# OSTEOGENESIS AND OSTEOINTEGRATION OF TISSUE ENGINEERED STRONTIUM HYDROXYAPATITE SCAFFOLD IN OSTEOPOROTIC RODENT AND OVINE MODELS

**SUNITHA CHANDRAN**

**Ph.D. THESIS**
**2016**

**SREE CHITRA TIRUNAL INSTITUTE FOR MEDICAL SCIENCES AND TECHNOLOGY**
**THIRUVANANTHAPURAM**
**INDIA**

# OSTEOGENESIS AND OSTEOINTEGRATION OF TISSUE ENGINEERED STRONTIUM HYDROXYAPATITE SCAFFOLD IN OSTEOPOROTIC RODENT AND OVINE MODELS

A THESIS PRESENTED BY

**SUNITHA CHANDRAN**

TO

SREE CHITRA TIRUNAL INSTITUTE FOR MEDICAL
SCIENCES AND TECHNOLOGY
THIRUVANANTHAPURAM
INDIA

IN PARTIAL FULFILMENT OF THE REQUIREMENTS
FOR THE AWARD OF
**DOCTOR OF PHILOSOPHY**

**2016**

# DECLERATION

I, Sunitha Chandran, hereby certify that I had personally carried out the work depicted in the thesis entitled, "*Osteogenesis and osteointegration of tissue engineered strontium hydroxyapatite scaffold in osteoporotic rodent and ovine models*", except where due acknowledgment has been made in the text. No part of the thesis has been submitted for the award of any other degree or diploma prior to this date.

Thiruvananthapuram — Sunitha Chandran

11-11-2016 — Reg.No: 2010/PhD/16

# CERTIFICATE

**SREE CHITRA TIRUNAL INSTITUTE FOR MEDICAL SCIENCES & TECHNOLOGY, TRIVANDRUM**

Dr. Annie John
Transmission Electron Microscopy Laboratory,
Department of Biomaterial Science and Technology
Biomedical Technology Wing,
Sree Chitra Tirunal Institute for Medical Sciences and Technology
Thiruvananthapuram.

This is to certify that Mrs. Sunitha Chandran in the division of Transmission Electron Microscopy Laboratory of this Institute has fulfilled the requirements prescribed for the Ph. D. degree of the Sree Chitra Tirunal Institute for Medical Sciences and Technology, Trivandrum. The thesis entitled, "***Osteogenesis and osteointegration of tissue engineered strontium hydroxyapatite scaffold in osteoporotic rodent and ovine models***" was carried out under my direct supervision. No part of the thesis was submitted for the award of any degree or diploma prior to this date.

* Clearance was obtained from the Institutional Ethics Committee/ Institutional Animal Ethics Committee for carrying out the study.

.

Trivandrum
11-11-2016

Dr. Annie John
(Research Supervisor)

The thesis entitled

***"Osteogenesis and osteointegration of tissue engineered strontium hydroxyapatite scaffold in osteoporotic rodent and ovine models".***

Submitted by

**Sunitha Chandran**

for the degree of

**Doctor of Philosophy**

Of

**SREE CHITRA TIRUNAL INSTITUTE**
**FOR MEDICAL SCIENCES AND TECHNOLOGY,**
**THIRUVANANTHAPURAM - 695011**

is evaluated and approved by

……. ……..

Dr. Annie John
(Research Supervisor)

Examiner

DEDICATED TO MY FAMILY &
TEACHERS

# ACKNOWLEDGEMENTS

*It is with deep sense of gratitude, satisfaction and with the divine blessings of God that I submit this dissertation. I take this opportunity with much pleasure to thank all who contributed in many ways for the success of this study.*

*I have no words to express my deepest sense of gratitude and respect to my supervisor Dr. Annie John, Scientist F, (TEM and DLAS) SCTIMST, who offered her continuous advice and encouragement throughout the course of study. I thank her for the systematic guidance and great effort that she put into for training me in the scientific field for preparation of this thesis. She was always accessible and willing to help with her advice and suggestions.*

*I thank members of doctoral advisory committee, Dr. T.V. Kumari (TIC), Dr. H. K. Varma (BCL) and Dr. Mira Mohanty (Rtd. from Histopathology) of SCTIMST for their timely suggestions, ideas and comments, which helped in the improvement of the quality of this work.*

*I thank Council of Scientific and Industrial Research, Govt. of India for the fellowship provided during the doctoral programme and Department of Science and Technology for funding the project. I also thank Department of Biotechnology, Govt. of India for funding for the international conference which I attended in China.*

*I am grateful to the Director of SCTIMST and the Head of BMT Wing for all support provided during the course of my work. I am thankful to Dean – Dr. Kallyana Krishnan, Associate Dean of Ph. D., Dr. Jayasingh - Deputy Registrar, all staff of academic division and Director's office for their assistance.*

*The valuable help and guidance from Dr. H.K Varma and Dr. Suresh for scaffold preparation has significantly contributed to this thesis. I gratefully acknowledge their personal support and encouragement at difficult times. I also acknowledge the service of Mr. Nishad for SEM evaluations.*

*I thank Dr. Umashankar for providing the facilities for large animal experiments in sheep model. My sincere thanks to Dr. Sachin, for his help with surgical procedures in sheep osteoporotic model. Sincere thanks to Dr. Harikrishnan V.S also, for helping with the surgical procedures in rat osteoporotic model. I thank all members of DIMT & DLAS, for their assistance during t he animal experiments.*

*I acknowledge the service from Dr. Mira Mohanthy, Dr. Sabareeswaran, Mr Joseph, Mrs Sulekha and Dr. Sowmya, Histopathology for the histology evaluations.*

*I would also like to thank Dr. Kallyana Krishnan, Mr Arun, Mr. Satheesh, Ms Lakshmi and all members of DPL for Micro-CT analysis. I also thank Mr Ramesh Babu and Staff of Precision fabrication facility for fabricating templates for different experiments. I also thank Dr. T.V. Anilkumar for helping with confocal laser scanning microscopy.*

*I am greatly indebted to all my colleagues at TEM lab: Mrs. Susan, Dr. Beena, Dr. Francis, Dr.Renu, Mr. Mir, Mrs. Resmi, Mrs. Ganga, Mrs. Sandhya Rani, Mr. Balu, Mr. Hadi, Mr Alwin and Mr. Joice for their support, encouragement & friendship throughout this odyssey.*

*My friends and teachers from within and outside the campus have helped in different ways. Co-operation from staff of various administrative departments and library of the Institute is fondly remembered. Cordial attitude and support from my fellow friends from other departments of the campus is also acknowledged*

*I have no words to express gratitude to my family members who provided the most precious support. I am indebted to my brother, sister in law - Rekha & Ajitha and my in-laws for their endless support, encouragement, love and prayers. I am deeply gratified to my parents for their love, care and support for overcoming the difficult times. My husband Dr. Renjith has been the pillar of my strength and has supported me wholeheartedly whenever it was most required. Last but not the least, smiling face of my little angel Nandana has relieved my tensions and anxieties throughout the course of study.*

***God, almighty I kneel down in your presence for giving me strength, courage and for providing good health for completing this work.***

# TABLE OF CONTENTS

# LIST OF FIGURES

# LIST OF TABLES

# ABBREVIATIONS

| | |
|---|---|
| ALP | :Alkaline phosphatase |
| ADMSCs | :Adipose derived mesenchymal stem cells |
| BMD | :Bone mineral density |
| BMP | :Bone morphogenetic proteins |
| BMU | :Bone remodelling units |
| CFU-F | :Clonogenic fibroblast precursor cells |
| DRIFT | :Diffuse reflectance |
| E-SEM | :Environmental Scanning Electron Microscope |
| FDA | :Food and Drug Administration |
| FTIR | :Fourier Transform Infrared Spectroscopy |
| HA | : Hydroxyapatite |
| HASi | :Silica coated HA |
| ICP | :Inductively Coupled Plasma |
| IGF | :Insulin-like growth factor |
| LAA | :L- Ascorbic Acid |
| MSCs | : Mesenchymal stem cells |
| MTT | :Thiazolyl Blue Tetrazolium Bromide |
| NBF | : Neutral buffered formalin |
| PBS | :Phosphate Buffered Saline |
| PDGF | :Platelet-derived growth factors |
| sADMSCs | : Sheep adipose derived MSCs |
| SBF | : Sterile simulated body fluid |
| Si | : Silica |
| Sr | : Strontium |
| TGF | :Transforming growth factors |
| Ti | :Titanium |
| UCBSCs | :Umbilical cord blood derived stem cells |
| XRD | :X-ray powder diffraction |
| β –GP | :β Glycerophosphate |

# ANNOTATIONS

| | |
|---|---|
| cm | : Centimetre |
| ml | : Millilitre |
| µg | : Microgram |
| µm | : Micrometre |
| mg | : Milligram |
| nM | : Nanomolar |
| °C | : Degree Celsius |
| mm | : Millimetre |
| h | : Hour |
| M | : Molar |
| min | : Minute |
| g | : Gram |

## SYNOPSIS

Incidence and prevalence of osteoporosis related disorders is on the rise worldwide. Approximately one in two women and one in four men above 50 years will have osteoporotic fractures. Further, aging also accelerates the extent of bone loss in postmenopausal women. In osteoporotic subjects, excessive bone loss is attributed to the increased activity of osteoclast cells and impaired activity of the osteoblast cells, thus increasing fracture susceptibility and incidence. Since such bone is unlikely to heal on its own, patients frequently undergo surgical procedures. But pull-out of implants (especially metals) is frequently observed and hence implants have to be anchored using screws, wires, or nails. Manipulation of fracture environment using tissue engineering applications of growth factors, scaffold and cells at the implant site has emerged as a promising strategy in the field of regenerative medicine.

In-house developed hydroxyapatite based scaffolds have proved to be highly osteoconductive and its efficacy has been proven in bone defect models in small and large animals. Improved *in vivo* osteogenic efficacy of tissue engineered ceramic systems (using stem cells- to incorporate osteoinductive properties) has also been reported. Though hydroxyapatite is found to be osteoconductive, they do not address the accelerated demineralization in the osteoporotic subjects at the defect site. Hence an ideal biomaterial for osteoporotic fracture should regulate bone resorption and

simultaneously favor osteogenesis, so as to attain better osteointegration and bone healing. Strontium (Sr) has recently gained interest for osteoporotic applications as it has shown to enhance osteoblast cell replication and simultaneously reduce osteoclast activity. Incorporation of Silica (Si) ions into bioactive ceramics is also of great interest, attributed to the improved apatite formation and osteointegration ability of Silica incorporated ceramic scaffolds. Therefore by local and targeted delivery of Si/Sr from the implant at the bone defect site, it is legitimate to assume that osteointegration and osteogenesis may be promoted. This work is focused on the hypothesis that cell-based tissue engineering in conjunction with Hydroxyapatite modified with Sr/Si may enhance bone defect healing in osteoporotic condition.

To prove the hypothesis, the defined objectives were –

(1) Phase I - Characterization of scaffold of choice: Test materials – Silica coated Hydroxyapatite (HASi) and 10% Strontium incorporated Hydroxyapatite (SrHA); Control material – Hydroxyapatite (HA).

(2) Phase II - Fabrication of tissue engineered scaffolds using rat derived Mesenchymal Stem Cells (rMSCs) followed by *in vitro* and *in vivo* evaluation in rat osteoporotic model.

(3) Phase III - Fabrication of tissue engineered scaffolds using sheep derived Mesenchymal Stem Cells (sMSCs) followed by *in vitro* and *in vivo* evaluation in sheep osteoporotic model.

Thesis is divided into following chapters – Introduction (Chapter 1), Literature review (Chapter 2), Materials and Methods (Chapter 3), Results (Chapter 4,5,6), Discussion (Chapter 7) and Summary and Conclusion (chapter 8).

**Chapter 1** gives an overview about osteoporosis, epidemiology of osteoporotic fractures, different treatment modalities and the challenges faced. The chapter also highlights the significance of tissue engineering application by the incorporation of bioactive molecules/ ions/ cells onto the ceramic scaffolds for regulating osteogenesis and excessive resorption in osteoporotic subjects.

**Chapter 2** covers an extensive review on basic bone biology, etiology of osteoporosis, fracture healing mechanism and factors associated with delayed healing in osteoporotic patients. Significance of the research methodology adopted in the present study including relevance of stem cells, role of Sr/Si therapy and significance of the animal models chosen is also mentioned.

**Chapter 3** includes a detailed depiction of protocols, materials and equipment used in the study. Scaffold materials – Hydroxyapatite (HA), Strontium incorporated HA (SrHA) and Silica coated HA (HASi) were synthesized and gifted by Bioceramic Laboratory, SCTIMST. The microstructure, porosity, phase composition, functional group analysis and degradation properties of the scaffolds were evaluated using Scanning Electron Microscopy (SEM), Micro CT, X-ray diffraction (XRD), Fourier transform infrared spectroscopy (FTIR) and Inductively Coupled Plasma techniques in Phase I. Cytocompatibility was evaluated using test on extract method. Phase II and Phase III involved adoption of techniques like primary stem cell isolation, MSC

characterization (using flow cytometry, lineage differentiation ability) and fabrication of tissue engineered constructs named as cHA, cHASi and cSrHA. Osteoporotic models were developed by combination of ovariectomy and Calcium deficient diet. Osteoporotic model development was evaluated by biochemical analysis, histology and micro CT. Surgical procedures adopted for implantation and post implantation evaluation techniques like radiography, histology and micro CT is also described.

**Chapter 4, 5, 6** illustrated the results of phase I, II and III studies respectively.

Phase I studies proved the scaffolds to be micro-porous with rough surface topography. HA and SrHA were found to have single phase, while HASi was found to have three phases. Micro CT studies revealed the porosity of scaffolds in the order HASi > HA > SrHA and apparent density in the reverse order. HASi exhibited highest *in vitro* degradation rate followed by SrHA and HA. Release of Sr from SrHA scaffolds were found to be within the therapeutic range, equivalent to 0.11mM per mg of the material. Cytocompatibility of the scaffolds were also proved using L929 cells.

Phase II results proved the *in vitro* cytocompatibility and *in vitro* osteogenic efficacy of all the three scaffolds using rat bone marrow derived MSCs -rBMSCs (rBMSCs were chosen owing to its high osteogenic differential potential) followed by *in vivo* osteogenic efficacy assessment in rat osteoporotic model. Isolated rBMSCs

were proven to be of mesenchymal origin with differentiation ability. HA, HASi and SrHA scaffolds supported *in vitro* osteogenic differentiation, as evident from the Alkaline Phosphatase assay. Meanwhile, the osteoclast pre-cursor cells seeded on SrHA scaffolds could not maintain their normal morphology compared to HA and HASi, indicative of the anti-osteoclastic activity of Sr incorporated scaffolds. Highest *in vivo* regeneration potential on par with material degradation was exhibited by cSrHA implants followed by SrHA, cHASi, HASi and HA. Since the improved therapeutical application of SrHA based implants has been signified from the rat studies, further investigation in sheep model proceeded with HA & SrHA scaffolds.

Phase III results proved the cytocompatibility and *in vitro* osteogenic efficacy of HA and SrHA implants using sheep adipose derived MSCs - sDAMSCs (sADMSCs were chosen as fat tissue may be procured with less morbidity compared to BMSCs and increased yield has also been reported). *In vitro* osteogenic differentiation studies proved the differentiation ability of the isolated sADMSCs and tissue engineered constructs proved to favour cell adhesion and proliferation. Implantation studies in osteoporotic sheep model revealed the improved osteointegration and osteogenic ability of cSrHA implants, evident from the radiographs, histology (in terms of regeneration efficiency -new bone formed /total defect area) and micro CT evaluations. Moreover an improved mineralization

efficiency of the *de-novo* bone was evident from the density histograms generated using micro CT.

The results obtained in the study are discussed in detail in **chapter 7**. Implantation studies in rat and sheep osteoporotic model emphasized the enhanced osteogenesis using cSrHA and SrHA implants. Supplementation of MSCs and Sr aided *in vivo* osteogenesis and possibly regulated the osteoclast activity enabling bone tissue in growth and osteointegration.

**Chapter 8** presents the summary and important conclusions derived from the study. The present study has been successful in validating the concept of fabrication of a scaffold to aid local delivery of Strontium ions and MSCs at the defect site in perspective of bone regeneration/repair in clinical osteoporotic situations. The acceptance of proposed scaffold material with *in vitro* data was further supported by performance in two animal models, paving hope for future applications using this indigenous technology for bone reconstructive surgery. SrHA may also be used as implant coating to improve fixation of metal implants and further research is warranted on this line. It is anticipated that tissue-engineered Strontium incorporated implants may revolutionize the current available geriatric osteoporotic defect treatment strategies in the Health Care System.

# CHAPTER 1

# INTRODUCTION

## 1. Bone

Bone is a dynamic tissue which provides structural support to the body and also plays an important role in maintaining calcium homeostasis in blood. Thus bone exerts a regulatory role in almost all the cell signalling pathways. Anatomically bone is comprised of the outer compact cortical bone and the inner less compact trabecular bone. Cortical bone forms 80% of the skeleton and contributes to the mechanical strength, whereas trabecular bone comprises of only 20%. But trabecular bones have larger surface area and are responsible for the stress responsive changes in bone mineral metabolism.

## 1.1. Composition:

Bone comprises of an organic matrix and a mineral phase. The organic matrix comprises of collagen (type I collagen) and different non collagenous proteins, which together influences the resistance of the bone towards tractional and torsional forces (Caetano-Lopes *et al.*, 2011). Non collagenous proteins include osteocalcin and glycoproteins including alkaline phosphatase (ALP), osteonectin etc. The organic matrix also includes growth factors like transforming growth factors (TGF–β), platelet-derived growth factors (PDGF), insulin-like growth factor (IGF) and a number of bone morphogenetic proteins (BMP) like BMP2, BMP4 and BMP6.

The mineral phase mainly includes Calcium (Ca) and Phosphorous (P). Other minerals include magnesium (Mg), sodium (Na), traces of fluorine (F), Strontium (Sr) (Dorozhkin, 2010). The Ca and P content determines the extent of crystallization in bone. Mature bone formation occurs by the process of crystallization followed by mineralization which ultimately leads to the formation of hydroxyapatite (HA) – the basic component of the bone.

## 1.2. Cellular composition:

Cellular composition of bone includes osteoclasts, osteoblasts and osteocytes. These cells act unanimously to maintain the normal bone remodelling cycle and thus help in maintaining a uniform bone mineral density (BMD). Osteoblast cells are descendants of bone marrow derived stem cells and are responsible for the synthesis of the collagenous protein. Osteoblast cells also organize Ca and P to form hydroxyapatite - the bone mineral phase (Manolagas, 2000). Osteocytes are the inactive or resting osteoblasts which get activated under physiological stress or stimuli and initiates bone remodelling process (Klein-Nulend *et al*., 2002). Osteoclast cells are the multinucleate jelly fish-like cells derived from the monocyte-macrophage lineages which are responsible for bone resorption process. Osteoclast cells have ruffled borders by which they attach to the bone surface and secrete acid and enzymes into the mineralized bone, which results in the demineralization of the bone. Stimulants of osteoclast cells include receptor activation of nuclear factor κ β-ligands (RANKL) and macrophage colony stimulating factors (M-CSF) (Lacey *et al*., 1998).

## 1.3. Bone remodelling:

Bone is in a state of continuous remodelling throughout the life. Remodelling is required to maintain the physiological structure and mineral homeostasis of bone. Optimum bone remodelling allows the skeleton to increase in size, respond to structural damages due to stress, fracture or fatigue and maintain the normal BMD. During childhood and adolescence, bone formation exceeds resorption, thereby denser and longer bones are formed. But as the growing stage attains maturity, both the process occurs in a balanced manner with equal resorption and formation. After adolescence, resorption exceeds formation and thus bone loss is initiated. Bone loss gets accelerated with menopause in women. Level of peak bone mass achieved at puberty/maturity determines the bone quality and later determines the extent of bone loss in women after menopause. Aging also contributes to rapid bone loss in both sexes. Age related decline in BMD in the trabecular bone is estimated to be 40% at the age of 50 (Seeman, 2008).

Bone remodelling (figure 1A) occurs in a non-targeted manner and consists of three consecutive phases: Phase I- resorption - osteoclasts digest old bone; Phase II – reversal - mononuclear cells appear on the bone surface; and Phase III - formation - osteoblasts lay down new bone until the resorbed bone is completely restored (Clarke, 2008). It occurs in definite sites known as the bone remodelling units (BMU). A healthy person will have approximately 4 million BMUs formed per year. BMU also occurs with the help of osteocytes at bone surfaces (Kennedy *et al.*, 2012). Rate of remodelling is higher in the trabecular bone.

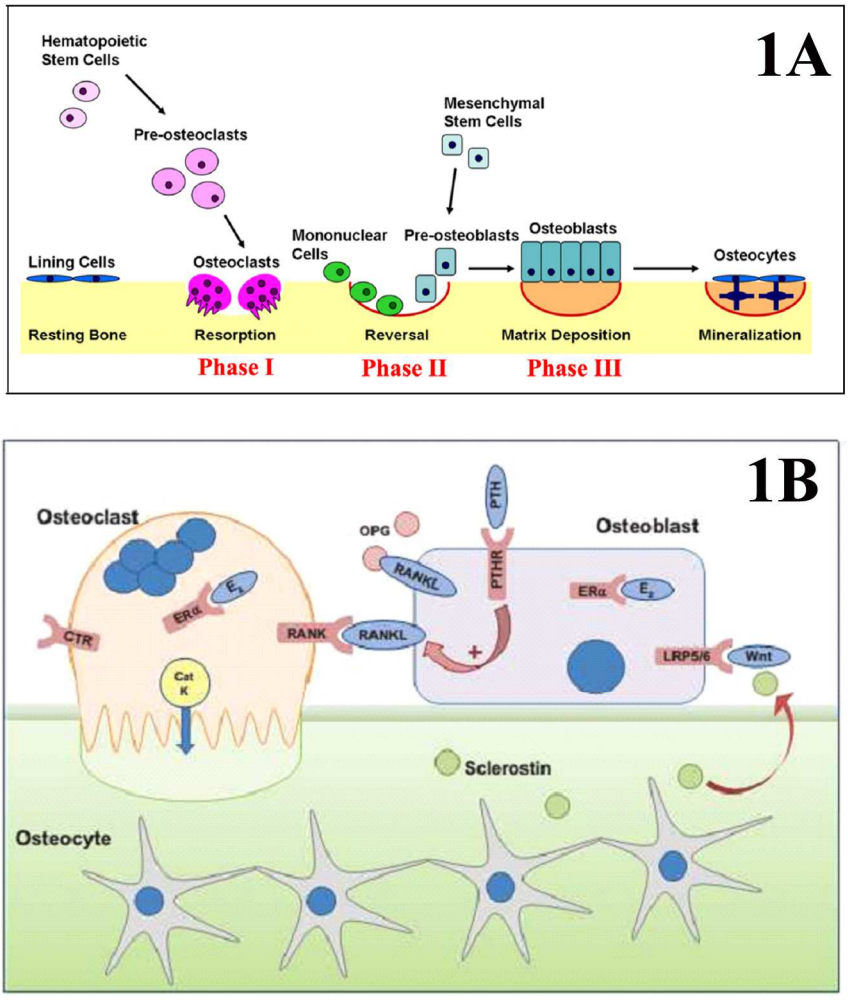


**Figure 1 - Bone remodelling cycle: 1A –**Bone formation by osteoblast cells and resorption by osteoclast cells (adapted from Kapinas and Delany, 2011); **1B:** key signalling pathways (adapted from Das and Crockett, 2013).

The osteoprotegerin / receptor activator of nuclear factor kappa-B / receptor activator of nuclear factor kappa-B (OPG/RANKL/RANK) the main system regulating osteoblast and osteoclast interaction (figure 1B). RANKL is found on the surface of osteoblast cells and is responsible for the activation of osteoclast cells. When RANKL binds to RANK receptor present on surface of osteoclast cells, Nuclear Factor Kappa-light-chain-enhancer of

cells (NF-κB) get translocated to the nucleus causing an increase in the of genes involved in osteoclastogenesis. RANK-RANKL interaction and could be inhibited solely by the decoy receptor osteoprotegerin (OPG), eventually terminates resorption of the osteoclast cells (Das and Crockett,

## 1.4. Osteoporosis:

Osteoporosis is a condition of skeletal fragility characterized by weak bone mass and increased fracture susceptibility (Grob, 2011). T-score value of zero is considered as the mean BMD of young female adult (Kanis *et al*., 2008). Osteoporosis is defined by World Health Organization (WHO) as a value for BMD 2.5 SD below from the mean BMD of female adult and is referred to as a T-score value of −2.5. Patients with osteoporosis suffer a reduction in bone mineral density, as a consequence of the increased demineralization by the osteoclast cells resulting in fragile bones. Morphological features of osteoporotic bone (figure 2) include cortical thinning and decrease in trabecular number which results in the reduction in bone quality. This ultimately lead to fracture, pain and disability in osteoporotic patients (Cooper, 1997). Since the advancement of the disease occurs insidiously, it is named as the “silent disease” and is often diagnosed when a clinical fracture occurs.

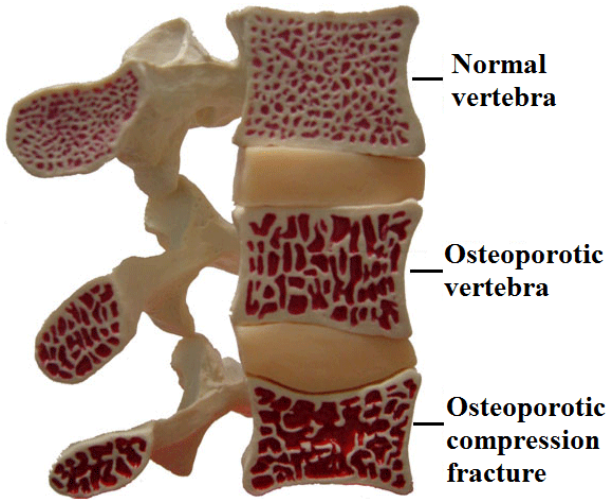


**Figure 2 - Morphological features of osteoporotic bones** (adapted from http://www.neuros.net/en/osteoporotic fractures.php).

Women are at a greater risk for osteoporosis due to lower peak bone mass and hormonal changes. Approximately one in two women and one in four men over the age 50 will have osteoporosis related fracture (Gudena *et al.*, 2011). This increased incident rate in women is because of the effect of hormonal changes during menopause, inadequate physical activity and low calcium intake. In aging population also, osteoporotic vertebral fractures are becoming more and more frequent and the increased incident rate is associated with significant morbidity and mortality.

## 1.5. Osteoporosis epidemiology

Osteoporosis is a well recognized public health problem worldwide and is associated with increased morbidity and health care costs. Osteoporosis has a common disease and it is estimated that worldwide 100-200 million people osteoporosis and associated fragility fracture (Cooper *et al.*, 1992) (figure 3). has been considered as an important factor for osteoporosis and associated The increased incidence is expected to reach to 800,000 hip fractures per year in

and up to 1.8 million in women (Dreinhöfer *et al*., 2005). A UK based study has predicted that one in two women and one in five men over the age of 50 years have osteoporosis related fractures (Das and Crockett, 2013), where as men risk rate of 15% compared to women with 40%. This accelerated bone loss in is due to the decreased estrogen level associated with menopause (Mullender *et* 2005). Shorter life expectancy and higher peak bone mass is found to be the behind the low incidence of osteoporosis in men (Kaufman *et al*., 2000). Age, genetic predisposition and family history also contribute to low BMD. osteoporosis has been associated with several factors such as drug treatment corticosteroid use), hypogonadism, malnutrition etc.

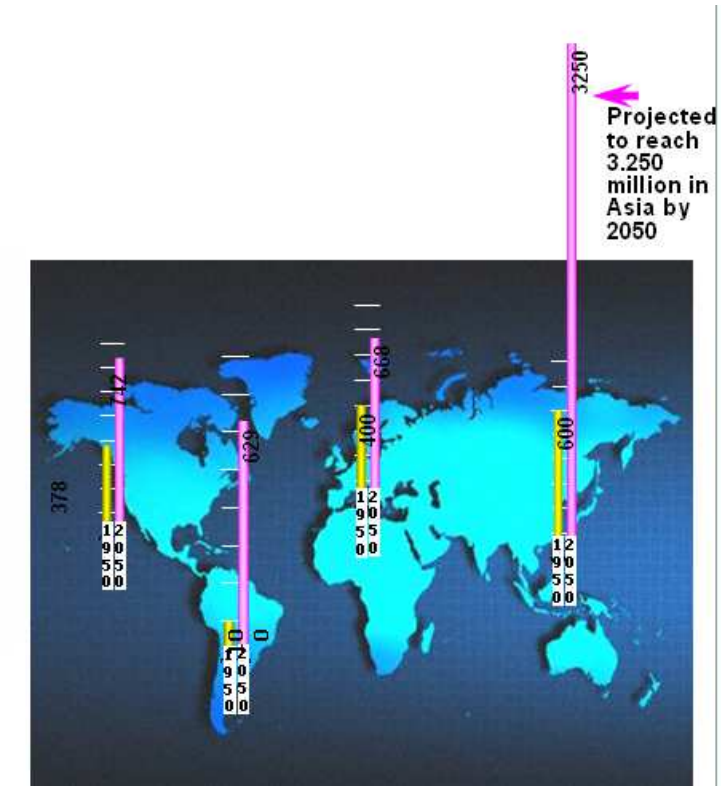


**Figure 3 - Osteoporosis epidemiology worldwide** (adapted from Cooper *et al.*, 1992).

## 1.6. Osteoporosis incidence in India:

In India, osteoporosis is emerging as a major orthopaedic challenge. Census study on Indian population, suggested that among 163 million aged people nearly 20% percent of women and 10-15% of men were affected by osteoporosis (Malhotra and Mithal, 2008). Even though in Western countries a high incidence is seen among the women population, in India majority of studies indicate that the incident rate is almost same in both sexes (Gupta *et al*., 2010). But it has also been reported that after menopause the incident rate is very high in women (Marwaha *et al*., 2011). Low Ca intake and low vitamin D level have been attributed to the increased incidence of osteoporosis in India. Even with high sunlight exposure, low vitamin D level is due to the genetic polymorphisms in the vitamin D receptor gene and estrogen receptor gene (Vupputuri *et al*., 2006). This could be attributed to differences in skeletal size and poor bone health status of Indians, which is a contributory factor for osteoporosis. Hence there is a pressing need to develop and validate a cost effective bone substitute for faster bone regeneration and fracture repair in osteoporotic patients in India.

## 1.7. Problems associated with fragility fractures:

Osteoporotic people have high bone turnover. Bone turnover is an determinant of the structural integrity of bone. Due to the poor quality of bone only is the risk of fracture high (Kanis *et al*., 2008) but also there is an increase fracture comminution. Increased bone porosity can produce a disproportionate reduction in bone strength and is associated with increased fracture risk. In

biomechanical stability in the fracture fragments is also important. leads to a lower degree of stem cell activation, which leads to delayed fracture healing. In osteoporotic condition reduced proliferation and differentiation the Mesenchymal Stem Cells (MSCs) and the osteoblast cells have been reported (Benisch *et al*., 2012). Increased susceptibility to fractures and inherent weak architecture increases the chances of implant failure and non union of the bone.

In osteoporosis, anchoring of screws, wires, or nails in bone is very difficult because of low bone mass. Consequently cut-out of implants and dislocations of bone fragments is frequently observed. Clinical reports have suggested that the absence of inherent osteointegrative ability of osteoporotic bone is the major cause of increased implant pull out and non-union. In most cases the fractures do not heal and often re-fracture at the same site, worsening the situation. Bonnaire *et al*., (2005) has reported that fracture at one site increases the incidence of further fractures in the vicinity by 2-3 times.

## 1.8. Osteoporotic fixation strategies:

With increase in the number of aging population, the medical and socio-economic burden associated with osteoporotic fractures increases. Treatment of osteoporotic fracture has a huge impact on a person's quality of life as bones are often associated with morbidity. Researches on osteoporosis and related have so far focused mainly on the pathophysiology, novel therapeutic agents for prevention and treatment of osteoporosis. Very few studies have focused on the

diagnosis and treatment of patients with osteoporotic fractures. Orthopaedic have understood that treatment strategies for osteoporotic fractures should not provide a mechanical support for the fractured bone but also address the pathology of the weak bone for better fracture fixation and bone regeneration.

In osteoporotic patients, when surgery is considered as the most advisable treatment, both rarefaction of bone and biological drawbacks due to local factor impairment (cytokines, growth factors etc) seem to be responsible for implant failures and non-union. Therefore, they require the adoption of particular surgical orthopedic strategies and adjuvant therapies that enhance integration and strength at the bone-implant interface.

Para Thyroid Hormone (PTH) supplementation has been considered as the most promising approach to treat osteoporosis as it enhances BMD by bone formation. But PTH administration also increases bone resorption. Bisphosphonate (BP) therapy which is known to inhibit bone resorption has also proven to inhibit bone turnover, thus helping in maintaining the bone density micro-architecture. But the therapeutic role of BP is prominent only in long supplementation studies. Recently, the concerns regarding the side effects with long term treatment has been raised as there are high chances of (Durie *et al*., 2005). Therefore neither PTH nor BP are preferred to attain early osteointegration and osteogenesis. PTH and BP also do not address the inherent impaired bone remodeling in osteoporosis (Gentleman *et al*., 2010). Therefore therapies that can aid faster osteointegration, osteogenesis with the ability to regulate bone remodeling ability may prove to be more beneficial.

## 1.9. Tissue engineering and osteoporosis:

Tissue engineering strategies may be adopted for osteoporotic applications, wherein the cellular part of the scaffold helps in bone regeneration and the scaffold/implant helps to maintain the contour and aesthetics of the fractured bone. This approach may be particularly relevant for large bone defects (trauma, tumors, etc.) or for osteoporotic patients for whom the number and renewal capability of osteoprogenitors are lower. Manipulation of both the local fracture environment in terms of application of growth factors, scaffolds, MSCs and systemic administration of agents promoting bone formation and bone strength have been considered as a treatment option in orthopedics from which promising results may arise.

### 1.9.1. Role of Mesenchymal Stem cells:

In aged and osteoporotic patients the number of resident MSCs and their proliferation, differentiation potential is reported to be impaired (Bonyadi *et al*., 2003). Stem cell therapy in osteoporotic fractures is expected to augment BMD and reduce fracture susceptibility by increasing the number and proliferation potential of resident stem cells (Antebi *et al*., 2014). Culture expanded MSCs may also be combined with bioactive ceramics or MSCs can be induced to differentiate into active osteoblasts on bioactive ceramics *in vitro* and then be implanted at the defect site (Nair *et al*., 2009a).

### 1.9.2. Significance of Strontium incorporation:

Studies have proven that Strontium (Sr) ions can decrease bone and increase bone formation simultaneously without affecting bone

(Meunier *et al*., 2002) raising the possibility that Sr may be a potential osteoporotic bone reconstruction. Strontium ranelate is being used widely for prevention and treatment of osteoporosis. But systemic oral administration of has only weak effect on osteoporotic bone healing and prolonged healing period be required for complete bone regeneration. Systemic and prolonged oral of Sr also might cause adverse reactions such as epidermal necrolysis. By local targeted delivery of Sr from the implant to the surrounding tissues, it is assume that it might inhibit excessive de-mineralization and promote osteointegration, osteogenesis. Incorporation of Sr may also improve the of the scaffolds and may aid in better *in vivo* tracking for assessing bone (López *et al*., 2014).

**1.9.3. Significance of Silica incorporation:**

Silica (Si) is found to play important role in the early bone calcification bone remodelling process (Carlisle, 1981). Si coated scaffolds have proved to better bone in growth and exhibit improved osteointegration ability *in vitro vivo* (Patel *et al*., 2002). Si incorporation also increases the dissolution property HA based scaffolds (Pietak *et al.*, 2007). The increased dissolution property also assist increased Ca release and thereby improve osteointegrative ability. and HA incorporation in PLGA composite improved the biocompatibility and osteoinductivity of the composite in rabbit bone defect model (He *et al.*, 2016). Together with the increased dissolution property, osteoconductive and osteointegrative ability - Silica incorporation in HA may aid osteoporotic bone healing and bone-implant bonding.

### 1.9.4. Carrier scaffold for local delivery of therapeutic agents:

Hydroxyapatite with the highest osteoconductive and osteointegrative ability may be chosen as the carrier to aid local factors that can hasten up the bone healing process in osteoporotic situations. HA has been proven effective for osteoporotic fracture fixation and have been used effectively as void fillers or for augmentation purposes, when metal implants are used. HA coated implants are also being currently used for osteoporotic applications. Therefore incorporation of additional bone regulatory agents/biologics with anti-resorptive and osteogenic ability may help in molding HA as a better scaffold for osteoporotic applications. Even though highly osteoconductive HA is devoid of any intrinsic osteoinductive property, incorporation of Si, Sr, growth factors, cells and related osteogenic hybrids may prove to be beneficial (Nair *et al.,* 2009b). Therefore HA based scaffolds may serve as an ideal carrier to aid local delivery of therapeutic ions at the fracture/bone defect site for osteoporotic bone reconstruction.

# CHAPTER 2

# REVIEW OF LITERATURE

## 2.1. Osteoporosis and fracture healing pathology:

Osteoporosis is associated with decreased mineral content of the bone the activity of osteoclast cells. Crystallinity of the HA phase in the bone along with increase in carbonate content, but there is a decrease in the acid level (Boskey *et al.,* 2005). These micro architectural changes lead to decrease the cross linking efficiency, bone thinning, decreased tolerance in response to mechanical stress and thus osteoporotic become more susceptible to fractures. Mechanical strength of the cortical bone decreases with the accelerated bone bone architecture becomes more and more porous. Cortical thinning pre-bone to fragility fractures. Not only there is reduction in bone density and mechanical strength, the composition and structural organisation are also osteoporosis (Currey *et al.,* 1996).

Osteoporosis increases fracture incidence. In certain cases the number of fractures may be limited to a single forearm fracture or hip fracture, but multiple numbers of fractures are also not rare. Fracture incidence at one site is known to increase the fracture incidence at nearby sites by two – three folds. classic fracture sites are hip, wrist and spine.

Fracture healing in osteoporotic bones exhibits a different than expected during normal bone healing process. Fracture healing ability is a

complex process which depends on the surrounding local niche, ensuing micro-vasculature and biomechanical condition. Etiological factors that cause like aging, hypogonadism, thyroid, parathyroid disorders - all contributes to fracture healing in osteoporotic condition. Accelerated bone loss further the bone regeneration potential. Osteoinductive nature of bone matrix decreases osteoporosis, as evident in ovariectomised rats (Cesnjaj *et al.,* 1991). It was from the *in vivo* studies using rat osteoporotic model that there is a prolonged of endoconrdal ossification as well as a higher phase of bone turnover that contributes to the delayed healing ability (Namkung-Matthai *et al.,* 2001). Bone formation rate in human osteoporotic patients is also adversely affected by bone formation due to diminished osteoblast activity (Marie *et al.,* 1989).

Compositional difference in vitamin D and local growth factors have considered as the key role players for delayed regeneration potential (Raisz, Estrogen deficiency in women adversely affects the vitamin D level and other cytokines which are responsible for bone formation. Estrogen plays a dominant in maintaining cortical bone formation and preventing bone resorption *al.,* 2011). Depletion of estrogen level in women after menopause accelerates the bone loss in them, making women population, a more vulnerable group to osteoporotic fractures. The regulatory role of estrogen is attributed to it's stimulatory effect on RANK L (Venken *et al.,* 2008). Increased RANK L leads to up regulation of osteoclast activity which enhances bone resorption in weak and fragile bones (Boyle *et al.,* 2003). In men testosterone plays a

role in maintaining BMD. Decline in PTH also results in decreased Ca and there by decrease in the bone density.

## 2.2. Osteoporosis and osteogenesis:

Cellular changes associated with osteoporosis include a decrease in the number, proliferation and osteogenic differentiation potential of MSCs residing the bone marrow micro-environment. MSCs residing in the bone marrow are recruited at the site of fracture healing and their interaction with the residing along with the local niche determines the bone healing efficacy. In adult or individuals red marrow forms the major part of bone marrow, but in condition marrow becomes populated with adipose cells resulting in white (Gimble *et al.,* 2007). This irreversible differentiation ability implies their to form mature bone during the bone healing process (Benisch *et al.,* 2012).

Bone regeneration ability in fracture healing is also seen impaired *et al.,*2012). It has been suggested that the impaired differential potential is to the impairment in type I collagen synthesis (Rodríguez *et al.,* 2000). Aging associated decline in the osteogenic differentiation potential also contributes to delayed healing in osteoporosis (Sethe *et al.,* 2006).

## 2.3. Osteoporosis and osteointegration:

High rate of implant failures has been reported in osteoporotic patients. most serious fragility fractures occur in the hip and an annual mortality rate of to 24% has been reported (Amin *et al.,* 2014). Implant failure statistics shows there is 2-10% non union, 4-40% mal-alignment after surgery and re-operation

of 3−23% (Syed *et al.,* 2004). Implant failure is also reported in the fractures associated with the metaphyseal region of long bones. Clinical reports suggest absence of inherent osteointegrative ability of the osteoporotic bone is the major cause of increased implant pull out and non-union. Regenerative capability of host bone also plays a crucial role in establishing a stable bone –implant (Fini *et al.,* 2004). Osteointegration is defined as the attainment of stable in the host bone by establishing direct chemical bonding between implant and (Albrektsson and Johansson, 2001). Histologically osteointegration is defined as direct anchorage of the implant in the host bone (implant gets surrounded by

Osteointegrative ability also depends on the osteoinductive and osteoconductive property of the implant. Researchers have focused on biomaterials/implants with better osteointegrative ability to suit osteoporotic applications. Strategies like increasing surface roughness and coating with HA have proven to improve osteointegration ability of the inert metals. But in osteoporotic patients, the number of cells with proliferative ability and local factors like growth factors are limited. Therefore osteoporotic bones need osteoinductive or osteoconductive implant materials to stimulate favour bone regeneration.

## 2.4. Osteoporotic fracture fixation:

Clinical reports have suggested osteoporosis as a risk factor for poor fixation especially in femoral and spine fractures (Schneider *et al.,* 2005). Due compromised healing ability and the weak architecture, treatment of

fractures is often complicated and there is higher chance of implant failure. Orthopaedic surgeons have realised that osteoporotic fracture should reduce further fracture incidence along with favouring bone defect (Dreinhöfer *et al.,* 2005).

Autografts have been considered as the most optimum substitute for engineering applications. Autografts exhibit better acceptance and along with functional outcome in aged patients (Tidermark *et al.,* 2003). Even aging has been associated with diminished osteogenic differentiation ability, satisfactory results were obtained from hip replacement studies using auto But the weak and compromised host bone limits the usage of such patients as source of autografts, especially in severe osteoporotic cases.

**2.4.1. Drugs and osteoporotic fracture fixation:**

Majority of the osteoporotic drugs exert their role by inhibiting bone resorption rather than favouring bone formation as increased resorption is the factor that leads to the impaired healing in osteoporotic patients. forms the major class of drugs that regulate the hyper activity of the osteoclasts. Other drugs include selective estrogen receptor modulators (SERMs), strontium ranelate and the more recent denosumab, all of which functions as resorbers (Das and Crockett, 2013). In contrast to the catabolic drugs, anabolic that favour bone formation include parathyroid hormone analog (PTH) and teriparatide. But for the drugs to be effective in accelerating fracture healing, a term systemic administration of drugs is required. And long term most of these drugs has been often associated with side effects such as

incidence of atypical fractures, thromboembolism and increased cardiovascular (Rheinboldt *et al.*, 2014). So a better strategy is to deliver these drugs locally at defect site using drug loaded implants. But drug loaded implant also do have limitation of drug release for a limited period and require reloading of the drug exert a long term effect on osteoporotic fracture haling. Hence, scaffolds with controlled drug release may also be suggested for prolonged osteoporotic applications.

**2.4.2. Surgical strategies and improvised implants:**

Reduced mechanical strength and weak osteoporotic bone presents an orthopaedic challenge to minimise the morbidity associated with surgical during fracture repair. Surgical procedure itself might create additional the nearby vicinity of the previous fracture. Surgical treatment aims at stability to fractured bone, with minimum treatment associated trauma. fixators are not usually recommended for osteoporotic fracture fixation due to poor anchorage of the fixator screws leading to screw pull out and non union. external circular fixators have been found useful to stabilize certain fractures using conventional wire to prevent non union. It has been suggested use of HA coated pin/screws help in providing better holding strength for the (Moroni *et al.*, 2001). Conventional plating techniques can also be used in combination with the use of HA coated screws or screws with improved threads (Kramer *et al.*, 2000).

Implants designed for fracture repair in normal bone may fail in bone of bone quality. Usage of inert metallic implants in osteoporotic condition, even

provides the desired mechanical strength, it is always associated with problems less osteointegration, inflammation associated with metal related stress fatigue, wearing at the bone implant interphase etc. Osteoporotic fracture fixation often augmentation using percutaneous cement injection (Kammerlander *et al.,* 2016) has become a widely accepted method (Levine *et al.,* 2000) . The aim is to a strong bone implant interphase and prevent implant failure. PMMA has been extensively used for augmentation purposes as it provides the desired strength (Bartucci *et al.,* 1985) (Alenezi *et al.,* 2016). Nevertheless, use of PMMA often associated with exothermal reaction, inflammation and difficulty in revision surgery is desired. Ideally, usage of osteoinductive or osteoconductive grafts maintains fracture reduction. Osteoconductive scaffolds provide a for *de novo* bone formation and favour bone in-growth at the bone implant interphase, thus aiding bone regeneration and osteointegration (Sterling and Guelcher, 2014).

### 2.4.3. Improved implant fixation using Hydroxyapatite:

Hydroxyapatite has been considered as the gold standard for applications because of its chemical similarity to human bone and its excellent activity (Costantino *et al.,* 1991). 95% of inorganic part of bone is composed of Important characteristic of hydroxyapatite scaffold is its interaction with the tissue and also it does not induce any foreign body reaction, toxic or response. HA is osteoconductive in nature and exhibit good osteointegration *In vivo* studies in small and large animal models have the proved the efficacy of house developed HA to favour bone in growth (Nair *et al.,* 2009a). Self setting

calcium phosphate cements (CPC) have also been used extensively as bone void fillers in osteoporotic fractures (Cornell *et al.,* 2003).

HA based scaffold possess the additional benefit, that the variations in its lattice and morphology help in ionic substitution – like Mg, Zn, Si, F, Cl, Sr etc *et al.,* 2012). Therefore HA with improved osteointegrative and osteoconductive nature may be used as a delivery vehicle to aid release of therapeutic ions at concentrations at the fracture healing site.

### 2.4.4. Local delivery of therapeutic ions at the defect site:

#### *2.4.4.1. Role of silica:*

Silicon is a trace element found in bone (100 ppm) (Schwarz, 1973). Si is found to play important role in the early bone calcification and its localization active bone forming areas have been reported (Carlisle, 1981). Supplementation has been reported to improve BMD in men and post menopausal women (Jugdaohsingh *et al.,* 2004). Silicon supplementation has also increased bone and strength in numerous animal models. A 30% increase in mineral osteogenesis was reported in ovariectomised rat models.

In addition, silica based HA scaffolds exhibit faster dissolution than bare demonstrating that Si incorporation in HA would distort and destabilize basic structure to dissolve rapidly. The increased dissolution property may also serve increased Ca release and thereby better apatite formation and osteogenesis at implant interphase. This may prove to be beneficial in improving the ability in osteoporotic patients. Follow up study of repair of a segmental

sheep model using tri calcium phosphate revealed that after 2 years Si incorporated material was completely resorbed on par with new bone formation (Mastrogiacomo *et al.,* 2007). The proposed mechanism of improved bioactivity (figure 4A) is due to the generation of more electronegative surface at the interphase that promotes osteogenesis or elemental silicon as such may be which directly stimulates the differentiation and proliferation of bone forming osteoblasts (Price *et al.,* 2013).

*In vitro* studies have proved the ability of Si to differentiate to mature osteoblast, thereby favouring better bone regeneration *in vivo al.,* 2009). Silica incorporated bioglass has also proved to form a strong bonding the host bone by the formation of HA layer at the implant interphase, indicative improved osteointegration ability (Hench, 1991). A better bone in growth and improved osteointegration ability was also evident from *in vivo* implantation in models studies using Silica coated HA (0.8 wt %) (HASi) (Patel *et al.,* 2002). application of Si becomes significant especially for orthopaedic applications in craniofacial, maxillofacial and periodontics.

The time required for forming the spontaneous precipitation of apatite layer is reported to increase with increasing silicate ion substitution. Si concentration in the human body is highly variable, ranging from plasma basal of 2–10 µM. A concentration of 10–20 µM elicited overexpression of collagen expression in MG63 cell line thereby improving osteogenic response. But a concentration above 50 µM revealed an inhibitory role (Reffitt *et al.,* 2003). studies have reported the inhibitory role of Si on $RAW_{264.7}$ cells, at a higher

concentrations of 200-500 µM (Costa-Rodrigues et al., 2016). Formation of very osteoclast cells with distorted morphology on 1.2% Silica containing HA, post days of culture substantiates the inhibitory effect of Si on osteoclast cells (Friederichs *et al.*, 2015), but not much is known about the mechanism.

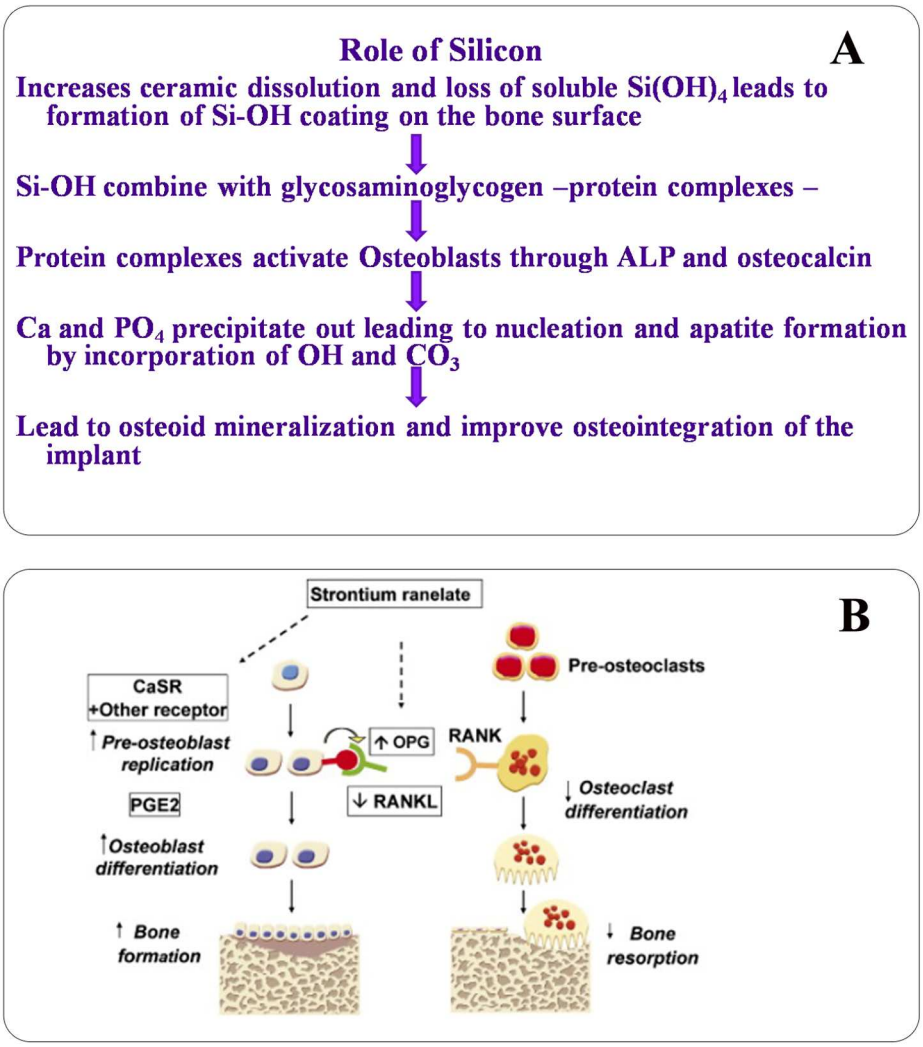


**Figure 4 -Therapeutic role of Silica and Strontium in bone tissue engineering: 4A –** anabolic role of Silica in osteogenesis and osteointegration (Adapted from Hench, 2006). **4B –** anabolic role of Strontium in osteogenesis catabolic role in osteoclast activity (adapted from Marie, 2006).

### *2.4.4.2. Role of Strontium in osteoporosis:*

Strontium has recently gained interest as it has shown to highly influence bone remodeling, where it not only favors bone formation and enhances proliferation (Canalis *et al.,* 1996) but also reduces osteoclast activity (Marie *et* 2001) (figure 4B). Studies indicate that strontium containing drugs like ranelate (sold under the trade name Protelos®) decreases bone resorption and maintains a high bone formation rate in osteoporotic rats, thereby preventing loss (Buehler *et al.,* 2001). The proposed cellular mechanisms behind the positive effects of strontium is in the prevention of formation of ruffled border by the osteoclast cells, thus preventing it from maturation and limits its pit formation (Bonnelye *et al.,* 2008). It has also been reported that Sr up regulates the Ca receptor activity by raising Ca concentration in the micro environment and promotes osteogenesis by the osteoblast cells (Canalis *et al.,* 1996).

The influence of Sr on bone metabolism has been subjected to research 1950's. The beneficial effect of Sr incorporated HA on bone mass at the bone implant interphase has been proven in rabbits (Beena *et al.,* 2013).Even though Strontium ranelate is not FDA approved, it is licensed (oral formulation of 2 for restricted use in case of vertebral and non-vertebral osteoporotic the European Union (EU). The prescribing guidelines also mention about the updates on the adverse effects of prolonged strontium ranelate treatment, skin rashes and deep vein thrombosis (Das and Crockett, 2013) on prolonged treatment.

### *2.4.4.3. Rational for 10% strontium incorporation in HA:*

Administration of strontium at low concentrations inhibits bone and hence Sr salts were formulated in many of the osteoporotic drugs for bone density (Meunier *et al.,* 2002). At high concentrations Sr is reported to the normal bone mineralization and alter the bone mineral profile in rodents. attributed to the increased substitution of Ca by Sr in the bone which also defective intestinal absorption of Ca (Dahl *et al.,* 2001). Accepted low dose of strontium is less than 4mmol Sr/kg/day (Marie *et al.,* 2001) and a dosage above mmol Sr/kg/day is found to negatively affect bone mineralization (Morohashi *et* 1995). Administration of Sr in the form of strontium carbonate at a very low 0.11–0.13 mmol Sr/kg/day for an osteoporotic person with 60kg body weight stimulated endosteal bone formation (Marie *et al.,* 2001). Sr incorporation has proven to improve the osteogenic efficacy as they up regulate the expression of when using 100% Sr incorporated bioglass scaffolds (Gentleman *et al.,* 2010).

Ca and Sr are alkaline earth metals and they resemble each other, with Strontium having a greater atomic radius than Ca. The chemical similarity the development of Sr incorporated Hydroxyapatite (SrHA) scaffolds by the replacement of Ca by desired concentration of Sr (Donazzon *et al.,* 1998). Sr easily be incorporated in bone by ion exchange mechanism (Likins *et al.,* 1959). uptake in human bone during adulthood occurs through this ionic exchange mechanism. But theoretical limitation for Sr substitution is one out of ten Ca (Boivin *et al.,* 1996). Sr replacement by more than 50% alters the crystallinity of scaffolds from monoclinic to rhombohedral. Therefore a lower concentration

in retaining the physcio-chemical properties of HA without affecting its (Qiu *et al.,* 2006a). But contradictions to this have been made by another group has proved that even 15% or more Sr incorporation may change the suggested 10% incorporation as optimum (Li *et al.,* 2007). It has been suggested 1-10% is the suggested optimum concentration for osteoporotic applications, and 10% seemed to improve *in vitro* osteoblast differentiation (Zhang *et al.,* Even though 5% SrHA is also expected to exhibit similar osteogenic efficacy to of 10% SrHA, the latter may exhibit better radiopacity too and thus aid in *vivo* tracking for assessing bone regeneration. If SrHA can aid in the local Sr at the desired concentration, then similar effects of strontium ranelate can be expected *in vivo* at the local implant site. Since HA is osteoconductive in nature, incorporation in HA would help in developing a better scaffold with improved osteointegrative ability, simultaneously incorporating the anti-resorptive ability suit osteoporotic applications.

**2.4.5. Role of stem cells:**

Stem cell research and therapy have got immense potential in skin, bone, cartilage tissue engineering etc. In aged osteoporotic patients, the number of MSCs and their differentiation potential is reported to be impaired (Bonyadi *et* 2003). Stem cell therapy in osteoporotic fractures is expected to augment the and reduce fracture susceptibility by increasing the number and proliferation potential of resident stem cells (Antebi *et al.,* 2014). Delivery of mesenchymal cells (MSCs) from PLGA microspheres too enhanced bone regeneration in bone defects in OVX rats (Yu *et al.,* 2012).

Stem cells can be procured from sources like bone marrow, adipose, umbilical cord, embryo etc. Recent studies have shown that umbilical cord blood derived stem cells (UCBSCs) also hold distinct therapeutical potential in osteoporotic application as they can be easily harvested without much morbidity, possess less immunogenic potential and exhibit strong differentiation potential. Application of human UCBSCs could effectively prevent OVX-mediated bone loss in nude mice (An *et al.,* 2013). Stem cells derived from dental pulp (DPSCs) and from that of exfoliated teeth have also proven to have strong application in orthopaedics (Alkaisi *et al.,* 2013), but the feasibility of their application in osteoporotic condition has to be validated.

Due to the intrinsic ability for osteogenic differentiation, ease of and possibility of genetic modification have made MSCs to be the most source (Antebi *et al.,* 2014). Out of all the sources, the highest osteogenic regeneration potential is expected from the bone marrow derived mesenchymal cells (BMSCs). But the differentiation potential and the overall number of has found to be inversely proportional with advancing age and osteoporosis.

In the mean time, Adipose derived mesenchymal stem cells (ADMSCs) emerging as a more reliable source, as ADMSCs can be easily isolated in without much morbidity and produce larger yield *in vitro.* The *in vitro* time required is also less compared to BMSCs (Liu *et al.,* 2012). Various studies have evaluated the functionality of ADMSCs from young and aged mice and aging to have minimum effect on its *in vitro* proliferation and differentiation (Chen *et al.,* 2012).

### 2.4.6. Bone Tissue engineering:

To effectively mimic the natural process of bone repair, tissue strategies have been optimized for the delivery of inductive growth and differentiation factors at the defect site, as well as the development of suitable biodegradable scaffolds (better mimicking the lost bone tissue) to support the attachment, proliferation and migration of osteoprogenitors. Bone defects that compromise the host source of osteoprogenitors would benefit from cell-based therapies in which cells with osteogenic potential are transferred to the site of loss (Antebi *et al.,* 2014). In a ground-breaking study, Friedenstein *et al.,* (1966), isolated cells; clonogenic fibroblast precursor cells (CFU-F) from whole bone marrow and showed that they were capable of forming bone and cartilage like colonies. Clinical and experimental studies have shown that marrow aspirates used in combination with biomaterials to improve bone formation. Systemic of MSCs have been used to treat children with severe forms of osteogenesis imperfecta (OI). Horwitz *et al.,* (2005) reported that patients subjected to the treatments showed reduced fractures in bones. Culture-expanded MSCs may combined with bioactive ceramics and implanted or MSCs can be induced to differentiate into active osteoblasts on bioactive ceramics *in vitro* and then be implanted at the defect site (Nair *et al.,* 2009b).

## 2.5. Need for an osteoporotic animal model:

The intended function of the proposed implant material is as an aid in healing of bone defects in females with osteoporosis. The US Food and Drug

Administration (FDA) Guidelines for pre-clinical and clinical evaluation of used in the treatment or prevention of postmenopausal osteoporosis therapeutic agents to be evaluated in two different animal species, first in ovariectomised rats followed by non-rodent large animal model which possesses Haversian systems and remodeling patterns similar to the human situation *al.,* 2001 and Pearce *et al.,* 2007). Therefore it is always desirable to study the efficacy of the proposed material first in a rat animal model. The selection a large osteoporotic animal model should be compatible with humans with anatomy, hormone profile, metabolism and bone architecture.

**2.5.1. Rat Osteoporotic model:**

Rat is the most frequently used laboratory animal for studying osteoporosis. Advantages of rat as a model are - inexpensive to purchase and maintain, grow rapidly, have a relatively short lifespan, have a well characterized skeleton and proven to be an excellent model for most common risk factors for osteoporosis. will give results more rapidly than other animals as they reach maturity in a span of life. Induction of osteoporosis by ovariectomy in rodents induced a significant trabecular bone loss with 3-6 months (Bagi *et al.,* 1997). A decrease BMD, cortical thickness and reduced fracture healing ability have also been

Zhang *et al*., 2013 has prepared strontium-incorporated mesoporous glass scaffolds and investigated the *in vivo* osteogenic efficacy in rat osteoporotic models developed by ovariectomy. In yet another study Cheng *et al.,* 2013 compared the regenerative efficacy of porous CaP/silk composite scaffolds in osteoporotic rats induced by bilateral ovariectomy.

### 2.5.2. Sheep Osteoporotic model:

The selection of an animal model for investigation in osteoporotic bone has so far been based on the comparable size of long bones in animals and humans, suitable for the implantation of human implants and prostheses. Sheep seems to be a promising model for osteoporotic studies for many reasons (Turner *et al.,* 2001 and Fini *et al.,* 2000):

- Sheep is used in 9-12% of orthopaedic research involving fractures
- Ewes ovulate spontaneously and have sex hormone profiles similar to women.
- Size and basic anatomy of the sheep skeleton are generally comparable with the human situation. Mechanical characteristics of the skeleton are comparable to humans which make their large vertebral bodies more suited to conventional surgical procedures.
- Sheep and humans have a similar pattern of bone in-growth into porous implants over time.
- They are docile and easy to handle.

Additionally, previous studies have also shown that sheep develop at various sites to different extents following ovariectomy (Hornby *et al.,* 1995), chronic steroid therapy (Chavassieux *et al.,* 1997) or combinations of these treatments along with diet restrictions (Lill *et al.,* 2000). Egermann *et al* (2005) established a sheep model for osteoporosis by combining estrogen deficiency, calcium and vitamin D-deficient diet with steroid medication (1800 mg methylprednisolone). It was also reported that BMD was reduced by 30% after weeks of induction and mimicked human osteoporotic situation with changes in the micro-architecture and mechanical properties (Egermann *et al.,*

In yet another study, Michele Rocca *et al.,* (2002) evaluated the osteointegration of HA-coated and uncoated titanium screws in the cortical long-term (24 months) ovariectomised sheep (OVX group) compared to sham-sheep (Control group). Cylindrical tapered screws - 3.5 mm in outer diameter mm in length were inserted into the diaphyseal cortex of femoral and tibial of the sheep model using 2.7 mm diameter drill. Post 12 weeks of implantation, animals were sacrificed and the histomorphometry analysis indicated that HA screws exhibited an affinity index (in terms of bone-implant contact) of compared to uncoated Ti screws of 61.15±13.12. The biomechanical and histomorphometry results achieved suggest employing HA-coated screws in osteopenic cortical bone. Long-term ovariectomised sheep can be used to study *vivo* osteointegration in the osteoporotic spine Nicoli *et al.,* (2002). HA coated screws proved to improve bone fixation and bone screw interface strength in and osteopenic animals. The histomorphometric and biomechanic results suggest that the role of HA coated steel in the improvement of the bone-screw interface strictly depends on the osteoconductivity of bioceramic materials nature of bone-implant bonding (Aldini *et al.,* 2002).

## 2.6. Development of Hypothesis:

Osteoporotic fracture healing is compromised due to the weak host bone structure, accelerated demineralization and together with the imbalance in bone remodelling, osteogenesis makes osteoporotic fracture fixation an orthopaedic challenge. . As a solution to this problem, review of literature portrays the use of

titanium and ceramic implants in osteoporotic rat and sheep models giving satisfactory results.

Nevertheless in this present study, we hypothesize that choosing an implant with better osteointegrative and osteogenic ability/delivery of local factors at the bone defect site would aid better bone regeneration in osteoporotic fractures. Hence Hydroxyapatite (gold standard for orthopaedic application) has been modified with silica /strontium and chosen as the carrier material for stem cell delivery rather than systemic administration of osteoporotic drugs to create anabolic effect on bone healing. Finally, the burden of proof of concept has been validated in osteoporosis induced rat and sheep models so as to extrapolate the data to clinical osteoporotic applications.

## 2.7. OBJECTIVES:

The main objective of the research study is to physcio-chemically characterize a hydroxyapatite scaffold modified with Silica or Strontium optimized for osteoporotic applications. It was also our interest to validate *in vitro* and *in vivo* osteointegrative and osteogenic ability of tissue engineered bioactive HA based constructs in osteoporotic animal models, so as to extrapolate the data to clinical application. To achieve these objectives and test the hypothesis, the study objectives were divided into following phases -

(1) Phase I- Characterization of scaffold of choice: Test materials – Silica coated Hydroxyapatite (HASi) and 10% Strontium incorporated Hydroxyapatite (SrHA); Control material – Hydroxyapatite (HA).

(2) Phase II- Fabrication of tissue engineered constructs using rat bone marrow derived Mesenchymal Stem Cells (rBMSCs) followed by *in vitro* and *in vivo* evaluation in rat osteoporotic model.

(3) Phase III -Fabrication of tissue engineered constructs using adipose derived Mesenchymal Stem Cells (ADMSCs) followed by *in vitro* and *in vivo* evaluation in sheep osteoporotic models.

# CHAPTER 3

# MATERIALS AND METHODS

## PHASE I – MATERIAL SYNTHESIS AND CHARACTERIZATION

## 3.1. Materials:

Bare hydroxyapatite (HA) as the control material, whereas HA modified with Silica coating (HASi) and HA modified with Strontium incorporation (SrHA), as the test materials were the scaffolds of choice. All materials were synthesized and developed at the Bioceramics Laboratory, SCTIMST, Trivandrum, India. All chemicals used for the synthesis were obtained from Rankem chemicals, India.

## 3.2. Material synthesis:

### 3.2.1. Synthesis of Hydroxyapatite:

Hydroxyapatite - $Ca_{10}(PO4)_6(OH)_2$ based scaffolds were synthesized by in-house developed method (Chandran *et al.,* 2016) (figure 5). Because of high solubility, calcium nitrate decahydrate ($Ca(NO_3)_2.4H_2O$) was taken as the salt and ammonium dihydrogen orthophosphate as the phosphate salt. HA was prepared by wet precipitation method involving slow addition of aqueous ammoniated solution of ammonium dihydrogen orthophosphate into the ammoniated solution of calcium nitrate under continuous stirring at 80˚C. procedure pH was maintained at the range of 10 to 11. The amount

of calcium and phosphate ions were retained in the mole ratio of 1.67. After the precipitate was collected by centrifugation, washed with de-ionized water to avoid impurities, oven-dried and calcined at 300˚C. Calcined precipitate were ball milled and sieved to collect HA powder below 125µm. HA powder was subjected to freeze drying for 24 hours and thereafter dispersed in polyvinyl solution and stirred along with glutaraldehyde (cross linking agent), benzoyl peroxide dispersed in benzene (initiator) and N-N-dimethyl aniline (activator). porous foam of slurry was then transferred into plastic moulds and kept for gelation at room temperature (RT). It was then severed into blocks, dried, fired at 600˚C to expel the additives and sintered at 1175˚C to get porous HA

$$10Ca(NO_3)_2 + 6NH_4H_2PO_4 + 4NH_4OH \rightarrow$$

$$Ca_{10}(PO_4)_6(OH)_2 + 10NH_4NO_3 + 4H_2O$$

### 3.2.2. Synthesis of Silica coated Hydroxyapatite:

To synthesize HASi scaffolds, porous HA blocks were synthesized as detailed in section 3.2.1. Silica sol was prepared alongside HA synthesis by the hydrolysis of Tetraethyl orthosilicate (TEOS) in ethanol water system. blocks were then dipped in silica sol gel (in ethanol–water system) for one and later sintered at 1230˚C for 2 h, to get a coating of Silica on HA. It has been confirmed from previous studies that HASi scaffolds developed using the same procedure ensured the presence of silica (15-17%), not only at the periphery but towards the internal core (Nair *et al.*, 2009a).

### 3.2.3. Synthesis of Strontium incorporated Hydroxyapatite:

To synthesize SrHA - $Ca_9Sr_1(PO4)_6(OH)_2$ the procedure used was almost similar to that employed in the fabrication of HA scaffold as in section 3.2.1. only difference was at the precipitation step where, 10 mol% of calcium nitrate solution was replaced with the corresponding amount of strontium nitrate *et al.*, 2016). Briefly, aqueous ammoniated solution of ammonium dihydrogen orthophosphate was dropped into aqueous solution containing calcium nitrate tetrahydrate and strontium nitrate in the mole ratio 1:9. During precipitation, kept above 10 and temperature at 80˚C. Resulting precipitate was subjected to various processes like aging, freeze-drying, and gelation at RT, followed by sintering at high temperature (1175˚C) to get porous SrHA blocks.

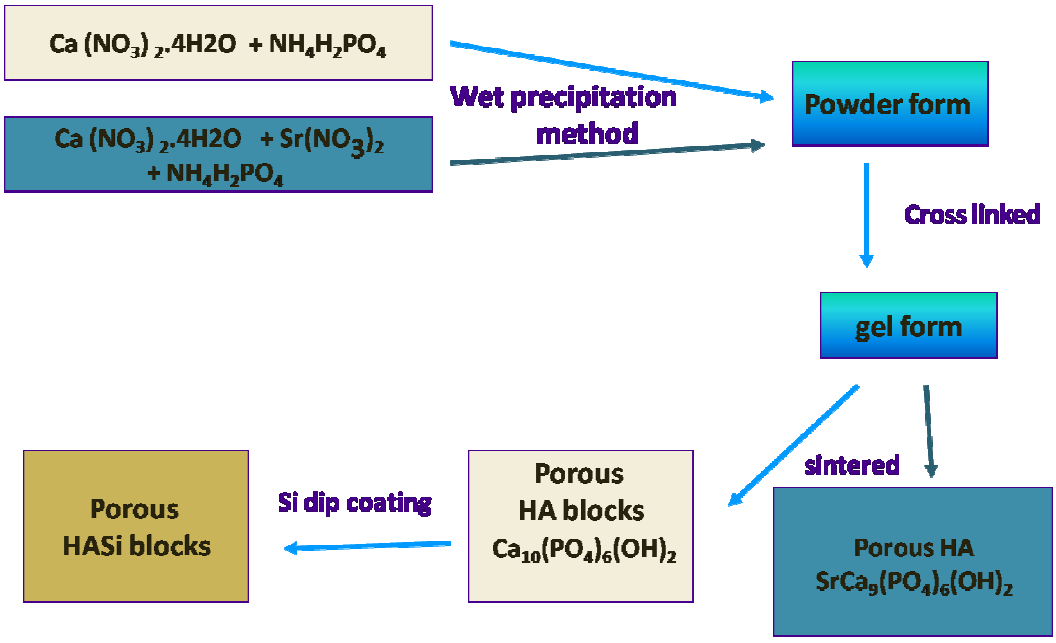


**Figure 5 - Flowchart for the synthesis of scaffold materials – HA, HASi and SrHA.**

### 3.2.4. Fabrication of experimental scaffolds:

Prior to *in vitro* and *in vivo* applications, ceramic blocks were shaped requisite size/shape to suit each experimental analysis.

- Disc shaped (5mm diameter x 1-2mm thickness) for the *in vitro* studies.
- Micro-granular (350-400μm) scaffolds for *in vitro* and *in vivo* studies in rat osteoporotic model. Micro granules were generated by manual crushing of ceramic blocks, which were then selectively sieved through specific sieves 350μm and 400μm.
- Cylindrical scaffolds (12 mm x 4mm) for *in vitro* and *in vivo* studies in sheep osteoporotic model. Polishing and shaping were done manually on the polisher (Buehler Ecomet, Germany).

### 3.2.5. Sterilization of scaffolds:

The scaffolds of desired dimensions (figure 6) were washed thrice with distilled water and subjected to ultrasonic cleaning (Bransonic, USA) for 10 each (5 times) at 37˚C, for the removal of fine powders and other impurities. the scaffolds were autoclaved by steam sterilization at 121˚C, 15 psi pressure for min.

## 3.3. Physicochemical characterizations of scaffolds:

#### 3.3.1. Microstructure evaluation – Scanning Electron Microscope:

For evaluating the surface morphology and micro structure, SrHA, HASi HA discs were gold coated using ion sputter (Hittachi E-1010) and viewed under Scanning Electron Microscope (Hitachi S-2400 – SEM, USA).

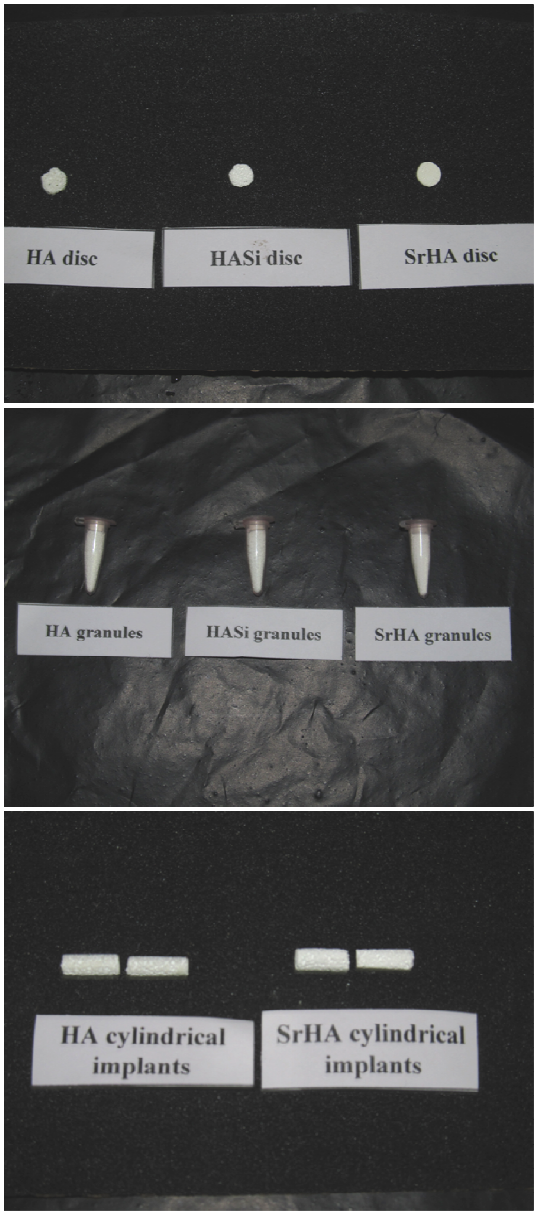


**Figure 6 - Gross images of different scaffold types used in the study.**

### 3.3.2. Pore Size & Porosity estimation - Micro CT:

Scaffolds were evaluated for its bulk porosity and pore size distribution micro CT desktop scanner CT 40, Scanco Medical AG (Bruttisellen, Scanning was performed at 70 kVp and 114µA. Pore size distribution was based on the data generated from approximately 300 numbers of slices of 20µm thickness. Bulk porosity (in terms of percentage) for each scaffold type was then calculated as given below -

$$\text{Porosity (\%)} = \{1- (Bv / TV)\}*100.$$

(Bv - Bone volume, TV - Trabecular Volume)

### 3.3.3. Phase analysis - X-ray diffraction:

Phase analyses of the scaffolds were determined using X-ray powder diffraction (XRD) measurement and compared with International Centre for diffraction data (ICDD) database for chemical identification. Scaffolds were powdered and XRD analysis was done with monochromatized Cu $k_\alpha$ radiation (Bruker D8 Advance, Germany) at an operational tube voltage of 40 kV and 30 mA and 2Theta range , n=20-50.

### 3.3.4. Functional group analysis - FTIR:

Functional group analysis of the synthesized scaffolds was done using Fourier Transform Infrared Spectroscopy (FTIR). This was performed on scaffold materials mixed with optical grade KBr powder using diffuse (DRIFT) mode in Thermo Nicolet 5700 spectrometer (USA). Pure KBr was

the control. FTIR spectra were recorded at a resolution of 4 $cm^{-1}$ and scanned between 400 and 4000 $cm^{-1}$ and 64 scans were done for each sample.

### 3.3.5. Density estimation - Micro CT:

For apparent density estimation, micro-CT desktop scanner CT 40 was as per the scan settings as in section 3.3.2. From the 2D slices generated, three-dimensional volumetric model reconstruction was performed using micro CT evaluation program V6.5. The apparent density of all the materials was evaluate the apparent opacity of the scaffolds.

### 3.3.6. Radiopacity evaluation - Radiography and image J analysis:

Radiopacity of the scaffolds were assessed from the radiographs taken at standard conditions using X ray film unit CR -30X (AGFA, USA). Generated radiographs were further evaluated using Image J software (Version 1.48v) compared against a standard curve plotted using an aluminium wedge (figure 7) (scaled 0.1- 1mm).


**Figure 7 - Aluminium wedge used for quantification of radiopacity of the scaffolds.**

## 3.4. Assessment of *in vitro* degradation ability in PBS – ICP:

Aseptic degradation studies were performed for 30 days in Calcium Magnesium free PBS. Scaffolds (10 x 10 x 2mm$^3$) of equal weight were sterilized and then immersed in 10ml PBS (pH – 7) in polypropylene vials at 37˚C for 30 with medium renewal every 3 days. The elemental analysis ($Ca^{2+}$, P, $Si^{2+}$ and of the degradation fluid in which the material was incubated was performed Inductively Coupled Plasma (ICP) optical emission technique (PerkinElmer (Waltham, MA) by Optical Emission Spectrometer ( Optima 5300 DV, USA)). to ICP analysis, collected fluids were acidified with nitric acid and were diluted known volume and then dissolution ratio per mg of the material was calculated.

## 3.5. Evaluation of *in vitro* apatite formation ability in SBF:

Aseptic degradation studies were performed in sterile simulated body (SBF) for 30 days (Kokubo and Takadama, 2006). Scaffolds (10 x 10 x 2mm$^3$) of equal weight were pre-sterilized. Scaffolds were then immersed in 10ml SBF 7.4) in polypropylene vials at 37˚C for 30 days, with medium renewal every 3 Incubated scaffolds were evaluated at regular intervals of 0, 7, 14, 21 days for formation using Environmental Scanning Electron Microscope (E-SEM) (FEI Quanta 200, Netherlands). Characterization of the apatite structure formed on scaffolds on 28$^{th}$ day of incubation was analyzed using FTIR as in section 3.3.4.

## 3.6. Cytotoxicity evaluation – MTT assay:

*In vitro* cytotoxicity was done using test on extract method. Extract was prepared by incubating disc scaffolds of equal weight in 1 ml DMEM LG USA) culture medium at 37±1˚C for 24 ± 2 hrs. Mouse fibroblast L929 cells 1, NCTC clone 929) (1000 cells per well) were cultured in 96 well plate and maintained for 24 hours at 5% $CO_2$ and 37±1˚C. Extracts of test and control were then added onto the cells cultured in the 96 well plates and incubated for another 24 hours. Phenol was chosen as the positive control. 5 mg/ml of Blue Tetrazolium Bromide (MTT) (Sigma, USA) reagent was added and after formazan crystals formed were dissolved in iso-propanol. Absorbance measured using an ELISA plate reader (BioRad systems, USA) (Measuring wavelength: 570nm, Reference wavelength: 630nm).

Metabolic activity of cells (Cm) expressed as percentage (Ayesh *et al.*, 2014) was calculated as follows:

$$Cm = (OD_{\text{of sample extract}} / \text{Mean } OD_{\text{cell alone control wells}}) \times 100$$

# PHASE II – *IN VITRO* & *IN VIVO* STUDIES USING rBMSCs IN RAT OSTEOPOROTIC MODEL

## ETHICAL STATEMENT:

All *in vitro* and *in vivo* studies using rat derived cells and rat osteoporotic model were performed as per the guidelines and recommendations of the for the Purpose of Control and Supervision of Experiments on Animals India and with the approval of the Institutional Animal Ethics Committee B Form No: B11122009 IV. Approval from Institutional Committee for Stem Research and Therapy (ICSCRT) was also obtained for the rat derived stem cell research work - Approval No:– SCT/IC-SCRT/08/Jun 2013.

## ANIMAL WELFARE:

Animals were housed in individually ventilated cages (IVC, Citizen Industries, India) at 22±2˚C and 55±10% Relative Humidity (RH). Light levels measured at 1 meter height less than 300 Lux and a 12:12 hour dark: light was maintained. Animals were fed with standard pelleted rat feed and drinking *ad libitum.* Animal colony was health monitored as per Federation for Animal Science Associations (FELASA) guidelines for parasitology (Rabbits *et* 2014) and was stamped negative of any infectious agents. The study also the Animal Research: Reporting of *Experiments* (ARRIVE) guidelines for the execution, evaluation and reporting of the *in vivo* study (Kilkenny *et al.,* 2011).

# PART A- *IN VITRO* EVALUATION OF HA, HASi AND SrHA DISC SCAFFOLDS USING rBMSCs

## 3.7. Isolation, culture and characterization of rBMSCs:

### 3.7.1. Isolation and culture of rBMSCs:

Rat Bone Marrow derived Mesenchymal Stem Cells (rBMSCs) were from the bone marrow of normal female rats aged 3- 6 months and weighing approximately 180-200mg. Rats were euthanized by $CO_2$ inhalation in a $CO_2$ chamber. The skin was shaved and disinfected with betadine solution. A skin incision of approximately 1-2 cm in length was made in the hind leg through the muscle flap and the femur, tibial bones were exposed. Bones were retrieved, removed off any muscle tissue and then collected in PBS with double of antibiotic -antimycotic (Gibco BRL, USA) (2ml antibiotics/100ml PBS).

Under sterile conditions inside a laminar air flow, each hind limb was bisected by cutting through the knee joint. Bones were exposed at the ends using bone cutter and bone marrow was flushed out through the bone shaft using an gauge needle into a centrifuge tube containing DMEM LG (Life technologies, growth medium. Marrow plug is dispersed in the medium followed by at 2500 rpm for 10 minutes. The pellet obtained was re- suspended in 5ml LG, seeded in tissue culture treated flasks and maintained in a $CO_2$ incubator 37˚C, 5% $CO_2$ and 95% RH. On the third day, medium was changed and supplemented with fresh growth medium to remove red blood cells and other adherent cells and were further cultured until confluency – $P_0$ passage.

On confluency, the cells were trypsinised by adding 0.25% Trypsin (Life technologies, USA) in the culture dish for 5 minutes. Fresh medium was to stop the action of trypsin, and the trypsinsed cell suspension was then at 2500 rpm for 10 minutes to collect the pellet. The pellet was re-seeded again and further cultured and passaged with medium renewal every 3 days till $P_3$

**3.7.2. Characterizations of rBMSCs:**

***3.7.2.1 Fluorescent staining –Actin and nuclear staining:***

To evaluate the morphology of isolated rBMSCs cells in $P_3$ passage were cultured on sterile cover slips for 24 hours and then fixed in 3.7% para-formaldehyde. Fixed cells were permeabalized using 0.1% triton (Sigma India) for 5 minutes followed by PBS wash. Fixed cells were initially stained Actin stain - rhodamine-phalloidin (Life technologies, USA) in 1: 100 dilution incubated for 30 minutes in dark at RT. After a gentle PBS wash, cells were counter stained with the nuclear stain – DAPI (Sigma chemicals, USA) for 10 minutes at RT in dark incubation. Stained cover slips were washed twice with mounted and imaged using fluorescent microscope DM 6000 (Leica, Germany).

***3.7.2.2. Surface marker analysis - Flow cytometry:***

For flow cytometry analysis, cells in $P_3$ passage were collected and twice in PBS. Cell suspension was then blocked with 3 % BSA for 30 minutes to prevent non-specific binding. After blocking cell pellet was obtained by centrifugation and following a PBS wash, cell suspension was subdivided. To cell suspension in tube, antibodies against CD 90 (Abcam) or CD 34 (Abcam)

added at 1:100 dilution and incubated for 2 hours in dark at 4°C. Following a PBS wash, FITC conjugated secondary antibody in 1:100 dilution specific to antibody was added into each suspension and further incubated for 1 hour in 4°C. Cells stained with secondary alone served as control. Stained cells were then fixed in 3.7% paraformaldehyde for 20 minutes and stored in 4°C until analysis. suspension was analysed using flow cytometer (FACS Aria, BD Biosciences) and percentage of FITC positive cells was quantified by applying suitable gating Diva software.

***3.7.2.3. Differentiation potential - Alizarin red & Oil red O staining:***

Osteogenic differentiation and alizarin red staining:

For osteogenic induction, $P_3$ cells were cultured in osteogenic medium (DMEM – LG containing 15% FBS, 10 mM β-glycerophosphate, $10^{-8}$ M dexamethasone, 0.05 mg / ml L-ascorbic acid (Sigma chemicals, USA) and 1% antibiotics). Further, the osteogenic induced cells were maintained in the induction medium for 14 days for osteogenic differentiation with medium every 3 days.

Cell-seeded cover slips were then washed thrice with PBS – 10 minute fixed in 3.7% paraformaldehyde and stained with 1% Alizarin red (Sigma Chemicals) to determine calcium deposition. Post staining the cover slips were mounted with anti-fadent (Dako, Denmark) and micrographed using DM 6000.

Adipogenic differentiation and oil red O staining:

For adipogenic induction, $P_3$ cells were cultured in adipogenic induction medium 100mM Iso butyl (sigma), 1mM dexamethasone (sigma), 1mM Indomethacin (sigma), 5g/ml insulin (Merk) , 10% FBS, 1% antibiotics) for 24 hours. After that the adipogenically induced cells were further maintained in adipogenic maintenance medium (5mg/ml Insulin (Merk), 10% FBS, 1% for 14 days with medium renewal every 3 days.

Cell-seeded cover slips were then washed thrice with PBS – 10 minute fixed in 3.7% paraformaldehyde and stained with oil red O (sigma, India) . staining, cover slips were mounted with anti-fadent (Dako, Denmark) and micrographed using DM 6000.

## 3.8. Fabrication & characterization of tissue engineered constructs - cHA, cHASi & cSrHA:

Isolated cells were cultured and expanded until $P_3$ passage. Scaffolds pre-conditioned in DMEM LG culture medium for 3-4 hours prior to tissue engineered (TE) constructs. Cells were seeded on the disc shaped scaffolds HA, HASi and SrHA at a density 1x10^4 cells to fabricate cHA, cHASi and respectively and maintained for 4-5 hours with minimum medium to allow maximum adhesion of cells onto scaffold surface. Subsequently, was added to immerse the cell-seeded scaffolds sufficiently and maintained in growth medium under culture conditions of 5% $CO_2$ and 37˚C for further *in* assessments.

### 3.8.1. *In vitro* cytocompatibility assessment:

#### *3.8.1.1. Cell adhesion on scaffolds - E-SEM:*

Tissue engineered constructs - cHA, cHASi and cSrHA cultured for 24 hours, were fixed in 1% glutaraldehyde and subsequently viewed under E-SEM under high vacuum.

### 3.8.2. Osteogenic induction of the TE constructs - cHA, cHASi and cSrHA:

To osteogenically induce the cells seeded on the TE constructs, post 24 of culture in the growth medium TE constructs were maintained in osteogenic induction medium containing $10^{-8}$ M Dexamethasone (dex), 0.05mg/ml L-Acid (LAA) and 10mM β Glycerophosphate (β–GP) for desired culture period.

### 3.8.3. *In vitro* osteogenic efficacy assessment:

#### *3.8.3.1. Cell adhesion on scaffolds – E-SEM:*

Post osteogenic induction (7 days), TE constructs were assessed for cell adhesion using E-SEM as in section 3.8.1.1.

#### *3.8.3.2. Osteogenic efficacy assessment – ALP assay:*

For *in vitro* osteogenic assessment, osteogenically induced TE constructs were evaluated using Alkaline Phosphatase activity (ALP) assay. ALP assay is on the hydrolysis of p-nitro phenyl phosphate (Sigma chemicals, USA) to p-nitro phenol. TE constructs (n=3), were assessed for ALP activity at 7, 14, 21 and 28 days of induction. TE constructs were collected at definite intervals, given PBS wash twice and kept at -80˚C until analysis.

Prior to ALP estimation, frozen cell seeded samples were thawed on ice for 20 min and lysed with 1% Triton X-100 for 50 min. Resultant cell lysate was

collected and 25 µl was taken for ALP assay. 125 µl ALP substrate (prepared using ALP buffer) was added to the lysate and incubated for 30 minutes at 37˚C. Reaction was stopped using 1N NaOH and centrifuged to collect the supernatant. Absorbance was measured at 405 nm using a multifunction plate reader (Hidex calibration line was plotted using different concentrations of p-nitro phenol (Sigma chemicals, India) using the same ALP buffer. ALP activity of TE constructs were expressed as concentration of pNP/30 minutes.

### 3.9. Compatibility of scaffolds using osteoclast pre-cursor cells - $RAW_{264.7}$:

Scaffolds – HA, HASi and SrHA were pre-conditioned in DMEM-LG for hours prior to seeding of the osteoclast pre-cursor cells – $RAW_{264.7}$ - National for Cell Sciences (NCCS, Pune, India). Pre- conditioned scaffolds – HA, HASi SrHA were then seeded with RAW cells at a density of 1x10^5 cells and 24 hours. Cell seeded scaffolds were then fixed in 1 % glutaraldehyde and then micrographed using E-SEM as in section 3.8.1.1.

## PART B - DEVELOPMENT & EVALUATION OF RAT OSTEOPOROTIC MODEL

### 3.10. Development of rat osteoporotic model – surgical procedure:

Osteoporosis was induced in female Wistar rats - Sctb: WI rats (figure 8) (Outbred Wistar rats) aged 3 months and weighing approximately 200 g by interventional bilateral ovariectomy (figure 9). Experiments were performed general anesthesia using 80 mg/kg ketamine (Anket, Neon Lab, and India) and 5 mg/kg xylazine (Xylaxin, Neon Lab, India). Briefly, the area for surgical

intervention was clipped and prepared with 5% Povidone iodine solution Win Media care, India). A longitudinal skin incision was made on the lateral the level of flank. Using a pair of fine tweezers, the peritoneal fat pad was and exteriorized to view the ovary and uterine horn on each side. The vascular to ovary was clamped using mosquito forceps and ovary was excised. After clamping the distal region of the uterine horn, a portion of the uterine horn was excised. Clamps were removed and ascertained that haemostasis was achieved. tissue and fat pad was retracted to the peritoneal cavity using the blunt end of a vascular forceps and skin was closed using 3-0 braided silk (Mersilk, Johnson Johnson, USA) in simple interrupted pattern. Povidone iodine solution was daily for 7 post operative days until the sutures were removed. Post surgery received subcutaneous injection of Analgesic- Meloxicam (Melonex, Indian Immunologicals Ltd, India) @ 1mg/kg S/C once daily and Buprenorphine (Buprigesic, Neon Lab, India) @ 0.05 mg/Kg i/m twice daily for 7 days. Induced animals were maintained for 10 months post induction to develop long term osteoporosis induced aged models (LOA). Animals aged 13 months were the age matched control group (n=5).

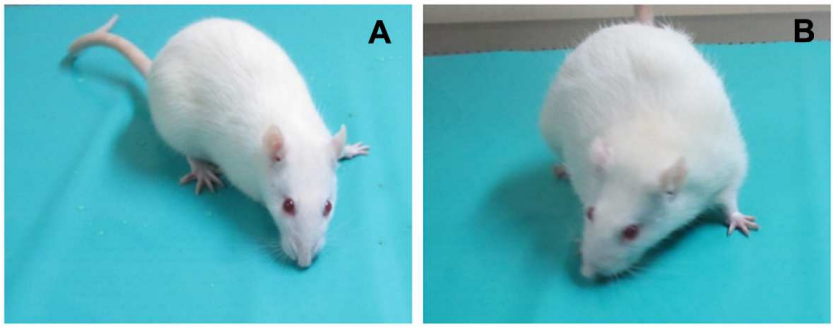


**Figure 8 - Rat model: A-** Control animal and **B-** long term osteoporosis induced aged models (LOA).

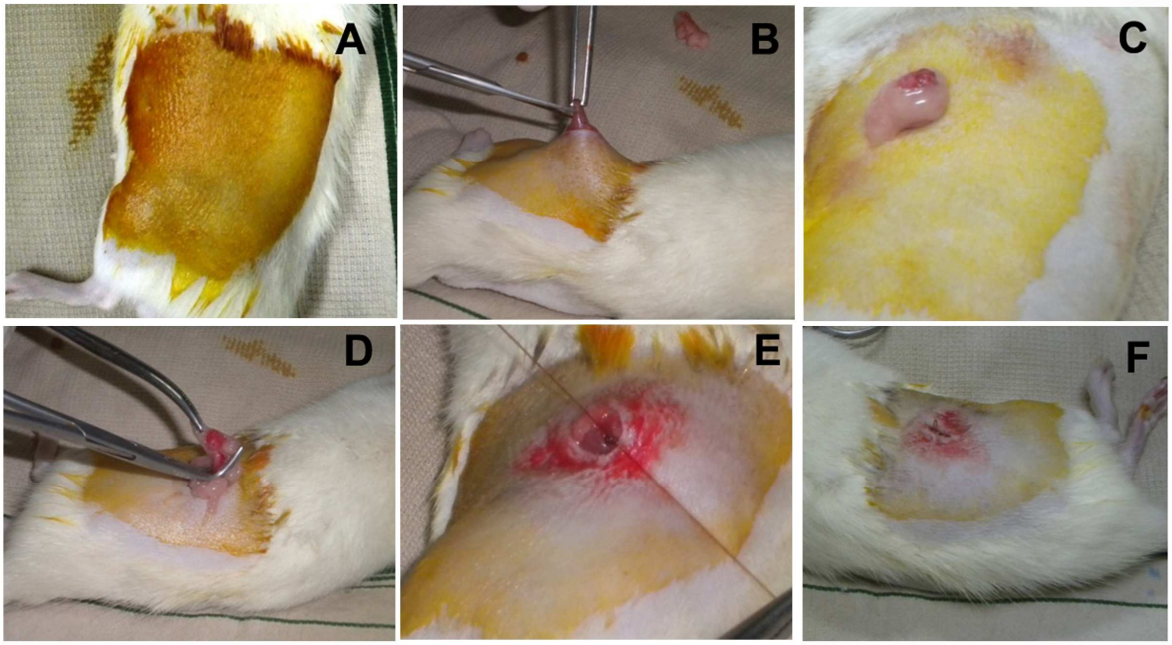


**Figure 9 - Surgical procedure for ovariectomy: A-F -** Osteoporosis induction in rat model.

## 3.11. Rat osteoporotic model evaluation:

### 3.11.1. Histology of excised tissue - H& E staining:

Ovaries collected during ovariectomy procedure were fixed in 10% neutral buffered formalin (NBF) and stored at RT until histological evaluation. For histological evaluation formalin fixed ovaries were dehydrated in ascending series of alcohol - 80% isopropyl alcohol (2 hours), 95%isopropyl alcohol (2 hours), 95% isopropyl alcohol (1 hour), 100% isopropyl alcohol (1 hour – three changes) followed by clearing in xylene (45 minutes – three changes) and infiltrated in paraffin wax (1 hour – two changes followed by 2 hours – one change).

Post processing, tissue capsules were embedded in cassettes into paraffin blocks and thin paraffin sections of approximately 4 micron thickness were taken

using rotary microtome (RM 2255, Leica, Germany). Sections were then transferred to the hot air oven set at 37˚C for one day.

For hematoxylin and eosin (H & E) staining, paraffin sections were first deparaffinised using xylene (15 minutes – 2 times), and then processed in descending series of isopropanol – 100%, 80% and 70% (3 minutes each), exposed to running tap water (5 minutes), stained with Haris Hematoxylin ( sigma chemicals, India) (12 minutes) and washed again in running tap water (5 minutes). Sections were then given two times fast 1% acid alcohol dip followed by incubation in 0.2% ammonia water solution (2 minutes). Sections were counterstained with Eosin (sigma chemicals, India) (5 minutes) and underwent dehydration in ascending series of alcohol – 95% and 100% (2 minutes each); three changes of xylene wash (15 minutes) and mounted using DPX. H & E stained sections were then viewed and micrographed using DM 6000 microscope.

**3.11.2. Evaluation of trabecular bone loss in the induced models:**

***3.11.2.1. Histological evaluation - H & E staining:***

Post 10 months of osteoporotic induction, animals were sacrificed and osteoporotic model development was assessed. Proximal tibial head was from LOA model, age matched control animal and fixed in 10% NBF for analysis. Bone tissues were decalcified using 12% EDTA prior to paraffin embedding. Paraffin sections were then taken from corresponding blocks of and induced group and stained using H& E staining procedure as in section The micrographs were then evaluated for qualitative trabecular bone loss.

***3.11.2.2. Micro CT evaluation:***

Quantitative and qualitative estimation of bone loss in the induced model were assessed using micro-CT desktop scanner CT 40, Scanco Medical AG. Metaphyseal cancellous bone at the tibial head region of the LOA model and animals were scanned using micro CT set at 70kVp and 114µA. Volume of (VOI) (trabecular bone) was chosen by selective contouring of approximately slices of 20µm thickness from the tibial plateau and three dimensional model reconstruction was performed using in built software V6.5. The bone parameters like trabecular number (Tb.N.), trabecular spacing (Tb.Sp.) and density at the trabecular area were assessed in the LOA model (n=5) and with the control group (n=5). Bone volume per total volume (Bv/Tv) was also analyzed within the contoured VOI zone and compared with that of age control rat.

**3.11.3. Biochemical evaluation of serum:**

Blood samples were collected from induced model (n=3) and age control animals at time period 0, 5 and 10 months post osteoporotic induction. was isolated from the animals by centrifugation at 1500 rpm at 37˚C for 10 and stored in freezer until analysis. Isolated serum were then analyzed for concentration based on the Arsenazo III method end point as per protocol (Cat No: BLT0001 Erba, Germany) (1 ml reagent mixed with 20 µl sample and absorbance read at 630 nm against blank). Calcium concentration calculated as

Calcium (mg/dl) = (absorbance of test/absorbance of standard) x concentration standard (mg/dl).

### 3.11.4. Evaluation of bone healing efficacy:

#### *3.11.4.1. Surgical procedure:*

*In vivo* healing efficacy at 3, 6 and 8 weeks (n=6) were assessed by sham defect (figure 10) of 3mm x 1.5mm in the femoral bone of LOA models. Xylazine-Ketamine anaesthesia @ 5mg/Kg& 80mg/kg respectively as in section 3.10, distal femur was exposed through a lateral approach and a defect was with surgical drill (Marathon, Saeyang microtech, Korea).

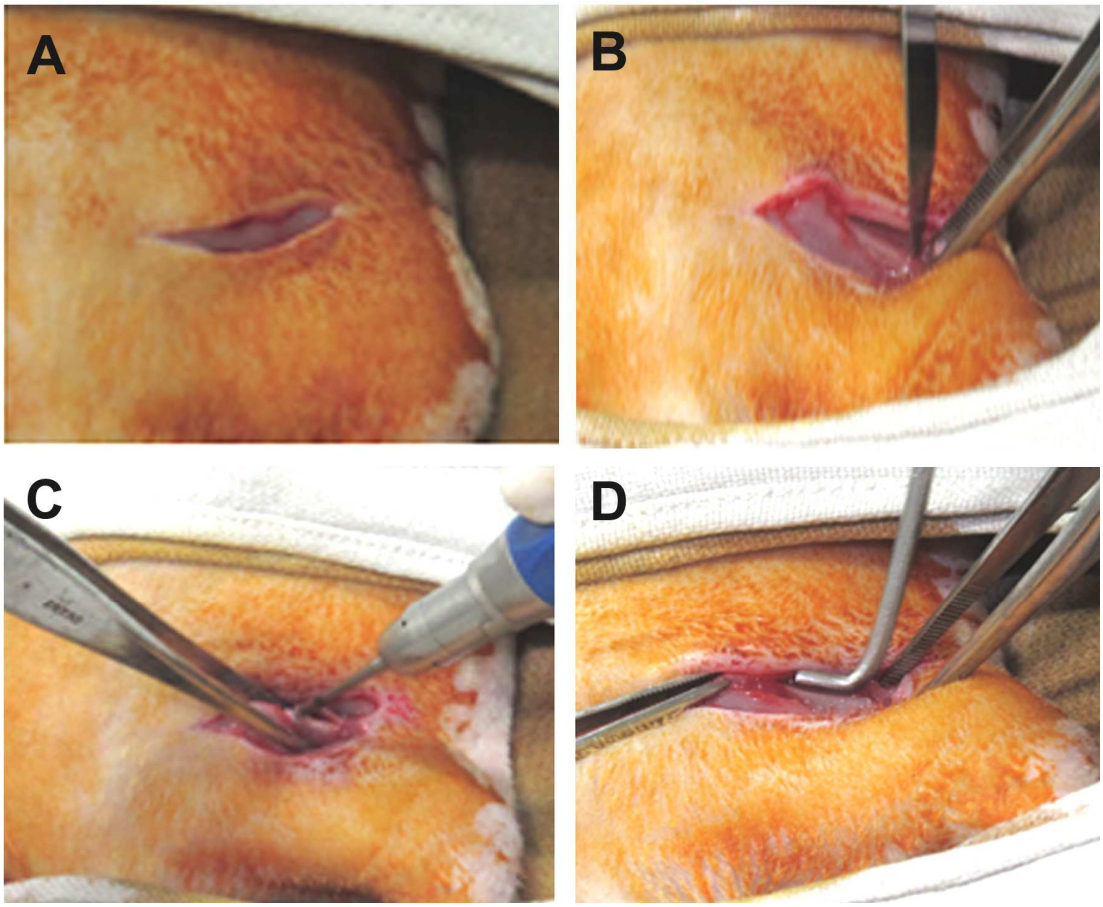


**Figure 10 - Implantation procedure: A-D** Sham defects created in the rat model.

Bone healing ability in LOA model was compared with that of control animals with the same sham defect size in the femur (8 weeks study). Post implantation, all rats received antibiotic and analgesic injection intramuscularly

seven postoperative days. Animals received subcutaneous injection of Analgesic-Meloxicam (Melonex, Indian Immunologicals Ltd, India) @ 1mg/kg S/C once and Buprenorphine (Buprigesic, Neon Lab, India) @ 0.05 mg/Kg i/m twice daily 7 days.

All animals were euthanized at the end of study period -3, 6 and 8 weeks implantation and implant site along with the adjacent host bone was dissected and fixed in 10% NBF. Gross evaluations of retrieved explants were done prior other evaluations.

***3.11.4.2. Micro CT evaluation:***

Effect of osteoporosis on bone healing ability was assessed from the fixed samples of 3, 6 and 8 weeks implantation studies in LOA model. The were scanned using desktop µCT (µCT 40, Scanco Medical AG, Brüttisellen, Switzerland) as in section 3.11.2.2. Scout selection was made including the 'drill hole' defect area in the tibial bone of osteoporotic-induced model and 2D and morphometry images generated from micro CT were assessed for evaluating overall healing efficacy. *In vivo* healing in the LOA models was compared with of control animal post 8 weeks of implantation. Also *de novo* bone (of the host bone and *de novo* bone) was assessed post 8 weeks of implantation the control and LOA models using density histograms generated from corresponding 2 D slices of control and induced group.

***3.11.4.3. Histological evaluation:***

Animals were euthanized eight weeks post surgery and the defect site with the adjacent bone was dissected out without disturbing the defect area. The retrieved bone samples were then formalin fixed and underwent series of

steps in isopropyl alcohol - 70% isopropyl alcohol (4 days), 80% isopropyl (4 days), 95% isopropyl alcohol (4 days), 100% isopropyl alcohol (2 days), alcohol: Acetone (1:1 ratio) (1 day), 100% isopropyl alcohol (2 days). Samples then infiltrated in MMA, followed by embedding in MMA containing 1% peroxide under vacuum in desiccator.

Embedded blocks were then sectioned at a thickness of 130-150 microns, using high-speed precision saw (Isomet TM 2000 Precision Saw, Buehler, USA). Plastic sections were polished down manually to 70–90 microns using variable speed grinder polisher (Ecomet 3000, Buehler, USA) and stained with Stevenal's blue and van Gieson's picrofuchsin (Mohan *et al.*, 2013). Briefly, the staining procedure was followed as – PMMA sections were incubated in hot water (3 minutes), immersed in the pre-heated Stevenal's blue stain (stain filtered and heated to a temperature of 60-65˚C) for (5-15 minutes), given water wash and counter stained with van Gieson's Picrofuchsin (3- 5minutes). Excess stain out with tissue paper and stained sections were then micro-graphed using DM microscope.

## PART C – EFFICACY ASSESSMENT OF MICRO-GRANULAR SCAFFOLDS IN RAT OSTEOPOROTIC MODEL

## 3.12. Fabrication and *in vitro* characterization of micro-granular scaffolds:

### 3.12.1. Fabrication of micro-granular scaffolds:

Micro-granules of HA, HASi and SrHA were generated by manual of the corresponding ceramic blocks as in section 3.2.1., 3.2.2. and 3.2.3.

respectively. Selective sieving ensured the micro-granules to be within the size of 350-400μm.

**3.12.2. Micro-structure and surface morphology evaluation - SEM:**

For evaluating surface morphology, micro-granular scaffolds were gold coated using ion sputter (Hittachi E-1010) and viewed under Scanning Electron Microscope (Hitachi S-2400 – SEM, USA).

**3.12.3. Radiopacity evaluation - Image J analysis:**

Radiopaque property of equal volume (50mg) of micro-granular were evaluated and quantified using image J analysis as in section 3.3.6.

**3.12.4. Cytocompatibility assessment:**

***3.12.4.1. Direct contact assay - phase contrast microscopy:***

Cytocompatibility of the micro-granular scaffolds was assessed by direct contact assay. rBMSCs were seeded at a density of 1x10^4 cells in 48 well plates incubated for culture expansion for 24 hours. Micro-granules (10 mg each) were added on to growing rBMSCs and evaluated using phase contrast microscopy assessing any change in morphology or growth of the cells in direct contact with micro-granules.

***3.12.4.2. Cytotoxicity - MTT assay:***

Cytotoxicity of the micro-granules (10 mg each) was evaluated using test extract method as in section 3.6.

***3.12.4.3. Cell adhesion on the micro-granules - E-SEM:***

Micro-granules (pre-conditioned for 4-5 hours) were seeded with (cHA, cHASi and cSrHA) at a density of 1x10^4 cells and cultured for 7 days in

growth medium. Micro-granular TE constructs were then evaluated for cell using E-SEM as in section 3.8.3.1.

## 3.13. *In vivo* osteogenic efficacy of tissue engineered micro-granules:

### 3.13.1. Surgical procedure for implantation:

For implantation study, 'drill hole' defects - 3mm x 1.5mm dimension made at the proximal end of each femur (figure 11) as in section 3.11.4.1. under general anesthesia distal femur was exposed through a lateral approach 'drill hole defect' was created with surgical drill (Marathon, Saeyang microtech, Korea) under profuse irrigation. Approximately 10mg of the micro-granules tight packed into the defects and muscle flap replaced. In-house developed and designed stainless steel canula with separate piston like holder was used to the micro-granular bare and TE constructs at the implant site. Post rats received antibiotic and analgesic for seven postoperative days. All animals maintained in individually ventilated cages until further analysis.

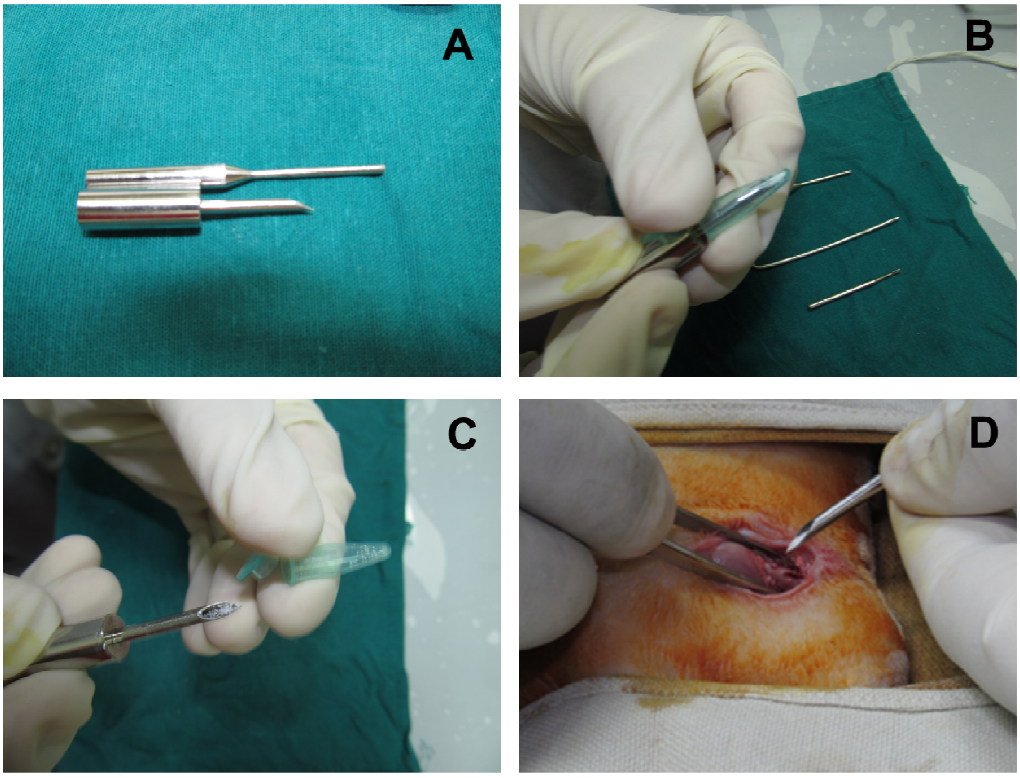


**Figure 11 - Surgical procedure in LOA model: A-D** - implantation of micro-granules in 'drill hole defect' in rat model.

Implantation experiments were designed (table 1) such that four implant sites each were made available for the implant types – HA, HASi, cHASi, SrHA and cSrHA. Sham group was also included.

| **Table : Experimental design in Osteoporosis induced rat model** | | | |
|---|---|---|---|
| **Sham** | **3 W (n=4)** | **6 W (n=4)** | **8 W (n=4)** |
| **HA** | | | **8 W (n=4)** |
| **HASi** | | | **8 W (n=4)** |
| **cHASi** | | | **8 W (n=4)** |
| **SrHA** | | | **8 W (n=4)** |
| **cSrHA** | | | **8 W (n=4)** |

### 3.13.2. Gross evaluation:

All animals were euthanized 8 weeks post implantation and implant site along with the adjacent host bone was dissected out. Femur was removed off any overlaying tissue and fixed in 10% NBF. Gross evaluations of retrieved explants were done prior to any other evaluations.

### 3.13.3. Histological evaluation - Plastic embedding and staining:

For histopathological evaluation formalin fixed explants underwent embedding in methyl methacrylate (MMA) as in section 3.11.4.3. PMMA were then stained using Stevenal's blue and van Gieson's picrofuchsin stain.

### 3.13.4. Histomorphometry analysis - Q win software:

Histomorphometry was done to assess the osteointegrative and ability of micro-granular scaffolds. Histomorphometric analysis was performed three consecutive sections of each implant and analyzed using image analyzing software (Leica Qwin, Germany). Bone formation indices were evaluated defect boundaries alone. Parameters measured included the total implant area area of *de novo* bone in-growth. Regeneration efficiency (RE) of implant was expressed as ratio of new bone formed to total defect area. Measurements taken from equidistant sites across sections under same magnification.

### 3.13.5. Micro CT evaluation:

To assess the extent of mineralization (in-terms of bone density) of the formed bone, explants were scanned using micro CT as described in section Scout selection was made including the 'drill hole' defect area in the tibial bone osteoporotic-induced model. *De novo* bone mineralization was assessed from the density histograms (included host bone and *de novo* bone) generated from 2 D

of control and test group. Mineralization was estimated from the density drawn on corresponding 2D slices.

**3.13.6. Estimation of Strontium accumulation in different organs - ICP:**

Post implantation, organs like kidney, liver and spleen were collected with explants, from the experimental animals to evaluate the accumulation of Sr leached out from the implant at any of these organs, which may be later for the survival of the animal model. Harvested organs (0.5g each) were washed any blood stains and stored at -80˚C until analysis. Ionic concentration of Sr each of the collected organs from the HA implanted group, HASi implanted and SrHA implanted group were analysed using ICP via pre-digestion in sand using pure grade nitric acid. Ion concentrations were calculated as in section

## PHASE III – *IN VITRO* AND *IN VIVO* STUDIES USING sADMSCs IN SHEEP OSTEOPOROTIC MODEL

### ETHICAL STATEMENT:

All *in vitro* and *in vivo* studies using sheep derived cells and sheep animal models were performed as per the guidelines and recommendations of the for the Purpose of Control and Supervision of Experiments on Animals India and with the approval from Institute Animal Ethics Committee (IAEC). – Form no: B462010 XVII. Approval from Institutional Committee for Stem cell Research and Therapy (ICSCRT) was also acquired for the research work - Approval No :– SCT/IC-SCRT/08/Jun 2013. ARRIVE guidelines for *in vivo* experiments in animals has also been followed in the study (Kilkenny *et al.,*

### ANIMAL WELFARE:

Animals were group housed in sheep house under natural conditions following CPCSEA guidelines for Laboratory Animal Facility under. Clinically healthy animals with unremarkable hematological and biochemical parameters selected for the experiment and randomly assigned to control and test arms. animals were fed in-house formulated sheep feed comprising of 30% Crude and 1.14 % of Calcium along with roughages. Water was provided *ad-libitum* to the animals. Ovarectomized animals were fed with commercial calcium sourced from Sai durga feeds; India partially along with in-house formulated feed prior to ovariectomy till implantation and was switched totally to Ca diet once they adjusted to the new feed in a two weeks period after implantation. roughages were fed to these animals.

# PART A - *IN VITRO* EVALUATION OF HA AND SrHA DISC SCAFFOLDS USING sADMSCs

## 3.14. Isolation, culture and characterization of sADMSCs:

### 3.14.1. Isolation and culture of sADMSCs:

Sheep adipose derived MSCs (sADMSCs) were isolated from fat pad of control sheep (figure 12) aged 6 months and weighing around 20- Under general anaesthesia and maintaining aseptic conditions, a skin incision made on the lateral side near the thigh area and approximately 5-10gm of fat was collected in PBS containing 2x antibiotics. MSC isolation was done in sterile condition inside a laminar hood. Briefly, Adipose tissue was thoroughly using 2x and 1x antibiotics (1 ml antibiotics per 100ml PBS), washed fat were fine minced and digested using type 1 collagenase (Sigma Aldrich, St. Louis, followed by centrifugation and the pellet obtained was re-suspended in DMEM complete growth medium. Cells were cultured and sub-cultured at 37˚C, 5% 95% humidity until P3.

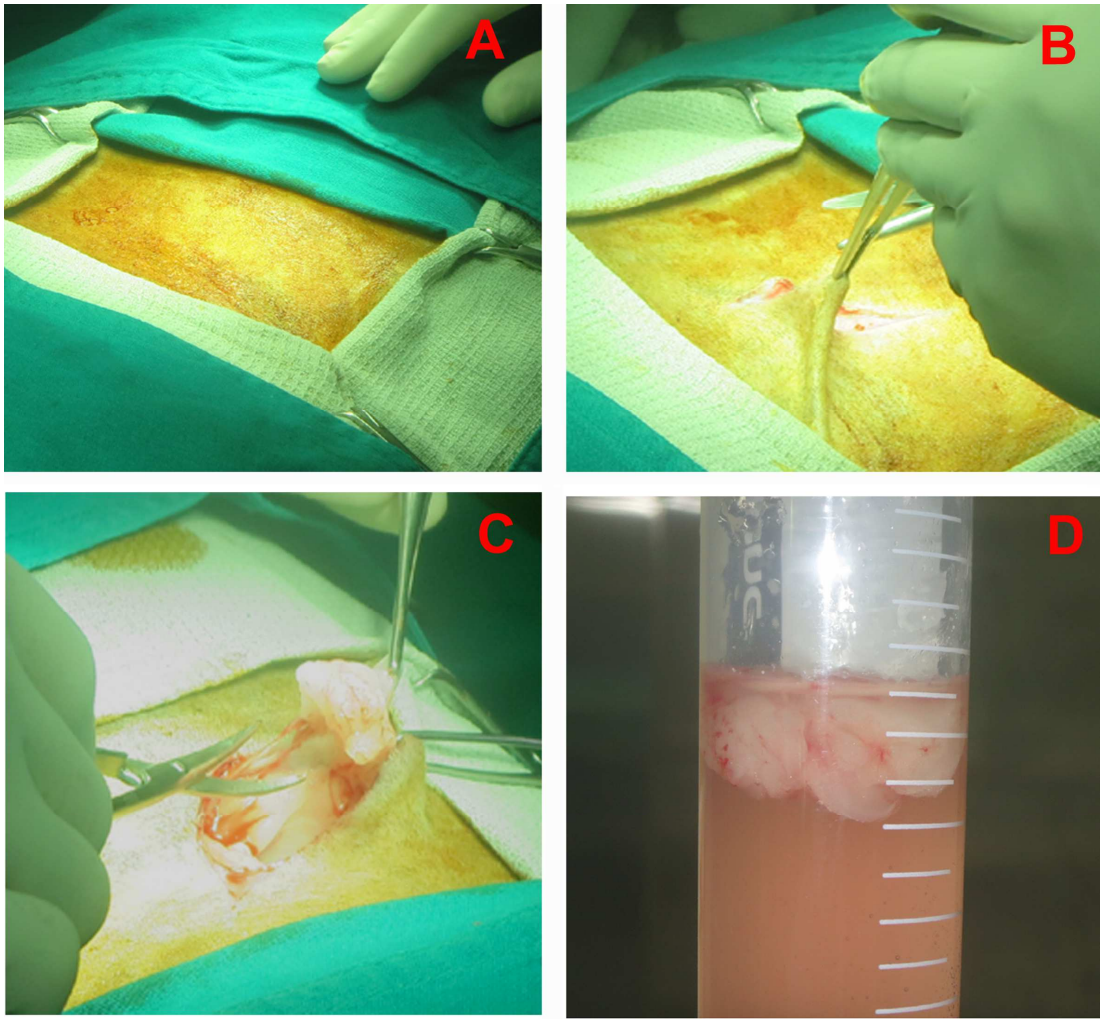


**Figure 12 - Surgical procedure for adipose tissue isolation: A-D -** isolation of subcutaneous adipose tissue from the sheep model.

### 3.14.2. Characterization of sADMSCs:

#### *3.14.2.1. Fluorescent staining – Actin and nuclear staining:*

sADMSCs from $P_3$ passage were seeded on sterile cover slips and maintained for 24 hours as in section 3.7.2.1. Cells were then fixed in 3.7 % paraformaldehyde and then stained using DAPI and rhodamine.

#### *3.14.2.2. Surface marker analysis - Flow cytometry:*

For flow cytometry analysis, cells in $P_3$ passage were trypsinised and underwent the procedure detailed in section 3.7.2.2. To each cell suspension in

antibodies against CD 44 (Abcam) and CD 34 (Abcam) were added at 1:100 Stained cell suspension was then kept for 2 hours in dark at $4^0$C. Cells were then washed with PBS. FITC conjugated secondary antibody in 1:100 dilution each antibody was added into each suspension and further incubated for 1 hour dark at $4^{\circ}$C. Cells stained with secondary antibody alone were used as a control analysis was done as in 3.7.2.2.

Stained cells were then fixed in 3.7% paraformaldehyde for 20 minutes and stored in 4˚C until analysis. Each suspension was analysed using flow cytometer (FACS Aria, BD Biosciences) and fluorescent intensity of each surface marker was quantified by applying suitable gating using Diva software.

***3.14.2.3. Differentiation potential - Alizarin red & Oil red O staining:***

Osteogenic differentiation and Alizarin red staining:

The cells in $P_3$ passage seeded on cover slips underwent osteogenic differentiation as in section 3.7.2.3. Cell-seeded cover slips were then washed with PBS – 10 minutes each, fixed in 3.7% paraformaldehyde and stained with Alizarin red (Sigma Chemicals).

Adipogenic differentiation and oil red O staining:

For adipogenic induction sADMSCs from $P_3$ passage were seeded on slips. They were further maintained in adipogenic induction and differentiation medium as in 3.7.2.3. Oil red O staining was also performed to assess the efficacy.

## 3.15. Fabrication & characterization of tissue engineered constructs - cHA and cSrHA:

Isolated sADMSCs were cultured and expanded to $P_3$ passage. Scaffolds HA and SrHA were pre-conditioned in DMEM LG culture medium as in section and cells were seeded on the disc shaped scaffolds at a density 1x10^4 cells to fabricate cHA and cSrHA respectively. TE constructs were then maintained for hours with minimum medium supplementation to allow maximum adhesion of onto scaffold surface. Later, required volume of medium was supplemented for promoting cell growth. TE constructs were maintained in growth medium in conditions of 5% $CO_2$ and 37˚C for further *in vitro* assessments.

### 3.15.1. *In vitro* cytocompatibility assessment:

#### *3.15.1.1 Direct contact assay-phase contrast microscopy:*

Direct contact assay was done using sADMSCs in direct contact with HA SrHA disc for 48 hours as in section 3.12.4.1

#### *3.15.1.2. Osteogenic induction of the TE constructs - cHA and cSrHA:*

To osteogenically induce the cells seeded on the TE constructs , post 24 of culture in the growth medium, TE constructs were maintained in osteogenic induction medium containing $10^{-8}$ M Dexamethasone (dex), 0.05mg/ml L-Acid (LAA) and 10mM β Glycerophospahte (β –GP) for desired culture periods.

#### *3.15.1.3. Cell adhesion on disc scaffolds – E-SEM:*

Cell adhesion on TE constructs – cHA and cSrHA was evaluated by seeding sADMSCs at a density 1x 10^ 4 cells and maintaining for 7 and 28 days in

osteogenic induction medium. Cell seeded scaffolds were then fixed in 1% glutaraldehyde and processed and further viewed using E-SEM as in section 3.8.1.1.

### 3.15.2. *In vitro* osteogenic efficacy assessment – ALP assay:

For *in vitro* osteogenic assessment, TE constructs were osteogenically induced and evaluated using ALP assay as in section 3.8.3.2.

## PART B - DEVELOPMENT AND EVALUATION OF SHEEP OSTEOPOROTIC MODEL

## 3.16. Development of sheep osteoporotic model - surgical procedure:

Ten mature female (10-12 years old) sheep (figure 13) with an average weight of 25-28 kg were used for the study. Out of the ten animals, only two served as the control, while eight animals were induced for osteoporosis (figure via ovariectomy and calcium deficient diet. Animals were anaesthetized with a combination of Atropine sulphate (@ 0.01mg/kg body weight) - Xylazine (@ 0.3mg/kg body weight) and Ketamine (@ 7mg/kg body weight). Animals were intubated with a size - 9 cuffed endotracheal tube after a bolus of Propofol (@ 3mg/kg body weight) intravenously. Sheep were then ventilated with a tidal of 10-12 ml/kg body weight to maintain an $EtCO_2$ at 30-35 mm of $H_2O$ under 1.8 Isofluorane for maintenance.

Following aseptic precautions, an oblique right flank incision was made, uterus was located and both ovaries were exteriorized, ligated. The ovarian along with the bursa was excised and uterus was replaced into the peritoneal Post surgery, wound was closed routinely. As post operative care, all animals given Strepto-penicillin (Indian Immunologicals Ltd, India) 15mg/kg body

antibiotic and Meloxicam (Indian Immunologicals Ltd, India) 0.5mg/kg as for 7 days. Ovariectomised animals were fed with commercial calcium deficient (Sai Durga feeds & foods company Pvt Ltd., India) and further maintained for months for osteoporosis induction (Lill *et al.*, 2002).

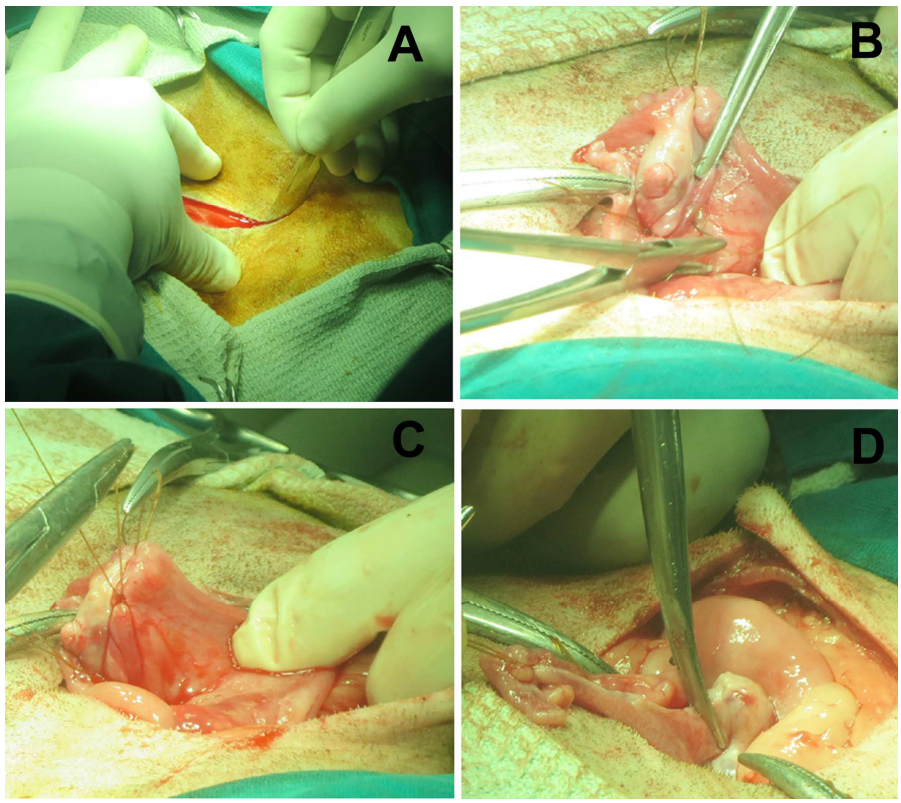


**Figure 13 - Surgical procedure for osteoporosis induction by ovariectomy (A-D) in sheep model.**

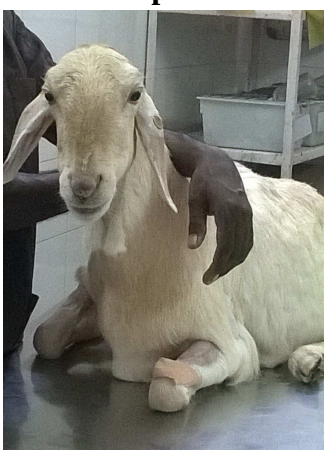

**Figure 14 - Sheep osteoporotic model developed by ovariectomy followed by maintenance under Calcium deficient diet.**

## 3.17. Validation of sheep osteoporotic model:

### 3.17.1. Histology of excised tissue - H& E staining:

Sheep ovary excised during ovariectomy was collected and fixed in 10% neutral buffered formalin for histology analysis using H& E staining as in section 3.11.1.

### 3.17.2. Evaluation of trabecular bone loss in the induced models – micro CT:

Bone loss in the osteoporosis induced models was estimated qualitatively quantitatively using micro CT (Scanco Micro CT 40, Switzerland). Post 10 of osteoporosis induction period, hind limbs were collected by sacrificing the model and same aged control animal. Distal end of tibia was scanned by micro 15µm voxel resolution, using x rays at energy of 70kVp and an intensity of A reference line was drawn at the distal end plate of the tibia so that each had the same starting point for analysis. From the reference line, a cylindrical of the trabecular area from similar anatomical location was selected and the induced model and control animal. Further on 3D morphology (trabecular thickness profile) was reconstructed using in built software. The trabecular parameters - Tb.N., Tb.Th., Tb.Sp. and Bv/Tv were compared with that of the control animal to quantify the extent of bone loss in the osteoporosis induced animals.

### 3.17.3. Biochemical evaluation of serum - Calcium and vitamin D3:

Blood samples were collected from induced osteoporotic model, post 10 months of osteoporosis induction and also from age matched control animals. was isolated from the animals by centrifugation at 1500 rpm at 37˚C for 10 and stored in freezer until analysis. Isolated serum was then analyzed for

concentration as in section 3.11.3. Serum collected was also analyzed for vitamin 3 level estimation using commercially available kit Disorne CLA (Italy).

# PART C - EFFICACY ASSESSMENT IN SHEEP OSTEOPOROTIC MO`DEL

## 3.18. Fabrication and *in vitro* characterization of cylindrical scaffolds:

### 3.18.1. Fabrication of cylindrical scaffolds:

Cylindrical scaffolds (12 mm x 4mm) were developed by manual trimming polishing of ceramic blocks of HA and SrHA as in section 3.2.4.

### 3.18.2. Micro-structure and surface morphology - SEM:

Cylindrical scaffolds were surface characterized using SEM analysis as in section 3.3.1.

### 3.18.3. Radiopacity evaluation - Image J analysis:

Radiopaque property of cylindrical scaffolds – HA and SrHA were and quantified using image J analysis of the radiographs as in section 3.3.6.

### 3.18.4. Fabrication of TE cylindrical constructs and cytocompatibility assessment:

Cylindrical scaffolds HA and SrHA were sterilized and pre-conditioned DMEM-LG growth medium for 4-5 hours. sADMSCs ($P_3$ passage) were then on to the pre-conditioned scaffolds at a density 1 x 10^ 4, to fabricate TE cHA

cSrHA and maintained in osteogenic induction medium for further *in vitro* or *in vivo* implantation studies.

***3.18.4.1. Cell adhesion on the scaffolds – DAPI staining:***

cHA and cSrHA were cultured for 7 days, fixed in 1% glutaraldehyde, processed and stained using the nuclear stain DAPI as in section 3.7.2.1.

***3.18.4.2. Cell viability assessment - Live dead assay:***

Post 7 days of culture of the TE constructs in osteogenic medium, representative scaffolds were assessed for cell viability, prior to implantation. viability on the scaffolds was assessed using live dead assay. Live dead assay was done using Acridine orange (AcrO) (10 µg/ml PBS) (Sigma chemicals) and bromide (EtBr) (15 µg/ml PBS) (Sigma chemicals) staining.

For live dead assay cell seeded scaffolds were cultured in osteogenic induction medium for 7 days and then washed in sterile PBS. TE constructs then incubated for 20 minutes at RT in solution mix containing 1:100 dilution and EtBr such that the scaffold gets fully immersed. Post staining, the scaffolds again washed in PBS (twice – 5 minutes each) and viewed using confocal Laser Scanning Microscope (cLSM) (Carl Zeiss LSM Meta) at an excitation and wavelength of 480nm / 526nm and 518nm / 605nm for AcrO and EtBr

## 3.19. *In vivo* osteogenic efficacy of tissue engineered cylindrical implants:

### 3.19. 1. Surgical procedure for bone implantation in sheep model:

Implantation (figure 15) was done in 10 months osteoporosis induced (n=4) to assess the osteogenic efficacy of HA, cHA, SrHA and cSrHA implants. Animals were anaesthetized with Atropine- Xylazine – Ketamine combination ventilated as in section 3.16. Following all aseptic precautions, a linear incision made on the distal one third of the lateral thigh to expose junction of tensor lata and biceps femoris muscle. The muscles were separated to expose the distal femur. Periosteum was elevated and the site was cleared for a 12mm X 4mm (Pearce *et al.,* 2007) created with 2mm drill bit using a micro-motor (Marathon, Saeyang microtech, Korea). A press fit method has been adopted for the implantation of cylindrical constructs and the defect area was approached as surgical procedure detailed by Nuss *et al.,* 2006. Muscles were then apposed and incision was closed routinely. Animals were under daily observation and given intramuscular injections of antibiotics (ceftriaxone) and anti inflammatory (Meloxicam) for 5 days postoperatively. Sutures were removed on seventh post operative day.

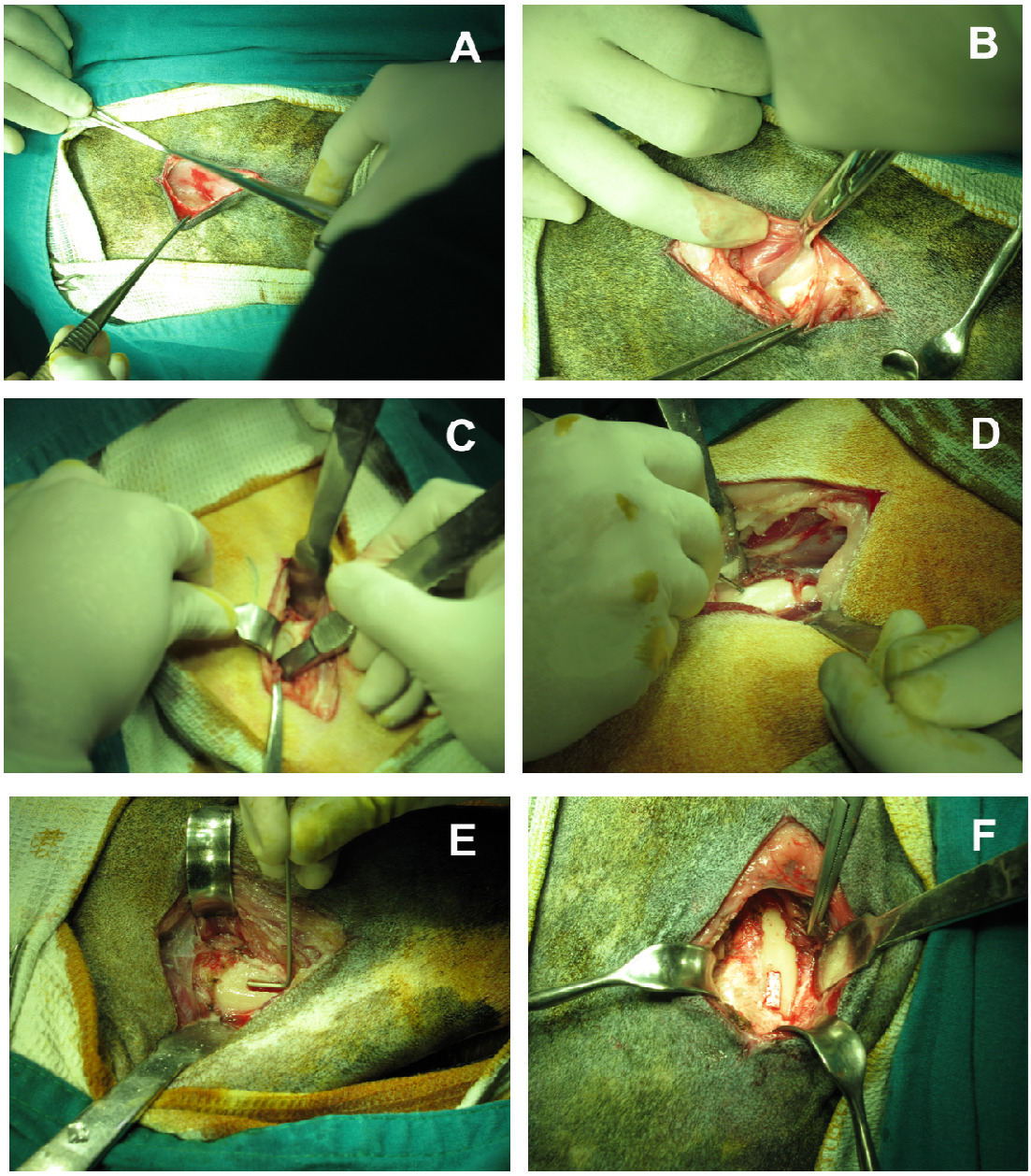


**Figure 15 - Surgical procedure - implantation of cylindrical implants: (A-F)-** Press fit method adopted in the osteoporosis induced sheep model.

Two implant sites were made (one defect per leg) in each animal, so as to provide for duplicate samples for each implant type.

| **Table 2: Experimental design in Osteoporosis induced sheep model. (2 defects per animal)** | |
|---|---|
| **HA** | **2 M (n=2)** |
| **cHA** | **2 M (n=2)** |
| **SrHA** | **2M (n-2)** |
| **cSrHA** | **2 M (n=2)** |

### 3.19.2. Serum analysis for inflammatory responses post implantation:

Blood was collected from the animals post zero day, one week, two weeks and two months of implantation to assess any inflammatory reactions associated the implanted scaffolds. Serum collected from blood samples by centrifugation 1500 rpm for 10 minutes and routine biochemical analysis was done using haematology analyser (Nihon Kohden) to assess the count of White Blood cells (WBC), Neutrophils, Lymphocytes and Eosinophils. The counts obtained from serum samples of experimental animals were compared with that of the values in healthy adult animals (table 3).

**Table 3**: **Reference range of serum parameters in normal sheep**

| | normal value |
|---|---|
| WBC - | 8 - 13 |
| Neut% - | 22-40 |
| Lymp% - | 50 -75 |
| Eos% | 1-8 |

### 3.19.3. Radiopacity of the implants *in vivo* - image J analysis:

Two months post explantation, bone samples were retrieved from the models without disturbing the implant area. Explants containing cHA and were radiographed at standard conditions using X ray film unit and imaging CR -30X (AGFA, USA) as in section 3.3.6. For estimating the radiopaque of the two months explanted sample, Image J analysis was further done on the radiographs.

### 3.19.4. Post implantation evaluation:

#### *3.19.4.1. Gross evaluation:*

All animals were euthanized by excess dose of anesthetics - Thiopentone (100mg/kg), Pancuronium Bromide (0.08mg/kg) and 35 ml of 7.5% w/v of Potassium chloride intravenously, post 2 months of implantation. Implant site with the adjacent host bone was dissected out. Femur was removed off any overlaying tissue and fixed in 10% NBF. Healing was uneventful and there was neither inflammation nor infection at the surgical site before humane killing of animals post 2 months implantation.

### *3.19.4.2. Radiographic evaluation:*

Radiographs taken as in section 3.19.3 at 0 day, 1 month and 2 months implantation were further assessed in detail to understand the osteointegrative of the implants – HA, cHA, SrHA and cSrHA based on the presence or absence radiolucent zones around the implant at the bone-implant interphase.

### *3.19.4.3. Histological evaluation:*

Retrieved bone explants were fixed in 10% NBF and embedded in methacrylate (MMA) as in section 3.11.4.3. PMMA sections were also stained Stevenal's blue and van Gieson's picrofuchsin stain. Histology images of 5x magnification were stitched together using in built software in DM 6000 so as to include the entire bone defect area as ROI and different bone could be assessed in detail. Evaluation of the complete defect area may enable a better understanding on bone regeneration on par with material resorption *in*

### *3.19.4.4. Histomorphometry:*

Blinded histomorphometric analysis was performed using image J software (Version 1.48v) by applying selective threshold to generate masked to specifically identify and quantify the new bone (NB), material remnants (MR) within in the entire defect area (TA) as reported by Egan *et al.,* 2012. efficiency (RE) was calculated based on the ratio of new bone formed per total defect area (NB/TA) and the ratio of material remnant present per total bone area (MR/TA). Degradation rate was estimated as (1- MR/TA)*100. Higher magnification images (20X) were further evaluated to assess the structural

organisation of the osteoid matrix within the *de novo* bone across different groups.

***3.19.4.5. Micro CT evaluation:***

Retrieved explants were scanned using micro CT desktop scanner. For evaluating the bone regeneration efficiency, ROI was chosen in such a manner that the scout selection was made comprising of the entire implant area (12 - 15mm long) in the sheep bone. Using in-built software, 2D slices were generated and analysed. Density histograms generated from respective 2D slices of HA, SrHA and cSrHA bone implants were assessed to evaluate the extent of mineralization in the *de novo* bone (in terms of bone density) at the bone implant interphase.

## 3.20. Statistical evaluations:

Results were analyzed and data's were expressed as mean ± standard deviation (SD). Statistical analyses and graphical representation was plotted Microsoft excel or using Graph pad prism (Version 6.01). p-value $< 0.05$ was considered statistically significant in all analysis.

*In vitro* osteogenic efficacy of HA, HASi and SrHA scaffolds with rBMSCs was evaluated by multiple comparison (Dunnet's test) using 2way analyses of (ANOVA). Significance of the data generated from micro CT for rat model evaluation was assessed using unpaired T test. For biochemical analyses serum calcium concentration 2 way ANOVA (with multiple comparisons) was Unpaired T test (two tailed) was performed to analyse the results of cytotoxicity assay using HA, HASi and SrHA micro-granules and L929 cells. One-way

were performed for evaluating the histomorphometry data obtained from the *vivo* studies. Multiple comparisons with Bonferronis's correction were applied assessing the statistical significance of the histomorphometry data. *In vitro* osteogenic efficacy of HA and SrHA scaffolds with sADMSCs was evaluated by multiple comparison (Dunnet's test) using 2way ANOVA. For analysis of the data obtained from the *in vivo* studies in sheep, multiple were done using 2-way ANOVA with Tukey test correction.

# RESULTS

The results of the present study are illustrated in this section. Findings of study are divided into three chapters - Chapter 4, chapter 5 and chapter 6.

CHAPTER 4 - **PHASE I - MATERIAL CHARACTERIZATONS**

CHAPTER 5 - **PHASE II– *IN VITRO* & *IN VIVO* STUDIES USING rBMSCs RAT OSTEOPOROTIC MODEL**

CHATER 6 - **PHASE III – *IN VITRO* AND *IN VIVO* STUDIES USING sADMSCs IN SHEEP OSTEOPOROTIC MODEL.**

# CHAPTER 4

## RESULTS – PHASE I - MATERIAL CHARACTERIZATIONS

## 4.1. Physicochemical characterizations of HA, HASi and SrHA:

### 4.1.1. Microstructure evaluation:

Scanning electron micrographs depicted that the scaffolds had a rough surface topography with interconnected pores. HA and HASi appeared to be porous compared to SrHA scaffolds (figure 16A-16C). Higher magnified micrographs (figure 16D-16F) revealed the amorphous nature of HASi and scaffolds in which the crystal boarders could not be recognized. But HA exhibited cubical crystals of almost uniform size with distinct borders.

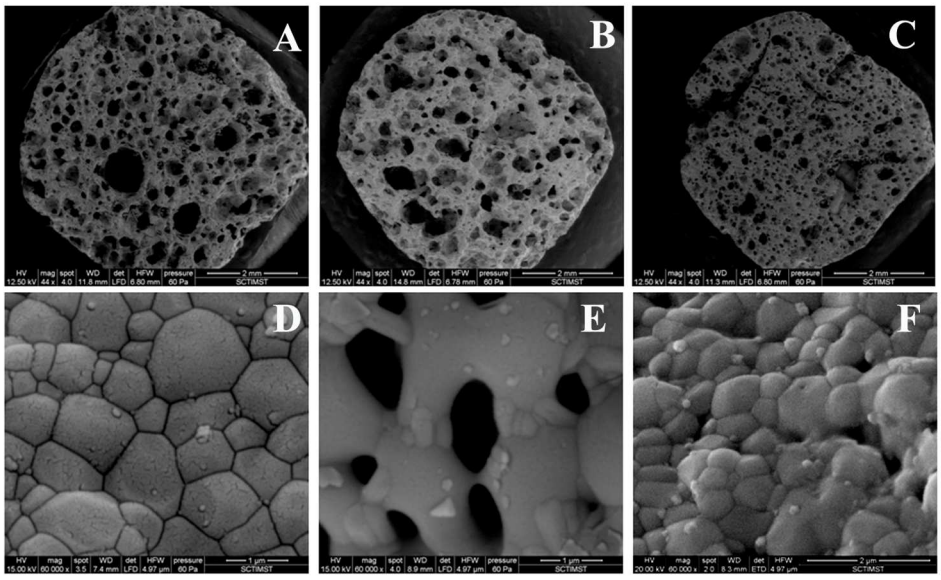


**Figure 16 - Surface characterization of the scaffold materials:** Rough and nature of HA, HASi and SrHA scaffolds evident in **A, B & C** respectively. magnification images (**D-F)** depicted the crystal boundary in HA, HASi and scaffolds (**A- C**: scale bar = 2mm; **D-F**: scale bar = 10µm).

### 4.1.2. Pore size & porosity estimation:

Micro CT studies evaluated the average pore size and overall porosity distribution in each scaffold. It was evident from the pore size distribution that HA scaffolds (figure 17 A) had the highest pore size range of 144-288 µm, whereas HASi (figure 17 B) and SrHA (figure 17 C) exhibited a pore size range 140-220 µm and 80-100 µm respectively.

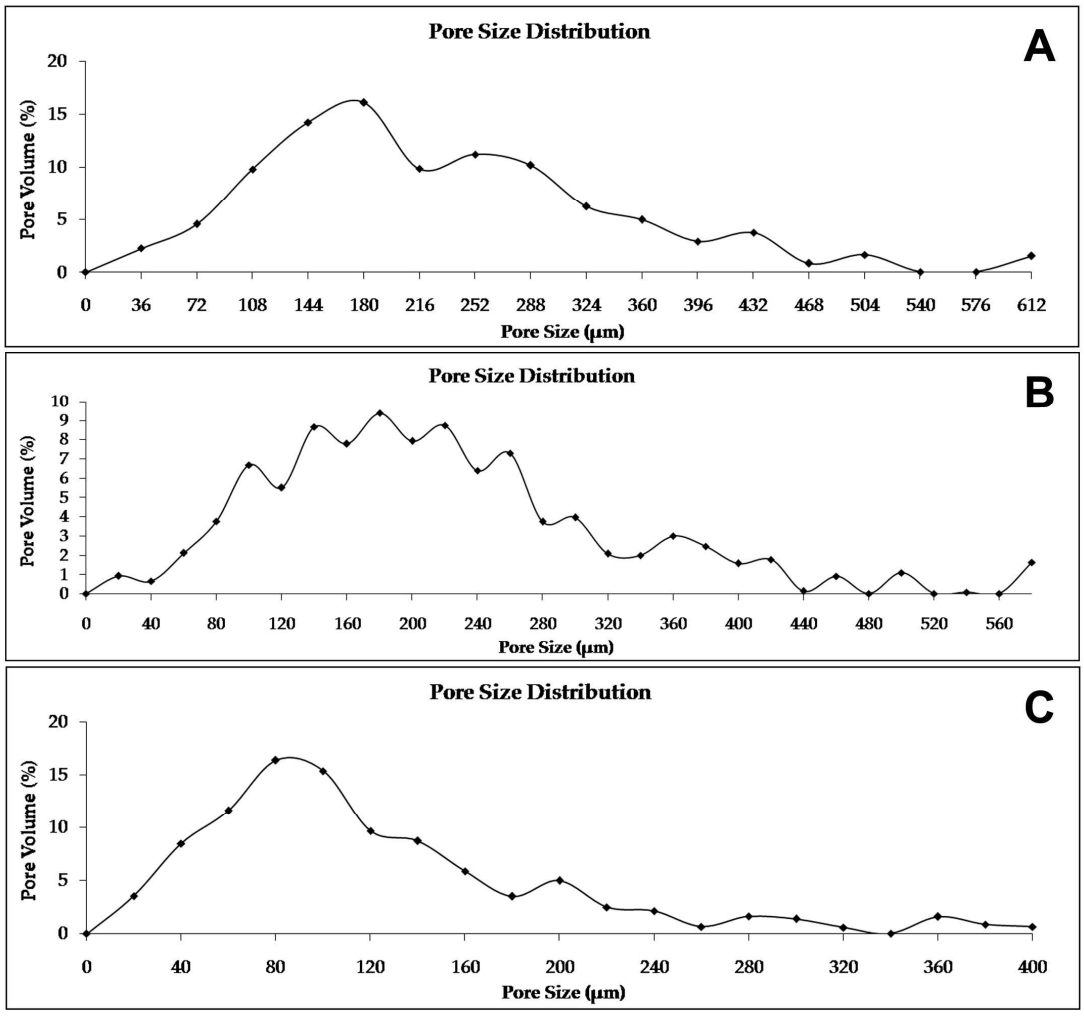


**Figure 17 - Pore size distribution graph of the scaffolds:** Micro CT generated size distribution graphs of HA, HASi and SrHA depicted in **A, B** and **C**

Percentage porosity calculated on the basis of Bv/Tv value indicated that HASi had the highest porosity of 37.05%, compared to HA and SrHA scaffolds 30.4% and 20.1% respectively (table 4).

**Table 4: Percentage porosity of the scaffolds – HA, HASi and SrHA.**

| Scaffolds | BV/TV | % porosity |
|---|---|---|
| **HA** | **0.696** | **30.4** |
| **HASi** | **0.6295** | **37.05** |
| **SrHA** | **0.799** | **20.1** |

**4.1.3. Phase analysis:**

XRD pattern of HA (figure 18) exhibited well defined and adequate around 2θ values of $25.9^0$, $31.8^0$ & $32.9^0$ which matched with the JCPDS Pattern PDF No. 09-0432. The presence of single crystalline phase in HA was also Whereas the XRD pattern of HASi (fig 19) matched to the JCPDS pattern PDF No. 09-0432, PDF No. 09-0348, PDF No. 09-0547 indicating the presence of apatite phase, calcium phosphate phase and wollastanite phase and confirmed triphasic nature. SrHA peak pattern (fig 20) corresponded to JCPDS pattern – No. 34-0484. Peaks at around 2θ values of $25.7^0$, $31.6^0$ & $32.8^0$ exhibited a similar pattern to that of XRD pattern of HA; indicating that Strontium incorporation did not induce any phase change in SrHA. Presence of sharper peaks in HA its crystalline nature compared to other scaffolds.

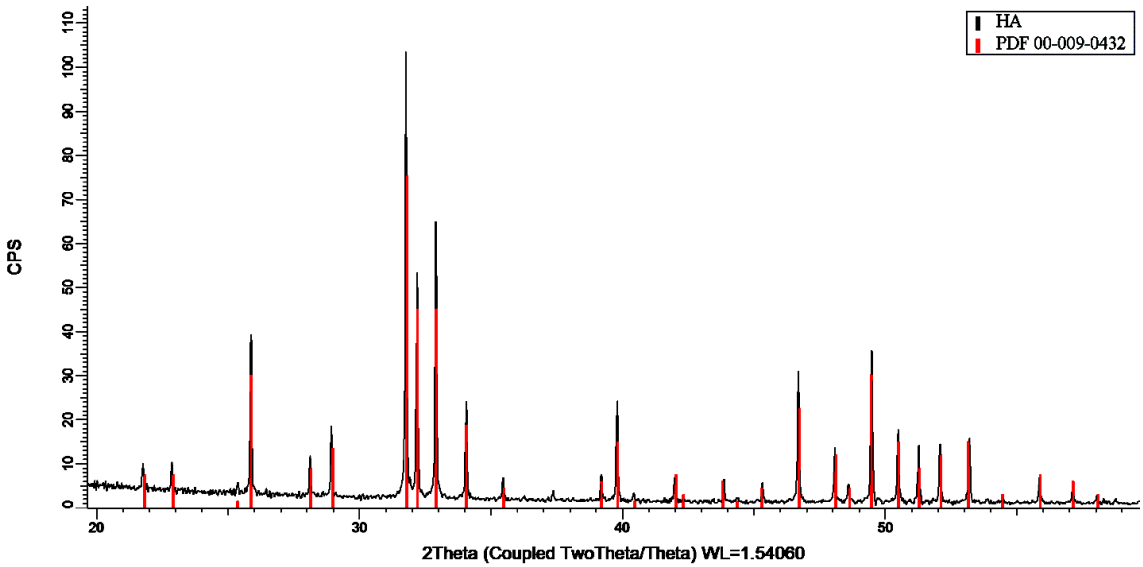


**Figure 18 - X-ray diffraction pattern of HA:** Peak of HA represented in black the matching JCPDS pattern no – PDF 00-009-0432 represented in red.

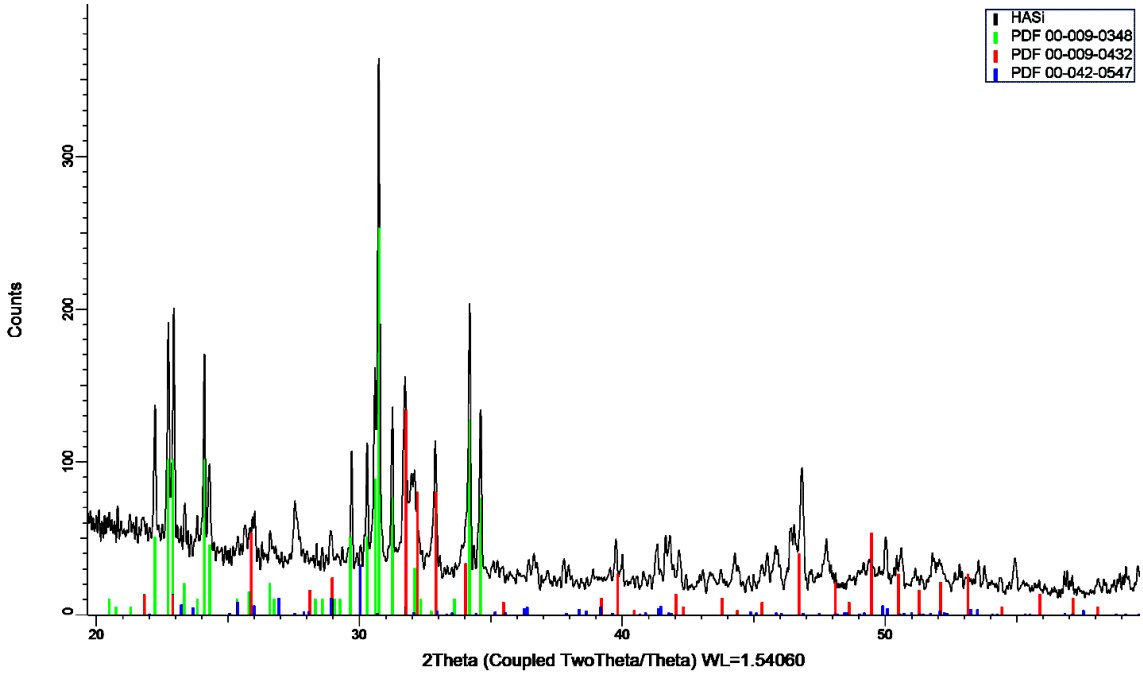


**Figure 19 - X-ray diffraction pattern of HASi:** Peak of HASi represented in and the matching JCPDS pattern no – PDF 00-009-0348, PDF 00-009-0432 and 00-042-0547 represented in green, red and blue respectively.

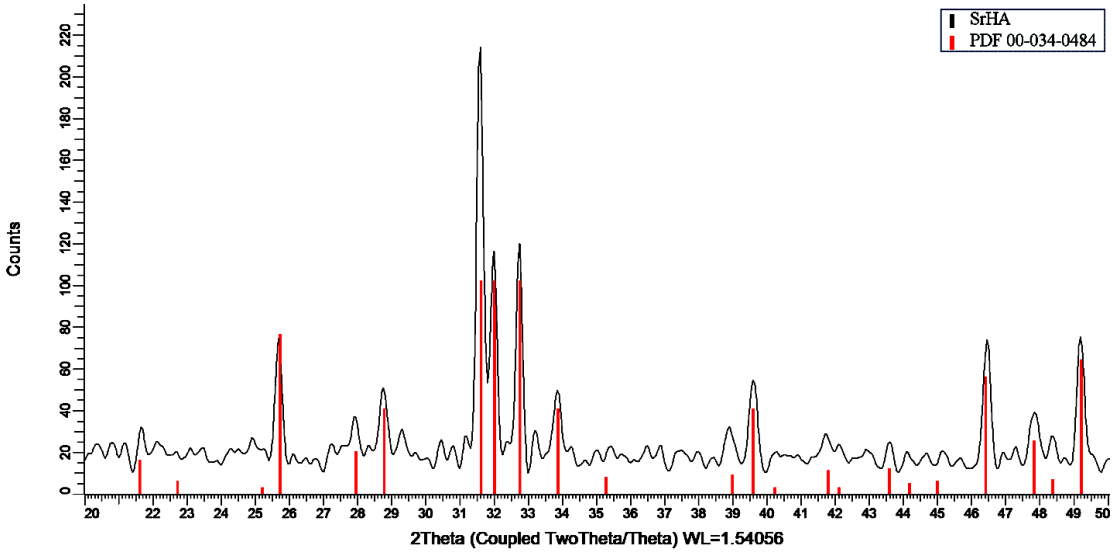


**Figure 20 - X-ray diffraction pattern of SrHA:** Peak of SrHA represented in and the matching JCPDS pattern no – PDF 00-034-0484 represented in red.

### 4.1.4. Functional group analysis:

The FTIR spectra exhibited the characteristic absorption bands to functional groups present in each scaffold. Characteristic HA bands were appreciated between wave numbers 3500 and 500. FTIR spectrum of HA (figure represented a typical structure containing sharp $PO_4$ stretching bands at 1200 - $cm^{-1}$ region and bending band at 650 -450 $cm^{-1}$. Presence of carbonate peak was identified at 1985 $cm^{-1}$ and hydroxyl group at 3569 $cm^{-1}$ and at 631 $cm^{-1}$. In additional peak at 436/424 $cm^{-1}$ corresponded to silicate group confirming Silica coating on HA (figure 22). Compared to FTIR spectrum of HA the OH bands at $cm^{-1}$ and 3569 $cm^{-1}$ disappeared gradually in SrHA (figure 23), while the bands remained as such.

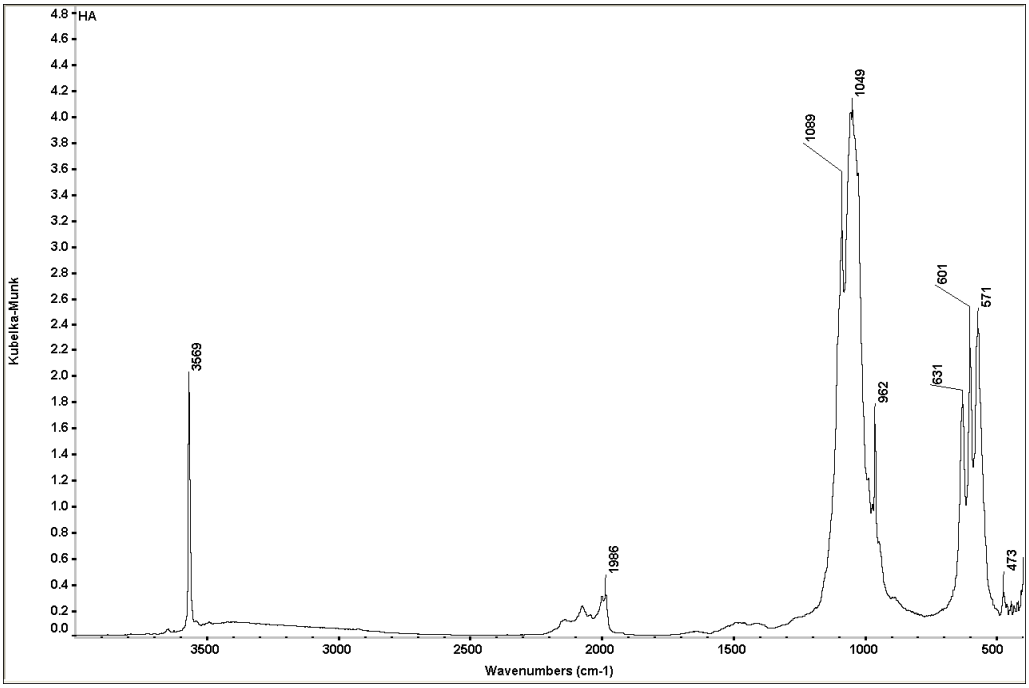


**Figure 21- Fourier Transform Infrared Spectrum of HA.**

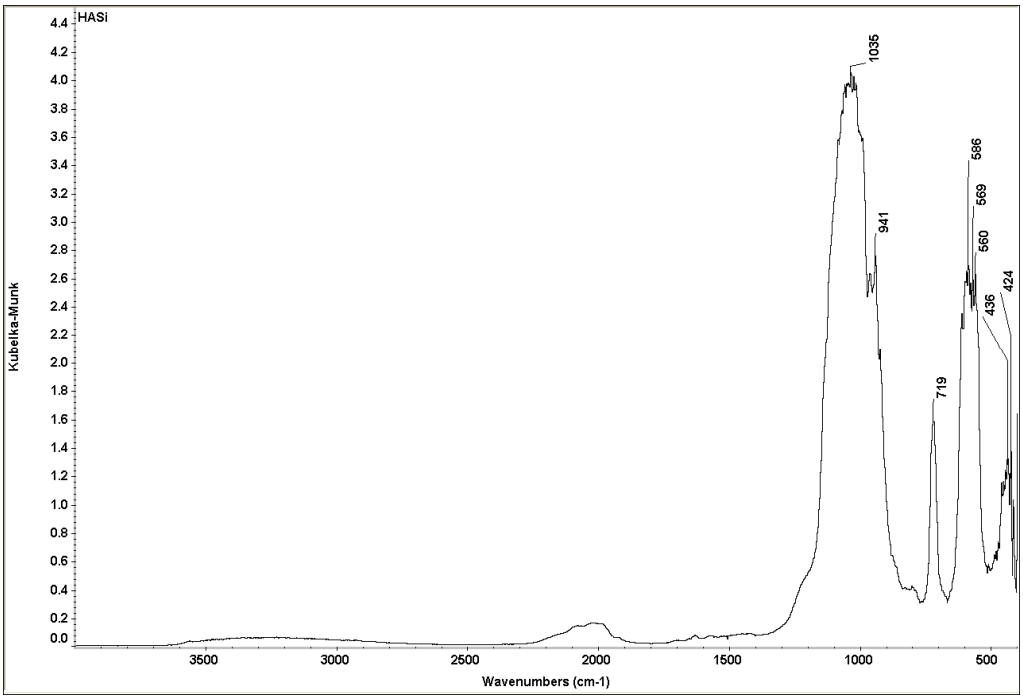


**Figure 22 - Fourier Transform Infrared Spectrum of HASi.**

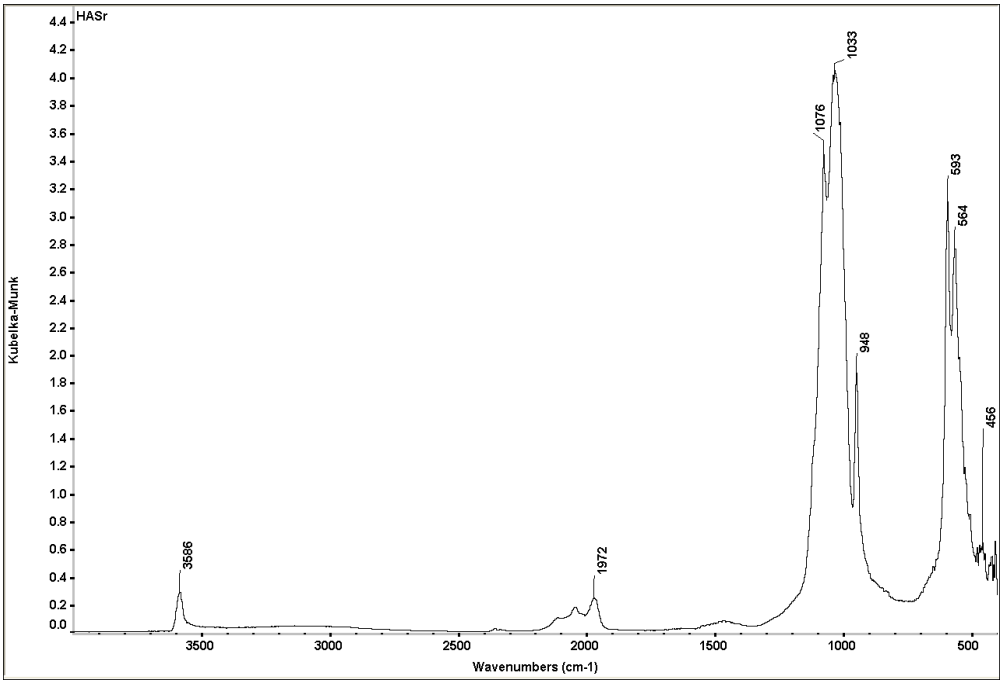


**Figure 23 - Fourier Transform Infrared Spectrum of SrHA.**

### 4.1.5. Density estimation:

Mean density of the scaffolds were evaluated using micro CT (figure 24) indicated that SrHA exhibited the highest density of 2439.91 mg HA/ccm, HA and HASi exhibited a lower density of 1744.71 mg HA/ccm and 1693.74 mg HA/ccm respectively.

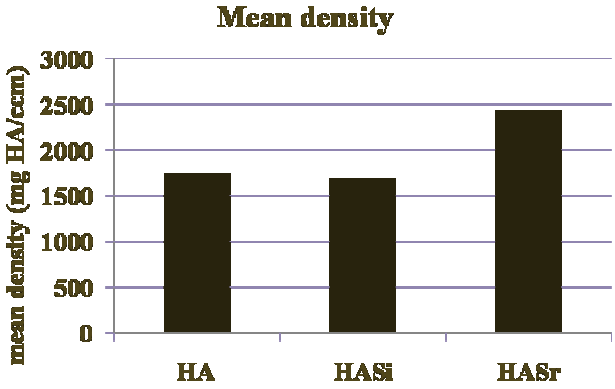


**Figure 24 - Mean density of the scaffolds:** Micro CT evaluation depicted the comparative density of HA, HASi and SrHA in terms of mg HA/ccm.

### 4.1.6. Radiopacity evaluation:

Radiopaque property of the scaffolds was evaluated using radiography 25) and quantified using Image J analysis software. It was estimated from the radiographs, that SrHA exhibited an improved radiopacity equivalent to thick aluminium, whereas HA and HASi exhibited radiopacity equivalent to and 0.52mm thick aluminium respectively (table 5).

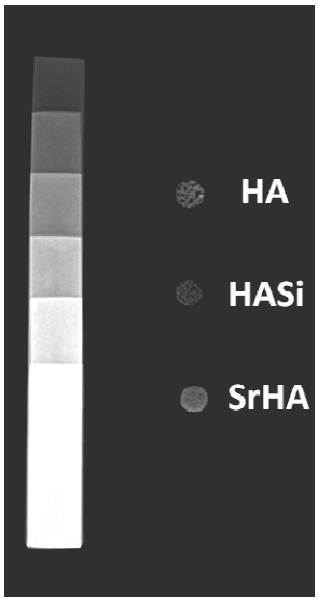


**Figure 25 - Radiopacity evaluation of the scaffolds:** Radiograph of HA, HASi SrHA scaffolds in comparison to aluminium wedge.

**Table 5: Radiopacity of the scaffolds compared to aluminium wedge.**

| | **HA** | **HASi** | **SrHA** |
|---|---|---|---|
| **Radiopacity (equivalent to aluminium thickness in mm)** | **0.80** | **0.52** | **0.99** |

## 4.2. Assessment of *in vitro* degradation ability in PBS:

*In vitro* degradation studies in PBS helped in the evaluation of ions from the scaffolds so as to predict the resorptive property of HA, HASi and scaffolds.

### 4.2.1. Calcium ion release profile:

ICP studies indicated that after an initial burst almost a steady release of $Ca^{2+}$ (figure 26) at the rate of approximately 0.009 µg/mg was exhibited by scaffolds. Highest release of 0.14 µg/mg was exhibited by HASi scaffolds, of its rapid degradation ability, which is in concurrent with the XRD data the study. SrHA seemed to have improved degradation ability (0.04 µg/mg) compared to HA scaffolds.

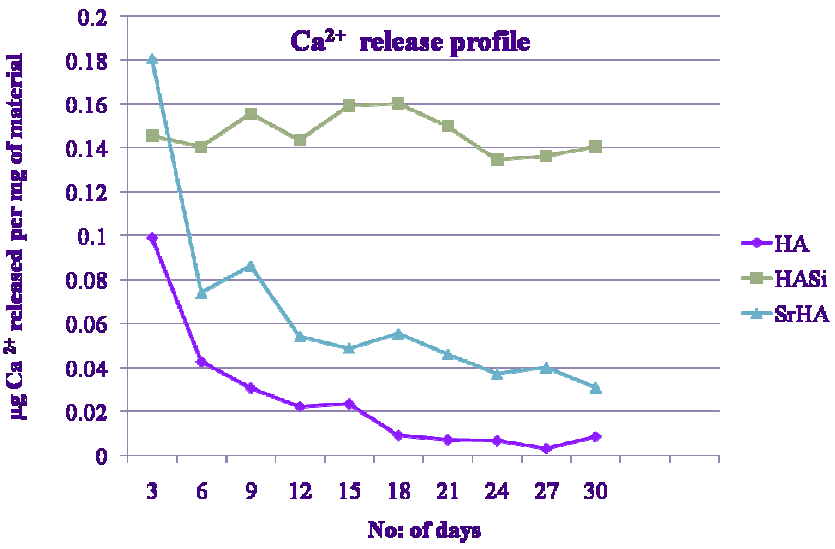


**Figure 26 - Calcium release profile in PBS:** ICP analysis indicated the highest release from HASi scaffolds compared to HA and SrHA scaffolds.

### 4.2.2. Phosphorus release profile:

Release of Phosphorus ions (figure 27) exhibited almost a steady pattern 1.1 to 1.5 µg per mg of the material in all the scaffolds. Even though HA exhibited a comparatively higher release, no significant difference was found in release pattern across the scaffolds.

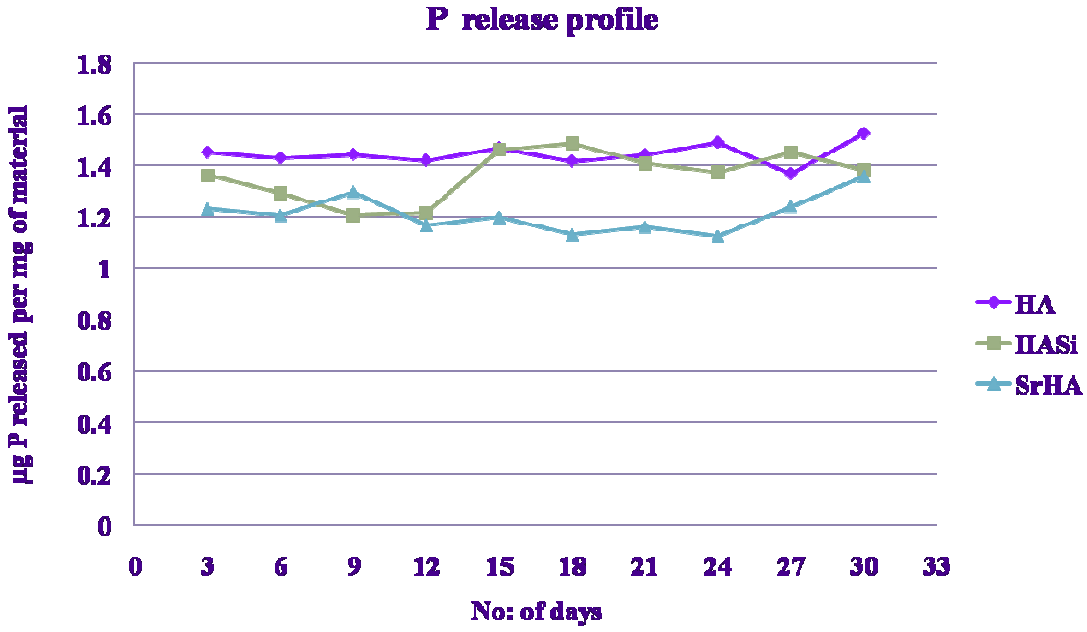


**Figure 27 - Phosphorous release profile in PBS:** ICP analysis indicated almost a uniform release pattern from the scaffolds HA, HASi and SrHA.

### 4.2.3. Silicon release profile:

Silicon release profile (figure 28) indicated a uniform release pattern HASi scaffolds. With the advancement in the incubation period there was a increase in the concentration of Silica released. On day 3 a release of 0.03 µg per was noted. Further on, Si release rate seemed to increase until 18$^{th}$ day, after steady release of 0.10 µg per mg was exhibited till the 27$^{th}$ day of analysis

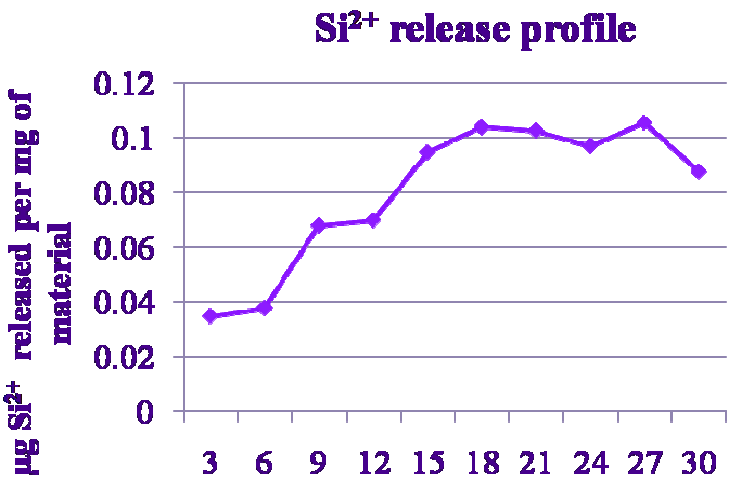


**Figure 28 - Silicon release profile in PBS:** ICP analysis indicated the Si release exhibit a steady increase until 18th day.

**4.2.4. Strontium release profile:**

The release of strontium ions (figure 29) from 10% SrHA needs to be in therapeutic range to enable its application in osteoporotic bone defect healing. studies implied that after an initial burst, a uniform release of 0.01 µg per mg of material could be attained post 12 days of incubation in PBS and further on a uniform release pattern was exhibited by the SrHA scaffolds.

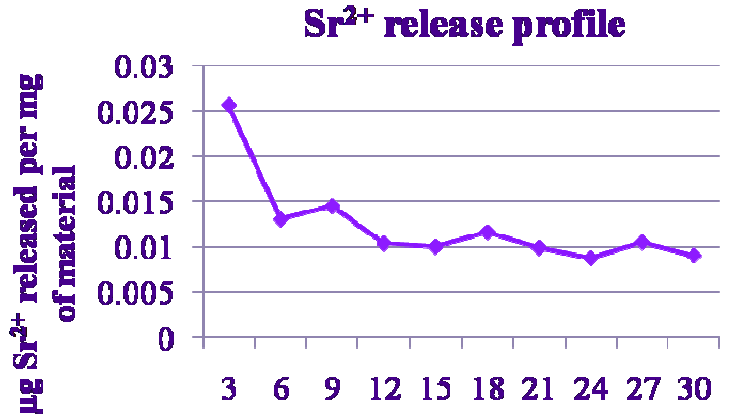


**Figure 29 - Strontium release profile in PBS:** ICP analysis indicated a steady release of Sr from the SrHA scaffolds on day 6 onwards.

## 4.3. Evaluation of *in vitro* apatite formation ability in SBF:

The *in vitro* bioactivity of the scaffolds was assessed by investigating the apatite formation ability post incubation in SBF for 30 days.

### 4.3.1. Assessment of apatite formed using E-SEM:

Apatite formation of the scaffolds across 0, 7, 14 and 21 days were using E-SEM (figure 30 and figure 31). On day 7, apatite formation ability was exhibited by HA, HASi and SrHA scaffolds. But it was interesting to observe 14$^{th}$ day and 21$^{st}$ day HASi and SrHA exhibited better apatite formation ability, compared to HA. E-SEM studies indicated that all the scaffolds supported formation when incubated in SBF. The layers consisted of inter-grown nodules formed by small entangled apatite crystals.

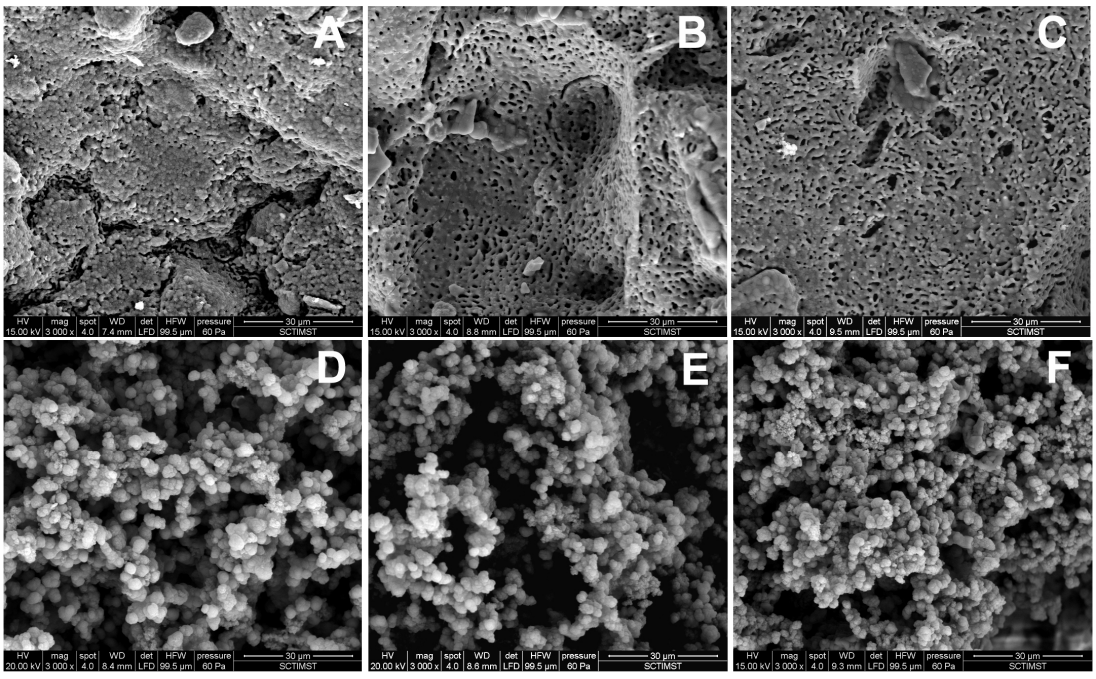


**Figure 30 - Apatite formation ability of the scaffolds (0, 7):** E-SEM images the nodular structures formed on the scaffolds HA **(A, D)**, HASi **(B, E**) and **(C, F)** post incubation in SBF for 0 and 7 days respectively (scale bar = 30µm).

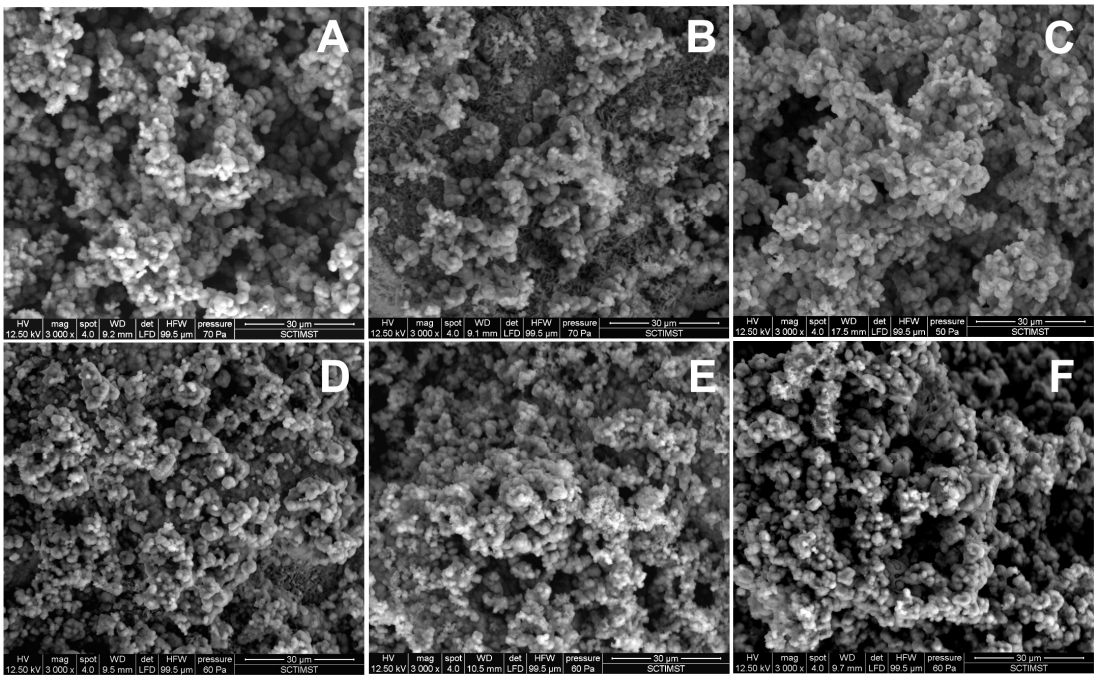


**Figure 31 - Apatite formation ability of the scaffolds (14, 21):** E-SEM images depict the nodular structures formed on the scaffolds HA **(A, D)**, HASi **(B, E**) and SrHA **(C, F)** post incubation in SBF for 14 and 21 days (scale bar = 30µm).

**4.3.2. FTIR analysis of apatite formed on scaffolds:**

To further assess the apatite formation ability of scaffolds, scaffolds incubated for 28 days in SBF were evaluated using FTIR (figure 32). FTIR of SrHA scaffolds indicated that a prominent carbonate peak at 1459 $cm^{-1}$ and a broad hydroxyl group at 3355 $cm^{-1}$. HASi scaffolds also exhibited a similar spectrum, but less prominent carbonate peak at 1419 $cm^{-1}$. In FTIR spectrum scaffolds hydroxyl group at 3571 $cm^{-1}$ was more prominent compared to group at 1459 $cm^{-1}$.

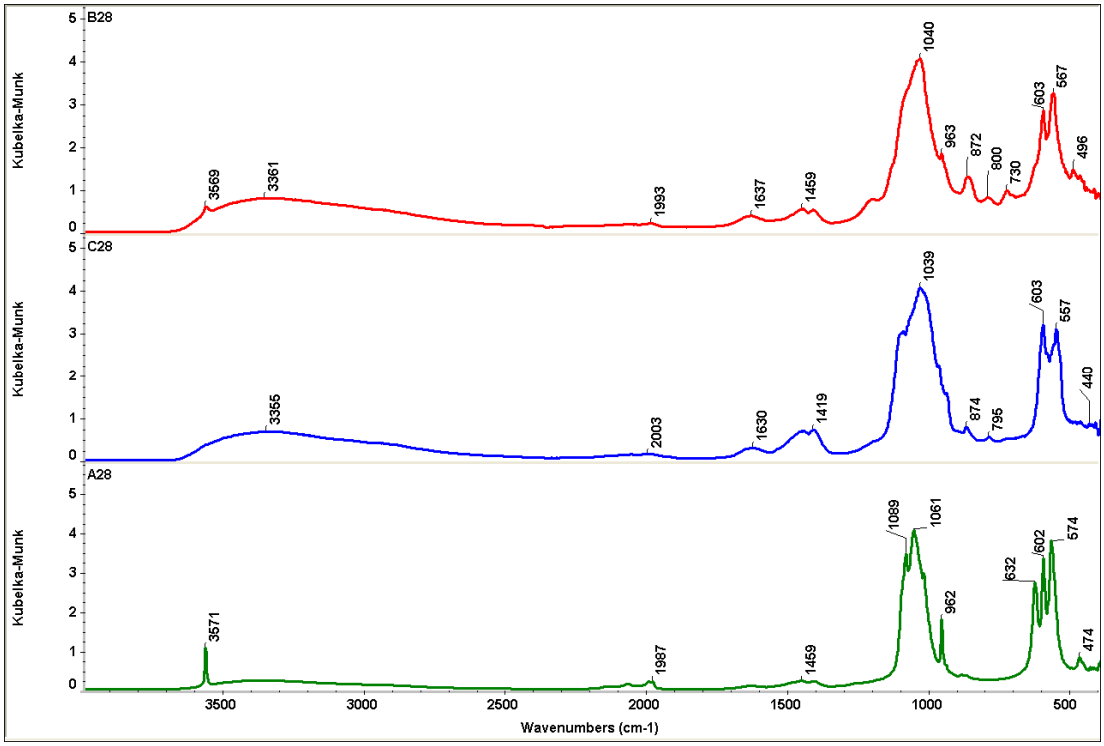


**Figure 32 – Apatite formation ability of the scaffolds assessed using FTIR:** Fourier Transform Infrared Spectra of scaffolds incubated in SBF (28 days) an improved apatite formation in SrHA scaffolds compared to HA and HASi scaffolds. HA (**A28** – green), HASi (**B-28** –red) and SrHA (**C28**-blue).

## 4.4. Cytotoxicity evaluation:

The cytotoxicity test done using test on extract method indicated that the L929 cells could maintain its morphology and proliferation ability in the the scaffold materials – HA, HASi and SrHA. MTT assay (figure 33) also that the cells metabolic activity was not affected even after 24hrs of incubation the scaffolds SrHA and HA exhibited a percentage cell metabolic activity of whereas HASi exhibited 82%, compared to control - cells alone. No significant difference was found in the metabolic activity of test materials – HASi (p value - 0.2710) and SrHA (p value - 0.6543) when compared to the control scaffold –

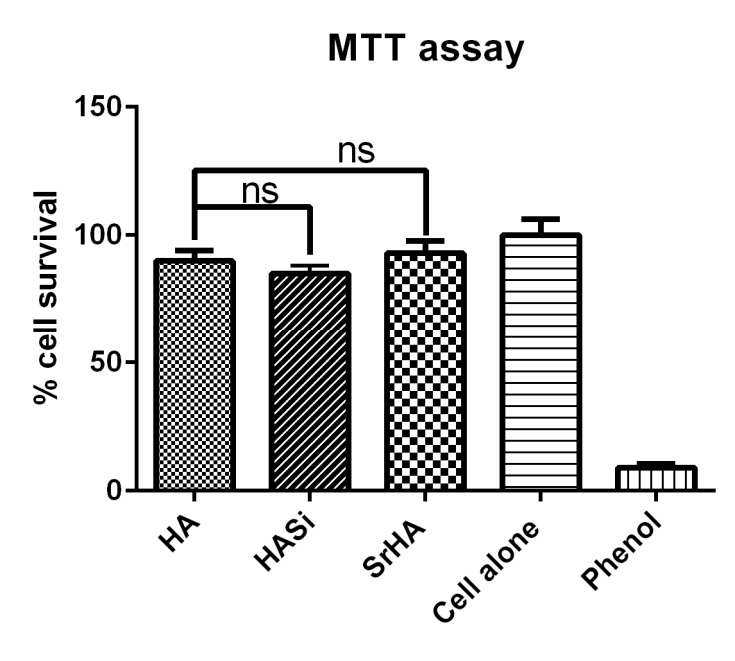


**Figure 33 – Cytotoxicity evaluation using MTT assay:** L929 cells exhibited a similar metabolic activity after culturing in the presence of HA, HASi and SrHA scaffolds for 24 hours. (ns – non significant; p value: HA vs. HASi - 0.2710; HA SrHA – 0.6543).

# CHAPTER 5

## PHASE II – *IN VITRO* & *IN VIVO* STUDIES USING rBMSCs IN RAT OSTEOPOROTIC MODEL

- **PART A - *In* vitro evaluation of HA, HASi and SrHA disc scaffolds using rBMSCs**
- **Part B - Development & Evaluation of rat osteoporotic model**
- **Part C - Efficacy Assessment of micro-granular HA, HASi, cHASi, SrHA and cSrHA in rat osteoporotic model**

# CHAPTER 5 - RESULTS

## PART A - *IN VITRO* EVALUATION OF HA, HASi AND SrHA DISC USING rBMSCs

## 5.1 Isolation, culture and characterization of rBMSCs:

### 5.1.1. Isolation and culture of rBMSCs:

rBMSCs were isolated from the rat bone marrow aspirate based on their adherence (figure 34). Even though rBMSCs proliferation was slow during the period of primary culture, they proliferated extensively and became confluent attaining the typical spindle morphology by 8–10 days.

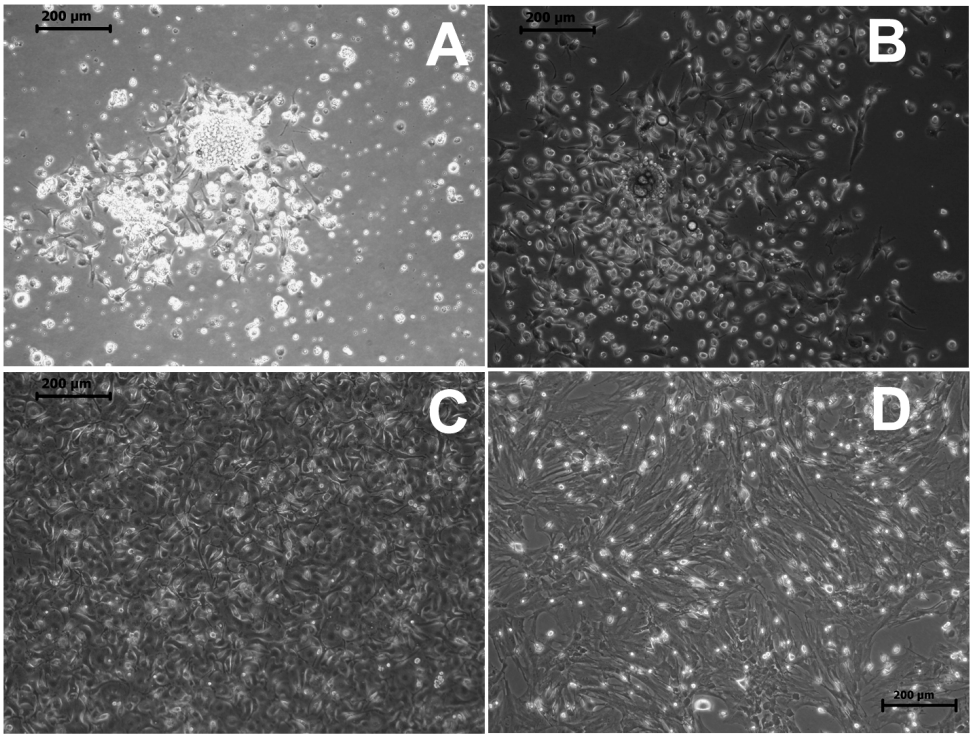


**Figure 34 -Phase contrast images of rBMSCs isolated from bone marrow: A** – $P_0$ passage (day 1), **B** - $P_0$ passage (day 5), **C**- $P_0$ passage (day 10), **D**- $P_3$ (scale bar = 200µm).

### 5.1.2. Characterization of rBMSCs:

#### *5.1.2.1 Fluorescent staining:*

Fluorescent staining using DAPI and rhodamine depicted the typical spindle morphology of the cultured rBMSCs on cover slips (figure 35).

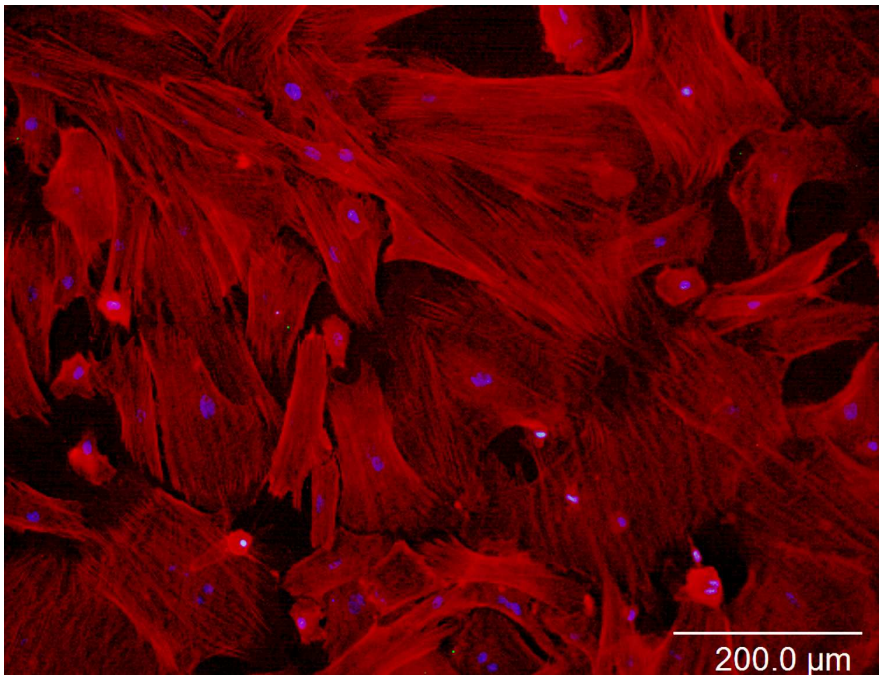


**Figure 35 – Fluorescent micrographs of rBMSCs on cover slips:** Actin fibers stained red with Rhodamine Phalloidin and nucleus stained blue with DAPI (scale bar = 200µm).

#### *5.1.2.2. Surface marker analysis:*

Quantitative characterization using flow cytometry indicated the cells to be 97% positive for the positive marker CD90 (figure 36B). Only 0.9% positivity was observed for the hematopoietic negative marker CD34 (fig 36C).

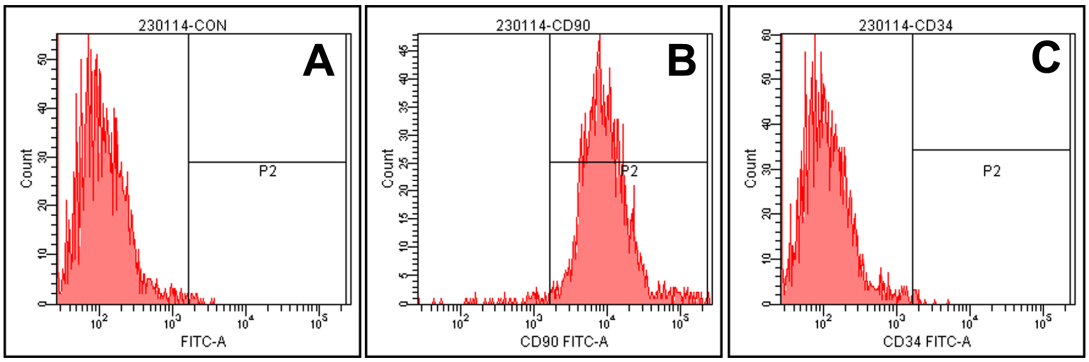


**Figure 36 - Flow cytometry analysis of the expression of CD 90 and CD34 on cultured rBMSCs: A** – Control cells, **B**- CD 90 stained cells, **C**- CD 34 stained cells.

### *5.1.2.3. Differentiation potential:*

Plasticity of the cultured cells was evaluated by assessing its ability. Alizarin red staining depicted the calcium deposited by the differentiated rBMSCs as reddish brown patches in the culture dish (figure red O staining indicated the presence of fat globules (stained as red globules) in adipogenically differentiated rBMSCs (figure 37B).

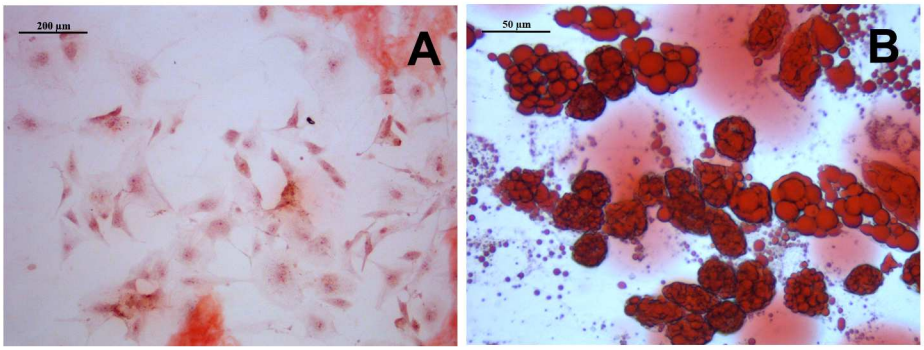


**Figure 37 – Light micrographs depicting differentiation ability of rBMSCs: A** - Osteogenic differentiation proved by alizarin red staining, **B** - adipogenic differentiation proved by oil red O staining (scale bar A = 200µm; B = 50µm).

## 5.2. *In vitro* cytocompatibility and osteogenic efficacy assessment of HA, HASi and SrHA scaffolds:

### 5.2.1 *In vitro* cytocompatibility assessment:

#### *5.2.1.1 Cell adhesion on disc scaffolds:*

Osteogenically induced rBMSCs were seeded on scaffolds and assessed using E-SEM. Scanning electron micrographs (Figure 38) depicted cell adhesion on all the scaffolds – HA, HASi and SrHA. Adhered cells maintained the typical spindle morphology post one day of culture.

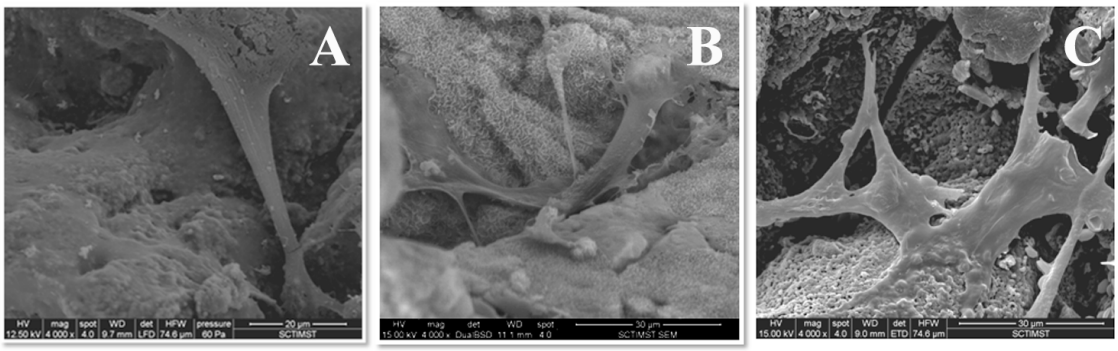


**Figure 38 - SEM images depicting cell adhesion on the scaffolds:** Scanning electron micrographs indicating cell adhesion on **A**- HA, **B**- HASi and **C**- SrHA scaffolds, post 24 hours of culture (scale bar = 30µm).

### 5.2.2. *In vitro* osteogenic efficacy assessment:

Osteogenic efficacy assessed in terms of ALP activity (figure 39) that HA, HASi and SrHA scaffolds favoured *in vitro* osteogenesis. All the TE constructs exhibited highest ALP activity by 21 days of culture, after which was a decline in the ALP level. Amongst the three scaffolds, cells seeded on scaffolds favoured a comparatively better ALP production of 13.89±1.5 µmol 30 minutes, whereas cells on HA and HASi exhibited ALP levels of 12.44±2.6

12.85±2.2 µmol pNp/30 minutes respectively. Multiple comparison (Dunnet's using 2way ANOVA in graph pad prism indicated no significant difference at time points in HASi or SrHA, compared to HA scaffolds. (p values - Day 7: HA HASi - 0.9737; HA vs. SrHA – 0.3866. Day 14: HA vs. HASi - 0.9461; HA vs. SrHA – 0.412. Day 21: HA vs. HASi - 0.927; HA vs. SrHA – 0.4256, Day 28: HA vs. HASi - 0.2404; HA vs. SrHA – 0.4868).

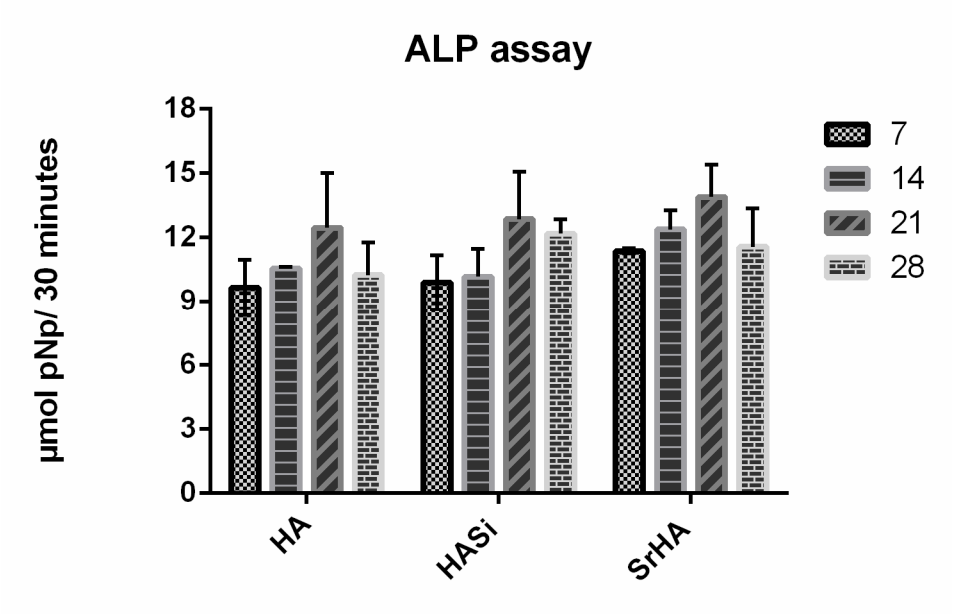


**Figure 39 – ALP activity of rBMSCs on HA, HASi and SrHA:** Biochemical estimation based on ALP assay for 7,14,21 and 28 days indicated that all the scaffolds exhibited high ALP activity at 21st day. SrHA exhibited comparitively (not significant) ALP expression on day 21 compared to HASi (day 21 - p values - HA vs. HASi - 0.927; HA vs. SrHA – 0.4256).

## 5.3. Compatibility of scaffolds using osteoclast pre-cursor cells - RAW264.7:

Osteoclast precursor cells were seeded on SrHA scaffolds and post 18 of seeding the cells exhibited a distorted elongated morphology, indicating its

adherence (figure 40C). It was interesting to note that the $RAW_{264.7}$ cells seeded HA and HASi scaffolds maintained their typical morphology – flattened cell numerous broad lamellopodia along with slender filopodia (figure 40A and 40B respectively).

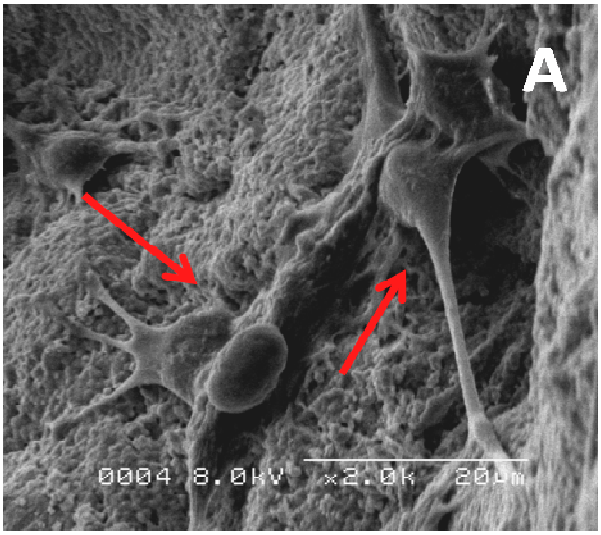


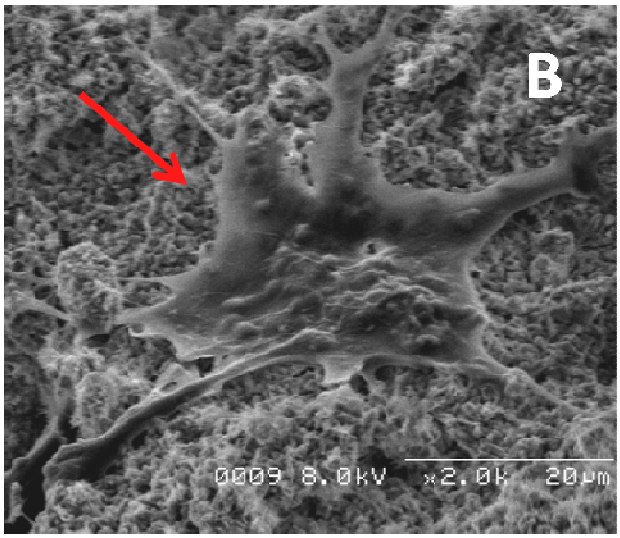

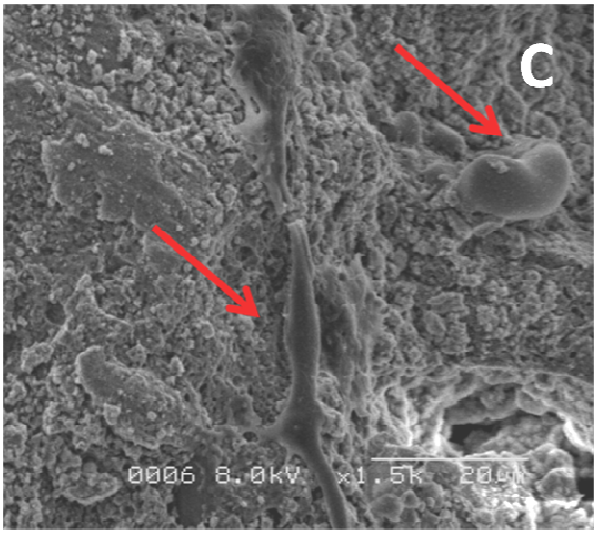


**Figure 40 - Adhesion of osteoclast precursor cells on the scaffolds:** Scanning electron micrographs depicted the adhesion of $RAW_{264.7}$ cells with numerous extensions on **A**- HA and **B**- HASi. Elongated and distorted morphology was on the cells seeded on **C**- SrHA scaffolds, post 18 hours of culture (scale bar = 20 µm).

## PART B -DEVELOPMENT & EVALUATION OF RAT OSTEOPOROTIC MODEL

Part B of chapter 5 includes the validation of the rat osteoporotic model developed by ovariectomy. Rat model was assessed for osteoporotic induction post 10 months of ovariectomy.

## 5.4. Validation of Rat Osteoporotic model:

### 5.4.1. Histology of excised tissue:

Histological evaluation of the excised ovary by H&E staining (figure 41) depicted the presence of primordial follicle, primary follicle and late primary which confirmed the typical ovarian organisation and cellular structure.

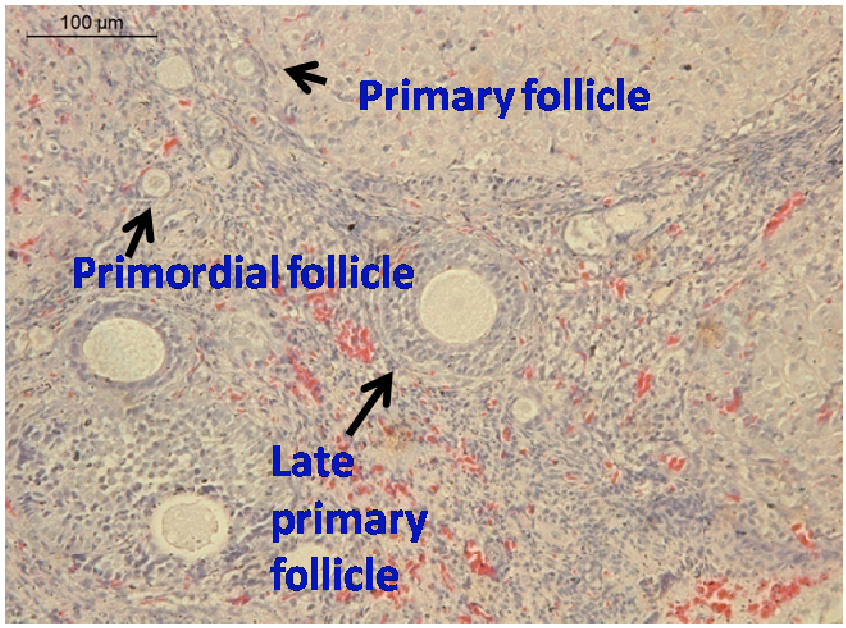


**Figure 41- H & E stained micrograph of rat ovary:** Histology images depicted the presence of follicles in the tissue confirming the structural features of tissue (scale bar = 100µm).

### 5.4.2. Evaluation of trabecular bone loss:

Trabecular bone loss at the tibial epiphyses of the induced rat osteoporotic models was qualitatively and quantitatively assessed.

#### *5.4.2.1. Histological evaluation:*

Histology sections of the proximal epiphysis of tibial bone, stained with indicated the extent of trabecular bone loss. Compared to the trabecular pattern normal rat model (figure 42A), ten months osteoporotic model exhibited a in the trabecular volume (figure 42B). Trabecular bone (TB) thinning with large spaces could also be appreciated from the histology image.

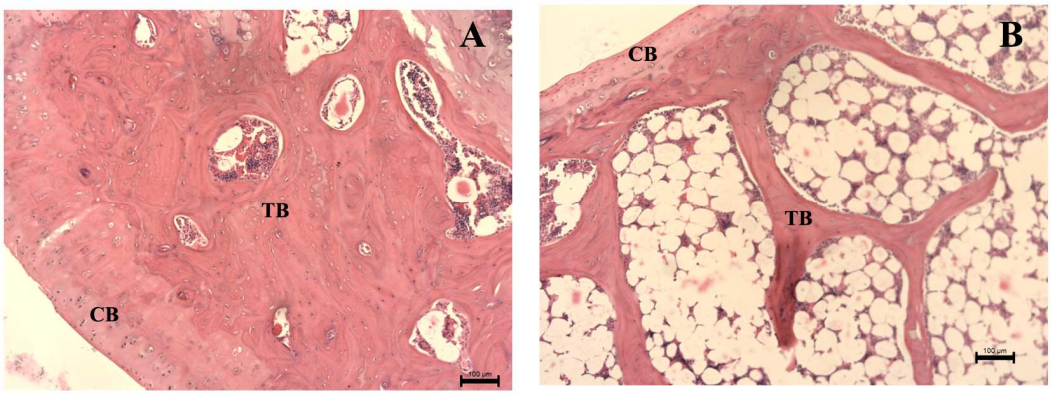


**Figure 42 - Evaluation of trabecular bone loss by histology:** H & E stained micrograph depicting the extent of trabecular bone loss in the proximal tibial bone in **A** - control rat and **B** - LOA model. Osteoporosis induction caused trabecular thinning and disruption. (CB – Cortical bone, TB- trabecular bone) (scale bar = 100µm).

***5.4.2.2. Micro CT evaluation:***

*2D* slices generated using micro CT from the tibial epiphyses of the model post six and ten months of induction, exhibited a decrease in the bone volume concurrent to the histological observations (figure 43B and 43C respectively). In the control animal presence of extensive trabecular bone was observed (figure 43A).

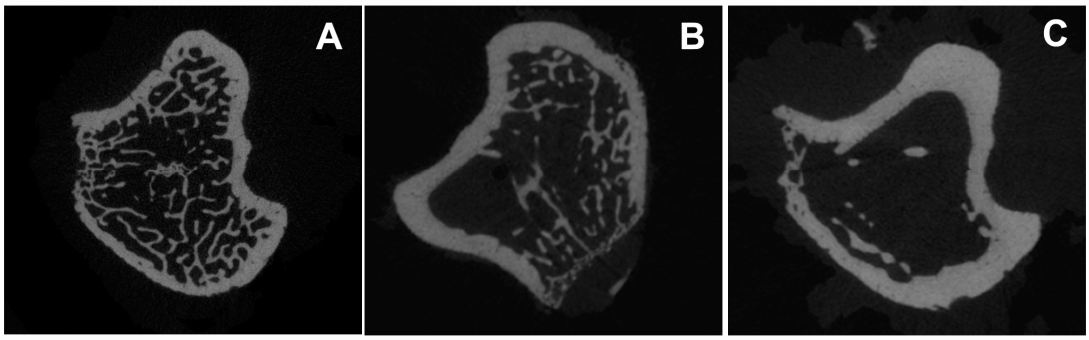


**Figure 43 - Evaluation of trabecular bone loss using micro CT:** 2D slices from micro CT depicted the trabecular bone loss in A - control animal, B - 6 months osteoporosis induction and C - 10 months post osteoporosis induction. Thinner trabeculae with less trabecular bone volume were evident in the induced

3D morphometry evaluation of trabecular volume at the proximal tibia induced model also indicated appreciable amount of bone loss compared to the similar aged control animals. Trabecular bone disruption was evident in the six ten months induced model (figure 44C and 44D respectively), since the network was seen only near the tibial head region. In the control animal (young aged - figure 44A and 44B) the trabecular network extended further down from tibial plateau. Presence of thick trabecular bone in the control animals can also appreciated from the color coded images. Greenish area represents a thicker trabeculae.

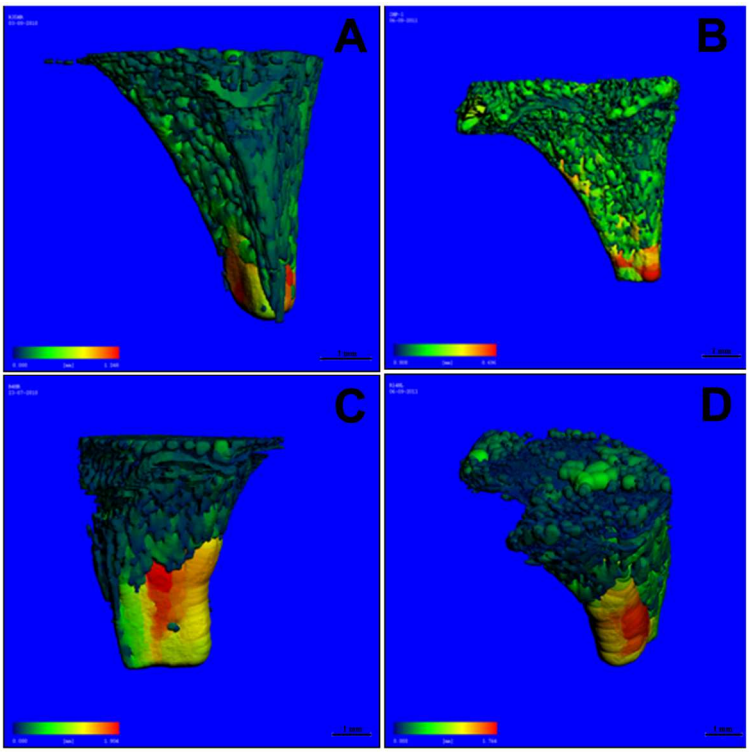


**Figure 44 - Evaluation of trabecular bone loss using 3D morphometry images: A & B -** 3D trabecular thickness of tibial epiphyses in young and aged control **C & D -** trabecular bone loss in the tibial region of 6 months and 10 months osteoporosis induced rat models (color coding – trabecular thickness increases green to red color; scale bar = 1mm).

Further quantification of bone loss was done by evaluating the bone parameters like Tb.N. and Tb.Sp. (figure 45 and 46 respectively). The of bone loss associated with the aging process in rats were assessed and in table 4. Micro CT evaluation indicated that in a normal rat, Tb.N. increased 2.79 1/mm to 3.63 1/mm at 12 months old. Further with aging associated bone was evident as the Tb.N. decreased to 3.12 (1/mm). Similarly control animals exhibited Tb.Sp. values of 0.36 mm, 0.26 mm and 0.2 mm at 6, 12 and 16 old, indicating aging associated bone loss only at 16 months.

At six months of induction Tb.N. decreased to 2.49 (1/mm) in the induced models (table 6). LOA rat models (n=5) were further evaluated post 10 months induction to assess the extent of bone loss. Trabecular number (Tb.N.) in the model exhibited a statistically significant (p value <.0001) decrease of 1.26±.04 (1/mm) compared to age matched control animals which had a Tb.N. of 3.63±.01 (1/mm). Trabecular space (Tb.Sp.) increased in the LOA models to 0.85±.03 when compared to control animals with a spacing of 0.26±.003 (mm) (p value <.0001). Bone density (trabecular) also decreased in the induced model, as the density in control animals were 331.1±14.54 (mg HA/ccm) and the induced had 223.2±6.5 (mg HA/ccm) (p value - 0.0025). Control animals exhibited a ratio of 0.278±0.007, whereas the LOA model exhibited a significantly low ratio of 0.205±0.009 (p value <0.05) (figure 47).

**Table 6: Trabecular bone parameters – Tb.N. Tb.Sp. and Tb.Th. in control animals aged 6, 12 and 16 months.**

| Control group age | Tb.N. | Tb.Sp. | Tb.Th. |
|---|---|---|---|
| 6 M | 2.79 | 0.36 | 0.062 |
| 12M | 3.637 | 0.2612 | 0.1003 |
| 16M | 3.12 | 0.32 | 0.108 |

**Table 7: Trabecular bone parameters – Tb.N., Tb.Sp. and Tb.Th. in 6 and 10 months osteoporosis induced LOA model.**

| OVVX group | Tb.N. | Tb.Sp. | Tb.Th |
|---|---|---|---|
| 6M OVX | 2.49 | 0.45 | 0.1085 |
| 10M OVX | 1.29 | 0.855 | 0.12 |

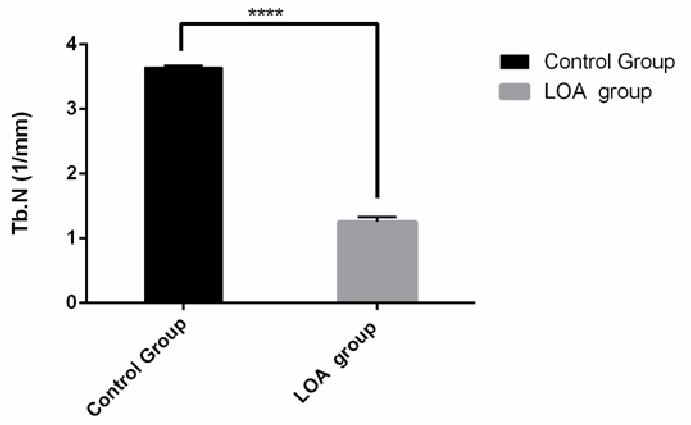


**Figure 45 – Quantification of trabecular bone loss – Tb.N.:** Graphical representation comparing the Tb.N. (1/mm) in control and LOA group (**** significant; p value <0.0001).

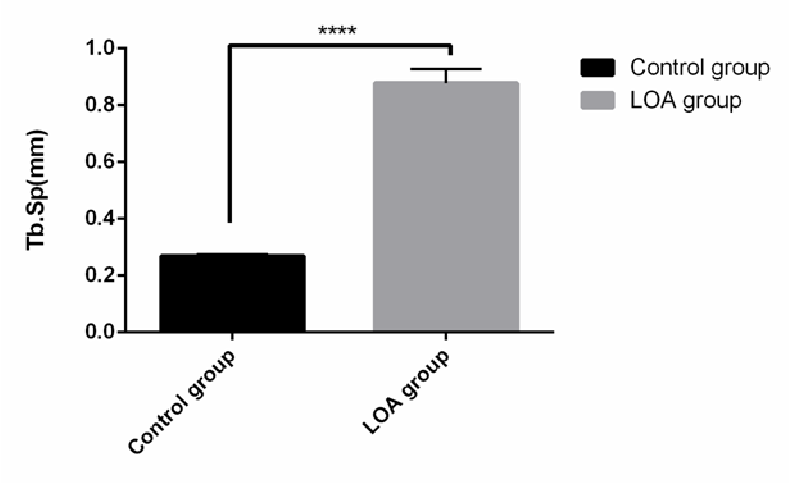


**Figure 46 – Quantification of trabecular bone loss – Tb.Sp.:** Graphical representation comparing the Tb.Sp. (mm) in control and LOA group (**** significant; p value <0.0001).

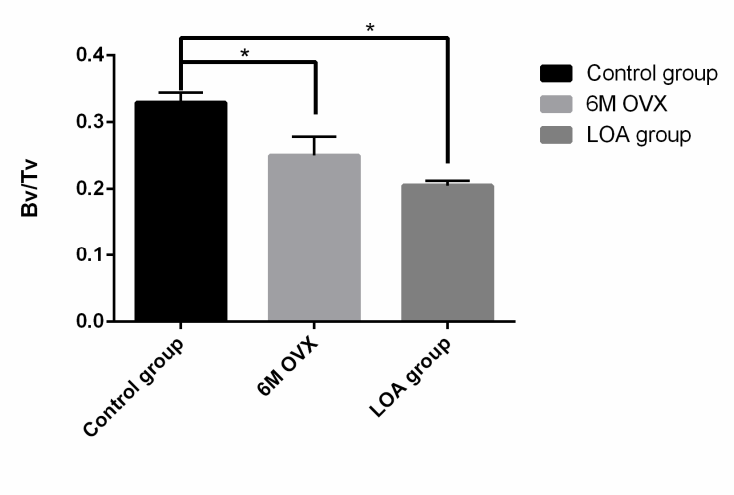


**Figure 47 – Quantification of trabecular bone loss –Bv/Tv:** Graphical representation comparing the Bv/Tv in control and LOA group (* significant; p value <0.05).

### 5.4.3. Biochemical analysis of serum:

LOA group exhibited a high calcium concentration of 16.77±.30 mg/dl 10 months of induction, whereas the control group exhibited a low value of

11.45±.56 mg/dl. No significant difference was observed at earlier time points of zero months and five months post induction (figure 48).

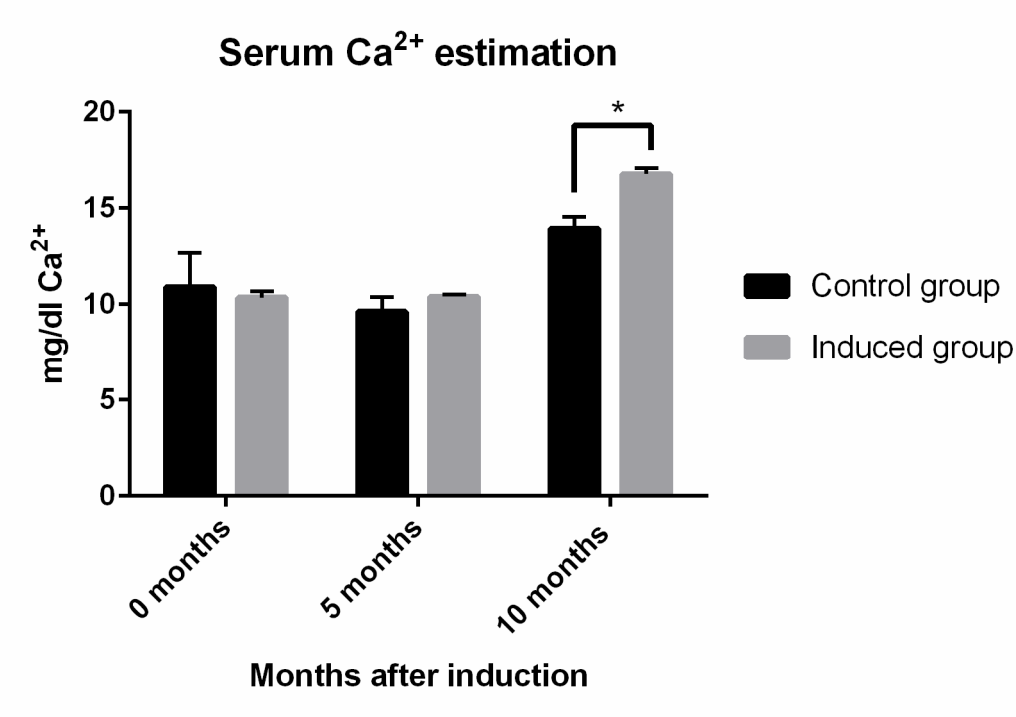


**Figure 48 – Biochemical analysis of serum Calcium:** Graphical representation of calcium concentration in the serum of the control and induced model at 0, 5 and 10 months (* p value – 0.0218).

**5.4.4. Evaluation of bone healing efficacy:**

All animals were euthanized at the end of study period and gross of retrieved explants was done prior to other evaluations. Gross evaluation uneventful healing, without any inflammatory response at the implant site at all periods.

***5.4. 4.1. Micro CT evaluation:***

3D morphology images of the defect area obtained from micro CT that defect area was clearly distinguishable at three and six weeks post surgery

LOA model (figure 49A and 49B). But eight weeks post surgery; defect area not be identified from the 3D images, indicative of wound closure in both LOA models (figure 49C and 49D).

Further analysis of the defect area from the 2D slices depicted that even though wound area seemed to be healed at eight weeks from the 3D images, healing was incomplete in the LOA models. The defect area was bridged at the peripheral region of the cortex, but void spaces could be appreciated towards marrow region. In Control animals cortical bridging was complete with new tissue filling the entire defect area without much void spaces.

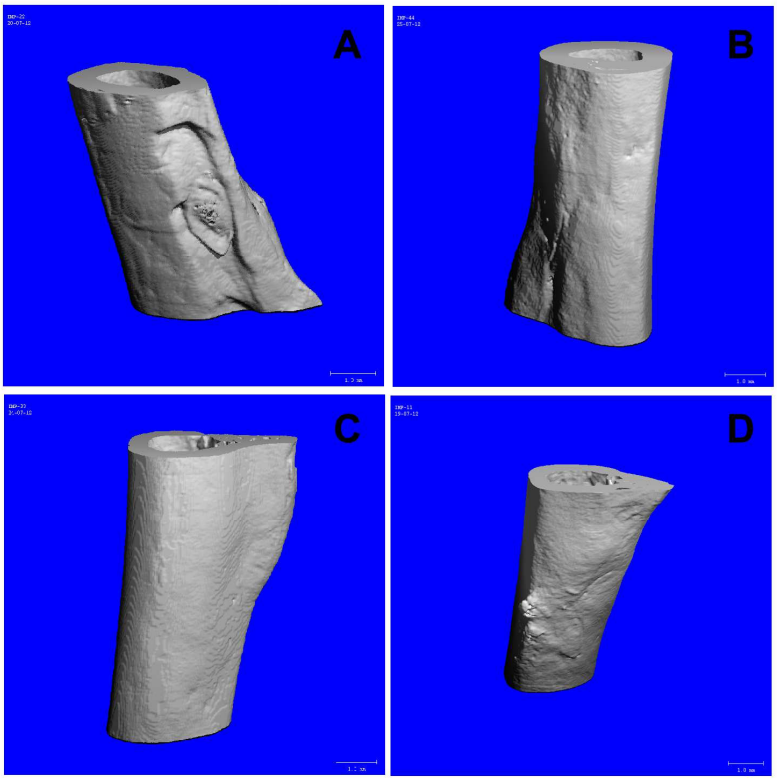


**Figure 49 – Healing of the sham defect site in control and LOA model:** 3D morphometry image depicting drill hole bone defect healing in **A** – post 3 weeks implantation in LOA model, **B** – post 6 weeks of implantation in LOA model, **C**- post 8 weeks of implantation in control animals and **D**- post 8 weeks of in LOA model (scale bar = 1mm).

A quantitative estimation of bone density across the defect area in the control (figure 50A) and LOA models (figure 50B) also depicted that the new bone formed in the LOA models were having a poor mineral content at eight weeks post implantation, as evident from the histograms generated from the corresponding 2D slices.

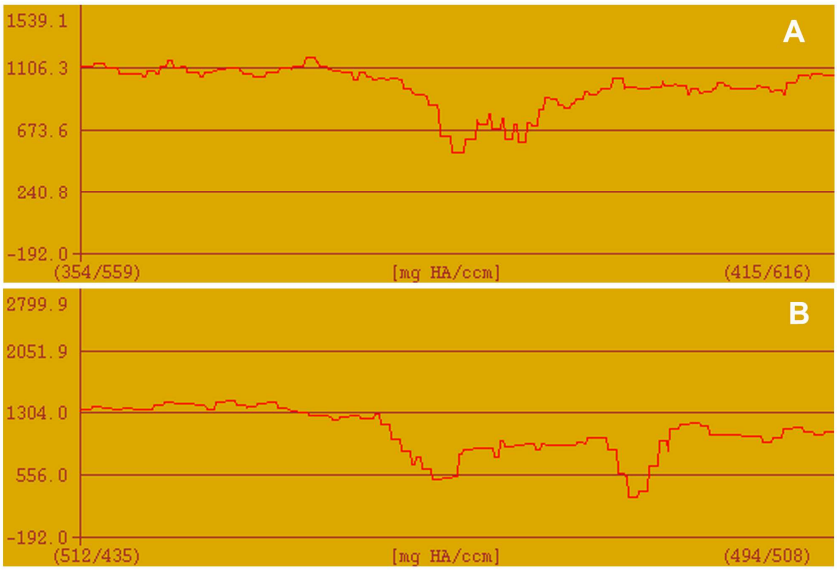


**Figure 50 - Density histograms of the bone defect site post 8 weeks of implantation: A -** control animal and **B -** LOA model; density histograms from 2D slices using micro CT.

***5.4. 4.2. Histological evaluation:***

Histological evaluation of the healing of sham defect (3 mm x 1.5 mm) carried out at eight weeks. In the Control animals (figure 51A), 8 weeks post the defect area was almost filled with new osseous tissue. But in the induced (figure 51B) even after eight weeks of surgery cortical bridging and closure of defect area was not evident. Loosely arranged osteocytes (immature bone organization) could be distinguished in the *de novo* bone matrix in the control

animals. But more void spaces with scarce new bone formation were evident in LOA models, indicative of poor healing.

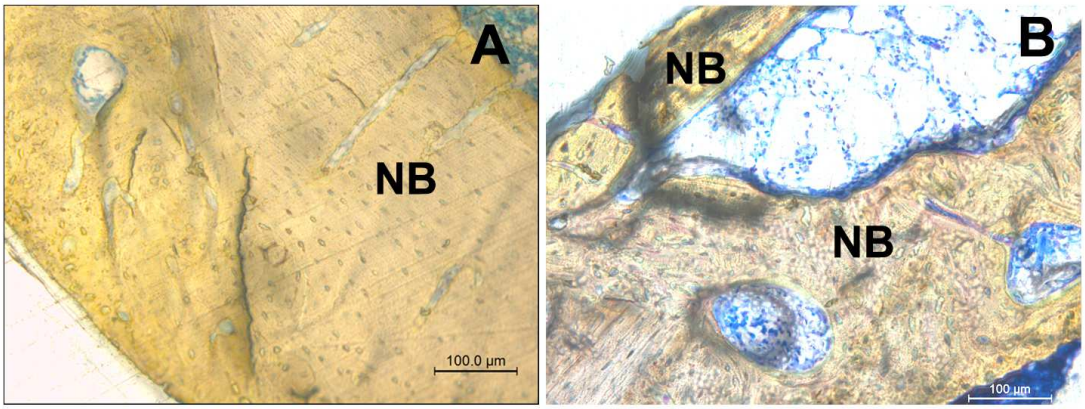


**Figure 51- Histological evaluation of bone defect healing:** Stevenal's blue and Gieson's picrofuchsin stained plastic sections depicting *in vivo* healing in control LOA rats 8 weeks after surgery. **A -** Defect area was almost bridged by the *de* bone tissue in control rats. **B-** Large void spaces in the defect area in the LOA indicates delayed healing in B (**NB**- New Bone) (scale bar = 100µm).

# PART C - EFFICACY ASSESSMENT OF MICRO-GRANULAR HA, HASi AND SrHA; cHASi AND cSrHA IN RAT OSTEOPOROTIC MODEL

## 5.5. *In vitro* characterization of micro-granular scaffolds:

### 5.5.1. Micro-structure and surface morphology:

Scanning Electron Micrographs of the HA, HASi and SrHA micro- depicted the 3D rough surface topography of the scaffolds (figure 52A, 52B and respectively) with inter connected pores in the size range of 350-400 microns.

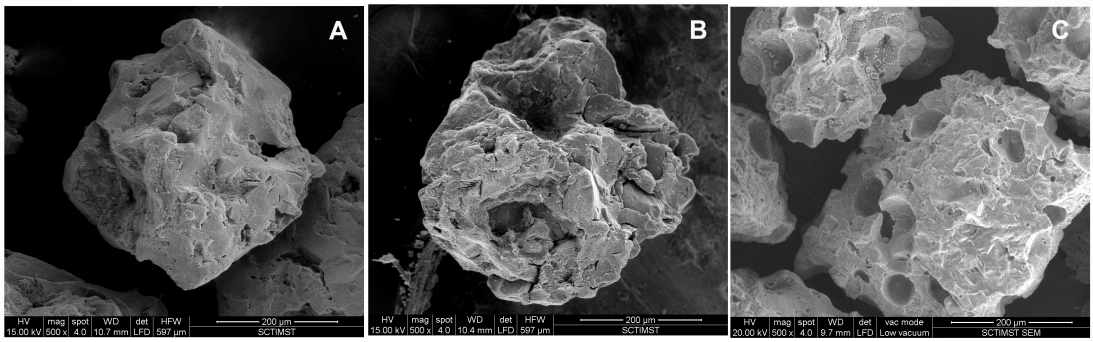


**Figure 52 Surface morphology of micro-granular scaffolds:** Scanning Electron Micrographs depicted rough and porous micro-granular – **A** - HA micro-HASi micro-granule and **C** – SrHA micro-granule (scale bar = 200µm).

### 5.5.2. Radiopacity evaluation:

Radiographic evaluation of SrHA micro-granules exhibited an improved radiopacity equivalent to 2.63 mm thick aluminium. HA and HASi revealed a radiopacity equivalent to 2.39 mm and 1.79 mm thick aluminium (figure 53).

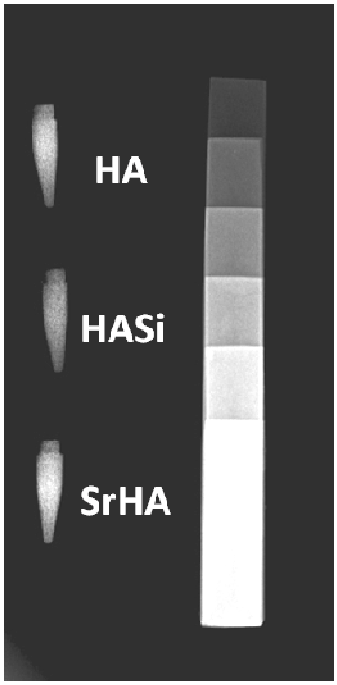


**Figure 53 – Radiopacity evaluation:** Radiograph depicts the radiopacity of HA, HASi and SrHA micro-granular scaffolds in comparison to aluminium wedge.

### 5.5.3. Cytocompatibility assessment:

#### *5.5.3.1. Direct contact assay:*

Cytocompatibility of the micro-granular scaffolds evaluated by direct assay indicated that the cells proliferated well in direct contact with L929 cells, 24 hours of incubation. The cells maintained their normal morphology and confluent proving the non toxicity of HA, HASi and SrHA micro-granules 54A, 54B and 54C respectively).

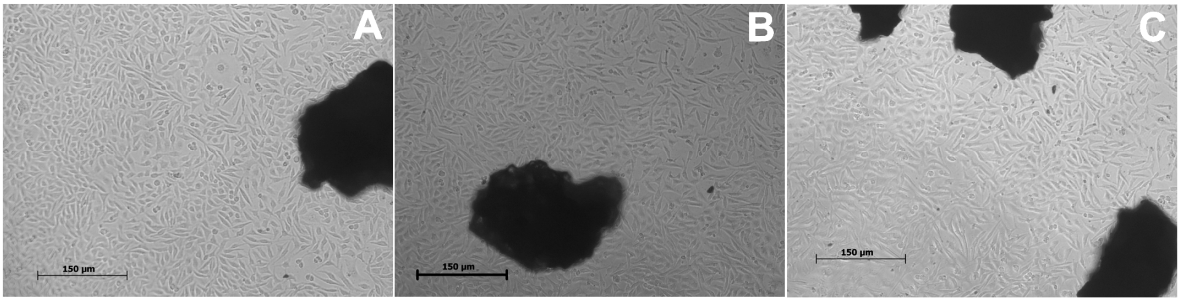


**Figure 54 - Cytocompatibility assessment of the micro-granules:** Phase contrast micrographs indicating the cytocompatibility of **A**- HA, **B** - HASi and **C** - SrHA micro-granular scaffolds in direct contact assay using L929 cells (scale bar = 150 µm).

#### *5.5.3.2. Cytotoxicity assay:*

Post 24 hours of incubation, MTT assay (figure 55) also proved the non-toxicity and cytocompatibility of the micro granules. Both HASi and SrHA exhibited an improved metabolic activity (in percentage) of 108.8 ± 11 and 111 compared to the cell alone control and HA micro granules. HA granules cells exhibited a metabolic activity of (in percentage) 112 ±7. One way analysis variance indicated a statistically significant increase in metabolic activity of cells incubated with SrHA (p value – 0.039) and HA (p value – 0.026), compared to alone control.

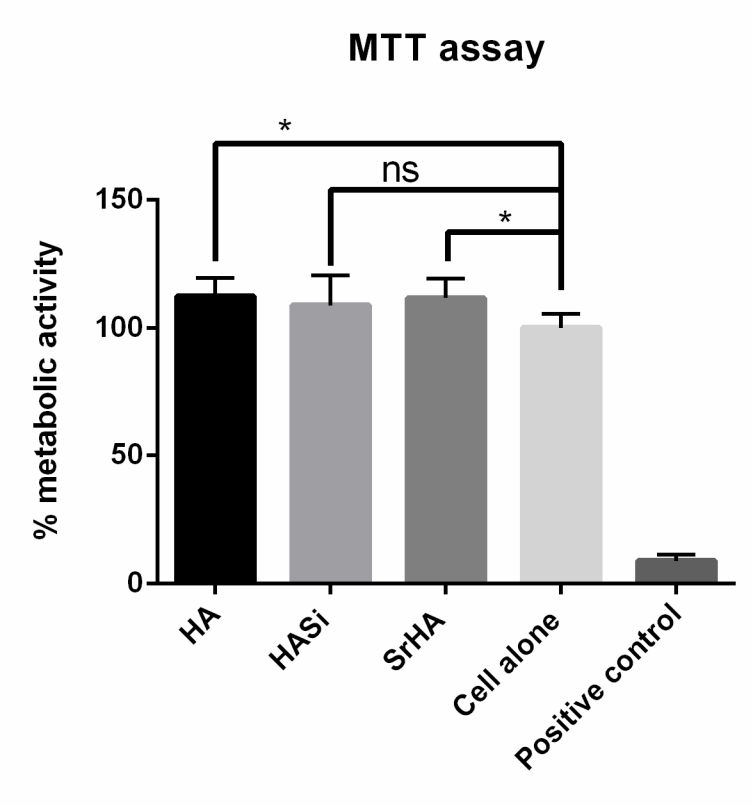


**Figure 55 – Cytotoxicity assay using micro-granules:** MTT assay indicated that HA, HASi and SrHA supported metabolic activity of L929 cells. (p value Cell vs. HA - * 0.026; Cell alone vs. HASi $^{ns}$ 0.154; Cell alone vs. SrHA * 0.039)

***5.5.3.3. Cell adhesion on the micro-granules:***

Adhesion of rBMSCs evaluated using E-SEM (Figure 56 A-C), depicted spindle morphology of the cells seen attached on the surface of the micro- Cells could adhere and spread well on the surface of micro-granules, without occluding the micropores present in them. All the scaffold materials favoured adhesion, again indicating the cytocompatibility of the micro-granules.

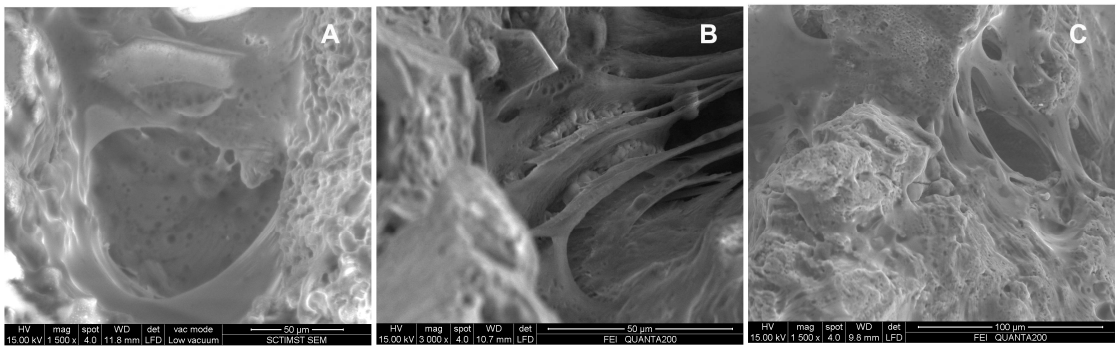


**Figure 56 - Cell adhesion on the micro-granular scaffolds:** Scanning electron micrographs indicating cell adhesion on **A** - HA, **B**- HASi and **C** - SrHA micro-granular scaffolds post 7 days of culture (scale bar = 50 µm).

## 5.6. *In vivo* osteogenic efficacy of tissue engineered micro-granules:

### 5.6.1. Gross evaluation:

Post implantation healing was uneventful in all the implantation in rat osteoporotic model, without any fibrous tissue formation and necrosis.

### 5.6.2. Histological evaluation:

In HA implanted group (figure 57C), there were distinct void spaces filled with cellular infiltration (cellular infiltration stained blue with Stevenal's blue) in between the newly formed osteoid sheet (stained yellow). Remnants of micro-granules (black) were also seen embedded in the *de novo* osteoid matrix at the defect site in HA, HASi (figure 58A) and cHASi (figure 58C) implanted groups. Whereas sham group exhibited a very poor regeneration ability (figure 57A), as more void spaces and less cellular infiltration were observed even after eight weeks of implantation.

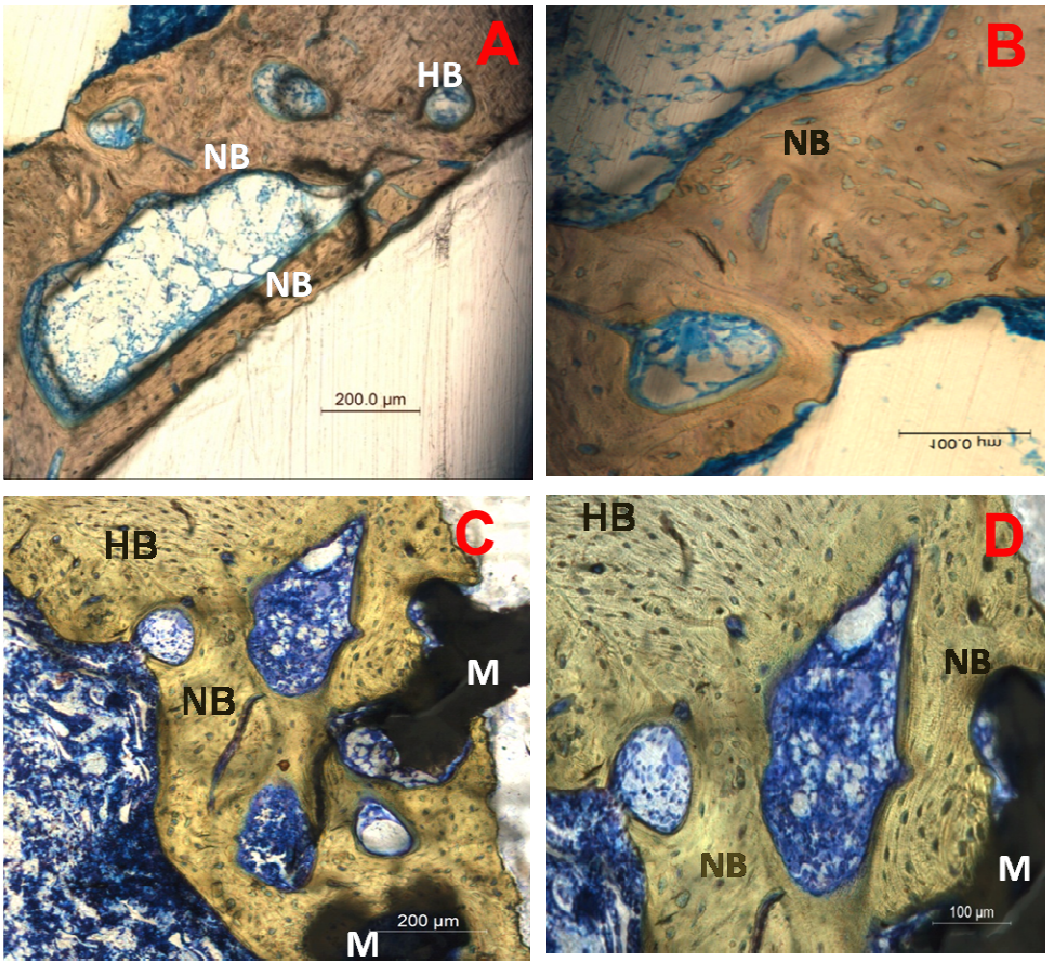


**Figure 57 - Histological evaluation of retrieved explants – sham & HA:** Stevenal's Blue and van Gieson's picrofuchsin stained histology images depicting the healing pattern in sham (**A&B**) and HA (**C&D**) implanted groups respectively. (**HB**-Host Bone, **NB**- New Bone, **VS** – Void Spaces, **M**- Material Remnants) (A &C - scale bar = 200µm, B&D – scale bar = 100 µm).

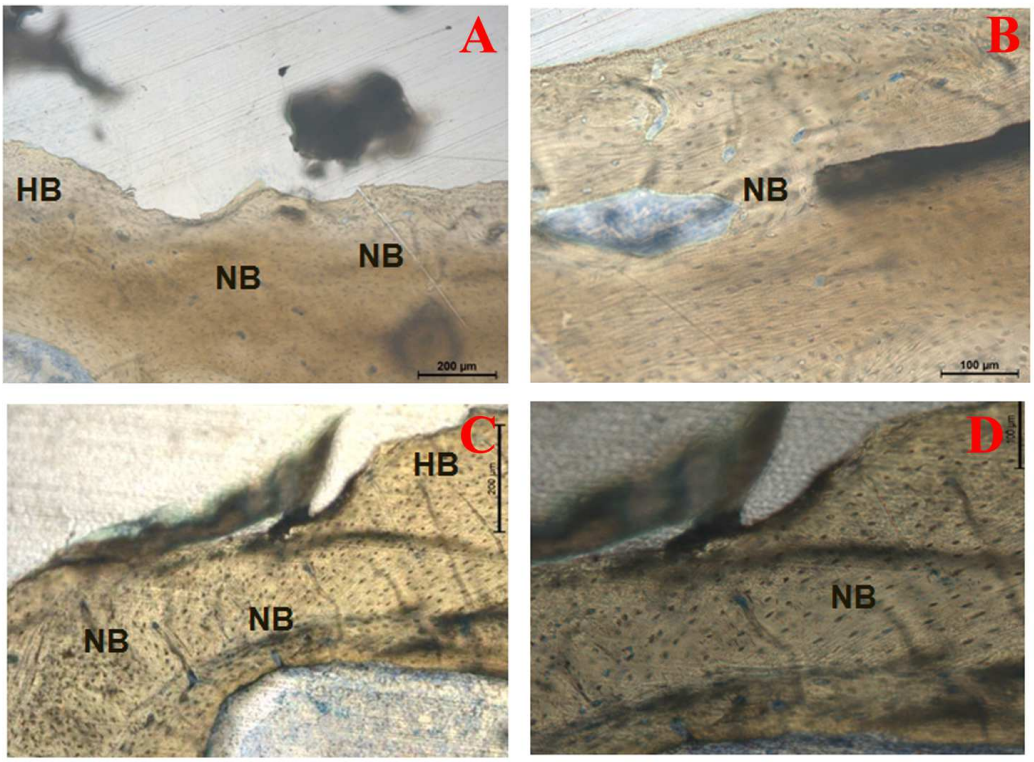


**Figure 58 - Histological evaluation of retrieved explants – HASi & cHASi:** Stevenal's Blue and van Gieson's picrofuchsin stained histology images depicting the healing pattern in HASi (**A&B**) and cHASi (**C&D**) implanted groups respectively. (**HB**-Host Bone, **NB**- New Bone, **VS** – Void Spaces, **M**-Material Remnants) (A &C - scale bar = 200µm, B&D – scale bar = 100 µm).

Undecalcified stained plastic sections demonstrated good osteointegration and improved osteoid formation (osteoid stained yellow with Van Gieson's picrofuchsin) across the defect area in cSrHA (figure 59C) and SrHA implanted group (figure 59A). Also, material remnants were not seen amidst the newly formed bone in HASi and SrHA (bare and cell seeded) implanted site, indicating the improved osteointegration ability of those scaffolds.

On a closer visualization, it was observed that in SrHA (bare and cell implanted group (figure 59B and 59D), *de novo* bone formed exhibited a more

lamellar pattern with uniform sized osteocytes oriented in line with the cells resembling typical mature bone. Where as in HASi (bare and cell seeded) implanted group, woven bone with scattered collagen fibers were seen (figure and 58D).

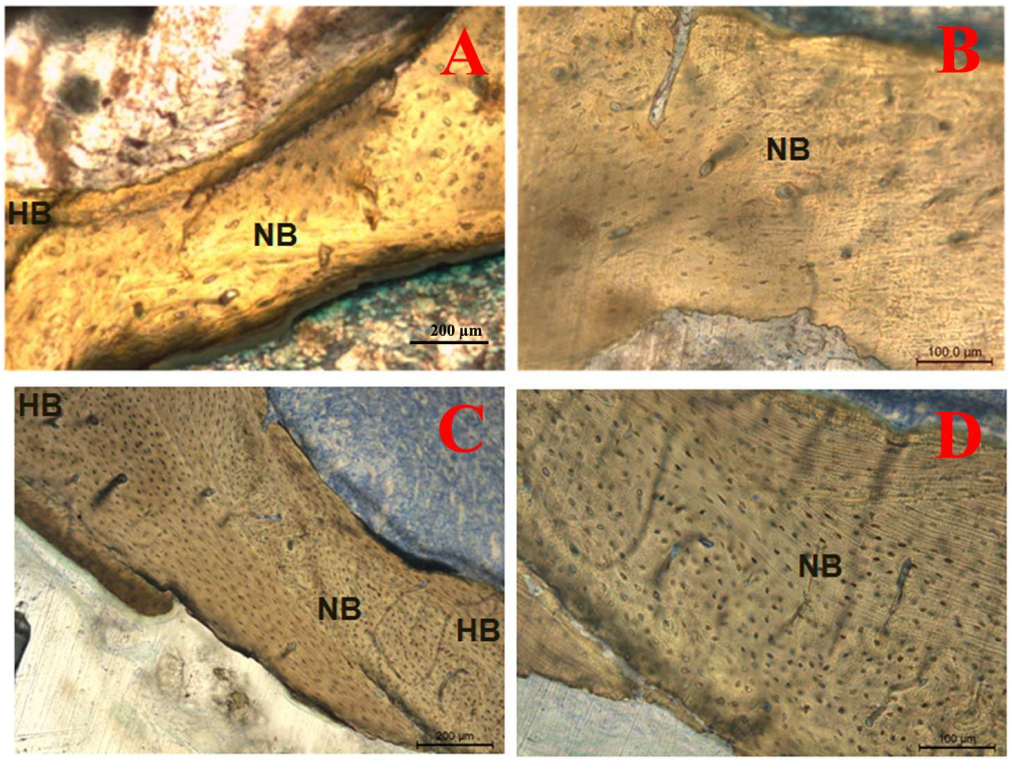


**Figure 59 - Histological evaluation of retrieved explants – SrHA & cSrHA:** Stevenal's Blue and van Gieson's picrofuchsin stained histology images the healing pattern in SrHA (**A&B**) and cSrHA (**C&D**) implanted groups respectively. (**HB**-Host Bone, **NB**- New Bone) (A &C - scale bar = 200µm, B&D scale bar = 100 µm).

### 5.6.3. Histomorphometry:

Osteogenic efficacy of implant materials assessed by histomorphometry demonstrated a significantly increased *de novo* osteoid formation in cSrHA implanted group. cSrHA implanted group exhibited the highest RE (New

defect area) ratio of 0.98 ± 0.01, followed by SrHA having a RE ratio of 0.97± whereas cHASi, HASi, HA and Sham group exhibited lower RE ratio of 0.92± 0.90± 0.04, 0.68± 0.08 and 0.65 ± 0.13 respectively. Statistical evaluation using way ANOVA indicated that cSrHA and SrHA implanted groups exhibited a significant (p value - <0.0001) increase in RE ratio compared to sham group. (p value - <0.0005) and cHASi (p value - <0.0002) implanted group also significant improvement in the RE ratio. But HA implanted group alone did not exhibit any statistically significant improvement (p value - 0.4275) in the RE indicating the relevance of other implant groups in the study.

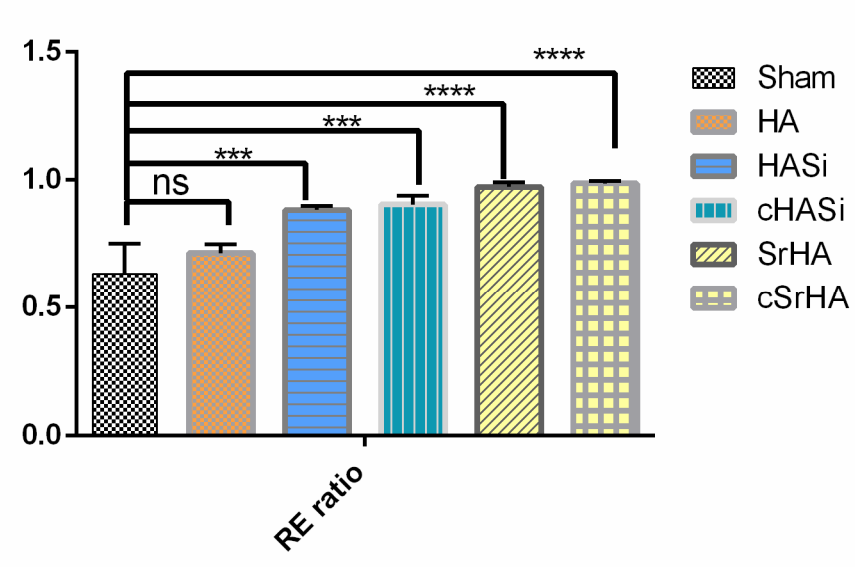


**Figure 60 – Quantitative evaluation of regeneration efficiency in LOA model:** SrHA and cSrHA implanted group exhibited significantly high RE ratio compared to other implant groups (significance: Sham vs. HA - ns- non-significant (p value - 0.4275), Sham vs. HASi - *** (p value - <0.0005), Sham vs. cHASi - *** (p value - <0.0002), Sham vs. SrHA - **** (p value - <0.0001), Sham vs. cSrHA - **** (p value - <0.0001).

### 5.6.4. Micro CT evaluation:

Mineralization of the new bone formed at the bone defect area was from the density histograms generated from corresponding 2D slices of different implant groups. New bone formed in sham and HASi implanted group (figure exhibited a poor mineralization efficiency compared to the mineral content of host bone. HA implanted group exhibited an improved mineralization of *de* bone. In SrHA and cSrHA implanted group (figure 62), better osteointegration was exhibited as the bone density (in terms of mg HA/ccm) of the *de novo* bone equalised to that of the host bone, indicating improved mineralization efficiency.

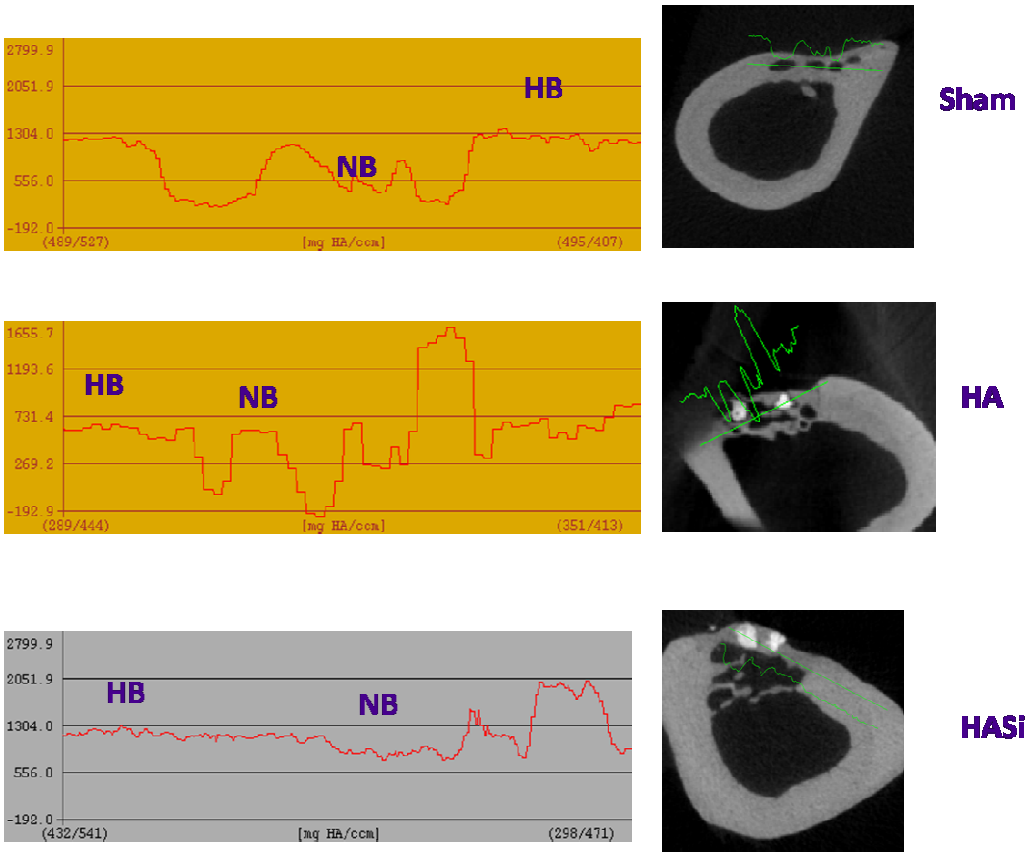


**Figure 61 - Density histograms of *de novo* bone and 2D slices of explants – Sham, HA & HASi:** Sham, HA and HASi post 8 weeks of implantation in LOA model.

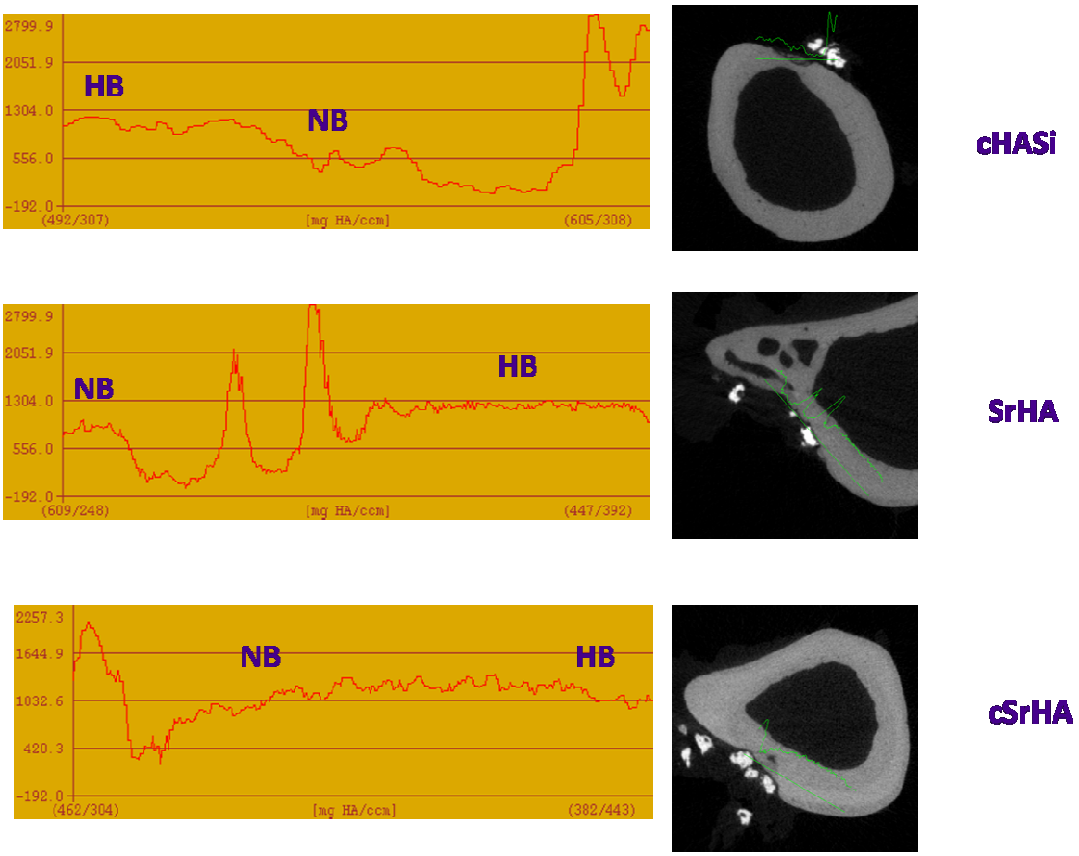


**Figure 62 - Density histograms of *de novo* bone and 2D slices of explants – cHASi, SrHA & cSrHA:** cHASi, SrHA and cSrHA post 8 weeks of implantation in LOA model.

### 5.6.5. Estimation of Strontium accumulation in different rat organs:

It was observed that Strontium levels in kidney and liver was less in SrHA implanted group compared to the organs collected from HA and HASi implanted groups. However, an increased strontium concentration was observed in the spleen of SrHA implanted group (table 8).

**Table 8: Strontium concentration in organs collected from HA, HASi and SrHA implanted LOA groups.**

| Organs | HA (µg/g) | HASi (µg/g) | SrHA (µg/g) |
|---|---|---|---|
| Kidney | 0.750 | 0.240 | 0.360 |
| Liver | 0.500 | 0.000 | 0.265 |
| Spleen | 0.600 | 0.450 | 1.980 |

# CHAPTER 6 - RESULTS

## PHASE III – *IN VITRO* AND *IN VIVO* STUDIES USING sADMSCs IN SHEEP OSTEOPOROTIC MODEL

- **Part A – *In vitro* evaluation of HA and SrHA disc scaffolds using sADMSCs**
- **Part B - Development & Evaluation of sheep osteoporotic model**
- **Part C - Efficacy Assessment of cylindrical HA, cHA, SrHA and cSrHA in sheep Osteoporotic Model**

# PART A - *IN VITRO* EVALUATION OF HA AND SrHA DISC SCAFFOLDS USING sADMSCs

Prior to *in vivo* application studies in sheep osteoporotic model, sADMSCs isolated and assessed for *in vitro* cytocompatibility and osteogenic efficacy.

## 6.1. Isolation, culture and characterization of sADMSCs:

### 6.1.1. Isolation and culture of sADMSCs:

sADMSCs were isolated from the sub-cutaneous fat tissue based on their adherence on TCPS (figure 63). Proliferation rate of sADMSCs during initial of primary culture was high and confluency was attained in $P_0$ stage by 6-8 With further passaging days for attaining confluency decreased to 3-4 days.

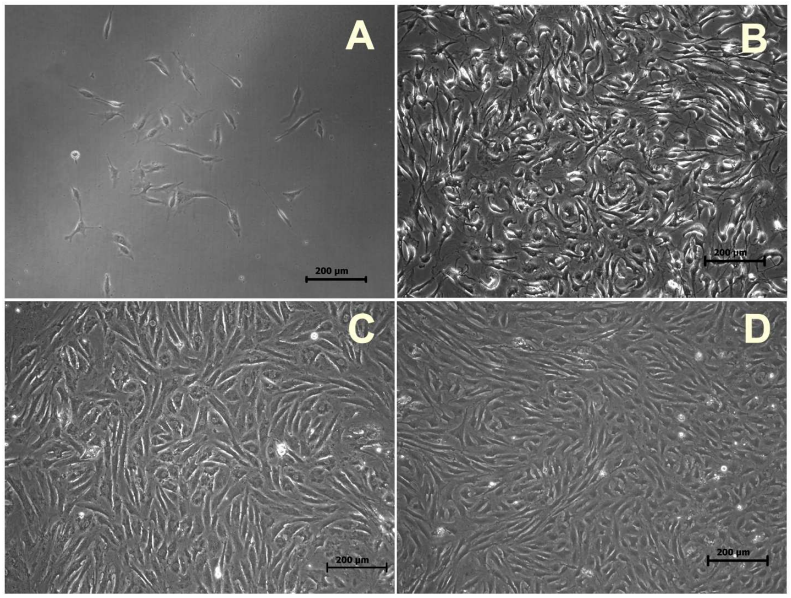


**Figure 63 - Phase contrast micrographs of sADMSCs isolated from adipose tissue: A** – $P_0$ passage (day 1), **B** - $P_0$ passage (day 5), **C**- $P_0$ passage (day 8), **D**- passage (scale bar = 200 µm).

### 6.1.2. Characterization of sADMSCs:

#### *6.1.2.1. Fluorescent staining:*

Fluorescent staining using DAPI and rhodamine depicted the typical morphology of the cultured sADMSCs (figure 64).

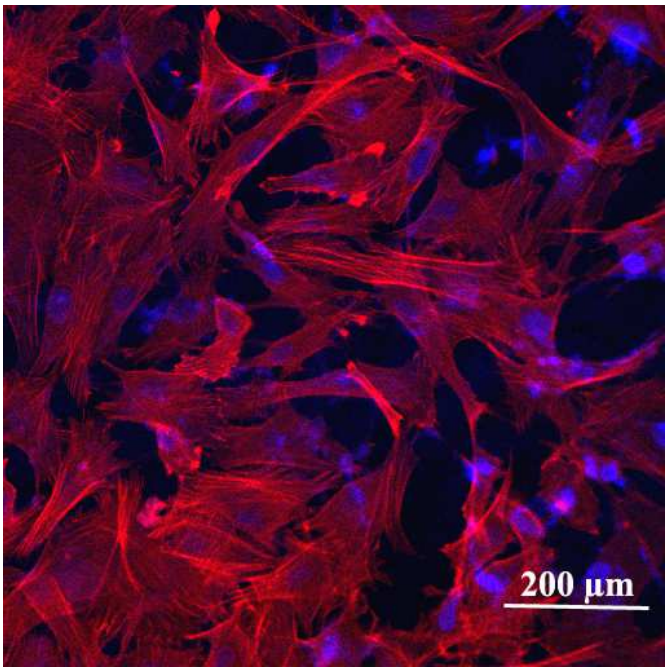


**Figure 64 - Fluorescent micrographs of sADMSCs on cover slips:** Actin fibers stained red with Rhodamine Phalloidin and nucleus stained blue with DAPI (scale bar = 200µm).

#### *6.1.2.2. Surface marker analysis:*

Quantitative characterization using flow cytometry indicated the cells to be 98.3% positive for the positive marker CD44 (figure 65C). Only 1.3% positivity was reported for the hematopoietic negative marker CD34 (figure

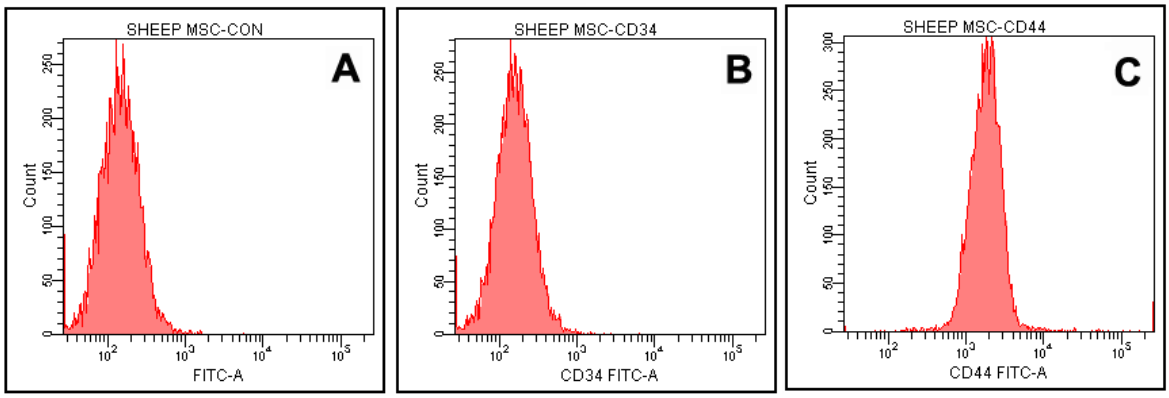


**Figure 65 - Flow cytometry analysis of the expression of CD 44 & CD 34 on cultured sADMSCs: A** – Control cells, **B**- cells stained with CD 34, **C**- cells stained with CD 44.

***6.1.2.3. Differentiation potential:***

Plasticity of the cultured cells was evaluated by assessing its ability towards osteogenic and adipogenic lineage. Alizarin red staining (figure depicted the calcium deposited by the osteogenically differentiated MSCs as brown patches. Oil red O staining (figure 66B) indicated the presence of fat (stained as red globules) by the adipogenically differentiated sADMSCs.

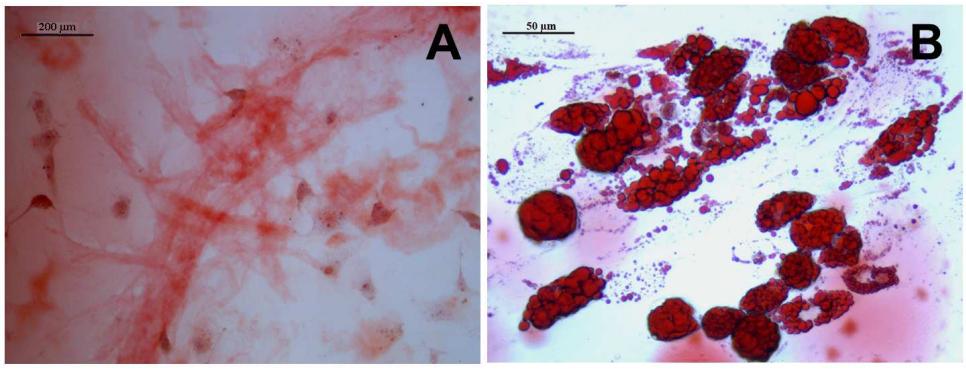


**Figure 66 : Light micrographs depicting differentiation ability of sADMSCs: A** - Osteogenic differentiation proved by alizarin red staining, **B** - adipogenic differentiation proved by oil red O staining (scale bar A= 200µm; B =50µm).

## 6.2. *In vitro* cytocompatibility and osteogenic efficacy assessment of the HA and SrHA scaffolds:

### 6.2.1. *In vitro* cytocompatibility assessment:

#### *6.2.1.1. Direct contact assay:*

Cytocompatibility of the scaffolds evaluated using direct contact assay indicated that sADMSCs proliferated well, post 48 hours of incubation with HA (figure 67A) and SrHA discs (figure 67B). The cells maintained their typical morphology and became confluent proving the non toxicity of these scaffolds.

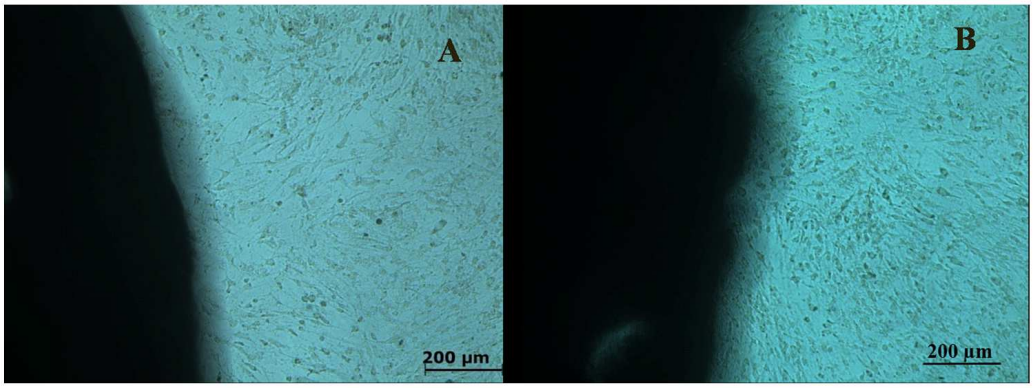


**Figure 67 - Cytocompatibility assessment of the scaffolds using sADMSCs:** Phase contrast micrographs indicating the cytocompatibility of **A**- HA, **B** – scaffolds in direct contact assay with sADMSCs (scale bar = 200 µm).

#### *6.2.1.2. Cell adhesion on disc scaffolds:*

sADMSCs were seeded on HA and SrHA scaffolds, osteogenically for 7 and 28 days and assessed using E-SEM. Scanning electron micrographs depicted cell adhesion on the HA and SrHA scaffolds post 7 days of culture 68A and 68C respectively). On day 28 cells proliferated and formed a canopy on surface of scaffolds HA and SrHA (figure 68B and 68D respectively).

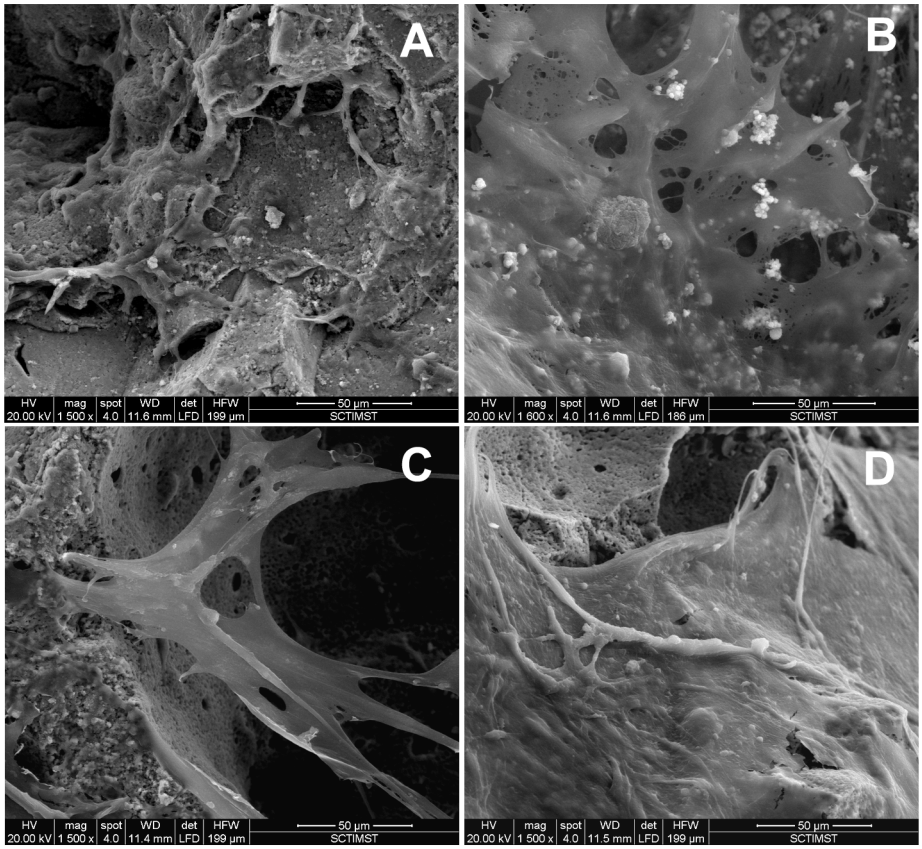


**Figure 68 - Cell adhesion on the scaffolds:** Scanning electron micrographs indicating cell adhesion on **A & C** – HA and SrHA post 7 days of culture; **B & D** HA and SrHA post 28 days of culture (scale bar = 50 µm).

### 6.2.2. *In vitro* osteogenic efficacy assessment:

Osteogenic efficacy assessed in terms of ALP activity indicated that both and SrHA scaffolds favoured *in vitro* osteogenesis (figure 69). But a higher level of ALP expression was exhibited by the cells seeded on HA scaffolds post 28 days of culture. In both scaffolds, ALP expression was seen to be post 21 days of culture. At 21 days cells seeded on HA expressed an ALP activity 24.5±1.9 µmol pNp/ 30 minutes, where as cells on SrHA expressed an activity of 20.08±.59 µmol pNp/ 30 minutes. HA scaffolds exhibited highest ALP activity at day 21, whereas SrHA scaffolds exhibited an increased ALP activity at day 14.

Statistical evaluation using 2way ANOVA indicated no significant difference in expression between the scaffolds at any time points. (p value : HA vs. SrHA day 0.9833, day 14 – 0.9873, day 21 - 0.0681, day 28 – 0.9899)

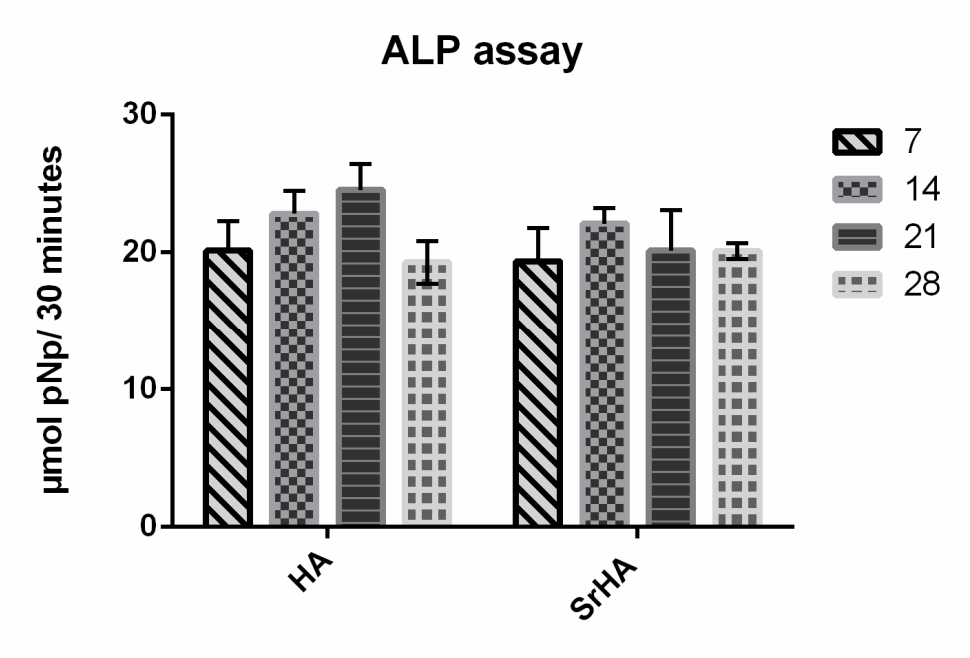


**Figure 69 – ALP activity of sADMSCs on HA and SrHA:** Biochemical based on ALP assay for 7,14,21 and 28 days indicated that HA scaffolds highest ALP activity at 21 days. SrHA seemed to exhibit highest ALP activity on 14 (p value HA vs. SrHA day 7 – 0.9833, day 14 – 0.9873, day 21 - 0.0681, day 28 0.9899).

## PART B - DEVELOPMENT AND EVALUATION OF SHEEP OSTEOPOROTIC MODEL

Part B includes the results of validation of the sheep osteoporotic model developed by ovariectomy and calcium deficient diet. Sheep model was assessed osteoporosis development post 10 months of induction.

## 6.3. Validation of sheep osteoporotic model:

### 6.3.1. Histology of excised tissue:

Post ovariectomy, the excised tissue was evaluated using histology (figure 70). H&E staining of the excised tissue depicted the presence of oocyte, growing follicle, atretic follicle etc, which in turn confirmed typical ovarian organisation cellular structure.

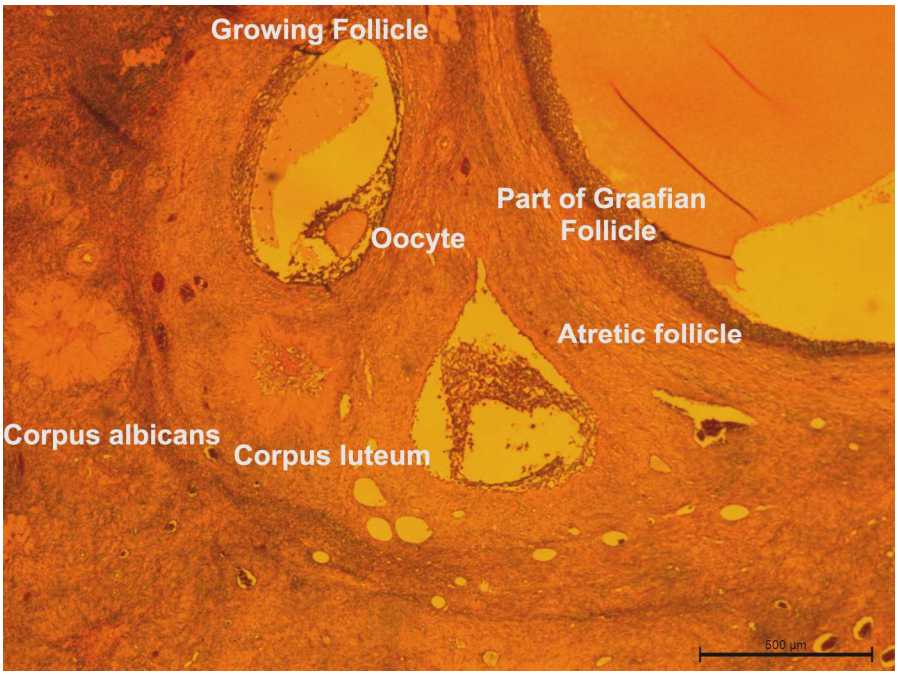


**Figure 70 - H & E stained micrograph of sheep ovary:** Histology images the presence of follicles in the tissue confirming the structural features of tissue (scale bar = 500µm).

### 6.3.2. Evaluation of trabecular bone loss:

Trabecular bone loss at the tibial epiphyses of the induced sheep models was qualitatively and quantitatively assessed using micro CT. 3D morphometry evaluation of trabecular volume in the distal epiphyses of tibia of induced model indicated appreciable amount of bone loss compared to age

control animals. Thickness profile (figure 71) of the trabecular bone at similar anatomical locations depicted bone loss in the induced model compared to animals. Large void spaces were seen from the proximal end towards the distal of the tibial bone. Presence of thicker trabecular bone in the control animals appreciated from the color coded images. Greenish yellow areas represent of thicker trabecular.

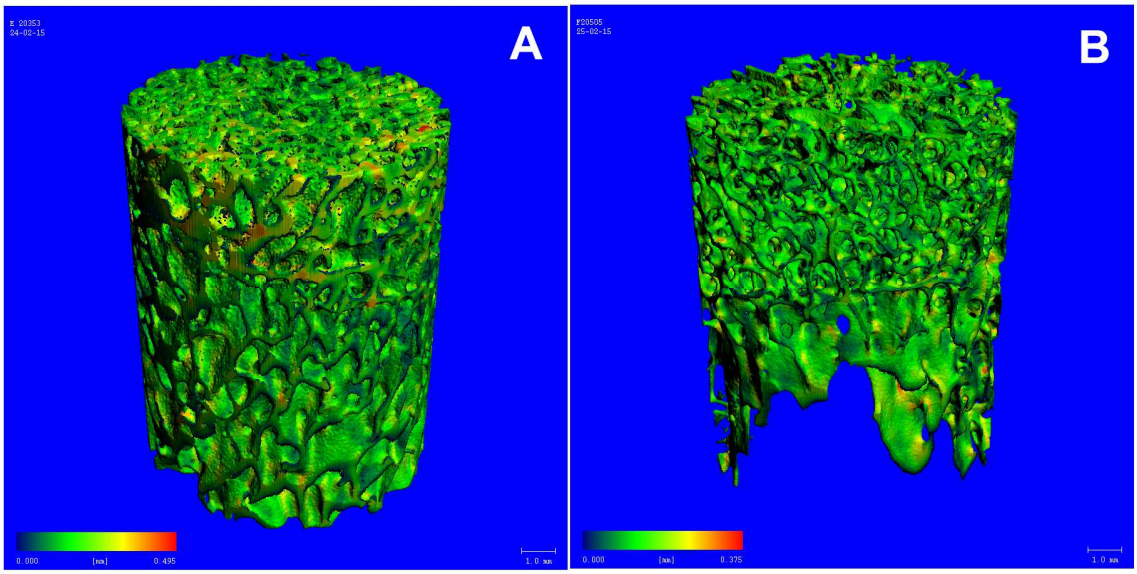


**Figure 71 -Evaluation of trabecular bone loss using 3D morphometry images: A & B** depict the 3D trabecular thickness of tibial epiphyses in control and induced sheep model. Extensive trabecular bone loss in the tibial region was at the proximal end of tibia in the induced model compared to control animal coding – trabecular thickness increases from green to red color) (scale bar =

Further, bone loss was estimated by evaluating the trabecular bone parameters like Tb.N., Tb.Sp. and Tb.Th. (figure 72). Induced model exhibited Tb.N. value of 0.64 (1/mm), whereas control animal exhibited a comparatively increased Tb.N. value of 1.51 (1/mm). Tb.Sp. increased to 1.62 (mm) compared control animals having a Tb.Sp. value of 0.66 (mm). Unlike the rat osteoporotic models, where no difference was found in the Tb.Th, in the osteoporosis induced

sheep model a decline in the Tb.Th. was also noted. Control animal had an trabecular thickness of – 0.19 mm, whereas the induced animal had a trabecular thickness of 0.13mm only. Bone density (trabecular) also decreased drastically the induced models, as the mean density in control animals were 257.91 (mg HA/ccm), compared to 76.79 (mg HA/ccm) in the induced models. Also control animals exhibited a Bv/Tv ratio of 0.2534, whereas the induced model exhibited low Bv/Tv ratio of 0.105.

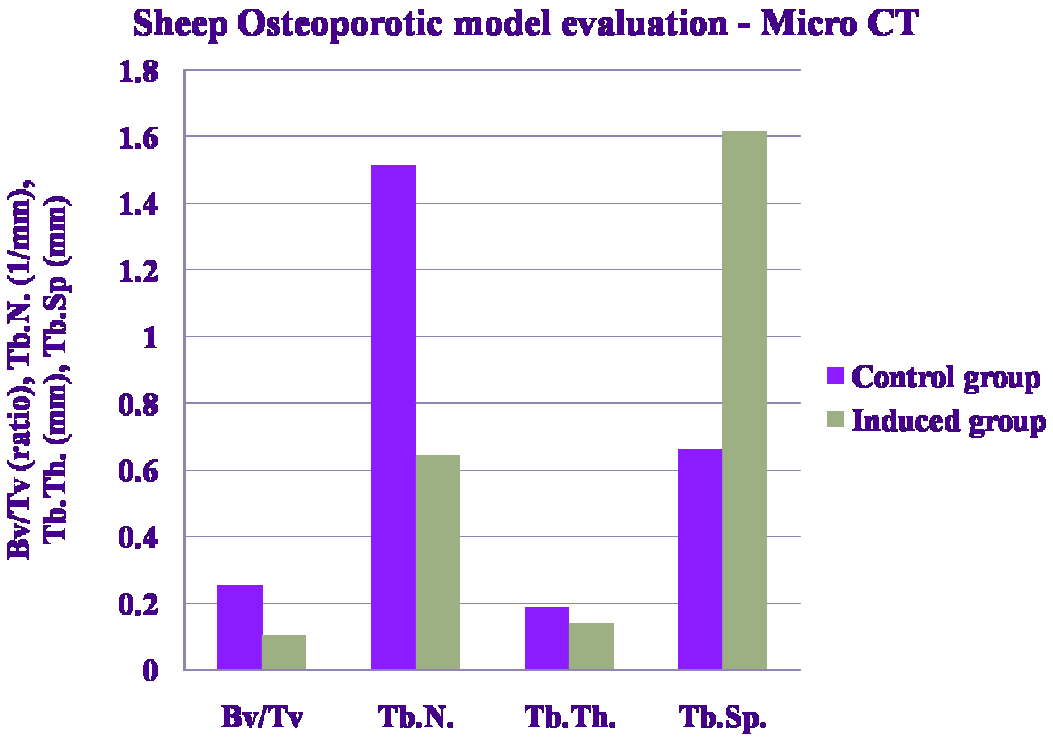


**Figure 72 – Evaluation of trabecular bone loss using micro CT:** Graphical representation comparing the Bv./Tv., Tb.N. (1/mm), Tb.Th. (mm) and Tb.Sp. in control and induced model.

### 6.3.3. Biochemical analysis of serum:

Biochemical analysis of serum was performed to evaluate serum calcium vitamin D level as markers for the onset of osteoporosis in the sheep model.

calcium concentration was 3.02±0.60 mg/dl before induction and with the onset osteoporosis, the level increased to 4.9±0.5 mg/dl, 6.48± 0.93 mg/dl and 6.17±0.86mg/dl post 3, 6, and 10 months respectively (figure 73).

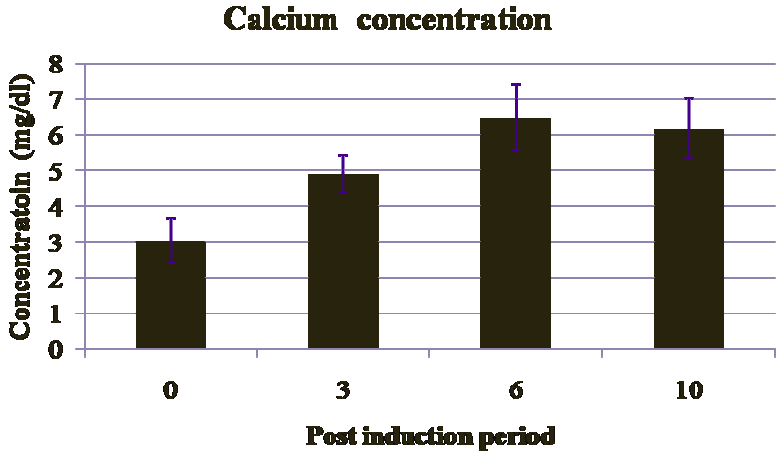


**Figure 73 – Biochemical evaluation of Ca in the serum of sheep osteoporotic model:** Serum Ca concentration increased with advancing induction period.

Meanwhile, vitamin D level in serum (figure 74) decreased, post 10 of induction. The induced model has a vitamin D cocentration of 35.75±3.74 whereas the age matchched control animal had 66±5.9 ng/dl.

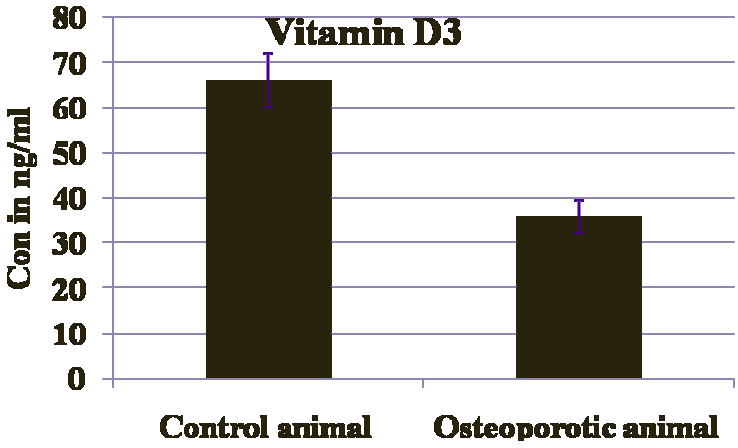


**Figure 74 – Biochemical evaluation of vitamin D in the serum of sheep osteoporotic model:** Vitamin D level seemed to decrease with increasing period.

# PART C - EFFICACY ASSESSMENT IN SHEEP OSTEOPOROTIC MODEL

## 6.4. Fabrication and *in vitro* characterization of cylindrical scaffolds:

### 6.4.1. Micro-structure and surface morphology:

Scanning Electron Micrographs of the cylindrical scaffolds – HA and depicted its 3D rough surface topography with interconnected pores.

### 6.4.2. Radiopacity evaluation:

Radiographic evaluation of SrHA cylindrical scaffolds (figure 75) an improved radiopacity equivalent to 0.98±0.2 mm thick aluminium, whereas exhibited radiopacity equivalent to 0.44±0.3 mm thick aluminium.


**Figure 75 - Radiopacity evaluation:** Radiograph depicts the radiopacity of HA SrHA scaffolds in comparison to aluminium wedge.

### 6.4.3. Cytocompatibility assessment:

#### *6.4.3.1. Cell adhesion on the scaffolds:*

Cell adhesion studies using DAPI staining (figure 76) indicated that the cylindrical scaffolds – HA and SrHA favoured cell adhesion. Nuclear stained fluorescent images depicted uniform distribution of sADMSCs on HA and scaffolds post 7 days of culture.

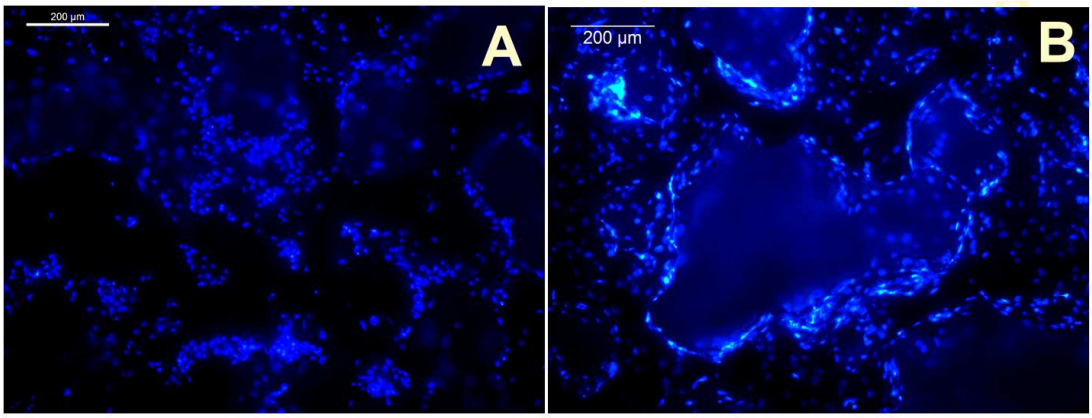


**Figure 76 - Fluorescent micrographs depicting cell adhesion and distribution:** DAPI staining depicted the sADMSCs to adhere on the surface of scaffolds **A** - and **B** - SrHA (scale bar = 200µm).

#### *6.4.3.2. Cell viability assessment:*

Post 7 days of culturing and prior to implantation studies representative constructs were evaluated using and live dead assay (figure 77). Fluorescent micrographs depicted the presence of live cells stained green which indicated viability of sADMSCs on the scaffolds.

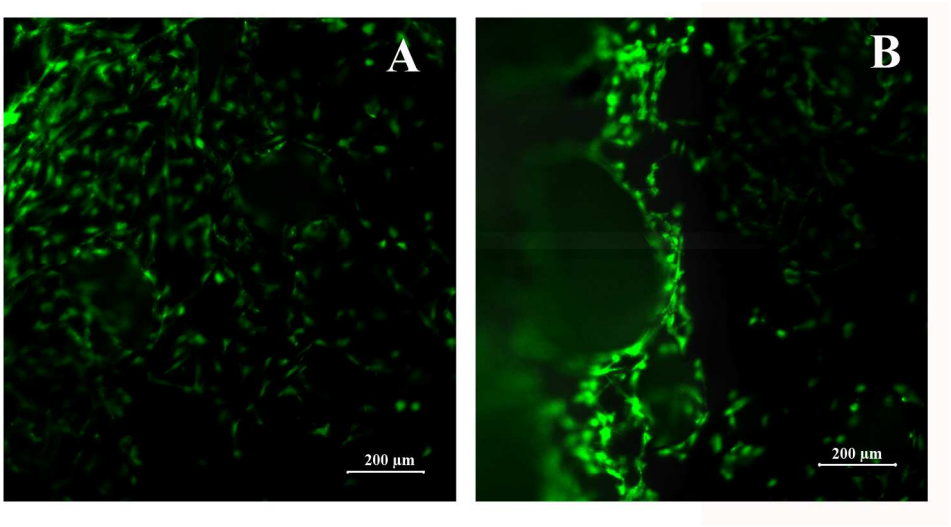


**Figure 77 – Evaluation of cell viability on the scaffolds:** Confocal laser scanning micrographs depicted viable cells on **A-** HA and **B -** SrHA scaffolds post 7 days culture (scale bar =200 µm).

## 6.5. Serum analysis for inflammatory responses post implantation:

Serum was collected from the animals before and after implantation at two weeks and two months of implantation to assess any inflammatory reactions associated with the implanted scaffolds (figure 78). It was noted from the haematology analysis that the WBC, lymphocyte and the eosinophil counts were within the reference range at all time points. But an exception of higher count of 73 was observed post one week of implantation, which later subsided to and 46 post two weeks and two months respectively.

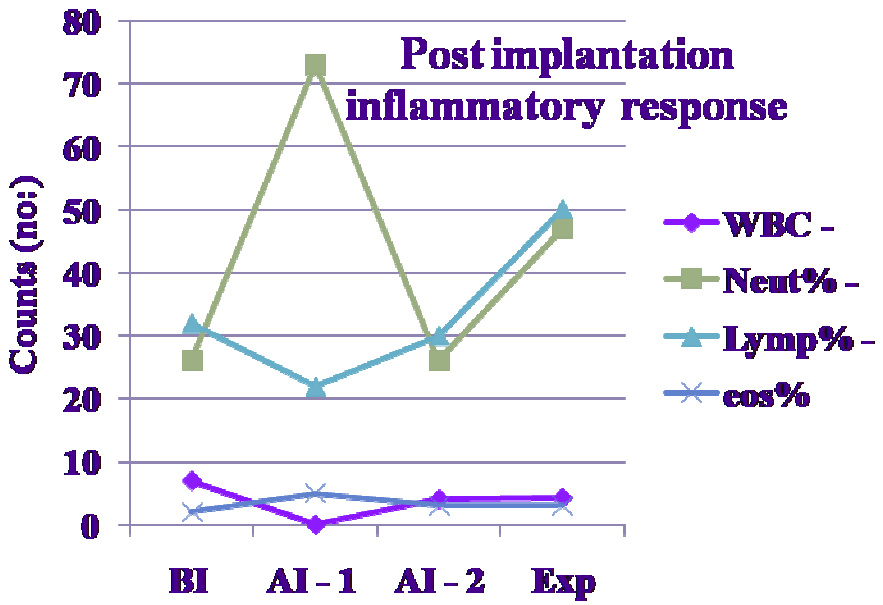


**Figure 78 – Evaluation of inflammatory responses post implantation:** Serum analysis done before (BI) and 1 week (AI-1), 2 weeks (AI- 2) and 2 months (Exp) post implantation indicated no acute inflammatory response in the implanted model.

## 6.6. Radiopacity of the implants *in vivo:*

Radiographic evaluation (figure 79) of the explants indicated that even two months of implantation, SrHA implants revealed an improved radiopacity equivalent to 0.67±0.01 mm thick aluminium, whereas HA implants exhibited a radiopacity equivalent to 0.46±0.01mm thick aluminium.

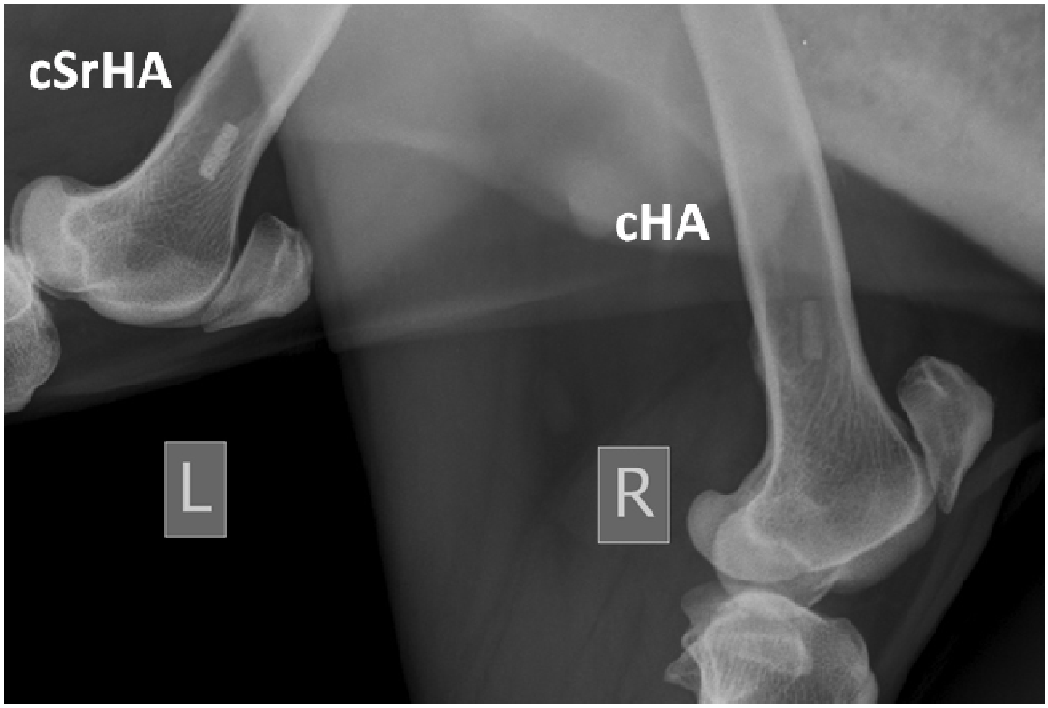


**Figure 79 -** ***In vivo*** **radiopacity evaluation of the implants:** Radiographs of cHA and cSrHA indicated the improved radiopacity of cSrHA scaffolds, post two months of implantation.

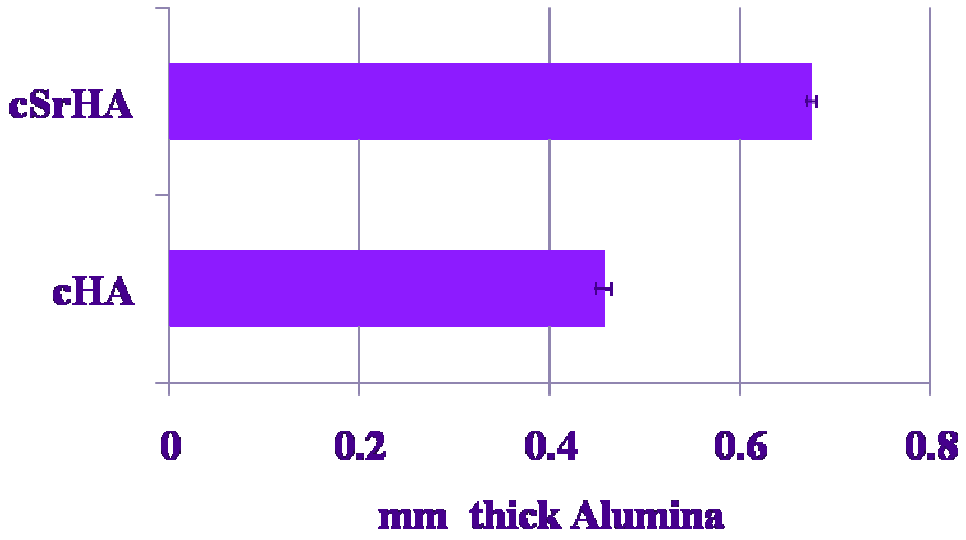


**Figure 80 – Quantification of Radiopacity of explants:** Image J analysis depicted improved radiopaque property of cSrHA implants compared to cHA.

## 6.7. *In vivo* osteogenic efficacy of tissue engineered implants:

### 6.7.1. Gross evaluation:

All animals survived the implantation procedures. Healing was and there was neither inflammation nor infection at the surgical site before killing of the animals post 2 months implantation. Gross evaluation of the further confirmed the absence of any fibrous tissue or inflammatory tissue area bone defect site.

### 6.7.2. Radiographic evaluation:

The osteointegrative ability of HA, cHA, SrHA and cSrHA implants was evaluated by close examination of host implant interface from the radiographs. month, *i.e.*, immediately after surgery, gaps between the implant and host bone well evident in the radiographs of HA, cHA, SrHA and cSrHA implanted press fit method was adopted for implantation procedure (figure 81A, 81D, 82A 82D respectively). One month post implantation, even though an improvement osteointegration ability was noted in all implant groups, HA & cHA implanted groups indicated clear zone of poor osteointegration (radiolucent areas marked arrows – figure 81B & 81E). But comparatively less radiolucent zones were appreciated around SrHA and cSrHA implants (figure 82B and 82E). Two post implantation, cSrHA became integrated with the host bone without any radiolucent zone at the host implant interface (figure 82F) and SrHA scaffolds exhibited an improved osteointegration with reduced radiolucent areas around implant (figure 82C). But in HA and cHA implanted groups, clear radiolucent still persisted post two months of implantation (figure 81C and 81F).

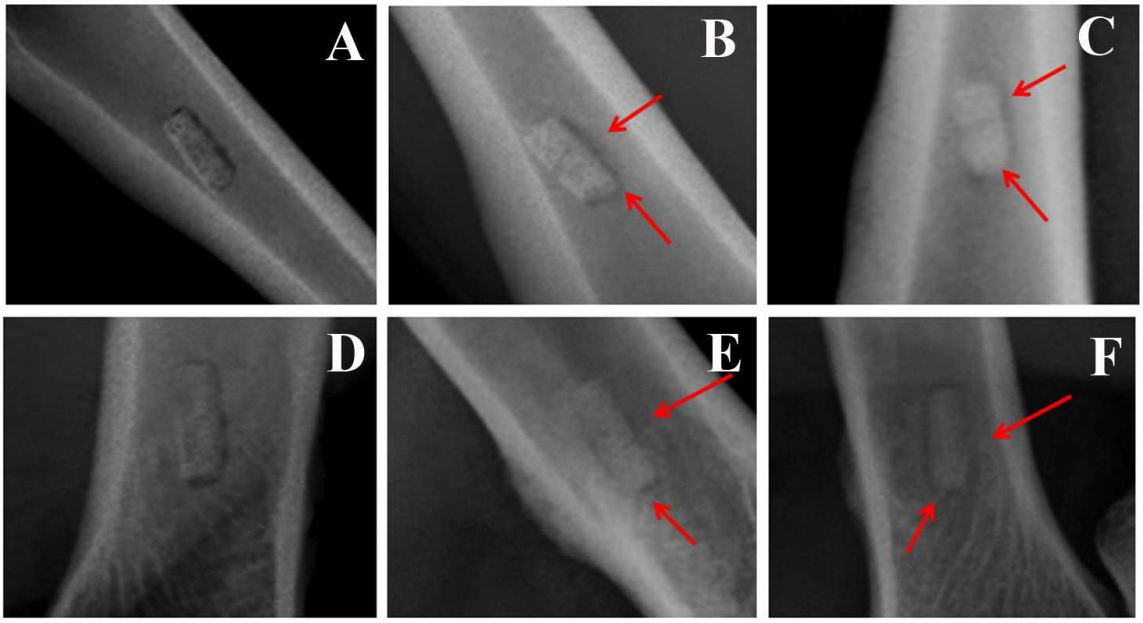


**Figure 81- Evaluation of osteointegrative ability of the scaffolds – HA & cHA:** Radiographs depict indicating the osteointegration ability post 0, 1, 2 months of implantation in HA **(A-C**) cHA **(D-F).** (Red arrow heads indicate poor osteointegration at bone implant interphase).

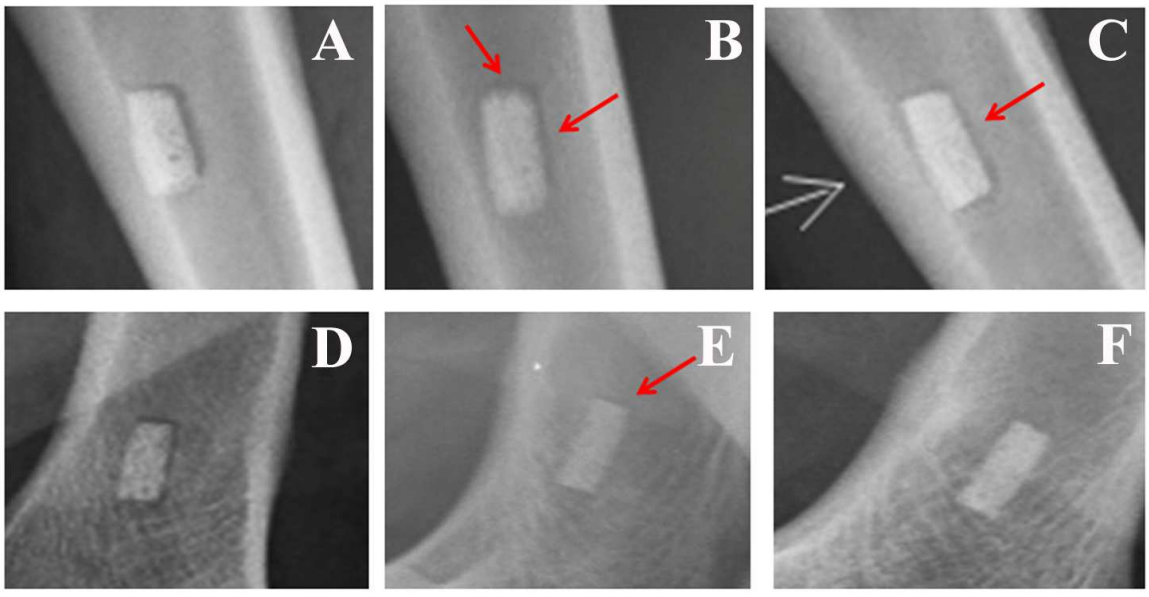


**Figure 82- Evaluation of osteointegrative ability of the scaffolds – SrHA & cSrHA:** Radiographs depict indicating the osteointegration ability post 0, 1, 2 months of implantation in SrHA **(A-C)** cSrHA **(D-F).** (Red arrow heads indicate poor osteointegration at bone implant interphase).

### 6.7.3. Histological evaluation:

Post implantation, undeclacified explants were evaluated by histology for their osteogenic efficacy and osteointegration. Stitched images of the Stevenal's & van Gieson's picrofuchsin stained plastic sections portrayed enhanced new formation in cSrHA implanted group (figure 83D) and the void spaces within cylindrical implants were almost filled with *de novo* bone (stained yellow). implants also lost its cylindrical morphology (material stained black), indicative its improved degradative property. Compared to bare material, an improved degradation was exhibited by the TE implants - cHA and cSrHA. Nevertheless implants (figure 83B) also exhibited improved osteogenesis within the pores of explant compared to bare HA and SrHA implants (figure 83A and 83C But HA implanted group exhibited the least osteogenic efficacy as large void could be identified with scarce osteoid formation and the retainment of morphology after two months of implantation indicates it poor degradative properties.

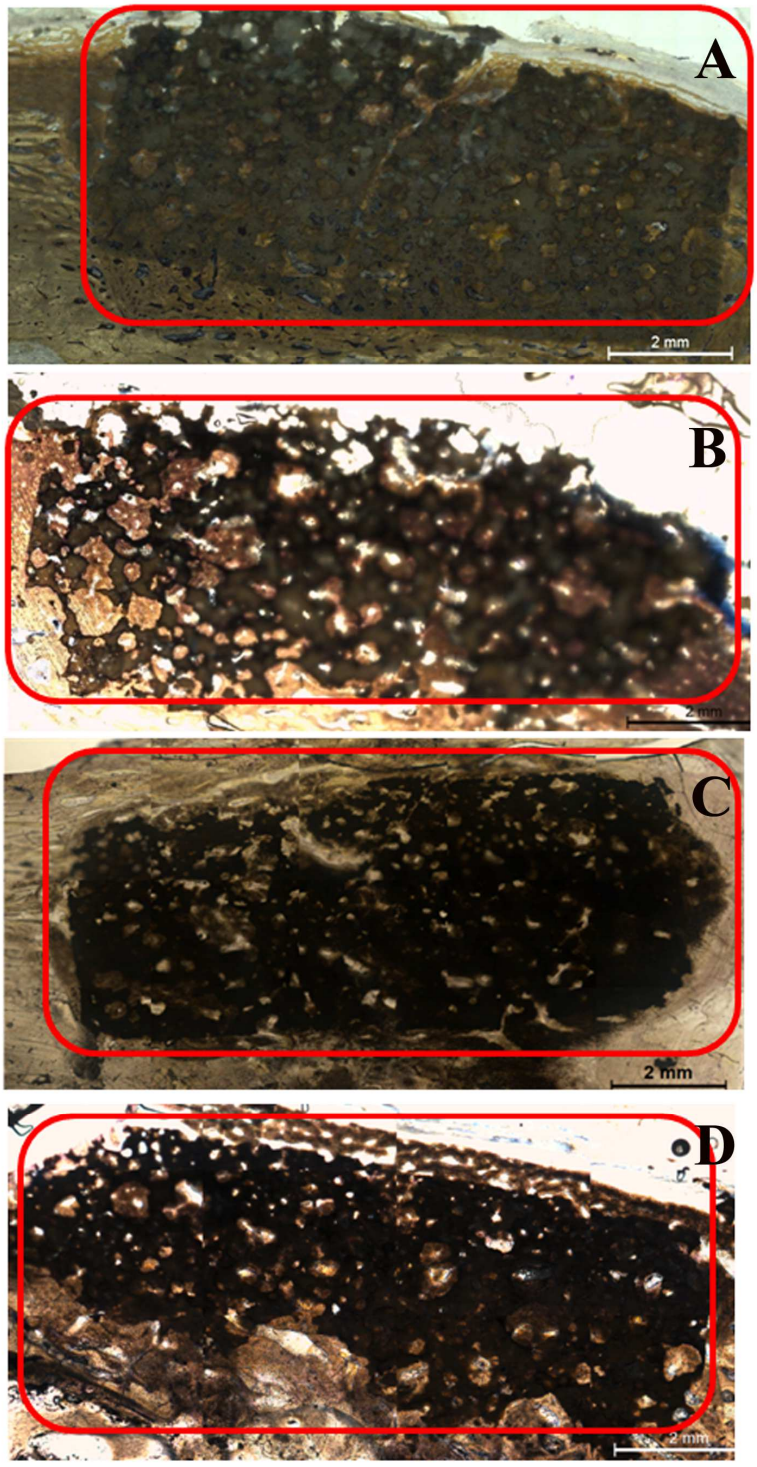


**Figure 83 - Histological evaluation of explants in sheep osteoporotic models: A, B, C & D** - stitched histology images of retrieved explants of HA , cHA, SrHA & cSrHA respectively, stained using Stevenal's Blue & van Gieson's picrofuchsin (scale bar = 2mm).

Detailed examination of the healing pattern across different implant groups were assessed from higher magnification histology sections. In HA implanted group (figure 84) the bone cells in the osteoid matrix were loosely arranged and distinct cellular infiltration zones (stained blue) were noticed. The cellular organisation depicted the initial phase of bone formation and hence exhibited early phase of bone healing. In cHA implanted group (figure 85) the defect area exhibited improved osteogenesis and the deposited new bone cells were seen to be arranged in line with other bone cells, but complete lamellar arrangement could not be appreciated from the histology images.

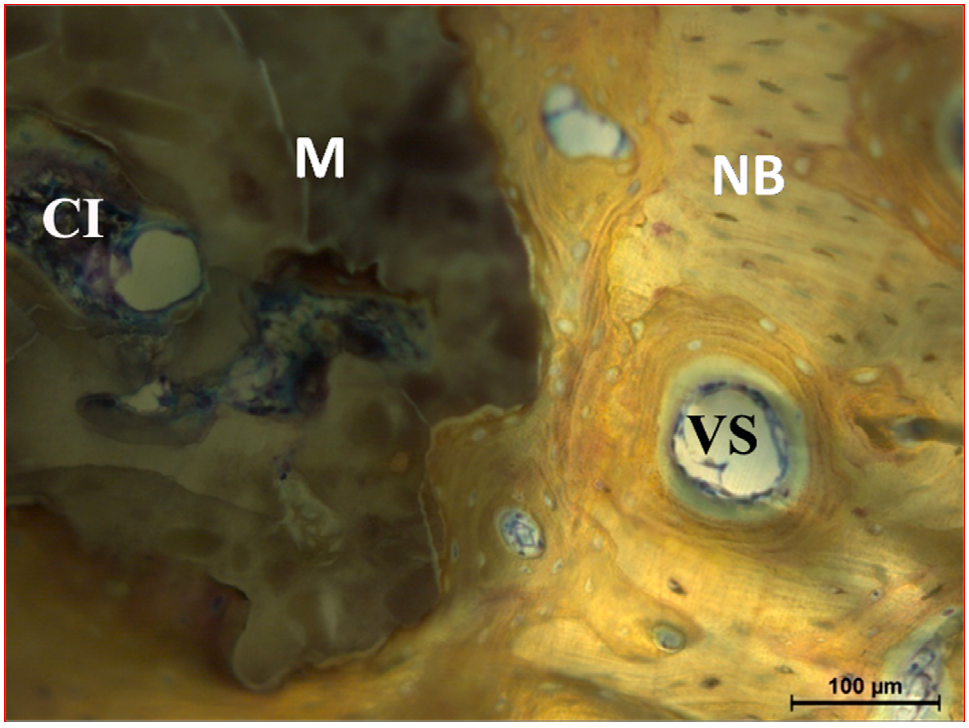


**Figure 84 - Histological evaluation of retrieved explants of HA:** Stevenal's Blue & Van Gieson's stained plastic embedded sections depicting the beginning of lamellar organisation in HA implanted group along with cellular infiltration. New Bone, **M** – Material remnant, **CI** – Cellular Infiltration, **VS** – Void Space) (scale bar = 100µm).

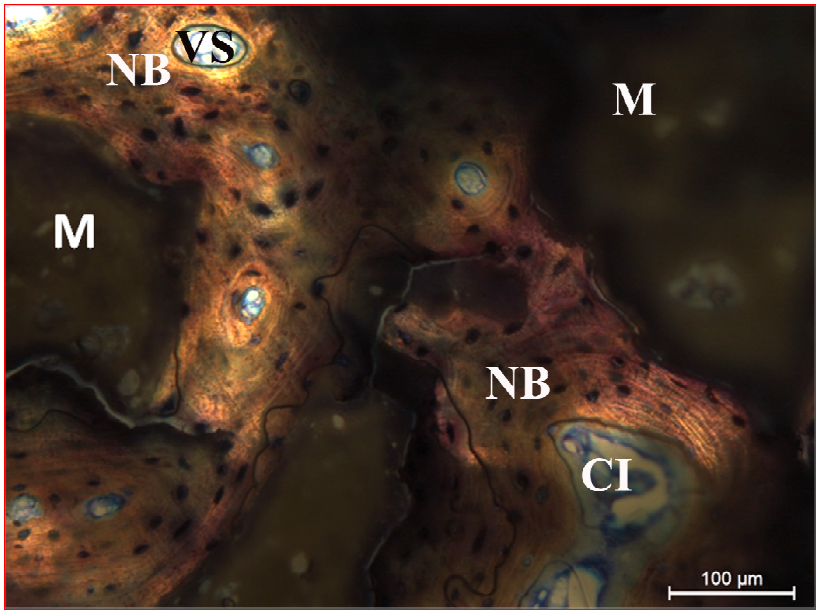


**Figure 85 - Histological evaluation of retrieved explants of cHA:** Stevenal's Blue & van Gieson's stained plastic embedded sections depicting the beginning of lamellar organisation. (**NB** – New Bone, **M** – Material remnant, **CI** – Cellular Infiltration, **VS** – Void Space) (scale bar = 100µm).

A detailed examination of the histology sections at higher magnification indicated improved bone formation with mature bone like organisation in cSrHA implanted group (figure 87). Moreover *de novo* bone formed, exhibited mature bone like morphology in cSrHA implanted group, as the newly formed bone cells were seen arranged in concentric rings of lamellae forming individual osteons, resembling Haversian organisation. In SrHA implanted group (figure 86), loosely arranged bone cells in the osteoid matrix leading to lamellar arrangement was noticed. Nevertheless prominent number of lamellar organisations was observed in cSrHA implanted group compared to SrHA implanted group.

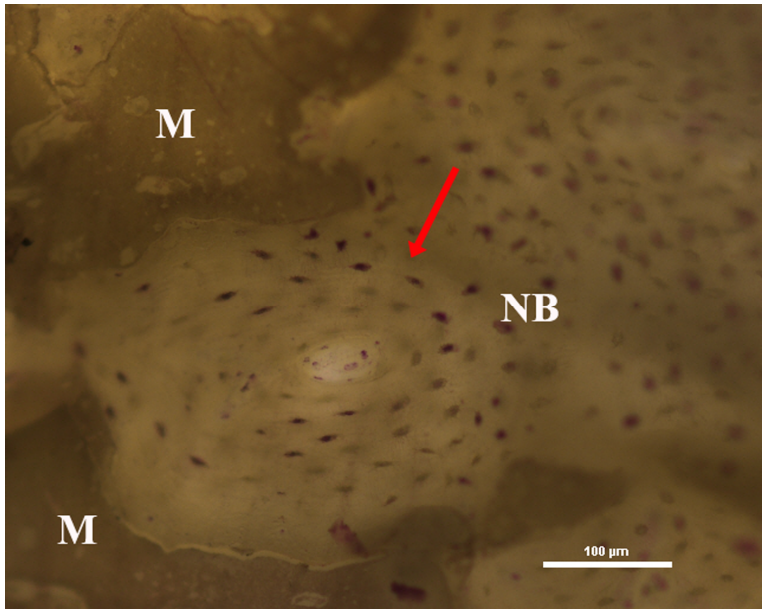


**Figure 86 - Histological evaluation of retrieved explants of SrHA:** Stevenal's Blue & van Gieson's stained plastic embedded sections depicting the formation of lamellar organisation (red arrow head) resembling mature bone like organisation. (**NB** – New Bone, **M** – Material remnant) (scale bar = 100µm).

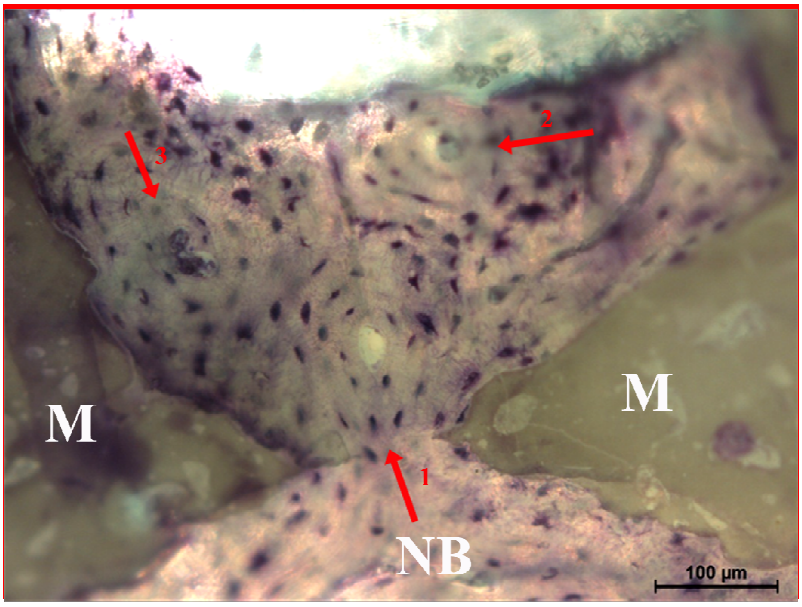


**Figure 87 - Histological evaluation of retrieved explants of cSrHA:** Stevenal's Blue & van Gieson's stained plastic embedded sections depicting complete (arrow 1, 2) and early phase of (arrow 3) lamellar organisation with mature bone like morphology. (NB – New Bone, M – Material remnant) (scale bar = 100µm).

### 6.7.4. Histomorphometry:

Osteogenic efficacy in terms of regeneration efficiency (RE) ratio (New bone formed per total defect area) of the implant materials – HA, cHA, SrHA and cSrHA was assessed by histomorphometry (figure 88). Statistically significant increase in *de novo* bone formation was evident in the cSrHA implanted group since they exhibited the highest RE ratio (New bone/Total defect area) of 0.52 ± 0.05 (p value - 0.006), followed by cHA implanted group having a RE ratio of 0.37± 0.06 (p value - 0.073). SrHA implanted group exhibited a RE ratio of 0.27±0.02 (p value - 0.840) and HA implanted group exhibited the least regeneration efficiency of 0.24±0.04.

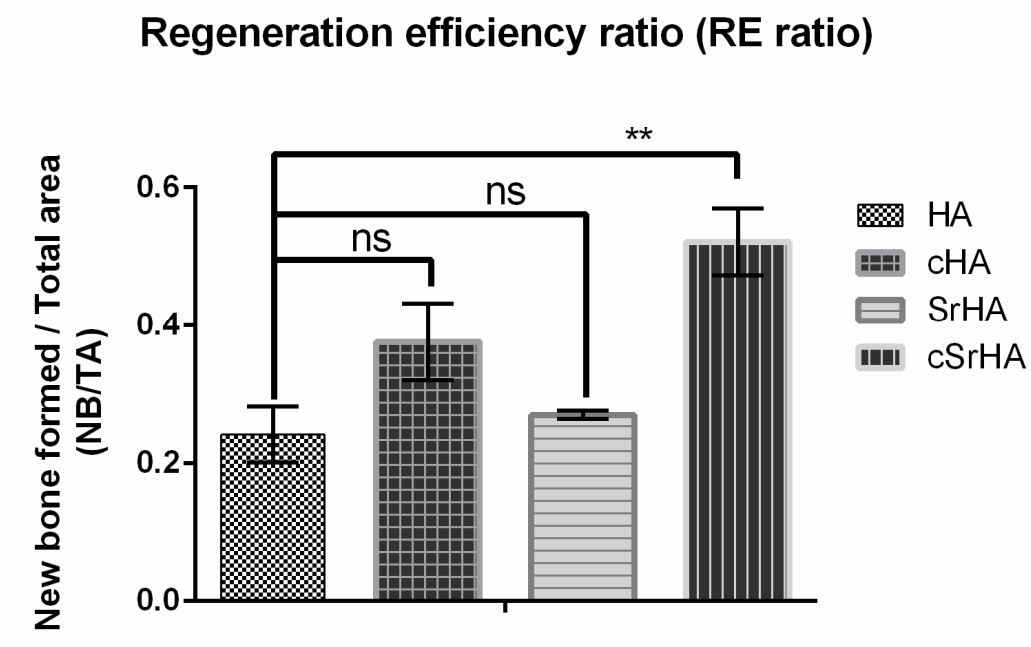


**Figure 88 – Histomorphometry analysis of the explants in terms of Regeneration Efficiency (RE):** RE ratio of HA, cHA, SrHA and cSrHA post 2 months of implantation in sheep model (p value – HA vs. cHA – $^{ns}$0.073; HA vs. SrHA – $^{ns}$0.840; HA vs. cSrHA - ** 0.006).

Material resorption ability (figure 89) was assessed in terms of material remnants per total defect area. Improved degradation ability was evident in the

cSrHA implanted group as they exhibited a MR/TA ratio of 0.36±.05 compared other implant groups HA, cHA and SrHA with MR/TA ratio of 0.68±0.03, and 0.75±0.03 respectively. Compared to HA implanted group, cSrHA group exhibited a statistically significant improvement in the resorption value - 0.005), whereas cHA exhibited an improved but non significant property.

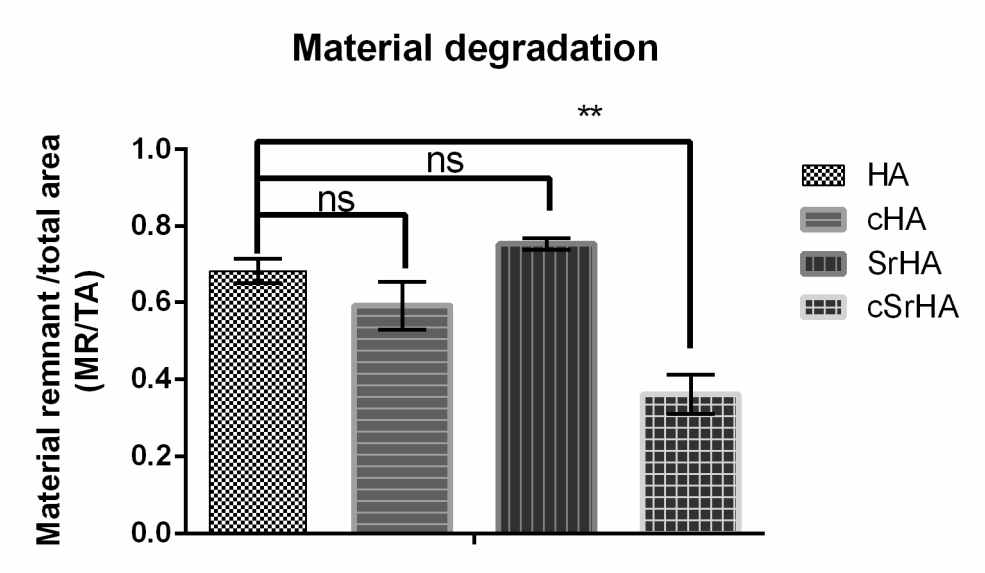


**Figure 89 – Histomorphometry analysis of the explants in terms of material remnants per total area (MR/TA):** Degradation ratio of HA, cHA, SrHA and cSrHA post 2 months of implantation in sheep model (p value – HA vs. cHA – $^{ns}$ 0.319; HA vs. SrHA – $^{ns}$0.559; HA vs. cSrHA - ** 0.005).

**6.7.5. Micro CT evaluation:**

3D morphology (figure 90A, B, C & D respectively) of the implants – HA, cHA, SrHA and cSrHA was evaluated using micro CT to assess the placement implants at the defect site and evaluate osteointegration. It was evident from the morphometry images that all implants became osteointegrated with the host establishing a bonding between host bone and the ceramic implant. Cylindrical

defect area (pointed by red arrow head) with the intact implant material was evident in the material alone implanted groups, even though not much evident TE implanted groups, especially in cSrHA implanted group.

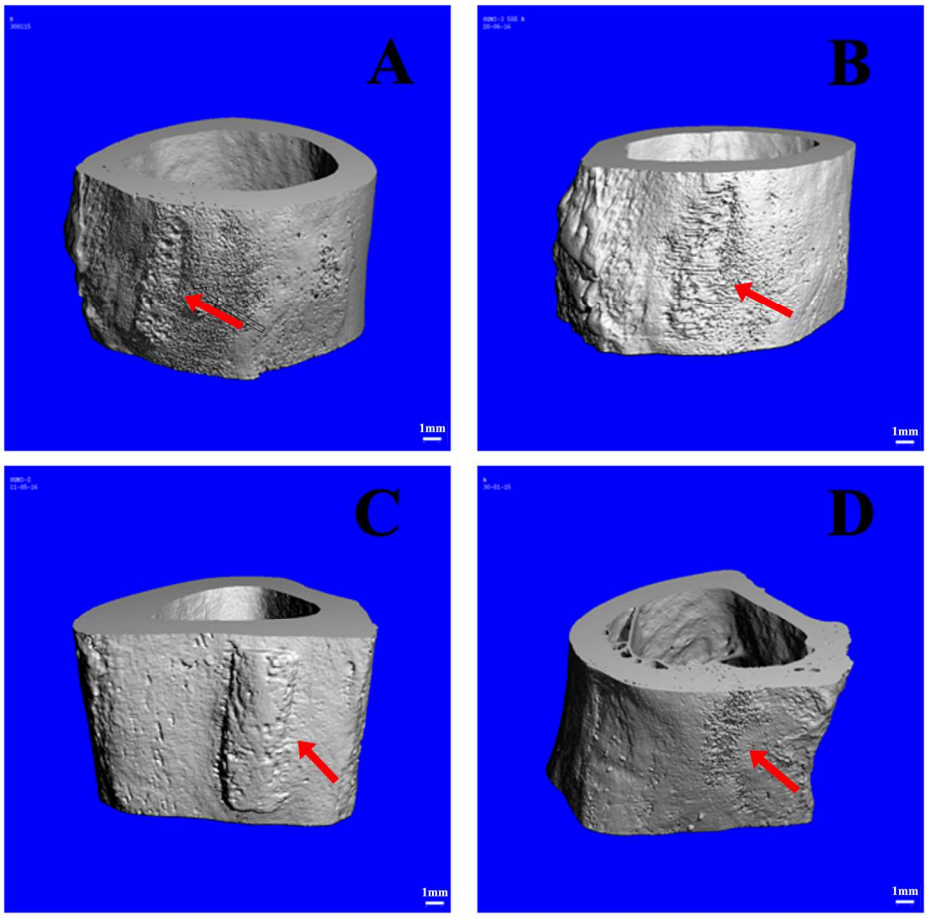


**Figure 90 – 3D morphology of the implants in sheep model:** Micro CT depicted the osteointegration of HA (**A**), cHA (**B**), SrHA (**C**) & cSrHA (**D**) post 2 months of implantation (red arrow pints towards the cylindrical bone area) (scale bar = 1mm).

Osteointegration ability of HA, cHA, SrHA and cSrHA implants was assessed using 2D slices and their corresponding density histograms generated micro CT. Representative 2D slices from HA, cHA, SrHA and cSrHA implanted groups (figure 91 A, C, E &G) confirmed the establishment of physical contact

between the implant and host bone in all groups. Evaluation of osteointegration ability in terms of bone density at the host bone implant interphase indicated even though physical contact was evident in all groups. In HA implanted group (figure 91B) bone density at the implant interphases was low compared to that host bone, whereas in SrHA implanted group (figure 91F) a comparatively bone density was observed at one of the interphase. The groups with the tissue engineered implants – cHA and cSrHA (figure 91D & H respectively), exhibited almost a comparable bone density with that of the host bone at both the indicative of the significance of cells in osteointegration

Density of the new bone formed within the pores of the material was compared to assess the osteogenic efficacy of each implant. It was interesting to that the *de novo* bone formed within the pores of SrHA and cSrHA exhibited an improved bone density compared to that of HA implants. Poor bone density was exhibited by the *de novo* bone formed within the pores of HA implants, whereas the cHA implanted group a comparable bone density with that of the host bone depicted. The results hint towards the improved osteointegrative and osteogenic efficacy of the strontium incorporated tissue engineered scaffolds.

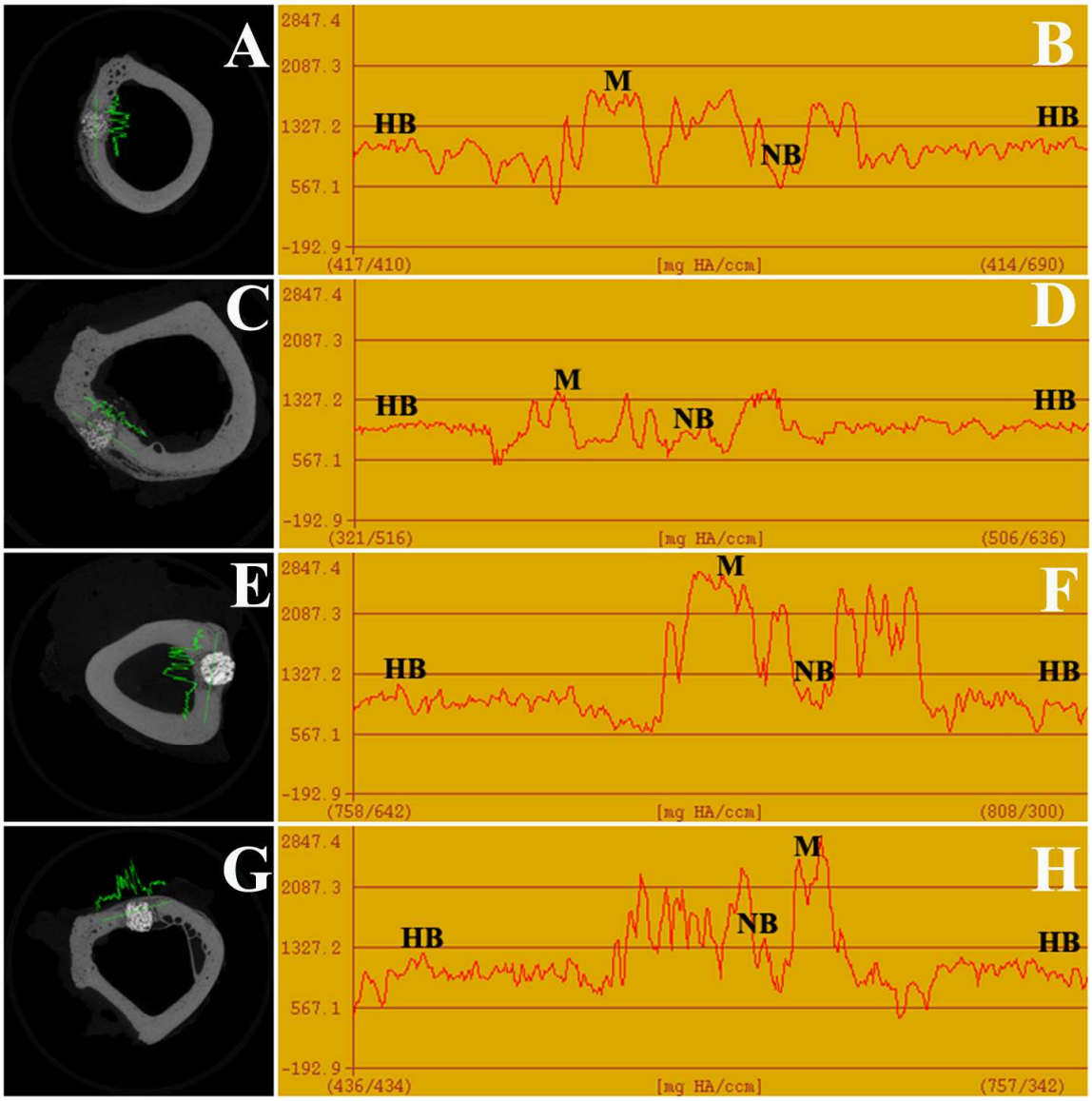


**Figure 91 – 2D slices and corresponding density histograms of the implants in sheep model: A, C, E & G** – 2D slices depicting osteointegration in HA, cHA, SrHA & cSrHA implanted group respectively, post two months of implantation. **D, F & H –** Corresponding density histograms depicting bone density (mg distribution across the bone defect site in HA, cHA, SrHA & cSrHA group respectively (**HB**- Host Bone, **NB**- New Bone, **M** – Material).

# CHAPTER 7

# DISCUSSION

Chapter 7 – Discussion of the results presented in Chapter 4, 5 and 6 interpretations and correlations to published literature. Significance of the also suggested intermittently to bring out the relevance of this work.

Chapter 7 is divided into three phases:-

**PHASE I - MATERIAL CHARACTERIZATONS**

**PHASE II– *IN VITRO* & *IN VIVO* STUDIES USING rBMSCs IN RAT OSTEOPOROTIC MODEL**

**PHASE III – *IN VITRO* AND *IN VIVO* STUDIES USING sADMSCs IN SHEEP OSTEOPOROTIC MODEL.**

# PHASE I - MATERIAL CHARACTERIZATONS

## 7.1. Scaffolds of choice for the study:

An ideal scaffold for orthopedic application should serve as a structural functional framework for the uniform distribution of host cells throughout its dimensional lattices, facilitating easy transportation of signaling molecules / chemokine factors to favor tissue in-growth (Kosuge *et al.,* 2013). HA has been proven to have inherent osteoconductive nature and possess the additional that variations in its lattice and morphology help in ionic substitution – like Si, F, Cl, Sr etc in HA (Ni *et al.,* 2012). Therefore HA was chosen as a delivery vehicle to aid controlled delivery of therapeutic ions at desired concentration at fracture healing site.

Synthetic HA powders may be produced by a variety of ceramic routes such as wet precipitation, sol-gel technique, combustion synthesis, hydrothermal synthesis, solid state reaction etc. Wet precipitation is widely used the synthesis of stoichiometric hydroxyapatite in bulk level because of low temperature, high yield and inexpensive equipment requirement (Sureshbabu 2012). In wet precipitation method, a homogenous dispersion/solution of is reacted with stoichiometric amount of phosphate solution to cause the of hydroxyapatite.

Bioactive glass systems are reported to be much more bioactive and than pure hydroxyapatite and are also proved to bind with soft tissue (Nair *et* 2009b). Supplementation of Si has been reported to improve BMD in men and menopausal women (Jugdaohsingh *et al.,* 2004). Silica incorporated bioglass has

proved to form a strong bonding at the implant interphase by formation of HA on their surface, indicative of its improved osteointegration ability (Hench, Silicon incorporation improves collagen deposition and mineralization ability contributing to improved osteointegrative ability and is osteoconductive in This may prove to be beneficial in improving the osteointegrative ability in osteoporotic patients. In the present study HASi scaffolds were fabricated by state reaction between the calcined HA scaffolds and silica sol. The amount of sol incorporated into the HA scaffold was so adjusted that it will not convert HA completely into TCP – wollastonite composite, but forms a triphasic system comprising HA-TCP- wollastonite. HASi scaffolds are chemically a bioactive system consisting of hydroxyapatite, tricalcium phosphate and wollastonite *al.*, 2008).

Strontium is reported to prevent the bone resorption activity of mature osteoclast by regulating the calcium sensing receptors (Canalis *et al.,* 1996). The chemical similarity between Ca and Sr helps in the development of SrHA of Ca replacement by desired concentration of Sr (Donazzon *et al.,* 1998). role of in-house developed Sr (50%) incorporated HA scaffolds in were evident from the *in vivo* studies in rabbit ulna defect model (Beena *et al.,* Post 12 weeks of implantation in critical-sized (1.5 cm) rabbit ulna defect model 50% Sr incorporated HA exhibited improved bone formation on par with resorption. High concentration of Sr substitution in HA, is reported to alter the crystallinity of HA (Qiu *et al.,* 2006a). It has been reported earlier that up to incorporation does not affect the physiochemical properties of HA (Li *et al.,* But a lower concentration of 1-10% has been suggested as the optimum

concentration in which Sr can be incorporated in HA, to exert its therapeutic inhibiting osteoclast activity and simultaneously promoting osteoblast (Zhang *et al.*, 2010). Sr incorporation is anticipated to improve radiopacity too may aid in better *in vivo* tracking and implant imaging for assessing bone regeneration (López *et al.*, 2014). 10% strontium incorporated HA is thus exhibit all physcio-chemical properties of HA and hence *in vitro* and *in vivo* osteogenic efficacy of the 10% SrHA scaffold was evaluated in the present

Prior to the evaluation of the biological performance of modified HA, it important to evaluate how each modification has affected the physiochemical properties of HA.

## 7.2. Physicochemical characterizations of scaffold materials:

One of the crucial aspects to be considered for orthopedic scaffolds is its surface property, as the surface is the first point of contact for the host following implant placement. The Scanning Electron Micrographs depicted the surface topography of the material to be uneven, rough and micro-porous in It has been suggested that implant materials with a rough and uneven topography induce three-dimensional growth and differentiation of cells osteogenic lineage by activation of several osteogenic-associated genes like collagen, alkaline phosphatase, osteonectin, osteopontin etc (Karageorgiou and Kaplan, 2005).

Porosity of the scaffold material also influences the osteogenic and osteointegrative property of implants. Scaffolds with increased porosity are to favor cell proliferation and bone in-growth, whereas scaffolds with lower

favor improved ALP activity and express more osteocalcin (Takahashi and 2004). Normal bone Haversian system is estimated to be 100-200 µm in and so it is suggested that scaffolds for orthopedic application should also fall this range, to exhibit optimum activity *in vivo* (Hulbert *et al.*, 1970). Micro CT emerged as a powerful tool to characterize ceramic scaffolds in terms of related architectural parameters, density etc (Bertoldi *et al.*, 2011). It was from the micro CT evaluation that HA and HASi scaffolds exhibited a pore size ranging from 150-200 µm with an average porosity of 30-35%. It has been that ceramic scaffolds with 150-220 µm porous scaffolds and 36% porosity with rabbit MSCs improved bone formation in nude mice ectopically (Chen *et* 2002). Similar results may be expected from the in-house developed ceramic scaffolds too. Sr incorporation in HA has decreased the porosity of SrHA and the average pore size was noted to be 80-100 µm. A minimum pore aperture diameter of 100 µm has been proven sufficient for an *in vivo* to encourage neo-vascularization that is required for initiation of bone (Hench and Jones, 2005). Degradation rate of scaffolds is also dependent on its porosity. So HASi scaffolds with high porosity are expected to exhibit an degradation rate.

Phase identification of the manufactured scaffolds using XRD helped in evaluating the medical application of materials. The crystalline phases present the degree of crystallinity influence the osteointegration and degradation ability the scaffolds. The narrow XRD pattern of the in-house developed HA scaffolds indicated high level of crystallinity of the apatite phase. Crystalline exhibit the slowest degradation compared to other amorphous hydroxyapatites

and Liu, 2008), limiting its orthopaedic application to a certain extent. HASi exhibited crystalline nature, but the crystallinity was less when compared to XRD pattern of HASi depicted the presence of three phases- apatite, tri calcium phosphate and wollastanite (Calcium Silicate). It is assumed that during coating of HA by sol gel dipping, silicate ions may have entered into some of sites of phosphates ions in HA and the process may have accompanied the of silicate with calcium ions to form calcium silicate phase. Again, this may have also reduced the Ca or Ca /P content in the material that the formation of TCP phase (Nair *et al.,* 2009b).

XRD pattern of 10% SrHA was very similar to that of HA, which imply Sr substitution in HA by 10 mol% Ca replacement did not induce any phase in HA. Thus, SrHA may exhibit almost similar physcio-chemical characters of the optimum scaffold for orthopedic applications. It was also mentioned that Sr incorporation by more than 15% affects the crystallinity of SrHA, wherein the monoclinic system would change to rhombohedral (Li *et al.,* 2007). This further supports the rational of our study in choosing the lower concentration of Sr for substitution in HA. Slightly broader crystalline peak of SrHA compared to HA indicative of its amorphous nature which may further increase its dissolution favor nucleation and apatite formation (Christoffersen *et al.,* 1997). Change in crystallinity may be due to the replacement of $Ca^{2+}$ in HA with $Sr^{2+}$, which is larger atomic radius.

The FTIR spectra showed the characteristic absorption band the functional groups present in each scaffold. HA scaffolds demonstrated

characteristic peaks for phosphate and hydroxyl groups (Walters *et al.,* 1990). Phosphate and silicate groups shared similar spaced vibrational modes due to structural similarity, and hence it was difficult to differentiate their peaks from spectra. It has been suggested that Silica ions gets incorporated as silicate ions onto phosphate sites in the HA lattice in HASi and the charge is maintained the loss of hydroxyl ions (Gibson *et al.,* 1999), which was evident from the weak intensity of hydroxyl group in the FTIR spectrum of HASi. The FTIR spectra of and SrHA exhibited different but comparable modes of molecular vibration characteristic of the apatites. However, the intensity of $OH^-$ bands at 3571 and $cm^{-1}$ seemed to be diminished due to the incorporation of Sr as already reported (Beena *et al.,* 2013).

Radiopacity is typically a clinical requirement for monitoring the and progress of implant aided healing *in vivo* (López *et al.,* 2014). Strontium and strontium chloride have been investigated for use as radio pacifiers for applications (Alkhraisat *et al.,* 2008). In addition to its reported therapeutic role regulating the osteoclast cells, incorporation of strontium fluoride or strontium chloride in smaller amounts has proven to improve the radiopacity of calcium phosphate based scaffolds.

Radiographical evaluation and micro CT studies proved the improved radiopaque property of in-house developed 10% Sr incorporated HA scaffolds. Increasing Sr concentration aid in improving the radiopacity of HA scaffolds *et al.,* 2013). However, in the present study the scaffolds are being tested for its application in osteoporotic condition; where the up regulated osteoclast cells

be regulated to aid osteogenesis and osteointegration. So far reported literatures suggest 1-10% Sr incorporation to regulate the osteoclast activity favorably. in the present study, the upper limit value of 10% Sr incorporation was chosen, to incorporate the dual characteristics of anti-osteoclastic activity and single scaffold.

## 7.3. Assessment of degradation ability – *in vitro* studies in PBS:

*In vitro* degradation ability was estimated in PBS to evaluate the release ions from the scaffolds. Highest Ca release was exhibited by HASi scaffolds, indicative of its high degradation ability which is concurrent with the XRD Amorphous nature of HASi scaffolds might have contributed to the increased dissolution property. Again, SrHA exhibited improved degradation ability to HA, which may be attributed to the Sr incorporation in the scaffold. Landi *et* has reported from their *in vitro* studies that Sr and Mg incorporated HA micro-granules exhibited an increased dissolution rate with the release of ionic (Landi *et al.,* 2013). HA scaffolds exhibited the least Ca release profile, its poor resorption properties.

ICP studies indicated that with the advancement in the incubation there was a steady increase in the concentration of Si released from HASi. This be attributed to the increased degradative property of the HASi scaffolds as from its Ca release profile. Gentlemen *et al.,* 2010 has also proved using ICP that release of Si from bioglass increase with incubation time. Human cultures treated with ionic dissolution products from bioactive glass (BG) has reported to increase collagen-I synthesis and enhance osteoblast differentiation

(Gupta *et al.*, 2010). Similar results may be expected from in-house developed scaffolds too.

ICP analyses also confirmed a stable release of Sr - 0.01µg (equivalent to 0.11 mM per mg) from SrHA scaffold. Schumacher *et al.*, (2013) has that release of 0.001–0.1 mM may be sufficient enough to regulate bone favourably, so as to exert its therapeutic role in osteoporosis pathology. Since a similar Sr release pattern could be attained using the in-house developed 10% *in vitro*, it is expected that SrHA scaffolds may exhibit a similar release pattern *vivo* too thereby promoting bone healing with controlled bone remodelling. Administration of Sr in the form of strontium carbonate (orally) at a very low 6.8-8 mmol Sr/day that is 0.11–0.13 mmol Sr/kg/day for an osteoporotic person 60kg body weight stimulated endosteal bone formation (Marie *et al.*, 2001). Therefore it is anticipated that if oral administration improved bone formation osteoporotic patients by 6 months, local delivery of same concentration of Sr at fracture healing site may help in better bone formation at a much earlier stage, facilitating faster rehabilitation in the osteoporotic subjects.

## 7.4. Evaluation of *in vitro* apatite formation ability in SBF:

*In vitro* bioactivity of scaffolds in SBF is an indirect indicator of its osteointegration ability *in vivo* (Kokubo and Takadama, 2006). It is well that the ability to form a bone-like apatite layer on the surface of scaffold plays important role in forming chemical bond between the implant and the living tissue (Ni and Chang, 2009). In this respect, all the scaffolds in this study formation of apatite layer as evident from the Scanning Electron Micrographs,

indicating that the surface is bioactive. The proposed mechanism of apatite has been well explained by Hench based on bioactivity of Bioglass in SBF and Paschall, 1973). He suggested that when immersed in SBF, rapid ion of alkali and alkaline-earth cations present in the scaffolds with $H^+$ or $H_3O^+$ SBF solution occurs, followed by loss of soluble silica $Si(OH)_4$. Later $SiO_2$-rich formed on the scaffold surface provides sites for phosphate nucleation growth of amorphous calcium phosphate followed by crystallization to form

Apatite formation is facilitated by the substitution of carbonate group at positions of hydroxyl groups. Hence to assess the apatite formation ability, the relative intensity of carbonate and hydroxyl in the scaffolds (28 days incubated) assessed using FTIR. SrHA scaffolds exhibited apatite formation ability HA and HASi scaffolds. Previous studies have also reported that Sr and Si from scaffolds can induce apatite formation and proved to be bioactive (Zhao *et* 2007). *In vitro* apatite formation on bioglasses indicated that, the extent of bone growth increased dramatically in terms of their apatite forming ability. HAp crystal spectral bands were recognized at about 1090, 566 and 603 $cm^{-1}$ as already reported by Zhang *et al.,* (2010). Therefore it is reasonable to expect HASi and SrHA scaffolds would help in improving the osteointegration ability scaffolds post implantation in osteoporotic models.

## 7.5. Cytotoxicity evaluation:

Cytotoxicity studies form an integral part of pre-clinical evaluation techniques for establishing the non toxicity of the scaffolds of choice before its engineering application *in vitro* or *in vivo* (Rose and Oreffo, 2002). MTT assay

proved the non toxic nature of the ionic products from HASi and 10% SrHA scaffolds on L929 mouse fibroblast-like cells suggesting the suitability of the scaffolds for tissue engineering applications. It was also reported previously concentration of Sr substitution (1-10% ) does not affect the cell viability and osteogenic ability in terms of ALP activity using the osteoblast cell line – and partial cytotoxicity is usually exhibited at 80% Sr substitution only (Qiu *et* 2006b). The results suggest HA, HASi and SrHA scaffolds to be compatible for tissue engineering applications, thus suggesting their therapeutic potential for tissue engineering applications.

## PHASE II– *IN VITRO* & *IN VIVO* STUDIES USING rBMSCs IN RAT OSTEOPOROTIC MODEL

### 7.6. *In vitro* evaluation of HA, HASi and SrHA disc using rBMSCs:

When a fracture occurs in bone, neutrophils and mast cells are initially recruited to the site (acute inflammatory response) followed by the infiltration MSCs and osteoblast progenitor cells through micro-capillaries to favour bone regeneration and mineralization (Ziats *et al.,* 1988). Nevertheless, under condition there is impairment in recruitment of the progenitors and the resident MSCs itself lack normal proliferation and osteogenic differentiation potential. such a pathological condition, effectiveness of bare scaffolds with nature alone may often be limited (El-Ghannam, 2005). Hence, ceramic based scaffolds incorporated with growth factors or osteogenic cells may induce osteoinductive properties for tissue engineering applications as discussed in the review of literature.

Tissue engineering necessitates the use of ceramic scaffolds for the of cells and bioactive molecules so as to accelerate the bone healing process *in* MSCs have been extensively used for *in vitro* and *in vivo* tissue engineering applications because of its multipotent nature. To reflect this aspect, the Society for Cellular Therapy (ICST) has declared an alternative terminology for Mesenchymal Stem Cells, referring to these cells as ‘‘multipotent mesenchymal stromal cells” (Horwitz *et al.,* 2002). When use of MSCs is planned for tissue engineering applications, it is crucial to obtain relatively pure autologous cells retain good multiplication/differentiation potential to enable/sustain tissue (Renjith *et al.,* 2014). Prior to *in vivo* applications, MSCs were for expression of surface markers and plasticity. No single specific surface that is unique to mesenchymal stromal cells has been reported till date. with literature, cells isolated in our study exhibited positivity for CD90, while negligible expression was exhibited for the negative marker CD34 (Sobh, 2014). Flow cytometry data together with the osteogenic and adipogenic potential of isolated cells confirmed the mesenchymal origin of the cells isolated from rat

Even though cell therapy using fresh marrow cells and enriched marrow been considered as a viable approach in tissue engineering, *in vitro* culturing of isolated MSCs from the marrow cells helps in amplifying the availability of cells 10 times even with single passaging (Jaiswal *et al.*, 1997). Culture expanded rat MSCs when combined with porous ceramics have improved *in vivo* osteogenic potential at a much earlier period in ectopic implantation sites (Goshima *et al.,* 1991). E-SEM analysis proved that HASi and SrHA scaffolds served in the of rBMSCs proving its cytocompatibility compared to HA scaffolds.

ALP activity is crucial for the bone mineralization process *in vitro* and *in vivo*; as the phosphatase enzyme acts on the organic phosphate releasing free phosphate ions and active transport of ions across the cell membrane initiates process of formation of calcium phosphate crystals leading to mineralization (Ciapetti *et al.,* 2003). Addition of osteogenic supplements on BMSC cultures up regulate the production of collagen-rich matrix, increased expression of non-collagenous proteins like ALP, osteocalcin etc (Ohgushi and Caplan, 1999). Osteogenic differentiation using dexamethasone (dex) and β glycerophosphate (βGP) is reported to accelerate the stem cell potential to fabricate a voluminous mineral matrix *in vitro* (Ohgushi *et al.,* 1989a). A similar approach has been employed in this study by fabrication of tissue engineered ceramic constructs rBMSCs, followed by their osteogenic differentiation on the scaffolds prior to implantation. In the present study, isolated rBMSCs were differentiated using osteogenic differentiation medium supplemented with dex, βGP and LAA.

ALP estimation of tissue engineered cHA, cHASi and cSrHA proved that the scaffolds supported osteogenic differentiation. Qiu *et al.,* (2006) could prove improved metabolic ability of Sr doped calcium phosphate scaffolds in terms of proliferation and ALP activity using rat OB sarcoma cells. The in-house tissue engineered ceramic with 50% Strontium substitution has also proved its efficacy for improved osteogenic ability *in vitro* using rabbit ADMSCs (Beena *et* 2013). Sr concentrations from 0.1 to 1 mM stimulate osteoblast formation *et al.,* 2008). Sr released from the in house developed 10% SrHA also falls the range, indicating the therapeutical potential of the scaffolds for osteoporotic applications. Studies on varying the Si concentration showed that orthosilicic

physiological concentrations (0–50 µM) could stimulate differentiation of osteoblast-like cells (Reffitt *et al.,* 2003). Studies using osteoblast cells have also proved that silica coated surfaces induce a much earlier bone nodule formation, indicating its improved bone bonding ability (Zhao *et al.,* 2007). Improved *in* osteogenic efficacy of in-house developed HASi scaffold using goat and rabbit ADMSCs has been proven (Nair *et al.,* 2009a and Fernandez *et al.,* 2012). Appropriate pore dimensions of the in-house developed scaffolds may have contributed towards the improved osteogenic differentiation, as it has been that a pore size within the range of 100 – 200 µm is optimum for promoting infiltration in 3D scaffolds. Again, interconnected micropores in scaffolds may better cell – cell interaction *in vitro,* thereby improving neo vascularisation and mineralization *in vivo* (Takahashi and Tabata, 2004).

## 7.7. Osteoclast precursor cell adhesion on the scaffolds:

Osteoclast originates from precursor monocytes and attachment of on to the scaffold surface occurs during the early period of implantation. extensive cellular micro extensions *viz.,* fillopodia is the typical morphology of osteoclast cells. To be functional, osteoclast cells need to adhere on to the apatite surface and maintain their flattened morphology with ruffled boarders which active centres that forms resorption pits, which ultimately causes bone demineralization (Saltel *et al.,* 2004 and Roy and Bose, 2012). Hence adhesion of osteoclast precursor cell -$RAW_{264.7}$ on the scaffolds was evaluated to assess the osteoclast ability of HA doped substitutes. HA and HASi scaffolds favoured cell adhesion and attached cells retained the typical morphology with extended

appendages, post 18 hours of culture. But lack of preferential attachment of osteoclast precursor cells, with typical morphology was evident on 10% SrHA scaffolds. Modulation of OPG and RANK L expression is reported to prevent formation of the ruffled borders (Bonnelye *et al.,* 2008). Since *in vitro* release proved that 10% SrHA releases Sr within the recommended therapeutic range osteoporotic applications, it is anticipated that the released Sr may have the expression of OPG and RANK L thereby altering the cell morphology. studies have also suggested that Sr at varying concentrations from 1% to 10% onto ceramic blocks regulate osteoclast activity *in vitro* (Capuccini *et al.,* 2009 Baier *et al.,* 2013).

The Sr release profile together with the SEM images thus supports the hypothesis that 10% Sr exerts a negative role in osteoclast activity. Even though incorporation in HA did not prove to be toxic to the RAW cells, presence of Sr the scaffold surface affected cell adhesion and typical morphology. Therefore it anticipated that in-house developed 10% SrHA scaffolds may regulate the activity *in vivo* also, signifying the therapeutic potential of Sr incorporation in for osteoporotic bone regeneration.

## 7.8. Development and evaluation of rat osteoporotic model:

Rat osteoporotic model has been considered as an optimum model as it many similarities to human pathological condition like the skeletal responses to depletion of estrogen, as well as the pharmacological effects on bone turn-over and Ezawa, 2011). There are various methods of inducing osteoporosis in rats as ovariectomy, low calcium diet, steroid administration etc (Lasota and

Klonowska, 2004). Most of the *in vivo* studies employ a short term period (3-4 months) of estrogen deficiency for osteoporotic induction (Habermann *et al.,* The effect of long-term estrogen deficiency in rat models to better mimic the situation in post-menopausal women has not been explored.

Aging also pre-disposes the bone to excessive bone loss and the incidence osteoporosis is also more prevalent among the aged population (Kerschan-*al.,* 2014). Impaired bone healing associated with senile osteoporosis is only in long term osteoporotic aged models (Oliver *et al.*, 2013). But most of the researches have been focused on rat osteoporotic models, induced in young rat models. Therefore osteoporotic animal models should consider the aging factor so as to better mimic the human clinical pathology. Various outcomes have reported on the short-term effects of estrogen deficiency on fracture healing. It suggested that young rat skeleton cannot be considered as an appropriate model osteoporosis because bone turnover in them is modelling (bone formation bone resorption) whereas, in human osteoporosis bone turnover is considered as remodelling (bone resorption precedes bone formation). However, it has also suggested that rat skeleton shows a gradual transition from modelling to with aging (Dennison *et al.,* 2005). So it is relevant to consider the bone site and of the rat model in research on therapeutic modalities.

The present study has evaluated the bone loss associated with prolonged ovariectomy in the aged rat model. The current surgical practice could be skillfully in bilateral ovariectomy - the muscle layer was perforated with a very nick to expose the ovary and a simple interrupted single suture was adequate to

the wound. Histology of proximal tibial head of LOA rat model exhibited a prominent decrease in the trabeculature, indicating bone loss associated with term osteoporosis induction. Cortical thickness was not affected by ovariectomy, which is concurrent with literature suggesting that osteoporosis mainly affects areas where bone remodelling occurs at a higher rate (Compston, 2011). area near the tibial epiphysis is one such area, where high bone turn-over slices from micro CT representing the tibial head of LOA models supported a similar pattern of bone loss where in, an appreciable loss in the trabecular compared to control animals was evident.

Qualitative and quantitative parameters evaluated using micro CT substantiated the bone loss. Pathology of osteoporosis in humans is a reduction in trabecular number and an increase in the trabecular separation *al.,* 2000). Animal models reviewed for osteoporosis induction also exhibited a similar trend in trabecular micro-architecture and demonstrated a loss of bone mass (Majumdar *et al.,* 1997). Similarly, results from our study also significant decrease in trabecular number compared to controls. Histological evaluation using H&E staining depicted the presence of thick trabecular the control group animals, whereas in the induced model the trabecular seen to be thinner with large void spaces.

## 7.9. Impaired bone healing in the long term osteoporosis induced aged rat model:

Meyer *et al.,* (2001) has reported that prolonged osteoporosis induction period significantly impair the process of fracture healing. Osteoinductive

the bone matrix is also reported to decrease with aging (Syftestad and Urist, Accordingly LOA rat model in the study was evaluated for assessing bone ability. In control animals, post 8 weeks of surgery a complete closure of the defect was observed. Presence of more woven bone at the defect site in the animals may have facilitated the bone remodelling process to occur normally promoted bone healing (Brüel *et al.*, 2011).

Impaired healing ability was evident in the LOA rat model. *De novo* trabecular bone formed at the bone defect site is reported to exhibit an irregular organisation indicating a histological impairment in wound healing (Wang *et* 2005) and was evident in plastic sections from LOA model too. The delay in ability in the induced models might be due to the suggested delay in cellular differentiation within the fracture callus. Impaired proliferation and potential of the resident MSCs has been reported to delay bone healing in osteoporotic subjects (Namkung-Matthai *et al.*, 2001). An impaired calcification the fracture callus has also been reported in osteoporotic animals (Li and 1994). A considerable delay in the remineralization of the fractured bone was evident in aged osteoporotic rats (Bak and Andreassen, 1989). In ovariectomised this could be due to an alteration in the composition of the mineral matrix and in local *milieu* including cytokines, growth factors etc, which is required for the normal healing of the bone (Giannoudis *et al.*, 2007). Reduced estrogen level in ovariectomised rats may lead to impaired bone metabolism and a reduced rate fracture healing (Walsh *et al.*, 1997).

## 7.10. Osteogenic efficacy assessment of micro-granular scaffolds in LOA model:

Improved drug delivery application of ceramic based micro-granules interconnected pore structure has been proven recently (Hong *et al.,* 2015). High surface area to volume ratio of micro-granules regulates the release of from the implants, thus making them relevant for drug delivery applications in tissue regeneration (Bracci *et al.*, 2009). In this perspective, HA, HASi and micro-granular scaffolds were fabricated using rBMSCs and the osteogenic, osteointegrative ability were assessed in LOA rat model.

Gross evaluation indicated no signs of inflammation or fibrosis. evaluation revealed that the bone defect area was bridged with newly formed bone in both HASi and SrHA (bare and cell seeded) groups post 8 weeks of implantation, indicative of the improved osteogenic ability of the modified HA scaffolds. It was interesting to note that the cell seeded scaffolds (cHASi and paved way for more osteoid formation compared to bare scaffolds. The osteogenically induced cells on the scaffolds might have released chemokine and other soluble factors that might have attracted more native cells to adhere scaffolds and generate more bony tissue. HA implants loaded with bone marrow have proven to improve bone healing in healthy rat models (Ohgushi *et al.,*

The addition of dopants like Si into tricalcium phosphate ceramics osteoinductive properties in HASi scaffolds (Fielding and Bose, 2013). In the study HASi and cHASi micro-granular scaffolds exhibited improved bone compared to bare HA scaffolds. The capability of silica incorporated scaffolds

facilitate cell migration and osteogenic differentiation were depicted in earlier using healthy rabbit and goat models (Fernandez *et al.,* 2012 and Nair *et al.,* Increasing Silica content in HA enhanced its dissolution property, which in turn promoted bone apposition in new Zealand white rabbits (Hing *et al.,* 2006). up study of repair of a segmental defect in sheep model using tri calcium phosphate revealed that Si incorporated material was completely resorbed on with new bone formation two years post implantation (Mastrogiacomo *et al.,* Hence the osteoinductive and osteoconductive nature of HASi scaffolds, with its resorptive properties favored bone healing process in the LOA rat

Cortical bridging was visible in HASi and SrHA implanted groups, but a better resurfacing and *de novo* bone organization at the defect area was evident cSrHA and SrHA implanted groups. This may be attributed to the improved bioactivity of the SrHA scaffolds to form apatite. Sr released from the implant have also contributed to better osteointegration as reported by Cardemil *et al.,* and Mohan *et al.,* 2013. Improved osteointegration with systemic administration Sr containing drugs have been proven in rat osteoporotic model (Li *et al.*, 2012). However, the improved osteointegration was evident only after 12 weeks of implantation, which is a very long duration in rats when the process of bone might have been completed. Interestingly, in the present study new bone on par with material resorption was evident post 8 weeks of implantation. Histomorphometry studies also proved marginal difference in osteogenic SrHA micro-granules implants *in vivo*.

Bioactivity and resorbability have been considered as important factors implant integration and stability (Dagang *et al.,* 2008). It was interesting to note in the HASi and SrHA implanted groups remnants of the micro-granular could not be appreciated within the bone defect site, even though micro- were seen attached towards the outer muscle flap at the bone defect site. This is concurrent to the results obtained from the *in vitro* degradation study, which predicted faster dissolution property of Sr and Si incorporated HA scaffolds compared to bare HA.

Micro CT is an efficient non-invasive tool to evaluate osteointegration bone density (Bouxsein *et al.,* 2010 and Sabareeswaran *et al.,* 2013). Micro CT depicted improved mineralization in the SrHA and cSrHA implanted group. It observed that *de novo* bone formed exhibited an improved mineral content to HA and HASi implanted group. Sr released from the SrHA implant may positively regulated the excessive mineralization and together with the inherent bioactivity of osteogenically induced cells, improved osteogenesis and was attained in the cSrHA implanted group. Furthermore, an analysis of the biomechanical properties of explants together with molecular analysis of genes involved in bone remodeling could have substantiated the healing cascades in long term osteoporosis induced pathology.

## 7.11. Strontium accumulation in LOA model:

The accumulation of the Sr in the organs of different implant groups was assessed using ICP, post eight weeks of implantation in the LOA model. It has reported that Sr released from scaffolds may be absorbed and retained in a

manner by which Ca is absorbed and gets trapped in the plasma, extracellular skeleton (Boivin *et al.,* 1996). Unbound Sr may also be excreted through urine feces. ICP studies indicated presence of Sr in kidney, liver and spleen in HA HASi implant groups, indicative of the fact that Sr is present in minimal level in organs (Takahashi *et al.,* 2000). It was evident from the ICP data that SrHA implanted group did not exhibit any comparative increase in Sr accumulation in kidney or liver. An increased Sr concentration compared to other groups was evident in the spleen. The average value of Sr found in the bone is 264µg/g and reported minimum toxic concentration of Sr is 10mg/kg (Iyengar *et al.,* 2004). Hence the observed spleen Sr concentration (1.98 µg/g) in the SrHA implanted falls much less than the minimum toxic concentration and is not expected to any adverse reaction in rats.

From the *in vitro* and *in vivo* studies in the rat osteoporotic model, it was evident that cSrHA scaffolds exhibited an improved osteogenic and ability compared to HA and HASi scaffolds. Therefore for further efficacy assessment studies (proof of concept) in large osteoporotic model cSrHA alone was chosen as the test material.

# PHASE III – *IN VITRO* AND *IN VIVO* STUDIES USING sADMSCs IN SHEEP OSTEOPOROTIC MODEL

## 7.12. Adipose derived MSCs - better cell source for tissue engineering applications:

Implants intended for osteoporotic application need to be specifically made and fabricated into living constructs taking into consideration of the status of the osteoporotic patient and the quality of bone stock. BMSC transplantation has been considered as a potential strategy to address the fracture healing in osteoporotic models (Ocarino *et al.,* 2010 and Wang *et al.,* 2006). BMSCs have been considered to exhibit improved osteogenic ability from the *in vivo* studies in rat osteoporotic model using in-house tissue engineered HA constructs (Chandran *et al.,* 2016). But bone marrow is associated with significant morbidity and requires a longer culture period *in* to obtain sufficient number of cells for clinical application (Pei *et al.,* 2015). from the deleterious effects of osteoporosis, aging has also got adverse effects on proliferation and differentiation potential of resident BMSCs (Giannoudis *et al.,* 2007). Thereby, the impaired osteogenic ability of BMSC also contributes to the delayed healing ability in osteoporotic models (Katsara *et al.,* 2011). So to clinical perspective in real pathological condition, a better source from which cells can be isolated without much morbidity should be considered.

ADMSCs have emerged as a suitable and viable source of stem cells for tissue engineering applications. Ease of tissue harvesting without much

abundant availability and osteogenic differentiation ability of fat derived stem signifies its therapeutical application. A comparative study on the osteogenic differentiation ability of ADMSCs from aged and young mice indicated minimal effect of aging on the *in vitro* differentiation potential (Chen *et al.,* 2012). But controversies do exist, as certain studies have shown the decreased proliferation differentiation potential of ADMSCs with aging (Liu *et al.,* 2012). *In vivo* studies osteoporotic aged sheep model using autologous and allologous MSCs suggested allologous cell based tissue engineering offers the potential for "Off the Shelf" tissue-engineered products (Berner *et al.,* 2013). Recently the therapeutic ADMSCs in re-establishing normal bone homeostasis and enhancing bone osteoporotic mice has been reported (Mirsaidi *et al.,* 2014). This supported the hypothesis of ADMSC based tissue engineering approach for osteoporotic bone regeneration If promising results emerges, the study may be further extended evaluating the *in vivo* efficacy of tissue engineered SrHA scaffolds using ADMSCs from osteoporotic animals.

## 7.13. *In vitro* evaluation of HA and SrHA disc scaffolds using sADMSCs:

In the present study Sheep ADMSCs were isolated from the fat pad of allogenic sheep model and cultured based on their plastic adherence on culture plates. Quantitative characterization indicated the cultured cells to be almost positive for the CD marker - CD44. CD 44 has been considered as a marker for characterization of sheep and human ADMSCs (Fadel *et al.,* 2011). Grzesiak *et* (2011) has reported a similar level of expression in the Somalian sheep model.

plasticity/differentiation ability of sADMSCs was demonstrated from the and adipogenic differentiation studies that confirmed the multipotent nature of MSCs.

Cytocompatibility studies using sADMSCs indicated that cells proliferated direct contact with the Sr incorporated scaffolds maintaining its typical spindle morphology. Tissue engineered constructs were fabricated and prior to *in vitro* cultured constructs were evaluated using live dead assay. SrHA discs to be cytocompatible with sADMSCs for tissue engineering applications. Cell adhesion studies indicated that the cylindrical scaffolds favoured cell adhesion retained their spindle morphology confirming the cytocompatibility of the Post 7 days of culture, DAPI staining indicated that the cells spread well on the cylindrical scaffolds and the live dead staining indicated the presence of viable As mentioned earlier it is assumed that osteogenically differentiated cells with the ECM secreted on the scaffolds would create an anabolic effect *vivo* osteogenesis under osteoporotic conditions.

Osteogenic potential exhibiting collagen synthesis and calcification of BMSCs on HA scaffold for bone tissue engineering applications has been by Sulaiman *et al.,* (2013). Similarly in the present study post 28 days of induction, thick cellular coating (cell sheet) was evident on the SrHA and HA scaffolds revealing cell-cell and cell-material interaction, proving their cytocompatibility. It has been well discussed in earlier sections that ECM the osteogenically differentiated stem cells on HA scaffold may pave way for improved osteoid synthesis and mineralization *in vitro*. A similar phenomenon

be anticipated with implanted tissue engineered SrHA and HA scaffolds with differentiated cells in osteoporotic sheep model. sADMSCs exhibited a (not statistically significant) osteogenic differentiation ability compared to HA scaffold. It has been reported that β glycerophospahte in the osteogenic media serves as a source of organic phosphate and induce mineralization *in vitro* the same has been supported with the bone like nodule formation in SrHA post two weeks of induction (Chang *et al.,* 2000). We have already reported that house developed 50% SrHA favour *in vitro* and *in vivo* osteogenic ability (Beena *al.,* 2013) in ulna segmental defects of healthy rabbits. On the contrary, in this only 10% Sr was incorporated so that the scaffolds may regulate the osteoclast activity rather than improve the osteogenic ability of the scaffolds. ADMSCs OVX animals have already proven to have *in vivo* osteogenic differentiation in different animal models (Ye *et al.,* 2014). Hence it is legitimate to assume that house developed 10% SrHA scaffolds in conjunction with osteogenically differentiated cells may exhibit an improved osteointegrative and osteogenic *in vivo*.

## 7.14. Development and evaluation of sheep osteoporotic model:

International standard recommends using large animal models like dog etc for evaluating biomaterials indented for orthopaedic application (Pearce *al.,* 2007). Sheep has been a preferred model for osteoporotic research as they docile, spontaneously ovulate, have similar hormone profile to that of humans sheep bones provide enough space to evaluate large bone implants (Wu *et al.,*

Severe osteoporosis can be induced in sheep by combined treatments of

ovariectomy, calcium/vitamin D-restricted diet, and steroids (Lill *et al.*, 2000). steroid administration in osteoporotic sheep model has exhibited to reverse the BMD with the discontinuation of steroid. Steroid administration is also with high chance of infection at the fracture site during implantation studies (Deloffre *et al.,* 1995). Sheep osteoporotic model induced by ovariectomy and calcium deficient diet for six months have shown to exhibit similar bone loss compared to human subjects (Lill *et al.,* 2002). However, short term induction period failed to exhibit BMD and biomechanical properties associated human osteoporosis (Fini *et al.,* 2000). Hence it has been suggested that 12-24 months of induction period induce statistically significant changes in histomorphometry and mechanical parameters in the induced sheep model (Lill 2002). It has also been suggested that 9-10 year old ewes exhibit a bone loss comparable to post menopausal women (Turner *et al.,* 2001). Also secondary remodelling exhibited by the human bone is evident only in aged ewes (Pearce 2007). To overcome these problems in our study, 9-11 years old sheep were with a combination regimen of ovariectomy and Calcium deficient diet. Post 10 months of induction a statistical significant loss in bone density and was evident in the tibial bones of the induced model, confirming the the osteoporotic model. So selection of aged sheep for osteoporotic induction combined induction method (OVX + Calcium deficient diet) employed in the study helped in developing an appropriate animal model for human

Induced osteoporotic sheep model was qualitatively and quantitatively assessed using micro CT. As already mentioned, trabecular bone parameters been considered as a good indicator for estimating bone loss in osteoporotic

as osteoporosis related bone loss is more evident in trabecular area of active remodelling. 3D morphometry image along with the evaluation of trabecular parameters at the proximal epiphyseal end of tibia indicated a significant bone the induced sheep model. Reduction in the trabecular parameter by more than has been considered as substantial to confirm model induction in sheep (Lill *et* 2002). In the present study the trabeculature was disrupted drastically, the age matched control model.

Vitamin D deficiency is associated with the metabolic bone diseases like osteoporosis and osteopenia and it is more prevalent in the aged population. Observational population based studies have suggested that decreased vitamin levels in serum is associated with fragility fractures and weak bone mass (Ohta *al.,* 2014). Herein too, the osteoporosis induced model exhibited a decline in vitamin D level confirming the onset of the disease. Also the serum Ca level to increase, further supporting bone loss in the induced sheep model.

## 7.15. Post implantation evaluation for inflammatory responses:

Inflammatory response towards an implant plays an immediate and role in regulating bone regeneration efficiency during bone defect healing *al.,* 2010). Inflammatory cells at the fracture site alter the local concentration of growth factors, cytokines and affect normal bone healing process. Neutrophils macrophages are the most representative leukocytes that form the first line of defence when tissues are exposed to a foreign implant material. Neutrophils first followed by macrophages (Mountziaris *et al.,* 2011). Serum analysis post day, two weeks and two months of implantation implied that WBC, lymphocyte

the eosinophil count were within the reference range at all time points. But the neutrophil level was seen elevated from the normal range post 1 week of implantation. Inflammatory modulators are reported to be regulated due to interventions in animal models and if the implant material is compatible, inflammatory mediators are expected to subside within few days. (Caetano-*al.,* 2011 and Pape *et al.,* 2010). Decline in the neutrophil count, post 2 weeks of implantation indirectly proved the biocompatibility of allogenic cell seeded scaffolds. These results are in line with the observations in mini-pigs by Guo *et* (2009) wherein allogenic MSCs resulted in a minimal immunological reaction implantation. Allogenic BMSCs were also safely delivered for scaffold based regeneration in a large segmental defect model in aged sheep (Berner *et al*., MSCs retain their immunological properties after *in vitro* osteogenic induction, signifying the potential clinical application of the in-house developed TE (Niemeyer *et al*., 2010).

## 7.16. Efficacy Assessment of tissue engineered SrHA constructs in sheep osteoporotic model:

Osteointegration is a pre-requisite for proper implant fixation during osteoporotic fracture healing. Implant instability and aseptic loosening are the problems faced by orthopaedic surgeons fixing osteoporotic fractures. plays significant role in fracture repair as they serve as a source for cell supply significant regeneration potential (De Bari *et al.,* 2001). However in natural the periosteum layer often tears away thereby further suppressing the ability. So in the present study, to mimic the clinical fracture situation, the

periosteum layer was removed prior to implant fixation. Sheep model provide advantage as they exhibit a similar pattern of bone in growth to that of humans, attributed to the greater amount of cancellous bone (Willi *et al.*, 2004).

ISO and ASTM standards recommend that implant dimensions must be chosen based on the size of the animal bone to avoid pathological fractures. ISO recommends a dimension of 4mm diameter and 12 mm length bone defect in the femur and tibia of sheep models to test the efficacy of the biomaterial (Pearce *et* 2007). It has also been suggested that in sheep model implant dimensions may to 5mm in diameter, provided the implantation is done at the tibia and (Huffer *et al.,* 2007). It has also been suggested that a minimum of 4 implant in rabbits or a minimum of 2 implant sites in higher animal models like sheep, or pig should be included in the study at each implantation period, through appropriate power calculations (Pearce *et al.,* 2007). Therefore in the present the materials were tested in duplicates in the sheep osteoporotic model.

A press fit method has been adopted in this study for the implantation of cylindrical constructs and the defect area was approached as per the surgical procedure detailed by Nuss *et al.,* (2006). Press fit method only provides a weak stability to the implants placed and so the success of the implant depends on growth into the material so as to establish structural and functional connection host implant interphase, *i.e.,* osteointegration (Borsari *et al.,* 2007). occurs when there is direct contact between the host bone and the implant without interposition of soft tissue. The radiographs clearly depicted the osteointegrative ability of cSrHA implants as there was hardly any area around

implant, without direct contact with the host bone. Disappearance of the zone post two months implantation compared to cHA implants clearly indicated improved osteointegration ability of SrHA and cSrHA implants. In the cHA and implanted groups there were distinct radiolucent zones even after two months implantation. The presence of radiolucent zone indicated non-union or low mineralization at the implant interface (Nair *et al.*, 2009b, 2009c). The radiopacity of SrHA implant compared to HA implant was also evident from radiographs. This gain in radiopacity is attributed to the incorporation of Sr may serve in the *in vivo* tracking of the implants.

Histological evaluation of stained plastic sections revealed that new bone formation was well osteoconducted over cSrHA implant surfaces, compared to other implant groups. Tissue engineered implants – cHA and cSrHA exhibited improved osteogenic efficacy, as majority of the pores in the implants were filled with *de novo* bone. Improved bone in growth and material resorption was also well evident from the histology studies. Post two months of implantation, cSrHA implants lost its cylindrical morphology compared to HA implants, indicative of the faster *in vivo* dissolution property. It is proposed that post implantation the bioactivity would be initiated by the host cell interaction at the implant interphase leading to material dissolution into the ECM (Chang *et al.*, 2000).

Again, secondary haversian organisation was also well identified in implanted group, indicative of its improved osteogenic differentiation ability. Compared to HA scaffolds bare SrHA also supported lamellar organisation, but prominent number of osteon units were identified in cSrHA implanted group.

results signified the therapeutic potential of Sr incorporated scaffolds to regulate bone remodelling process to pave way for mature bone formation. remodelling in sheep is more prevalent in mature aged sheep. It has been that strontium leached out from the implant regulate excessive resorption at the implant interphase and better osteointegration may be attained (Liebschner, The osteogenic differentiated cells, their secreted ECM and optimum pore size scaffolds that encouraged bone in-growth may attribute to the improved bone maturation and haversian organisation in cSrHA implanted group. Accelerated dissolution of Sr incorporated implants, lead to rapid Sr release and earlier have suggested the positive influence of the Sr in regulating the bone positively and favouring bone implant integration, facilitating better bone in- (Tao *et al*., 2016 and Newman *et al*., 2014).The mechanism of osteointegration explained by Wong *et al.,* using SrHA bone cement samples using Transmission Electron Microscopy. It was reported that SrHA paved way for mature bone formation, as collagen fibres in the *de novo* bone was perpendicularly arranged seen in mature rabbit bone (Wong *et al.,* 2004).

Micro CT results further substantiated the improved osteointegration of cSrHA and SrHA implants in osteoporotic condition. Compared to cHA an improved bone density at the host implant interface comparable to that of bone was depicted in the cSrHA implants. Similar results have been reported in rabbit model using 100% Sr incorporated implants (Sabareeswaran *et al.,* the present study even at two months post implantation using 10% cSrHA, osteointegration was attained. But the improved osteointegrative ability and osteogenic ability cannot be attributed to the osteogenically differentiated cells

scaffold alone, as in SrHA implanted group also, *de novo* bone exhibited mineralization, indicative of mature bone formation. In a study where osteointegration among young, aged and osteoporotic sheep models in a similar bone defect were assessed using titanium and titanium coated with HA rough surfaces, it was observed that HA coated implants influenced the ability in osteoporotic condition (Borsari *et al.,* 2007). Implants that aid the local delivery of drugs like bisphosphonate at the bone defect site improved bone and exhibited a better fixation of implant in osteoporotic sheep models *et al.,* 2008). Local delivery of bisphosphonate served in regulating the excessive resorption paved way for earlier implant fixation. Similarly, in-house developed SrHA served in local delivery of Sr at the defect area in the sheep bone, thereby facilitating better osteointegration.

Therefore the results indicate that a combination of strontium ions and cells together exert a positive role in osteogenesis and osteointegration in osteoporotic condition, thus supporting the proposed hypothesis thereby the relevance of the work in the clinical perspective.

## 7.17. Limitations of the study:

1. Evaluation of the osteointegration ability based on mechanical pull out studies of the implant would have helped in validating the cSrHA for better implant fixation in terms of mechanical parameters. But there limitations in the number of animals sanctioned for the present study. However an increase in the implant pull out force is expected since

depicted an increased bone in-growth and improved osteogenesis in osteoporotic models.

2. Ceramic scaffolds are usually not recommended for large segmental bone replacements due to its limited mechanical strength. In the present study SrHA scaffolds are proposed for the functional restoration of the impaired osteoblast and osteoclast cells at the fracture site, rather than for providing mechanical support. Hence future studies may be directed towards development and validation of SrHA coated metal implants in view of clinical application in large segmental bone defects.

## 7.17. Future perspective:

1. Molecular analysis of the explants would provide more insights into the genetic mechanism behind the improved osteointegration of cSrHA
2. Considering the optimum strategy for clinical application in osteoporotic condition, the most promising approach would be the use of autologous ADMSCs from OVX animals and research on this front may be
3. The suitability of SrHA coated metallic implants may also be investigated for application in load bearing bone defects.

# CHAPTER 8

# SUMMARY AND CONCLUSIONS

## 8.1. Summary and conclusion:

In orthopedic reconstructive surgery, mending of osteoporotic fractures formidable challenge. Combined effect of aging and osteoporosis results in weak bone mass and delayed bone healing ability, thus resulting in poor fracture and non-union. The frequent incidence of fractures in such patients often surgical procedures for fracture fixation. High rate of metal implant failures in osteoporotic patients have been reported due to poor implant anchorage and osteointegrative ability. Currently, implants are anchored using additional wires or nails or augmentation with hydroxyapatite based bone cements. But of screws and nails creates additional morbidity to the already weak bone, increasing the fracture susceptibility at nearby sites.

Hence, novel strategies/bone substitutes are required for treating fractures. Manipulation of the fracture environment *via* tissue engineering comprising of growth factors, scaffold and cells has been considered as a therapeutic strategy. In this context, an ideal biomaterial is a necessity to bone resorption and simultaneously favor osteogenesis to attain better osteointegration and prevention of implant pull out/failure. This work was on the hypothesis that cell-based tissue engineering in conjunction with hydroxyapatite modified with strontium/silica may stimulate osteogenesis to osteoporotic bone defect healing.

In-house developed HA, HASi and SrHA scaffolds were physio-characterized and found suitable for bone tissue engineering applications in porosity, degradation, non toxic nature and apatite formation ability. SrHA and scaffolds exhibited an improved degradation rate and dissolution property to HA scaffolds. Bone bonding ability in terms of apatite formation was also HASi and SrHA scaffolds indicative of the improved osteointegrative property both the scaffolds. Release of Sr ions from SrHA was found to be concurrent to required therapeutic dose of 0.1mM/mg in perspective of osteoclast regulation. 'combination product' of cells and HA based scaffolds – cHA, cHASi and were fabricated using osteogenically induced mesenchymal stem cells and for its cytocompatibility and *in vitro* osteogenic ability prior to *in vivo* The *in vitro* analysis indicated the compatibility of the in house developed towards rBMSCs.

Post implantation evaluation by histology in rat osteoporotic models revealed that HASi and SrHA scaffolds promoted bone healing in osteoporotic condition. But a complete bridging of the defect area by *de novo* bone with mature bone like morphology was evident in SrHA and cSrHA implant group only, indicative of its improved osteogenic ability. The bone cells were of uniform sized and oriented in line with the neighboring cells, resembling mature bone in the Sr implanted groups. Histomorphometry data indicated that the *in vivo* osteogenic efficacy followed the order - cSrHA > SrHA > cHASi > HASi > HA. Since significant outcomes were obtained from Sr incorporated scaffolds in rat osteoporotic model, validating the same in a large animal model which better mimics the human pathological condition will help in extrapolating the proposed study to real clinical situation. Sheep has been

considered as a preferred model for human osteoporosis as they spontaneously ovulate, have similar hormone profile and provide enough space to evaluate large bone implants.

Tissue engineered constructs were fabricated from adipose derived MSCs which is a suitable source from which cells can be isolated without any morbidity. *In vitro* cytocompatibility studies using sADMSCs confirmed the therapeutical application of sADMSCs seeded on HA and SrHA for *in vivo* bone tissue engineering applications. Absence of translucent zone at the bone implant post two months of implantation in sheep clearly indicated the improved osteointegration ability of cSrHA implants. SrHA and cSrHA served in local delivery of Sr at the defect area, thereby facilitating better osteointegration. of MSCs and Strontium incorporation in HA aided osteogenesis quantitatively terms of regeneration efficiency (new bone formed /total defect area) and regulated the osteoclast activity enabling bone tissue in growth and Again, secondary Haversian organisation was also visible in cSrHA implanted group, indicative of its improved osteogenic differentiation ability. Micro CT evaluation of the explants further confirmed the improved osteointegrative ability of Sr incorporated scaffolds. Hence, cSrHA proved to be osteoinductive, osteointegrative and degradative in nature, without the intervention of fibrous at the defect site in sheep osteoporotic models. Absence of any inflammatory response associated with the TE constructs post implantation; signify the clinical application of the in-house developed TE scaffold. The radiopaque scaffolds served in clinical imaging also.

The concept of local delivery of Strontium ions and osteogenically induced allogenic MSCs at the implant site *via* HA carrier achieved better osteogenesis osteointegration in osteoporotic condition. Acceptance of materials with *in vitro* supported further by its performance *in vivo* in rat and sheep osteoporotic predicts the clinical application of tissue engineered Strontium incorporated for osteoporotic applications.

## 8.2. Clinical relevance of proposed project:

The study has got significant clinical application in terms of the cell used and the simplicity in the material preparation. Although the clinical use of engineered scaffolds is still in its state of infancy the present findings that the local delivery of Sr and MSCs significantly contributed to osteoporotic regeneration and healing process. The study also hints towards the safe use of allogenic cells for clinical translations as “Off the Shelf TE Products” (OSTEP). anticipated that in-house developed tissue-engineered Strontium incorporated implants may likely revolutionize the currently available geriatric osteoporotic treatment strategies in a cost effective way - “a reality to be accomplished in the health care system”.

# REFERENCES


Albrektsson, T., Johansson, C., 2001. Osteoinduction, osteoconduction and osseointegration. Eur. Spine J. Off. Publ. Eur. Spine Soc. Eur. Spinal Deform. Soc. Eur. Sect. Cerv. Spine Res. Soc. 10 Suppl 2, S96–101.

Aldini, N.N., Fini, M., Giavaresi, G., Giardino, R., Greggi, T., Parisini, P., 2002. Pedicular fixation in the osteoporotic spine: a pilot in vivo study on long-term ovariectomized sheep. J. Orthop. Res. Off. Publ. Orthop. Res. Soc. 20, 1217–

Alenezi, S., Jerban, S., Elkoun, S., 2016. Importance of the PMMA viscoelastic rheology on the reduction of the leakage risk during osteoporotic bone augmentation: A numerical leakage model through a porous media. J. Mech. Behav. Biomed. Mater. 65, 29–41. doi:10.1016/j.jmbbm.2016.08.009

Alkaisi, A., Ismail, A.R., Mutum, S.S., Ahmad, Z.A.R., Masudi, S. 'an, Abd Razak, N.H., 2013. Transplantation of human dental pulp stem cells: enhance bone consolidation in mandibular distraction osteogenesis. J. Oral Maxillofac. Surg. Off. J. Am. Assoc. Oral Maxillofac. Surg. 71, 1758.e1–13.

Alkhraisat, M.H., Mariño, F.T., Rodríguez, C.R., Jerez, L.B., Cabarcos, E.L., 2008. Combined effect of strontium and pyrophosphate on the properties of brushite cements. Acta Biomater. 4, 664–670.

Amin, S., Achenbach, S.J., Atkinson, E.J., Khosla, S., Melton, L.J., 2014. Trends in fracture incidence: a population-based study over 20 years. J. Bone Miner. Res. Off. J. Am. Soc. Bone Miner. Res. 29, 581–589. doi:10.1002/jbmr.2072

An, J.H., Park, H., Song, J.A., Ki, K.H., Yang, J.-Y., Choi, H.J., Cho, S.W., Kim, S.W., Kim, S.Y., Yoo, J.J., Baek, W.-Y., Kim, J.-E., Choi, S.J., Oh, W., Shin, C.S., 2013. Transplantation of human umbilical cord blood-derived mesenchymal stem cells or their conditioned medium prevents bone loss in ovariectomized nude mice. Tissue Eng. Part A 19, 685–696.

Antebi, B., Pelled, G., Gazit, D., 2014. Stem cell therapy for osteoporosis. Curr. Osteoporos. Rep. 12, 41–47. doi:10.1007/s11914-013-0184-x

Ayesh, B.M., Abed, A.A., Faris, D.M., 2014. In vitro inhibition of human leukemia THP-1 cells by Origanum syriacum L. and Thymus vulgaris L. extracts. BMC Res. Notes 7. doi:10.1186/1756-0500-7-612

Bagi, C.M., Ammann, P., Rizzoli, R., Miller, S.C., 1997. Effect of estrogen deficiency on cancellous and cortical bone structure and strength of the femoral neck in rats. Calcif. Tissue Int. 61, 336–344.

Baier, M., Staudt, P., Klein, R., Sommer, U., Wenz, R., Grafe, I., Meeder, P.J., Nawroth, P.P., Kasperk, C., 2013. Strontium enhances osseointegration of calcium phosphate cement: a histomorphometric pilot study in ovariectomized rats. J. Orthop. Surg. 8, 16.

Bak, B., Andreassen, T.T., 1989. The effect of aging on fracture healing in the rat. Calcif. Tissue Int. 45, 292–297.

Bartucci, E.J., Gonzalez, M.H., Cooperman, D.R., Freedberg, H.I., Barmada, R., Laros, G.S., 1985. The effect of adjunctive methylmethacrylate on failures of fixation and function in patients with intertrochanteric fractures and osteoporosis. J. Bone Joint Surg. Am. 67, 1094–1107.

Benisch, P., Schilling, T., Klein-Hitpass, L., Frey, S.P., Seefried, L., Raaijmakers, N., Krug, M., Regensburger, M., Zeck, S., Schinke, T., Amling, M., Ebert, R., Jakob, F., 2012. The transcriptional profile of mesenchymal stem cell populations in primary osteoporosis is distinct and shows over expression of osteogenic inhibitors. PloS One 7, e45142.

Berner, A., Reichert, J.C., Woodruff, M.A., Saifzadeh, S., Morris, A.J., Epari, D.R., Nerlich, M., Schuetz, M.A., Hutmacher, D.W., 2013. Autologous vs. allogenic mesenchymal progenitor cells for the reconstruction of critical sized segmental tibial bone defects in aged sheep. Acta Biomater. 9, 7874–7884.

Bertoldi, S., Farè, S., Tanzi, M.C., 2011. Assessment of scaffold porosity: the new route of micro-CT. J. Appl. Biomater. Biomech. JABB 9, 165–175.

Boivin, G., Deloffre, P., Perrat, B., Panczer, G., Boudeulle, M., Mauras, Y., Allain, P., Tsouderos, Y., Meunier, P.J., 1996. Strontium distribution and interactions with bone mineral in monkey iliac bone after strontium salt (S 12911) administration. J. Bone Miner. Res. Off. J. Am. Soc. Bone Miner. Res.

Bonnaire, F., Zenker, H., Lill, C., Weber, A.T., Linke, B., 2005. Treatment strategies for proximal femur fractures in osteoporotic patients. Osteoporos. Int. J. Establ. Result Coop. Eur. Found. Osteoporos. Natl. Osteoporos. Found. USA 16 Suppl 2, S93–S102. doi:10.1007/s00198-004-1746-7

Bonnelye, E., Chabadel, A., Saltel, F., Jurdic, P., 2008. Dual effect of strontium ranelate: Stimulation of osteoblast differentiation and inhibition of osteoclast formation and resorption in vitro. Bone 42, 129–138.

Bonyadi, M., Waldman, S.D., Liu, D., Aubin, J.E., Grynpas, M.D., Stanford, W.L., 2003. Mesenchymal progenitor self-renewal deficiency leads to age-dependent osteoporosis in Sca-1/Ly-6A null mice. Proc. Natl. Acad. Sci. U. S. A. 100, 5840–5845.

Borsari, V., Fini, M., Giavaresi, G., Rimondini, L., Consolo, U., Chiusoli, L., Salito, A., Volpert, A., Chiesa, R., Giardino, R., 2007. Osteointegration of titanium and hydroxyapatite rough surfaces in healthy and compromised cortical and trabecular bone: in vivo comparative study on young, aged, and estrogen-deficient sheep. J. Orthop. Res. Off. Publ. Orthop. Res. Soc. 25,

Boskey, A.L., DiCarlo, E., Paschalis, E., West, P., Mendelsohn, R., 2005. Comparison of mineral quality and quantity in iliac crest biopsies from high- and low-turnover osteoporosis: an FT-IR microspectroscopic investigation. Osteoporos. Int. J. Establ. Result Coop. Eur. Found. Osteoporos. Natl. Osteoporos. Found. USA 16, 2031–2038.

Bouxsein, M.L., Boyd, S.K., Christiansen, B.A., Guldberg, R.E., Jepsen, K.J., Müller, R., 2010. Guidelines for assessment of bone microstructure in rodents using micro-computed tomography. J. Bone Miner. Res. Off. J. Am. Soc. Bone Miner. Res. 25, 1468–1486.

Boyle, W.J., Simonet, W.S., Lacey, D.L., 2003. Osteoclast differentiation and activation. Nature 423, 337–342.

Bracci, B., Torricelli, P., Panzavolta, S., Boanini, E., Giardino, R., Bigi, A., 2009. Effect of Mg(2+), Sr(2+), and Mn(2+) on the chemico-physical and in vitro biological properties of calcium phosphate biomimetic coatings. J. Inorg. Biochem. 103, 1666–1674.

Brüel, A., Olsen, J., Birkedal, H., Risager, M., Andreassen, T.T., Raffalt, A.C., Andersen, J.E.T., Thomsen, J.S., 2011. Strontium is incorporated into the fracture callus but does not influence the mechanical strength of healing rat fractures. Calcif. Tissue Int. 88, 142–152.

Buehler, J., Chappuis, P., Saffar, J.L., Tsouderos, Y., Vignery, A., 2001. Strontium ranelate inhibits bone resorption while maintaining bone formation in alveolar bone in monkeys (Macaca fascicularis). Bone 29, 176–

Caetano-Lopes, J., Lopes, A., Rodrigues, A., Fernandes, D., Perpétuo, I.P., Monjardino, T., Lucas, R., Monteiro, J., Konttinen, Y.T., Canhão, H., Fonseca, J.E., 2011. Upregulation of inflammatory genes and down regulation of sclerostin gene expression are key elements in the early phase of fragility fracture healing. PloS One 6, e16947.

Canalis, E., Hott, M., Deloffre, P., Tsouderos, Y., Marie, P.J., 1996. The divalent strontium salt S12911 enhances bone cell replication and bone formation in vitro. Bone 18, 517–523.

Capuccini, C., Torricelli, P., Boanini, E., Gazzano, M., Giardino, R., Bigi, A., 2009. Interaction of Sr-doped hydroxyapatite nanocrystals with osteoclast and osteoblast-like cells. J. Biomed. Mater. Res. A 89, 594–600.

Cardemil, C., Elgali, I., Xia, W., Emanuelsson, L., Norlindh, B., Omar, O., Thomsen, P., 2013. Strontium-doped calcium phosphate and hydroxyapatite granules promote different inflammatory and bone remodelling responses in normal and ovariectomised rats. PloS One 8, e84932.

Carlisle, E.M., 1981. Silicon: a requirement in bone formation independent of vitamin D1. Calcif. Tissue Int. 33, 27–34.

Cesnjaj, M., Stavljenić, A., Vukicević, S., 1991. Decreased osteoinductive potential of bone matrix from ovariectomized rats. Acta Orthop. Scand. 62,

Chandran, S., S, S.B., Vs, H.K., Varma, H.K., John, A., 2016. Osteogenic efficacy of strontium hydroxyapatite micro-granules in osteoporotic rat model. J. Biomater. Appl. 0885328216647197. doi:10.1177/0885328216647197

Chang, Y.L., Stanford, C.M., Keller, J.C., 2000. Calcium and phosphate supplementation promotes bone cell mineralization: implications for hydroxyapatite (HA)-enhanced bone formation. J. Biomed. Mater. Res. 52, 270–278.

Chavassieux, P., Buffet, A., Vergnaud, P., Garnero, P., Meunier, P.J., 1997. Short-term effects of corticosteroids on trabecular bone remodelling in old ewes. Bone 20, 451–455.

Chen, F., Mao, T., Tao, K., Chen, S., Ding, G., Gu, X., 2002. Bone graft in the shape of human mandibular condyle reconstruction via seeding marrow-derived osteoblasts into porous coral in a nude mice model. J. Oral Maxillofac. Surg. Off. J. Am. Assoc. Oral Maxillofac. Surg. 60, 1155–1159.

Chen, H.-T., Lee, M.-J., Chen, C.-H., Chuang, S.-C., Chang, L.-F., Ho, M.-L., Hung, S.-H., Fu, Y.-C., Wang, Y.-H., Wang, H.-I., Wang, G.-J., Kang, L., Chang, J.-K., 2012. Proliferation and differentiation potential of human adipose-derived mesenchymal stem cells isolated from elderly patients with osteoporotic fractures. J. Cell. Mol. Med. 16, 582–593.

Cheng, N., Dai, J., Cheng, X., Li, S. ’e, Miron, R.J., Wu, T., Chen, W., Zhang, Y., Shi, B., 2013. Porous CaP/silk composite scaffolds to repair femur defects in an osteoporotic model. J. Mater. Sci. Mater. Med. 24, 1963–1975.

Christoffersen, J., Christoffersen, M.R., Kolthoff, N., Bärenholdt, O., 1997. Effects of strontium ions on growth and dissolution of hydroxyapatite and on bone mineral detection. Bone 20, 47–54.

Chu, P.K., Liu, X., 2008. Biomaterials Fabrication and Processing Handbook. CRC Press.

Ciapetti, G., Ambrosio, L., Savarino, L., Granchi, D., Cenni, E., Baldini, N., Pagani, S., Guizzardi, S., Causa, F., Giunti, A., 2003. Osteoblast growth and function in porous poly epsilon -caprolactone matrices for bone repair: a preliminary study. Biomaterials 24, 3815–3824.

Clarke, B., 2008. Normal bone anatomy and physiology. Clin. J. Am. Soc. Nephrol. CJASN 3 Suppl 3, S131–139.

Compston, J., 2011. Age-Related Changes in Bone Remodelling and Structure in Men: Histomorphometric Studies. J. Osteoporos. 2011, 1–4.

Cooper, C., 1997. The crippling consequences of fractures and their impact on quality of life. Am. J. Med. 103, 12S–17S; discussion 17S–19S.

Cooper, C., Campion, G., Melton, L.J., 1992. Hip fractures in the elderly: a world-wide projection. Osteoporos. Int. J. Establ. Result Coop. Eur. Found. Osteoporos. Natl. Osteoporos. Found. USA 2, 285–289.

Cornell, C.N., Lane, J.M., Poynton, A.R., 2003. Orthopedic management of vertebral and long bone fractures in patients with osteoporosis. Clin. Geriatr. Med. 19, 433–455.

Costantino, P.D., Friedman, C.D., Jones, K., Chow, L.C., Pelzer, H.J., Sisson, G.A., 1991. Hydroxyapatite cement. I. Basic chemistry and histologic properties. Arch. Otolaryngol. Head Neck Surg. 117, 379–384.

Costa-Rodrigues, J., Reis, S., Castro, A., Fernandes, M.H., 2016. Bone Anabolic Effects of Soluble Si: In Vitro Studies with Human Mesenchymal Stem Cells and CD14+ Osteoclast Precursors. Stem Cells Int. 2016.

Currey, J.D., Brear, K., Zioupos, P., 1996. The effects of ageing and changes in mineral content in degrading the toughness of human femora. J. Biomech. 29, 257–260.

Dagang, G., Kewei, X., Yong, H., 2008. The influence of Sr doses on the in vitro biocompatibility and in vivo degradability of single-phase Sr-incorporated HAP cement. J. Biomed. Mater. Res. A 86, 947–958.

Dahl, S.G., Allain, P., Marie, P.J., Mauras, Y., Boivin, G., Ammann, P., Tsouderos, Y., Delmas, P.D., Christiansen, C., 2001. Incorporation and distribution of strontium in bone. Bone 28, 446–453.

Das, S., Crockett, J.C., 2013. Osteoporosis - a current view of pharmacological prevention and treatment. Drug Des. Devel. Ther. 7, 435–448.

De Bari, C., Dell’Accio, F., Luyten, F.P., 2001. Human periosteum-derived cells maintain phenotypic stability and chondrogenic potential throughout expansion regardless of donor age. Arthritis Rheum. 44, 85–95.

Deloffre, P., Hans, D., Rumelhart, C., Mitton, D., Tsouderos, Y., Meunier, P.J., 1995. Comparison between bone density and bone strength in glucocorticoid-treated aged ewes. Bone 17, 409S–414S.

Dennison, E., Cole, Z., Cooper, C., 2005. Diagnosis and epidemiology of osteoporosis. Curr. Opin. Rheumatol. 17, 456–461.
Donazzon, B., Dechambre, G., Lacout, J.L., 1998. Calcium-strontium hydroxyapatite: Hydrothermal preparation. Ann. Chim. Sci. Matér. 23, 53–
Dorozhkin, S.V., 2010. Amorphous calcium (ortho)phosphates. Acta Biomater. 6, 4457–4475.
Dreinhöfer, K.E., Anderson, M., Féron, J.-M., Herrera, A., Hube, R., Johnell, O., Lidgren, L., Miles, K., Tarantino, U., Simpson, H., Wallace, W.A., 2005. Multinational survey of osteoporotic fracture management. Osteoporos. Int. J. Establ. Result Coop. Eur. Found. Osteoporos. Natl. Osteoporos. Found. USA 16 Suppl 2, S44–53.
Durie, B.G.M., Katz, M., Crowley, J., 2005. Osteonecrosis of the jaw and bisphosphonates. N. Engl. J. Med. 353, 99–102; discussion 99–102.
Egermann, M., Goldhahn, J., Holz, R., Schneider, E., Lill, C.A., 2008. A sheep model for fracture treatment in osteoporosis: benefits of the model versus animal welfare. Lab. Anim. 42, 453–464. doi:10.1258/la.2007.007001
Egermann, M., Goldhahn, J., Schneider, E., 2005. Animal models for fracture treatment in osteoporosis. Osteoporos. Int. J. Establ. Result Coop. Eur. Found. Osteoporos. Natl. Osteoporos. Found. USA 16 Suppl 2, S129–138.
El-Ghannam, A., 2005. Bone reconstruction: from bioceramics to tissue engineering. Expert Rev. Med. Devices 2, 87–101.
Fadel, L., Viana, B.R., Feitosa, M.L.T., Ercolin, A.C.M., Roballo, K.C.S., Casals, J.B., Pieri, N.C.G., Meirelles, F.V., Martins, D. dos S., Miglino, M.A., Ambrósio, C.E., 2011. Protocols for obtainment and isolation of two mesenchymal stem cell sources in sheep. Acta Cirúrgica Bras. Soc. Bras. Para Desenvolv. Pesqui. Em Cir. 26, 267–273.
Fernandez, F.B., Shenoy, S., Suresh Babu, S., Varma, H.K., John, A., 2012. Short-term studies using ceramic scaffolds in lapine model for osteochondral defect amelioration. Biomed. Mater. Bristol Engl. 7, 035005.
Fielding, G., Bose, S., 2013. SiO2 and ZnO dopants in three-dimensionally printed tricalcium phosphate bone tissue engineering scaffolds enhance osteogenesis and angiogenesis in vivo. Acta Biomater. 9, 9137–9148.
Fini, M., Giavaresi, G., Torricelli, P., Borsari, V., Giardino, R., Nicolini, A., Carpi, A., 2004. Osteoporosis and biomaterial osteointegration. Biomed. Pharmacother. Bioméd. Pharmacothérapie 58, 487–493.
Fini, M., Pierini, G., Giavaresi, G., Biagini, G., Mattioli Belmonte, M.M., Nicoli Aldini, N., Rocca, M., Martini, L., Giardino, R., 2000. The ovariectomised sheep as a model for testing biomaterials and prosthetic devices in osteopenic bone: a preliminary study on iliac crest biopsies. Int. J. Artif. Organs 23, 275–
Friederichs, R.J., Brooks, R.A., Ueda, M., Best, S.M., 2015. In vitro osteoclast formation and resorption of silicon-substituted hydroxyapatite ceramics. J. Biomed. Mater. Res. A 103, 3312–3322. doi:10.1002/jbm.a.35470
Gentleman, E., Fredholm, Y.C., Jell, G., Lotfibakhshaiesh, N., O'Donnell, M.D., Hill, R.G., Stevens, M.M., 2010. The effects of strontium-substituted bioactive glasses on osteoblasts and osteoclasts in vitro. Biomaterials 31, 3949–3956.
Giannoudis, P., Tzioupis, C., Buckley, R., 2007. Fracture healing in osteoporotic fractures: is it really different.Basic science perspective.Injury 38 Suppl

Gibson, I.R., Best, S.M., Bonfield, W., 1999. Chemical characterization of silicon-substituted hydroxyapatite. J. Biomed. Mater. Res. 44, 422–428.
Gimble, J.M., Katz, A.J., Bunnell, B.A., 2007. Adipose-derived stem cells for regenerative medicine. Circ. Res. 100, 1249–1260.
Goshima, J., Goldberg, V.M., Caplan, A.I., 1991. The osteogenic potential of culture-expanded rat marrow mesenchymal cells assayed in vivo in calcium phosphate ceramic blocks. Clin. Orthop. 298–311.
Grob, G.N., 2011. From aging to pathology: the case of osteoporosis. J. Hist. Med. Allied Sci. 66, 1–39
Grzesiak, J., Krzysztof, M., Karol, W., Joanna, C., 2011. Isolation and morphological characterisation of ovine adipose-derived mesenchymal stem cells in culture. Int. J. Stem Cells 4, 99–104.
Gudena, R., Werle, J., Johnston, K., 2011. Bilateral femoral insufficiency fractures likely related to long-term alendronate therapy. J. Osteoporos. 2011, 810697. doi:10.4061/2011/810697
Gupta, G., Kirakodu, S., El-Ghannam, A., 2010. Effects of exogenous phosphorus and silicon on osteoblast differentiation at the interface with bioactive ceramics. J. Biomed. Mater. Res. A 95A, 882–890
Habermann, B., Kafchitsas, K., Olender, G., Augat, P., Kurth, A., 2010. Strontium Ranelate Enhances Callus Strength More Than PTH 1-34 in an Osteoporotic Rat Model of Fracture Healing. Calcif. Tissue Int. 86, 82–89.
He, S., Lin, K.-F., Fan, J.-J., Hu, G., Dong, X., Zhao, Y.-N., Song, Y., Guo, Z.-S., Bi, L., Liu, J., 2016. Synergistic Effect of Mesoporous Silica and Hydroxyapatite in Loaded Poly(DL-lactic-co-glycolic acid) Microspheres on the Regeneration of Bone Defects. BioMed Res. Int. 2016, 9824827.
Hench, L., Jones, J., 2005. Biomaterials, Artificial Organs and Tissue Engineering. Elsevier.
Hench, L.L., 1991. Bioceramics: From Concept to Clinic. J. Am. Ceram. Soc. 74, 1487–1510.
Hench, L.L., 2006. The story of Bioglass. J. Mater. Sci. Mater. Med. 17, 967–978. doi:10.1007/s10856-006-0432-z
Hench, L.L., Paschall, H.A., 1973. Direct chemical bond of bioactive glass-ceramic materials to bone and muscle. J. Biomed. Mater. Res. 7, 25–42.
Hing, K.A., Revell, P.A., Smith, N., Buckland, T., 2006. Effect of silicon level on rate, quality and progression of bone healing within silicate-substituted porous hydroxyapatite scaffolds. Biomaterials 27, 5014–5026.
Hong, M.-H., Choi, H.-J., Ko, Y.-M., Lee, Y.-K., 2015. Engineered microstructure granules for tailored drug release rate. Biotechnol. Bioeng.
Hornby, S.B., Ford, S.L., Mase, C.A., Evans, G.P., 1995. Skeletal changes in the ovariectomised ewe and subsequent response to treatment with 17 beta oestradiol. Bone 17, 389S–394S.
Horwitz, E.M., Gordon, P.L., Koo, W.K.K., Marx, J.C., Neel, M.D., McNall, R.Y., Muul, L., Hofmann, T., 2002. Isolated allogeneic bone marrow-derived MSCs engraft and stimulate growth in children with osteogenesis imperfecta: Implications for cell therapy of bone. Proc. Natl. Acad. Sci. 99, 8932–8937.
Huffer, W.E., Benedict, J.J., Turner, A.S., Briest, A., Rettenmaier, R., Springer, Walboomers, X.F., 2007. Repair of sheep long bone cortical defects filled with

COLLOSS, COLLOSS E, OSSAPLAST, and fresh iliac crest autograft. J. Biomed. Mater. Res. B Appl. Biomater. 82, 460–470.

Hulbert, S.F., Young, F.A., Mathews, R.S., Klawitter, J.J., Talbert, C.D., Stelling, F.H., 1970. Potential of ceramic materials as permanently implantable skeletal prostheses. J. Biomed. Mater. Res. 4, 433–456.

Iyengar, G.V., Kawamura, H., Dang, H.S., Parr, R.M., Wang, J.W., Cho, S.Y., Natera, E.S., 2004. Contents of cesium, iodine, strontium, thorium, and uranium in selected human organs of adult asian population. Health Phys. 87,

Jaiswal, N., Haynesworth, S.E., Caplan, A.I., Bruder, S.P., 1997. Osteogenic differentiation of purified, culture-expanded human mesenchymal stem cells in vitro. J. Cell. Biochem. 64, 295–312.

Jugdaohsingh, R., Tucker, K.L., Qiao, N., Cupples, L.A., Kiel, D.P., Powell, J.J., 2004. Dietary silicon intake is positively associated with bone mineral density in men and premenopausal women of the Framingham Offspring cohort. J. Bone Miner. Res. Off. J. Am. Soc. Bone Miner. Res. 19, 297–307.

Kalu, D.N., 1991. The ovariectomized rat model of postmenopausal bone loss. Bone Miner. 15, 175–191.

Kammerlander, C., Neuerburg, C., Verlaan, J.-J., Schmoelz, W., Miclau, T., Larsson, S., 2016. The use of augmentation techniques in osteoporotic fracture fixation. Injury, Osteoporotic fracture fixation — a biomechanical perspective 47, Supplement 2, S36–S43. doi:10.1016/S0020-1383(16)47007-5

Kanis, J.A., McCloskey, E.V., Johansson, H., Oden, A., Melton, L.J., Khaltaev, N., 2008. A reference standard for the description of osteoporosis. Bone 42,

Kapinas, K., Delany, A.M., 2011. MicroRNA biogenesis and regulation of bone remodeling. Arthritis Res. Ther. 13, 220. doi:10.1186/ar3325

Karageorgiou, V., Kaplan, D., 2005. Porosity of 3D biomaterial scaffolds and osteogenesis. Biomaterials 26, 5474–5491.

Katsara, O., Mahaira, L.G., Iliopoulou, E.G., Moustaki, A., Antsaklis, A., Loutradis, D., Stefanidis, K., Baxevanis, C.N., Papamichail, M., Perez, S.A., 2011. Effects of donor age, gender, and in vitro cellular aging on the phenotypic, functional, and molecular characteristics of mouse bone marrow-derived mesenchymal stem cells. Stem Cells Dev. 20, 1549–1561.

Kaufman, J.M., Johnell, O., Abadie, E., Adami, S., Audran, M., Avouac, B., Sedrine, W.B., Calvo, G., Devogelaer, J.P., Fuchs, V., Kreutz, G., Nilsson, P., Pols, H., Ringe, J., Van Haelst, L., Reginster, J.Y., 2000. Background for studies on the treatment of male osteoporosis: state of the art. Ann. Rheum.

Kennedy, O.D., Herman, B.C., Laudier, D.M., Majeska, R.J., Sun, H.B., Schaffler, M.B., 2012. Activation of resorption in fatigue-loaded bone involves both apoptosis and active pro-osteoclastogenic signaling by distinct osteocyte populations. Bone 50, 1115–1122.

Kerschan-Schindl, K., Mikosch, P., Obermayer-Pietsch, B., Gasser, R., Dimai, H.-P., Fahrleitner-Pammer, A., Dobnig, H., Roschger, P., Preisinger, E., Klaushofer, K., Resch, H., Pietschmann, P., 2014. Current Controversies in Clinical Management of Postmenopausal Osteoporosis. Exp. Clin. Endocrinol.

Kilkenny, C., Browne, W., Cuthill, I.C., Emerson, M., Altman, D.G., National Centre for the Replacement, Refinement and Reduction of Amimals in Research, 2011. Animal research: reporting in vivo experiments--the ARRIVE guidelines. J. Cereb. Blood Flow Metab. Off. J. Int. Soc. Cereb. Blood Flow Metab. 31, 991–993. doi:10.1038/jcbfm.2010.220

Klein-Nulend, J., Sterck, J.G.H., Semeins, C.M., Lips, P., Joldersma, M., Baart, J.A., Burger, E.H., 2002. Donor age and mechanosensitivity of human bone cells. Osteoporos. Int. J. Establ. Result Coop. Eur. Found. Osteoporos. Natl. Osteoporos. Found. USA 13, 137–146.

Kokubo, T., Takadama, H., 2006. How useful is SBF in predicting in vivo bone bioactivity? Biomaterials 27, 2907–2915.

Kolar, P., Schmidt-Bleek, K., Schell, H., Gaber, T., Toben, D., Schmidmaier, G., Perka, C., Buttgereit, F., Duda, G.N., 2010. The early fracture hematoma and its potential role in fracture healing. Tissue Eng. Part B Rev. 16, 427–434.

Kosuge, D., S. Khan, W., Haddad, B., Marsh, D., 2013. Biomaterials and Scaffolds in Bone and Musculoskeletal Engineering. Curr. Stem Cell Res.

Kramer, A., Angst, M., Gasser, B., Ganz, R., 2000. [Increasing bone screw anchoring in the femur head by cement administration via the implant--a biomechanical study]. Z. Für Orthop. Ihre Grenzgeb. 138, 464–469.

Lacey, D.L., Timms, E., Tan, H.L., Kelley, M.J., Dunstan, C.R., Burgess, T., Elliott, R., Colombero, A., Elliott, G., Scully, S., Hsu, H., Sullivan, J., Hawkins, N., Davy, E., Capparelli, C., Eli, A., Qian, Y.X., Kaufman, S., Sarosi, I., Shalhoub, V., Senaldi, G., Guo, J., Delaney, J., Boyle, W.J., 1998. Osteoprotegerin ligand is a cytokine that regulates osteoclast differentiation

Laib, D.A., Barou, O., Vico, L., Lafage-Proust, M.H., Alexandre, C., Rügsegger, P., 2000. 3D micro-computed tomography of trabecular and cortical bone architecture with application to a rat model of immobilisation osteoporosis. Med. Biol. Eng. Comput. 38, 326–332.

Landi, E., Uggeri, J., Medri, V., Guizzardi, S., 2013. Sr, Mg cosubstituted HA porous macro-granules: potentialities as resorbable bone filler with antiosteoporotic functions. J. Biomed. Mater. Res. A 101, 2481–2490.

Lasota, A., Danowska-Klonowska, D., 2004. Experimental osteoporosis--different methods of ovariectomy in female white rats. Rocz. Akad. Med. W Białymst. 1995 49 Suppl 1, 129–131.

Levine, S.A., Perin, L.A., Hayes, D., Hayes, W.S., 2000. An evidence-based evaluation of percutaneous vertebroplasty. Manag. Care Langhorne Pa 9, 56–60, 63.

Li, Y., Li, X., Song, G., Chen, K., Yin, G., Hu, J., 2012. Effects of strontium ranelate on osseointegration of titanium implant in osteoporotic rats. Clin. Oral Implants Res. 23, 1038–1044.

Li, Z.Y., Lam, W.M., Yang, C., Xu, B., Ni, G.X., Abbah, S.A., Cheung, K.M.C., Luk, K.D.K., Lu, W.W., 2007. Chemical composition, crystal size and lattice structural changes after incorporation of strontium into biomimetic apatite. Biomaterials 28, 1452–1460.

Liebschner, M.A.K., 2004. Biomechanical considerations of animal models used in tissue engineering of bone. Biomaterials 25, 1697–1714.

LIKINS, R.C., POSNER, A.S., KUNDE, M.L., CRAVEN, D.L., 1959. Comparative metabolism of calcium and strontium in the rat. Arch. Biochem. Biophys. 83, 472–481.
Lill, C.A., Fluegel, A.K., Schneider, E., 2000. Sheep model for fracture treatment in osteoporotic bone: a pilot study about different induction regimens. J. Orthop. Trauma 14, 559–565; discussion 565–566.
Lill, C.A., Fluegel, A.K., Schneider, E., 2002. Effect of ovariectomy, malnutrition and glucocorticoid application on bone properties in sheep: a pilot study. Osteoporos. Int. J. Establ. Result Coop. Eur. Found. Osteoporos. Natl. Osteoporos. Found. USA 13, 480–486.
Liu, H.-Y., Chiou, J.-F., Wu, A.T.H., Tsai, C.-Y., Leu, J.-D., Ting, L.-L., Wang, M.-F., Chen, H.-Y., Lin, C.-T., Williams, D.F., Deng, W.-P., 2012. The effect of diminished osteogenic signals on reduced osteoporosis recovery in aged mice and the potential therapeutic use of adipose-derived stem cells. Biomaterials 33, 6105–6112. Li, X., Nishimura, I., 1994. Altered bone remodeling pattern of the residual ridge in ovariectomized rats. J. Prosthet.
López, A., Montazerolghaem, M., Engqvist, H., Ott, M.K., Persson, C., 2014. Calcium phosphate cements with strontium halides as radiopacifiers. J. Biomed. Mater. Res. B Appl. Biomater. 102, 250–259.
Majumdar, S., Genant, H.K., Grampp, S., Newitt, D.C., Truong, V.-H., Lin, J.C., Mathur, A., 1997. Correlation of Trabecular Bone Structure with Age, Bone Mineral Density, and Osteoporotic Status: In Vivo Studies in the Distal Radius Using High Resolution Magnetic Resonance Imaging. J. Bone Miner. Res. 12, 111–118. Malhotra, N., Mithal, A., 2008. Osteoporosis in Indians. Indian J. Med. Res. 127, 263–268.
Malhotra, N., Mithal, A., 2008. Osteoporosis in Indians. Indian J. Med. Res. 127, 263–268.
Manolagas, S.C., 2000. Birth and death of bone cells: basic regulatory mechanisms and implications for the pathogenesis and treatment of osteoporosis. Endocr. Rev. 21, 115–137.
Marie, P.J., 2006. Strontium ranelate: a dual mode of action rebalancing bone turnover in favour of bone formation. Curr. Opin. Rheumatol. 18 Suppl 1, S11-15. doi:10.1097/01.bor.0000229522.89546.7b
Marie, P.J., Ammann, P., Boivin, G., Rey, C., 2001. Mechanisms of action and therapeutic potential of strontium in bone. Calcif. Tissue Int. 69, 121–129.
Marie, P.J., Sabbagh, A., de Vernejoul, M.C., Lomri, A., 1989. Osteocalcin and deoxyribonucleic acid synthesis in vitro and histomorphometric indices of bone formation in postmenopausal osteoporosis. J. Clin. Endocrinol. Metab. 69, 272–279.
Marwaha, R.K., Tandon, N., Garg, M.K., Kanwar, R., Narang, A., Sastry, A., Saberwal, A., Bhadra, K., Mithal, A., 2011. Bone health in healthy Indian population aged 50 years and above. Osteoporos. Int. J. Establ. Result Coop. Eur. Found. Osteoporos. Natl. Osteoporos. Found. USA 22, 2829–2836.
Mastrogiacomo, M., Papadimitropoulos, A., Cedola, A., Peyrin, F., Giannoni, P., Pearce, S.G., Alini, M., Giannini, C., Guagliardi, A., Cancedda, R., 2007. Engineering of bone using BMSCs and a silicon-stabilized TCP: evidence for a coupling between bone formation and scaffold resorption. Biomaterials

Meunier, P.J., Slosman, D.O., Delmas, P.D., Sebert, J.L., Brandi, M.L., Albanese, C., Lorenc, R., Pors-Nielsen, S., De Vernejoul, M.C., Roces, A., Reginster, J.Y., 2002. Strontium ranelate: dose-dependent effects in established postmenopausal vertebral osteoporosis--a 2-year randomized placebo controlled trial. J. Clin. Endocrinol. Metab. 87, 2060–2066

Meyer, R.A., Tsahakis, P.J., Martin, D.F., Banks, D.M., Harrow, M.E., Kiebzak, G.M., 2001. Age and ovariectomy impair both the normalization of mechanical properties and the accretion of mineral by the fracture callus in rats. J. Orthop. Res. Off. Publ. Orthop. Res. Soc. 19, 428–435.

Mirsaidi, A., Genelin, K., Vetsch, J.R., Stanger, S., Theiss, F., Lindtner, R.A., von Rechenberg, B., Blauth, M., Müller, R., Kuhn, G.A., Hofmann Boss, S., Ebner, H.L., Richards, P.J., 2014. Therapeutic potential of adipose-derived stromal cells in age-related osteoporosis. Biomaterials 35, 7326–7335. doi:10.1016/j.biomaterials.2014.05.016

Mohan, B.G., Shenoy, S.J., Babu, S.S., Varma, H.K., John, A., 2013. Strontium calcium phosphate for the repair of leporine (Oryctolagus cuniculus) ulna segmental defect. J. Biomed. Mater. Res. A 101, 261–271.

Mohan, B.G., Suresh Babu, S., Varma, H.K., John, A., 2013. In vitro evaluation of bioactive strontium-based ceramic with rabbit adipose-derived stem cells for bone tissue regeneration. J. Mater. Sci. Mater. Med. 24, 2831–2844.

Morohashi, T., Sano, T., Harai, K., Yamada, S., 1995. Effects of strontium on calcium metabolism in rats. II. Strontium prevents the increased rate of bone turnover in ovariectomized rats. Jpn. J. Pharmacol. 68, 153–159.

Moroni, A., Faldini, C., Marchetti, S., Manca, M., Consoli, V., Giannini, S., 2001. Improvement of the bone-pin interface strength in osteoporotic bone with use of hydroxyapatite-coated tapered external-fixation pins. A prospective, randomized clinical study of wrist fractures. J. Bone Joint Surg. Am. 83-A,

Mountziaris, P.M., Spicer, P.P., Kasper, F.K., Mikos, A.G., 2011. Harnessing and Modulating Inflammation in Strategies for Bone Regeneration. Tissue Eng. Part B Rev. 17, 393–402.

Mullender, M.G., Tan, S.D., Vico, L., Alexandre, C., Klein-Nulend, J., 2005. Differences in osteocyte density and bone histomorphometry between men and women and between healthy and osteoporotic subjects. Calcif. Tissue Int. 77, 291–296.

Nair, M.B., Bernhardt, A., Lode, A., Heinemann, C., Thieme, S., Hanke, T., Varma, H., Gelinsky, M., John, A., 2009a. A bioactive triphasic ceramic-coated hydroxyapatite promotes proliferation and osteogenic differentiation of human bone marrow stromal cells. J. Biomed. Mater. Res. A 90, 533–542.

Nair, M.B., Suresh Babu, S., Varma, H.K., John, A., 2008. A triphasic ceramic-coated porous hydroxyapatite for tissue engineering application. Acta Biomater. 4, 173–181.

Nair, M.B., Varma, H.K., Menon, K.V., Shenoy, S.J., John, A., 2009a. Tissue regeneration and repair of goat segmental femur defect with bioactive triphasic ceramic-coated hydroxyapatite scaffold. J. Biomed. Mater. Res. A 91, 855–865. doi:10.1002/jbm.a.32239

Nair, M.B., Varma, H.K., Menon, K.V., Shenoy, S.J., John, A., 2009b. Reconstruction of goat femur segmental defects using triphasic ceramic-

hydroxyapatite in combination with autologous cells and platelet-rich plasma. Biomater. 5, 1742–1755. doi:10.1016/j.actbio.2009.01.009

Namkung-Matthai, H., Appleyard, R., Jansen, J., Hao Lin, J., Maastricht, S., Swain, M., Mason, R.S., Murrell, G.A., Diwan, A.D., Diamond, T., 2001. Osteoporosis influences the early period of fracture healing in a rat osteoporotic model. Bone 28, 80–86.

Newman, S.D., Lotfibakhshaiesh, N., O'Donnell, M., Walboomers, X.F., Horwood, N., Jansen, J.A., Amis, A.A., Cobb, J.P., Stevens, M.M., 2014. Enhanced osseous implant fixation with strontium-substituted bioactive glass coating. Tissue Eng. Part A 20, 1850–1857. doi:10.1089/ten.TEA.2013.0304

Ni, G.-X., Shu, B., Huang, G., Lu, W.W., Pan, H.-B., 2012. The effect of strontium incorporation into hydroxyapatites on their physical and biological properties. J. Biomed. Mater. Res. B Appl. Biomater. 100, 562–568.

Ni, S., Chang, J., 2009. In vitro degradation, bioactivity, and cytocompatibility of calcium silicate, dimagnesium silicate, and tricalcium phosphate bioceramics. J. Biomater. Appl. 24, 139–158.

Niemeyer, P., Szalay, K., Luginbühl, R., Südkamp, N.P., Kasten, P., 2010. Transplantation of human mesenchymal stem cells in a non-autogenous setting for bone regeneration in a rabbit critical-size defect model. Acta Biomater. 6, 900–908. doi:10.1016/j.actbio.2009.09.007

Nuss, K.M.R., Auer, J.A., Boos, A., von Rechenberg, B., 2006. An animal model in sheep for biocompatibility testing of biomaterials in cancellous bones. BMC Musculoskelet. Disord. 7, 67

Ocarino, N. de M., Boeloni, J.N., Jorgetti, V., Gomes, D.A., Goes, A.M., Serakides, R., 2010. Intra-bone marrow injection of mesenchymal stem cells improves the femur bone mass of osteoporotic female rats. Connect. Tissue

Ohgushi, H., Caplan, A.I., 1999. Stem cell technology and bioceramics: from cell to gene engineering. J. Biomed. Mater. Res. 48, 913–927.

Ohgushi, H., Goldberg, V.M., Caplan, A.I., 1989. Repair of bone defects with marrow cells and porous ceramic. Experiments in rats. Acta Orthop. Scand. 60, 334–339.

Ohta, H., Uemura, Y., Nakamura, T., Fukunaga, M., Ohashi, Y., Hosoi, T., Mori, S., Sugimoto, T., Itoi, E., Orimo, H., Shiraki, M., Adequate Treatment of Osteoporosis (A-TOP) Research Group, 2014. Serum 25-hydroxyvitamin D level as an independent determinant of quality of life in osteoporosis with a high risk for fracture. Clin. Ther. 36, 225–235.

Oliver, R.A., Yu, Y., Yee, G., Low, A.K., Diwan, A.D., Walsh, W.R., 2013. Poor histological healing of a femoral fracture following 12 months of oestrogen deficiency in rats. Osteoporos. Int. J. Establ. Result Coop. Eur. Found. Osteoporos. Natl. Osteoporos. Found. USA 24, 2581–2589.

Omi, N., Ezawa, I., 2011. [Animal models for bone and joint disease. Low calcium diet-induced rat model of osteoporosis]. Clin. Calcium 21, 173–180.

Ozawa, S., Ogawa, T., Iida, K., Sukotjo, C., Hasegawa, H., Nishimura, R.D., Nishimura, I., 2002. Ovariectomy hinders the early stage of bone-implant integration: histomorphometric, biomechanical, and molecular analyses. Bone 30, 137–143.

Pape, H.-C., Marcucio, R., Humphrey, C., Colnot, C., Knobe, M., Harvey, E.J., 2010. Trauma-induced inflammation and fracture healing. J. Orthop. Trauma 24, 522–525.

Patel, N., Best, S.M., Bonfield, W., Gibson, I.R., Hing, K.A., Damien, E., Revell, P.A., 2002. A comparative study on the in vivo behavior of hydroxyapatite and silicon substituted hydroxyapatite granules. J. Mater. Sci. Mater. Med. 13, 1199–1206.

Pearce, A.I., Richards, R.G., Milz, S., Schneider, E., Pearce, S.G., 2007. Animal models for implant biomaterial research in bone: a review. Eur. Cell. Mater. 13, 1–10.

Pei, M., Li, J., McConda, D.B., Wen, S., Clovis, N.B., Danley, S.S., 2015. A comparison of tissue engineering based repair of calvarial defects using adipose stem cells from normal and osteoporotic rats. Bone 78, 1–10. doi:10.1016/j.bone.2015.04.040

Pietak, A.M., Reid, J.W., Stott, M.J., Sayer, M., 2007. Silicon substitution in the calcium phosphate bioceramics. Biomaterials 28, 4023–4032. doi:10.1016/j.biomaterials.2007.05.003

Price, C.T., Koval, K.J., Langford, J.R., 2013. Silicon: a review of its potential role in the prevention and treatment of postmenopausal osteoporosis. Int. J. Endocrinol. 2013, 316783.

Qiu, K., Zhao, X.J., Wan, C.X., Zhao, C.S., Chen, Y.W., 2006a. Effect of strontium ions on the growth of ROS17/2.8 cells on porous calcium polyphosphate scaffolds. Biomaterials 27, 1277–1286.

Rabbits, F. working group on revision of guidelines for health monitoring of rodents and, (Convenor), M.M., Berard, M., Feinstein, R., Gallagher, A., Illgen-Wilcke, B., Pritchett-Corning, K., Raspa, M., 2014. FELASA recommendations for the health monitoring of mouse, rat, hamster, guinea pig and rabbit colonies in breeding and experimental units. Lab. Anim. 48, 178–192. doi:10.1177/0023677213516312

Rachner, T.D., Khosla, S., Hofbauer, L.C., 2011. Osteoporosis: now and the future. Lancet Lond. Engl. 377, 1276–1287.

Raisz, L.G., 1993. Local and systemic factors in the pathogenesis of osteoporosis. World Rev. Nutr. Diet. 72, 92–101.

Reffitt, D.M., Ogston, N., Jugdaohsingh, R., Cheung, H.F.J., Evans, B. a. J., Thompson, R.P.H., Powell, J.J., Hampson, G.N., 2003. Orthosilicic acid stimulates collagen type 1 synthesis and osteoblastic differentiation in human osteoblast-like cells in vitro. Bone 32, 127–135.

Reffitt, D.M., Ogston, N., Jugdaohsingh, R., Cheung, H.F.J., Evans, B. a. J., Thompson, R.P.H., Powell, J.J., Hampson, G.N., 2003. Orthosilicic acid stimulates collagen type 1 synthesis and osteoblastic differentiation in human osteoblast-like cells in vitro. Bone 32, 127–135.

Renjith P. Nair, K.K., 2014. Feasibility of Dermal Substitute Construction on Hybrid Scaffold Made of Poly(ε-caprolactone) and Bio Mimetic Fibrin Composite. J. Biomater. Tissue Eng. 4.

Rheinboldt, M., Harper, D., Stone, M., 2014. Atypical femoral fractures in association with bisphosphonate therapy: a case series. Emerg. Radiol. 21, 557–562.

Rocca, M., Fini, M., Giavaresi, G., Aldini, N.N., Giardino, R., 2002. Osteointegration of hydroxyapatite-coated and uncoated titanium screws in long-term ovariectomized sheep. Biomaterials 23, 1017–1023.

Rodríguez, J.P., Montecinos, L., Ríos, S., Reyes, P., Martínez, J., 2000. Mesenchymal stem cells from osteoporotic patients produce a type I collagen-deficient extracellular matrix favoring adipogenic differentiation. J. Cell. Biochem. 79, 557–565.

Rose, F.R.A.J., Oreffo, R.O.C., 2002. Bone tissue engineering: hope vs hype. Biochem. Biophys. Res. Commun. 292, 1–7.

Roy, M., Bose, S., 2012. Osteoclastogenesis and osteoclastic resorption of tricalcium phosphate: effect of strontium and magnesium doping. J. Biomed. Mater. Res. A 100, 2450–2461.

Sabareeswaran, A., Basu, B., Shenoy, S.J., Jaffer, Z., Saha, N., Stamboulis, A., 2013. Early osseointegration of a strontium containing glass ceramic in a rabbit model. Biomaterials 34, 9278–9286.

Saltel, F., Destaing, O., Bard, F., Eichert, D., Jurdic, P., 2004. Apatite-mediated actin dynamics in resorbing osteoclasts. Mol. Biol. Cell 15, 5231–5241.

Schneider, E., Goldhahn, J., Burckhardt, P., 2005. The challenge: fracture treatment in osteoporotic bone. Osteoporos. Int. J. Establ. Result Coop. Eur. Found. Osteoporos. Natl. Osteoporos. Found. USA 16 Suppl 2, S1–2.

Schumacher, M., Lode, A., Helth, A., Gelinsky, M., 2013. A novel strontium(II)-modified calcium phosphate bone cement stimulates human-bone-marrow-derived mesenchymal stem cell proliferation and osteogenic differentiation in vitro. Acta Biomater. 9, 9547–9557.

Schwarz, K., 1973. A bound form of silicon in glycosaminoglycans and polyuronides. Proc. Natl. Acad. Sci. U. S. A. 70, 1608–1612.

Seeman, E., 2008. Structural basis of growth-related gain and age-related loss of bone strength. Rheumatol. Oxf. Engl. 47 Suppl 4, iv2–8.

Sethe, S., Scutt, A., Stolzing, A., 2006. Aging of mesenchymal stem cells. Ageing Res. Rev. 5, 91–116

Shie, M.-Y., Ding, S.-J., Chang, H.-C., 2011. The role of silicon in osteoblast-like cell proliferation and apoptosis. Acta Biomater. 7, 2604–2614. doi:10.1016/j.actbio.2011.02.023

Sobh, M.A., 2014. Adipogenesis of Sprague Dawely rats mesenchymal stem cells: a morphological, immunophenotyping and gene expression follow-up study. Anat. Cell Biol. 47, 83–90.

Stadelmann, V.A., Gauthier, O., Terrier, A., Bouler, J.M., Pioletti, D.P., 2008. Implants delivering bisphosphonate locally increase periprosthetic bone density in an osteoporotic sheep model. A pilot study. Eur. Cell. Mater. 16,

Sterling, J.A., Guelcher, S.A., 2014. Biomaterial scaffolds for treating osteoporotic bone. Curr. Osteoporos. Rep. 12, 48–54.

Sureshbabu, S., Komath, M., Varma, H.K., 2012. In Situ Formation of Hydroxyapatite – Alpha Tricalcium Phosphate Biphasic Ceramics with Higher Strength and Bioactivity. J. Am. Ceram. Soc. 95, 915–924.

Syed, A.A., Agarwal, M., Giannoudis, P.V., Matthews, S.J.E., Smith, R.M., 2004. Distal femoral fractures: long-term outcome following stabilisation with the LISS. Injury 35, 599–607.

Syftestad, G.T., Urist, M.R., 1982. Bone aging. Clin. Orthop. 288–297.
Takahashi, S., Takahashi, I., Sato, H., Kubota, Y., Yoshida, S., Muramatsu, Y., 2000. Determination of major and trace elements in the liver of Wistar rats by inductively coupled plasma-atomic emission spectrometry and mass spectrometry. Lab. Anim. 34, 97–105.
Takahashi, Y., Tabata, Y., 2004. Effect of the fiber diameter and porosity of non-woven PET fabrics on the osteogenic differentiation of mesenchymal stem cells. J. Biomater. Sci. Polym. Ed. 15, 41–57.
Tao, Z.-S., Bai, B.-L., He, X.-W., Liu, W., Li, H., Zhou, Q., Sun, T., Huang, Z.-L., Tu, K.-K., Lv, Y.-X., Cui, W., Yang, L., 2016. A comparative study of strontium-substituted hydroxyapatite coating on implant's osseointegration for osteopenic rats. Med. Biol. Eng. Comput. doi:10.1007/s11517-016-1494-9
Tidermark, J., Blomfeldt, R., Ponzer, S., Söderqvist, A., Törnkvist, H., 2003. Primary total hip arthroplasty with a Burch-Schneider antiprotrusion cage and autologous bone grafting for acetabular fractures in elderly patients. J. Orthop. Trauma 17, 193–197.
Tsigkou, O., Jones, J.R., Polak, J.M., Stevens, M.M., 2009. Differentiation of fetal osteoblasts and formation of mineralized bone nodules by 45S5 Bioglass conditioned medium in the absence of osteogenic supplements. Biomaterials 30, 3542–3550.
Turner, R.T., Maran, A., Lotinun, S., Hefferan, T., Evans, G.L., Zhang, M., Sibonga, J.D., 2001. Animal models for osteoporosis. Rev. Endocr. Metab. Disord. 2, 117–127.
Venken, K., Callewaert, F., Boonen, S., Vanderschueren, D., 2008. Sex hormones, their receptors and bone health. Osteoporos. Int. J. Establ. Result Coop. Eur. Found. Osteoporos. Natl. Osteoporos. Found. USA 19, 1517–1525.
Vupputuri, M.R., Goswami, R., Gupta, N., Ray, D., Tandon, N., Kumar, N., 2006. Prevalence and functional significance of 25-hydroxyvitamin D deficiency and vitamin D receptor gene polymorphisms in Asian Indians. Am. J. Clin. Nutr. 83, 1411–1419.
Walsh, W.R., Sherman, P., Howlett, C.R., Sonnabend, D.H., Ehrlich, M.G., 1997. Fracture healing in a rat osteopenia model. Clin. Orthop. 218–227.
Walters, M.A., Leung, Y.C., Blumenthal, N.C., LeGeros, R.Z., Konsker, K.A., 1990. A Raman and infrared spectroscopic investigation of biological hydroxyapatite. J. Inorg. Biochem. 39, 193–200.
Wang, J., Li, W., Xu, S., Yang, D., Wang, Y., Lin, M., Zhao, G., 2005. Osteoporosis influences the middle and late periods of fracture healing in a rat osteoporotic model. Chin. J. Traumatol. Zhonghua Chuang Shang Za Zhi Chin. Med. Assoc. 8, 111–116.
Wang, Z., Goh, J., Das De, S., Ge, Z., Ouyang, H., Chong, J.S.W., Low, S.L., Lee, E.H., 2006. Efficacy of bone marrow-derived stem cells in strengthening osteoporotic bone in a rabbit model. Tissue Eng. 12, 1753–1761.
Willie, B.M., Bloebaum, R.D., Bireley, W.R., Bachus, K.N., Hofmann, A.A., 2004. Determining relevance of a weight-bearing ovine model for bone ingrowth assessment. J. Biomed. Mater. Res. A 69, 567–576.
Wong, C.T., Lu, W.W., Chan, W.K., Cheung, K.M.C., Luk, K.D.K., Lu, D.S., A.B.M., Deng, L.F., Leong, J.C.Y., 2004. In vivo cancellous bone remodeling

strontium-containing hydroxyapatite (sr-HA) bioactive cement. J. Biomed. Res. A 68, 513–521.

Wu, Z., Lei, W., Hu, Y., Wang, H., Wan, S., Ma, Z., Sang, H., Fu, S., Han, Y., 2008. Effect of ovariectomy on BMD, micro-architecture and biomechanics of cortical and cancellous bones in a sheep model. Med. Eng. Phys. 30, 1112–

Ye, X., Zhang, P., Xue, S., Xu, Y., Tan, J., Liu, G., 2014. Adipose-derived stem cells alleviate osteoporosis by enhancing osteogenesis and inhibiting adipogenesis in a rabbit model. Cytotherapy 16, 1643–1655.

Yu, Z., Zhu, T., Li, C., Shi, X., Liu, X., Yang, X., Sun, H., 2012. Improvement of intertrochanteric bone quality in osteoporotic female rats after injection of polylactic acid-polyglycolic acid copolymer/collagen type I microspheres combined with bone mesenchymal stem cells. Int. Orthop. 36, 2163–2171.

Zhang, M., Zhai, W., Lin, K., Pan, H., Lu, W., Chang, J., 2010. Synthesis, in vitro hydroxyapatite forming ability, and cytocompatibility of strontium silicate powders. J. Biomed. Mater. Res. B Appl. Biomater. 93, 252–257.

Zhao, W., Chang, J., Wang, J., Zhai, W., Wang, Z., 2007. In vitro bioactivity of novel tricalcium silicate ceramics. J. Mater. Sci. Mater. Med. 18, 917–923.

Ziats, N.P., Miller, K.M., Anderson, J.M., 1988. In vitro and in vivo interactions of cells with biomaterials. Biomaterials 9, 5–13.

Zreiqat, H., Ramaswamy, Y., Wu, C., Paschalidis, A., Lu, Z., James, B., Birke, O., McDonald, M., Little, D., Dunstan, C.R., 2010. I incorporation of Sr and zinc into a calcium-silicon ceramic for bone tissue engineering. Biomaterials 31, 3175–3184.

# PATENT

1. Porous scaffolds of strontium containing dual phase calcium phosphate for bone tissue engineering (under preparation)

# LIST OF PUBLICATIONS

1. **Sunitha Chandran,** Suresh Babu, Harikrishnan V.S. , H.K. Varma and John; Osteogenic efficacy of Strontium Hydroxyapatite micro-granules in osteoporotic rat model. (J Biomater Appl. October 2016 vol. 31 no. 4 499-

2. **Sunitha Chandran**, Harikrishnan V.S. and Annie John; Characterisation of the Ovariectomised and Long Term Induced (OLI) Rat Model for Osteoporotic Applications (Veterinary evidence – final copy edit )

3. **Sunitha Chandran**, Suresh Babu, Sachin J Shenoy , Renjith P Nair, H.K. Varma and Annie John; Osteointegration of bioactive Strontium hydroxyapatite – preliminary evaluation in sheep osteoporotic model. (Under review - Biofabrication)

4. Joice Tom, **Sunitha Chandran** and Annie John; Assessment of bone quality with ageing (Under preparation) .

5. Remya K.R, **Sunitha Chandran**, Annie John and P.Ramesh; Pamidronate encapsulated electrospun nanofibrous polycaprolactone scaffolds as a potential drug eluting scaffold for the treatment of osteoporotic bone defects (Under preparation) .

6. Remya K.R, **Sunitha Chandran**, Annie John and P.Ramesh; Hybrid Polycaprolactone/Polyethylene oxide scaffolds with tunable fiber surface morphology, improved hydrophilicity and biodegradability for bone tissue engineering applications (Under preparation) .

# PAPER PRESENTATIONS AND CONFERENCE PROCEEDINGS:

1. **Sunitha Chandran and Annie John** "Osteoporotic fracture treatment strategies: How your bones can be protected – a review". ICFST – JSPS, Trivandrum, 2011 (Poster).

2. **Sunitha Chandran,** Suresh Babu, Harikrishnan V.S. , H.K. Varma and John - "Tissue engineered Strontium incorporated Hydroxyapatite (SrHA) substitute for Osteoporotic rat femur defect model- A pre-clinical during the XXIII Conference of the Society for Biomaterials and Artificial Organs (India) at the IISc. Bangalore, 2012 (Poster).

3. **Sunitha Chandran,** Suresh Babu, Harikrishnan V.S., H.K. Varma and John;- "Osteoporotic fracture healing in rat model using Strontium bone substitute" at the XXV KSC at Technopark, 2013 (Poster).

4. **Sunitha Chandran,** Suresh Babu, Harikrishnan V.S., H.K. Varma and John- "Strontium Incorporated Hydroxyapatite (Sr .HA) Micro-granules Osteoporotic Application" at TERMIS-AP 2013, China, 2013 (Oral).

5. **Sunitha Chandran,** Suresh Babu, Sachin Shenoy, H.K. Varma and Annie John- Bioactive Strontium Hydroxyapatite– Reinforcing Osteoporotic Women And Beyond' in Indo-Australian Conference On Biomaterials, Engineering, Drug Delivery System & Regenerative Medicine, 2015 (Oral).

6. **Sunitha Chandran,** Suresh Babu, Harikrishnan V.S. , H.K. Varma and John- Bone healing response with a bi-functional bioactive hydroxyapatite in osteoporotic rat model; Science fete, SCTIMST, India, 2014 (Oral).

7. **Joice Tom J, Sunitha Chandran**, and Annie John- "Assessment of Bone Quality and Stem Cell potential with aging" at Third Euro-India Conference on Nanomedicine and Tissue Engineering, Kerala, 2013

# CURRICULUM VITAE

## Education

- **Ph.D. Scholar (CSIR fellowship)** (March 2010- present) at Sree Chitra Tirunal Institute for Medical Sciences and Technology, Biomedical Technology Wing, Thiruvananthapuram, Kerala, India.
- **Post Graduation:** Masters Degree in Biotechnology, K.V.M. College; University of Science and Technology, Distinction & CGPA score - 8.73 in 2009.
- **Graduation:** Bachelors degree in Biotechnology with Botany (double main course), St Xavier's College; Kerala University, Distinction and 86% of

## Achievements

- **Qualified CSIR–JRF June-2009 - 276$^{th}$ Rank on all India Basis.**
- **Junior Research Fellowship** (2010-2012) by Council of Scientific and Industrial Research (CSIR), New Delhi, India.
- **Senior Research Fellowship** (2012-2015) by Council of Scientific and Industrial Research, New Delhi, India.
- **Best Paper Presentation Award (Oral),** "Bioactive Strontium Hydroxyapatite Reinforcing Osteoporotic Bones In Women And the Indo-Australian Conference – BiTERM 2015, India.
- Joice Tom J, **Sunitha Chandran**, and Annie John- **(Best poster award) -** "Assessment of Bone Quality and Stem Cell potential with aging" at Euro-India International Conference on Nanomedicine and Tissue Engineering, Kerala, 2013.
- DBT travel Grant to attend TERMIS-AP Annual Meeting at Wuzhen & Shanghai, China and gave an oral presentation entitled on October 24,

# APPENDIX

1. **SBF buffer**

| | |
|---|---|
| Sodium Chloride | : 8.05g |
| Sodium carbonate | : 0.355g |
| Potassium Chloride | : 0.225 g |
| Dipotassium hydrogen phosphate | : 0.261g |
| Magnesium Chloride hexahydrate | : 0.311g |
| 1 M Hydrochloric acid | : 35 ml |
| Calcium Chloride Dihydrate | : 0.55 g |
| Sodium Sulphate | : 0.072 g |
| Tris | : 6.60 g |

2. **Alkaline phosphatase buffer (pH 9.8)**

| | | |
|---|---|---|
| Diethanol amine | - | 0.1 M |
| Triton X-100 | - | 1% |
| $MgCl_2$ | - | 1 mM |

3. **Alkaline phosphatase substrate:**

   20 mg 4-paranitrophenyl phosphate (Sigma chemicals) in 20 mL ALP substrate buffer.

4. **Stevenal's blue stain:**

   Methylene Blue – 1 gm in 75 ml distilled water

   Potassium permanganate – 1.5 gm in 75 ml distilled water

5. **Van Gieson's Picrofuchsin stain:**

   Acid Fuchsin – 0.1 gm in 10 ml distilled water

   Saturated picric acid – 100ml